Universidade do Minho
Escola de Engenharia

João Pedro Vasconcelos Silva

Integration of a Model for Volatile Release in the CFD Simulation of an Industrial Biomass Boiler

dezembro de 2022

Integration of a Model for Volatile Release in the CFD Simulation of an Industrial Biomass Boiler

João Silva

UMinho | 2022

REPÚBLICA PORTUGUESA | CIÊNCIA, TECNOLOGIA E ENSINO SUPERIOR
FCT Fundação para a Ciência e a Tecnologia
NORTE 2020 CENTRO 2020
ALENTEJO 2020
POCH
PORTUGAL 2020
UNIÃO EUROPEIA
Fundo Europeu de Desenvolvimento Regional

Universidade do Minho
Escola de Engenharia

João Pedro Vasconcelos Silva

Integration of a Model for Volatile Release in the CFD Simulation of an Industrial Biomass Boiler

Doctoral Thesis for PhD degree in

Leaders for Technical Industries

Work developed under the supervision of:

Professor José Carlos Fernandes Teixeira

Professor Senhorinha de Fátima Capela Fortunas Teixeira

December 2022

ACKNOWLEDGMENTS

The road to complete this thesis was long but gratifying. However, that work was not the result of my solitary commitment but the result of the support of many people and institutions. Here is my opportunity to acknowledge all people I have been involved with during the past four years. I will be forever grateful to them!

In the first place, I am grateful to Professors José Carlos Teixeira and Senhorinha Teixeira, my supervisors, for the opportunity in doing this research, for their guidance, and for creating all the conditions to develop my work. I must also say that their sense of responsibility, attitude, professional ethics, and their perseverance are a golden standard for my professional career. It was a pleasure and privilege to collaborate with them.

A special thanks go to Professor Bernhard Peters from the University of Luxembourg for providing me the opportunity to use the numerical model developed by their research center, the possibility to use their computational resources, and also the interesting ideas and observations.

I am also grateful to Fundação para a Ciência e a Tecnologia for sponsoring my research, through the grant SFRH/BD/130588/2017.

During my research work, I visited the Biomass Power Plant of Mortágua, Portugal, for a period of two weeks. I want to express my deepest gratitude to Élson Grilo and Carlos Ferreira from Altri and EDP for their brilliant guidance, help, and support. Their friendship, the care taken with me during my stay in Mortágua, and the moments experienced will never be forgotten. It was a rewarding experience both scientifically and personally.

The development of my experimental work was only possible due to the collaboration with different laboratories and with different institutions for that I am deeply grateful. Hence, I would like to express here my gratitude to the Wastes Valorization Centre, Biological Engineering Centre, and ECOTORO.

I would especially like to express my gratitude to my colleagues from Mechanical Engineering Department for their encouragement, support, and contagious enthusiasm. They created a wonderful working atmosphere at the University.

I would like to also address my deepest gratitude to my parents for giving me their encouragement, patience, and all the conditions and comfort to develop my work. Finally, I would like to express all my gratitude to Eliana for their never-ending encouragement, love, and constant moral support, and the belief in my ability to do the work was tremendous.

STATEMENT OF INTEGRITY

I hereby declare having conducted this academic work with integrity. I confirm that I have not used plagiarism or any form of undue use of information or falsification of results along the process leading to its elaboration.

I further declare that I have fully acknowledged the Code of Ethical Conduct of the University of Minho.

RESUMO

Integration of a Model for Volatile Release in the CFD Simulation of an Industrial Biomass Boiler

Motivada por sua disponibilidade, abundância generalizada e preocupações ambientais, a biomassa sólida tornou-se uma opção competitiva para diversificar a produção de eletricidade entre os recursos de energia renovável. Este trabalho tem como objetivo caraterizar o comportamento da combustão de espécies de biomassa frequentemente utilizadas em centrais termoelétricas para suportar o desenvolvimento de um modelo numérico para modelação eficiente e precisa da conversão de biomassa numa caldeira industrial a grelha. A eficiência da caldeira numa central de 35 MWth foi calculada como sendo aproximadamente 80%.

Amostras selecionadas de biomassa de eucalipto, pinheiro, acácia e oliveira foram testadas com o analisador térmico Hot Disk TPS 2500S. A condutividade térmica ficou compreendida entre 0,239 e 0,404 W/mK. Além disso, a capacidade calorífica apresentou uma variação entre 0,855 e 2,442 MJ/m^3K, e a difusividade térmica entre 0,187 e 0,258 mm^2/s. Para a análise final e aproximada foram utilizados os equipamentos LECO TruSpec CHN Macro e LECO CS-200 e uma mufla, respetivamente. Os dados revelaram uma maior reatividade do eucalipto, cerca de 2 vezes superior aos outros combustíveis, e a propensão da acácia a produzir emissões poluentes (principalmente à base de azoto) e problemas de deposição de cinzas devido à sua composição química.

Amostras de pequenas dimensões (cerca de 10 mg) foram usadas para medir a perda de massa e a sua reatividade num analisador termogravimétrico (TGA) da TA Instruments, modelo SDT 2960. Os testes foram realizados em atmosfera oxidante, a uma taxa de aquecimento entre 5 e 100 °C/min, até 900 °C. Observou-se que numa ampla faixa de temperaturas, a conversão do combustível segue uma sequência de secagem, desvolatilização e combustão do resíduo carbonoso.

Amostras de maiores dimensões foram testadas num reator construído para esse fim, e que simula o processo de desvolatilização de forma controlável. Neste, a perda de massa foi medida continuamente ao longo do tempo enquanto os compostos da fase gasosa foram recolhidos em sacos para posterior análise num cromatógrafo gasoso da Bruker Scion 456-GC equipado com um detetor de condutividade térmica. Ao contrário dos dados do TGA, concluiu-se que na oxidação de biomassas, utilizando partículas maiores, não é possível distinguir as sucessivas etapas de conversão, devido à maior resistência interna de difusão. Avaliando a influência da esbelteza da amostra (rácio comprimento/espessura), concluiu-se que a taxa de desvolatilização depende apenas da sua espessura e não do volume. Além disso, para temperaturas mais altas do reator, a taxa de perda de massa é independente do tipo de biomassa. Os compostos gasosos libertados durante a conversão térmica do eucalipto apresentaram forte correlação com a temperatura do reator, sendo CO_2 e CO sempre os principais produtos de desvolatilização. A dependência da temperatura de ambos os compostos apresentam, para o CO, um aumento de 8 a 13% entre 600 e 800°C, enquanto o de CO_2 aumenta apenas ligeiramente de 11 a 12%.

O modelo eXtended Discrete Element Method foi usado para descrever a desvolatilização no reator. Os resultados foram comparados com os dados experimentais e, embora tenha sido observada uma boa concordância, concluiu-se que a oxidação do resíduo carbonoso necessita de um modelo de difusão.

A simulação do escoamento no interior da caldeira foi feita utilizando o software ANSYS Fluent. Neste, um modelo empírico externo para prever a conversão de biomassa ao longo da grelha é acoplado a um modelo CFD para prever o escoamento reativo dentro da caldeira. Os resultados destacaram a contribuição da contração na seção intermédia da fornalha, e a necessidade de um maior caudal de ar secundário para reduzir as emissões de CO. Os resultados mostram que modificando a razão entre o ar primário e secundário de 79/21 para 40/60, obteve-se uma redução da fração mássica de CO de 0.009 para 0.0003.

Palavras-chave: Biomassa, Caldeira de grelha, CFD, Combustão, Modelação, Resíduos Florestais.

ABSTRACT

Integration of a Model for Volatile Release in the CFD Simulation of an Industrial Biomass Boiler

Motivated by their availability, widespread abundance, and environmental concerns, solid biomass has become a competitive option to diversify electricity production amongst the renewable energy resources. This work aims to characterize the combustion behavior of solid biomass species frequently used in power plants as a route to support the development of a numerical model for efficient and accurate modeling of biomass conversion in an industrial grate-fired boiler. The boiler efficiency of a power plant rated at 35 MWth was calculated as approximately 80%.

Selected samples of biomass (eucalyptus, pine, acacia, and olive) were tested with a Hot Disk Thermal Constants Analyzer TPS 2500S. The thermal conductivity, varied in the range of 0.239 to 0.404 W/mK. In addition, the heat capacity is within 0.855 to 2.442 MJ/m^3K, and the thermal diffusivity is between 0.187 and 0.258 mm^2/s. The ultimate and proximity analysis was carried out on the fuel samples using LECO TruSpec CHN Macro and LECO CS-200 equipment and a muffle furnace, respectively. The data revealed a higher reactivity of eucalyptus, which is around 2 times higher than that of other fuels, and the propensity of the acacia to produce pollutant emissions (mostly Nitrogen based) and ash deposition problems due to their chemical composition.

Small size samples (around 10 mg each) were used to measure the mass loss and their reactivity in a thermogravimetric analyzer (TGA) from TA Instruments, model SDT 2960. The tests were carried out on an oxidizing atmosphere at a heating rate between 5 and 100 °C/min up to 900 °C. It was observed that over a wide range of temperatures, fuel conversion follows a sequence of drying, devolatilization, and char combustion.

Larger samples of heartwood were tested in a purpose built reactor that simulates the devolatilization process under a controllable manner. In this, the mass loss was continuously measured along the time while the gas phase compounds were collected in bags for subsequent analysis in a gas chromatograph Bruker Scion 456-GC equipped with a thermal conductivity detector. As opposed to the TGA data, it was concluded that all fuels show that the combustion of large particles does not exhibit separate consecutive conversion stages, due to internal diffusion resistance. This was further highlighted by varying the sample aspect ratio. It was concluded that the devolatilization rate depends on the smallest dimension and not on the bulk size. Furthermore, at higher reactor temperatures, the mass loss profile is independent of the biomass. The gas compounds released with eucalyptus presented a strong correlation with the reactor temperature, being CO_2 and CO always the main devolatilization products. The temperature dependence of both compounds shows, for CO, an increase from 8 to 13% between 600 and 800 °C, while the CO_2 yield is only slightly increasing from 11 to 12%.

The eXtended Discrete Element Method model was implemented to describe the devolatilization inside the reactor. The results were compared with the experimental data and, while a good agreement was observed, it was concluded that the char oxidation needs to be also represented by a diffusion model.

The numerical model was developed using the ANSYS Fluent software. In this, a user defined empirical model to predict the biomass conversion along the grate was coupled with a freeboard model to predict reactive flow inside the boiler. The results highlighted the contribution of the converging sections in the middle section of the furnace and the need for a higher secondary air flow rate to reduce CO emissions. The results show that a reduction of the CO mass fraction from 0.009 to 0.0003 was possible with a modification of the primary to secondary air split ratio from 79/21 to 40/60.

Keywords: Biomass, CFD, Combustion, Forest residues, Grate-fired boiler, Modeling.

TABLE OF CONTENTS

LIST OF FIGURES

LIST OF TABLES

NOMENCLATURE

List of Symbols

Latin Symbols

A	Empirical constant equal to 0.6 or Pre-exponential factor (s^{-1}) or Area (m^2)
a	Gas mixture absorption coefficient (m^{-1}) or linearized coefficient of the algebraic equation (-)
B	Empirical constant equal to 0.5 or Burnout performance (-)
Bi	Biot number (-)
C	Comprehensive index (%/min^2T^3)
c	Heat capacity (J/kg.K)
$C_{i\varepsilon}$	Turbulence model constants (i = 1, 2, and 3)
c_p	Specific heat (J/kg.K)
D	Diameter (m)
Da	Damkohler number (-)
E	Total energy (J) or Activation energy (J/mol)
$\vec{F}$	External body force (N)
$\vec{g}$	Gravitational acceleration (m/s^2)
G_b	Generation of turbulence kinetic energy due to buoyancy (m^2/s^2)
G_k	Generation of turbulence kinetic energy due to the mean velocity gradients ($kg/m.s^3$)
H	Reaction enthalpy (J/kg)
h	Convective heat transfer coefficient ($W/m^2.K$), or Height (m)
h_j	Sensible enthalpy of species j

I	Ignition performance index (%/min^3) or Radiant intensity or Unit tensor (-)
$\vec{J}_i$	Diffusion flux of specie i (m^2/s)
$\vec{J}_j$	Diffusion flux of species j (m^2/s)
K	Permeability (m^2)
k	Turbulent kinetic energy (J/kg), or Rate constant (s^{-1}), or Thermal conductivity (W/m.K)
k_{eff}	Effective conductivity (W/m.K)
$k_{f,r}$	Forward rate constant for reaction (-)
m	Mass (kg)
$\dot{m}$	Mass flow rate (kg/s)
M_w	Molecular weight of the gas (kg/kmol)
$M_{w,i}$	Molecular weight of species i (kg/kmol)
$M_{w,j}$	Molecular weight of product j (kg/kmol)
$M_{w,\Re}$	Molecular weight of reactant $\Re$ (kg/kmol)
N_p	Number of products (-)
N_r	Number of reactants (-)
Nu	Nusselt number (-)
P	Power (W)
p	Static pressure (Pa)
p_{op}	Operating pressure (Pa)
Pr	Prandtl number (-)
$\dot{Q}$	Heat flux (W)
$\dot{q}$	Specific heat flux (W/m^2)

R	Universal gas constant (J/mol.K)
R_i	Net rate of production of specie i by chemical reaction (kg/m³.s)
$R_{i,r}$	Net rate of production of specie i due to reaction r (kg/m³.s)
Re	Reynolds number (-)
r	Radius (m)
$\vec{r}$	Position vector (m)
S	Deformation tensor
S_{Bi}	Rate of creation by addition from the biomass dispersed phase (kg/m³.s)
S_h	Energy source (from chemical reactions or radiation) (kg/m³.s)
S_i	Source term for the i (*x*, *y* or *z*) momentum equation (kg/m³.s)
S_m	Mass source from the biomass to the continuous phase (kg/m³.s)
Sc	Schmidt number (-)
Sh	Sherwood number (-)
s	Distance (m)
$\vec{s}$	Direction vector (m)
T	Temperature (K)
t	Time (s)
Th	Thiele number (-)
u_i	Velocity component for the i (*x*, *y* or *z*) direction (m/s)
V	Volatile matter release performance (%/T³) or Cell volume (m³)
$\vec{v}$	Velocity vector of the continuous phase (m/s)
$v'_{i,r}$	Stoichiometric coefficient for reactant i in reaction r (-)
$v'_{\Re,r}$	Stoichiometric coefficient for reactant $\Re$ (-)

$\nu''_{j,r}$	Stoichiometric coefficient for product j in reaction r (-)
Y_i	Local mass fraction of specie i (-)
Y_M	Contribution of the fluctuating dilatation incompressible turbulence to the overall dissipation rate
Y_P	Mass fraction of any product specie, P (-)
$Y_{\Re}$	Mass fraction of a particular reactant, $\Re$ (-)

Greek Symbols

α	Extent of reaction (-), or Thermal diffusivity (m^2/s), or Gas absorption coefficient
$f(\alpha)$	Reaction model (-)
$g(\alpha)$	Integral form of the reaction model (-)
β	Heating rate (K/min)
Γ	Diffusion coefficient (m^2/s)
ΔT	Difference of temperature (K)
ε	Turbulent dissipation rate (m^2/s^3) or Particle porosity (-) or Emissivity (-)
η	Constant of the Turbulence model (-)
κ	Absorption coefficient (m^{-1})
μ	Viscosity of the continuous phase (Pa.s)
μ_t	Turbulent (or eddy) viscosity (Pa.s)
ρ	Density of the continuous phase (kg/m^3)
σ	Stefan Boltzmann constant (W/m^2K^4)
σ_s	Scattering coefficient (m^{-1})
σ_ε	Turbulent Prandtl number for ε
σ_k	Turbulent Prandtl numbers for k

$\overline{\overline{\tau}}$	Stress tensor (N/m^2)
Φ	Phase function (-)
ϕ	Solution value (variable)
$\dot{\omega}$	Consumption or generation of the species (kg/m^3.s)
Ω	Solid angle (rad)

Subscripts

0	Initial
b	Burnout
cd	Conduction
cv	Convection
DP	Dew point
eff	Effective
$evap$	Evaporation
f	Final or Face
fg	Flue gas
g	Gas
i	Instantaneous
ig	Ignition
in	Initial decomposition
max	Peak
nb	Neighbor
op	Operational
P	Peak
p	Product or Particle

r	Reactant
rad	Radiation
ref	Reference
t	Time
vol	Volatiles

Superscripts

T	Temperature
$\eta'_{i,r}$	Rate exponent for reactant species j in the reaction r

List of Acronyms

ar	As received
AI	Alkali Index
AB	Acacia Branch
AT	Acacia Trunk
BFB	Bubbling Fluidized Bed
CFB	Circulating Fluidized Bed
CFD	Computational Fluid Dynamics
CLD	Chemiluminescence Detector
CPD	Chemical Percolation Devolatilization
CR	Coats-Redfern
CVR	Centro para a Valorização de Resíduos
DAEM	Discrete Activation Energy Model
db	Dry basis
DEM	Discrete Element Method
DGEG	Direção Geral de Energia e Geologia
DNS	Direct Numerical Simulation
DP	Dew Point
DPM	Discrete Particle Model
DOM	Discrete Ordinates Model
DTG	Derivative thermogravimetry
DTRM	Discrete Transfer Rate Model
DSC	Differential Scanning Calorimetry
EB	Eucalyptus Branch
EBA	Eucalyptus Bark

EBU	Eddy Break-up model
ED	Eddy Dissipation
EDC	Eddy Dissipation Concept
EDM	Eddy Dissipation Model
EDS	Energy Dispersive Spectrometer
ET	Eucalyptus Trunk
EU	European Union
EWT	Enhanced Wall Treatment
FC	Fixed Carbon
FCT	Fundação para a Ciência e Tecnologia
FG-DVC	Functional Group Depolymerization Vaporization Crosslinking
FGR	Flue Gas Recirculation
FGT	Flu Gas Temperature
FI	Fouling Index
FID	Flame Ionization Detector
FLIC	FLuid dynamic Incinerator Code
FR	Finite Rate
FTIR	Fourier-transform infrared spectroscopy
GC	Gas Chromatography
GHG	Greenhouse Gas Emissions
HHV	Higher Heating Value
ICNF	Instituto da Conservação da Natureza e das Florestas
ICTAC	International Confederation for Thermal Analysis and Calorimetry
IRENA	International Renewable Energy Agency
KAS	Kissinger-Akahira-Sunose linear integral method

LHV	Lower Heating Value
LTI	Leaders for Technical Industries
MIT	Massachusetts Institute of Technology
MS	Mass Spectrometry
MSW	Municipal Solid Wastes
NA	Not available
NDIR	Nondispersive Infrared Analysis
OB	Olive Branch
OFA	Over Fire Air
OFW	Ozawa-Flynn-Wall linear integral method
PA	Primary Air
PB	Pine Branch
PISO	Pressure-Implicit with Splitting of Operators
PNEC	Plano Nacional Energia e Clima
PT	Pine Trunk
RANS	Reynolds-Averaged Navier-Stokes
$R_{b/a}$	Ratio Base/Acid
RE	Renewable Energy
RDF	Refuse Derived Fuel
RNC	Roteiro para a Neutralidade Carbónica
RNG	Re-Normalization Group
RTE	Radiative Transfer Equation
SA	Secondary Air
SI	Slag Viscosity Index
SIMPLE	Semi-Implicit Method for Pressure-Linked Equations

SST	Shear Stress Transport
SEM	Scanning Electron Microscope
SWT	Standard Wall Treatment
TA	Thermogravimetric Analyzers and Total Alkalis
TCD	Thermal Conductivity Detectors
TG	Thermogravimetry
TGA	Thermogravimetric Analysis
TPS	Thermal Plane Source
UDFs	User-Defined Functions
VM	Volatile Matter
WSGGM	Weight-Sum-of-Gray-Gases Model
XDEM	eXtended Discrete Element Model
XRD	X-ray Diffraction
XRF	X-ray Fluorescence Spectroscopy
2D	2-Dimensional
3D	3-Dimensional

CHAPTER 1

INTRODUCTION

Currently, the energy sector is facing a strong regulatory pressure, higher competition, and a demand to provide greater flexibility and environmentally friendly solutions. Due to this, at this time, it is necessary to respond effectively, and rapidly, to the fast-changing context of the electricity market. The energy transition is in fact on top of the agenda, and computer-aided methods from the field of Computational Fluid Dynamics (CFD) have been, in part, one of the cornerstones enabling such a paradigm shift. Concerning electricity production using biomass, grate firing is currently the most common technology, as well as for the incineration of household residual wastes and household-type commercial wastes. Thus, CFD is increasingly being used in its development and design. The development and application of CFD for further optimization of grate firing systems is the subject of this work.

1.1 Contextualization and Motivation

The energy demand has increased over the years due to population growth, and industrial and socio-economic developments, cornerstones of human civilization. As fossil fuels have been the cornerstone of energy supply worldwide, they are linked with climate change and global warming. Besides the protection of the environment, the depletion of fossil fuels resources is an important aspect that needs to be overcome. Consequently, using alternative energy sources to reduce environmental problems and limited reservoirs is a primary concern nowadays.

The European Union (EU) aims to be climate-neutral by 2050 with an economy with net zero Green House Gas (GHG) emissions [1]. To achieve this objective, which is the essence of the European Green Deal ambitions and in line with the Paris Agreement, Europe needs to deploy a wide range of low carbon technologies and solutions in the different sectors of the economy in order to reduce the global temperature rise below 2 °C, considering the pre-industrial levels [2]. The EU has been progressively reducing GHG with the targets defined for climate and energy to 2020 and the new targets defined for 2030. In this latest iteration at least 55% reduction in GHG emissions, compared to 1990 levels, and at least 32% share for renewable energy and improvement in energy efficiency are expected [3]. Regarding the total GHG emissions, the energy sector is responsible for 78% of the EU's emissions, where transport and heat and electricity production are the major contributors (46%) [4]. Despite these initiatives and considering the most recent data on the renewable energy sector contribution in the European Union in gross final consumption in 2020, your share is already 2% above the target for this year (20%) [5]. Portugal ranked fifth among the 27 Member States, with a share of 34%.

As an alternative clean energy source, biomass appears a very interesting option as it is considered a sustainable, renewable, and CO_2 neutral energy source [6], even though this has been seriously debated recently [7–11]. Furthermore, its abundance and availability not depending on weather conditions make this resource an attractive and valuable alternative for energy supply in both domestic and industrial sectors. The utilization of biomass in the industrial sector has been a strong incentive as it allows the reduction of the amount of fuel in woodlands and lowers the risk of forest fires which brings extra benefits to society, the environment, and the economy [12,13]. These are essential aspects mentioned in a particular recent bibliometric analysis from 1998 to 2017 performed by Mao et al. [14]. In this recent survey, it was found that energy production and consumption and a sustainable energy system that can effectively promote the development of the national economy and strengthen the protection of the environment can be achieved using biomass. Banja et al. [15] noted that biomass is the main contributor

to EU renewable energy markets and, due to the lower carbon footprint, has a significant contribution to a low carbon economy which results in a key role within the EU policy in the support for renewable energy sources. Furthermore, the International Energy Agency Roadmap - Net Zero Emissions by 2050 - identifies bioenergy as an important source of energy, representing 18% of the total energy supply in 2050, and playing a key role in the transition toward a carbon-neutral society [16]. This number considers either through the direct replacement of fossil fuels or to counterbalance emissions indirectly through the combined use of bioenergy with carbon capture and storage. In 2019, the replacement of fossil fuels by biomass avoided 290 $MtCO_2eq$ emissions, equivalent to approximately 8% of the EU27 GHG emissions [17].

Portugal recently faced the urgent need to prevent wildfires and the Portuguese government introduced a scheme to support biomass energy installations and coerce the forest owners to clean their properties and use the forest residues to produce biomass energy [18]. There are already some municipal areas implementing a system for local harvesting and storage of biomass, which can be further used for energy valorization. This strategy involved the concession of an additional 60 MWe for residual forest biomass power plants. Since 2017, when devastating wildfires reached the central and northern regions of Portugal, new dedicated biomass power plants were built with a total capacity of around 100 MW and there are currently more than 20 solid biomass power plants delivering over 600 MW to the national power grid. The main owners that contribute to this installed power are the pulp and paper companies (Altri and The Navigator).

In 2020, according to the last data published by the Portuguese *Direção Geral de Energia e Geologia* (DGEG) [19,20], the contribution of biomass to renewable energy production was approximately 50%. However, although 64% of biomass has been converted into other forms of energy, specifically in dedicated thermal power plants and cogeneration plants, only about 10% of solid biomass energy contributes to the total renewable electricity production. In addition, despite the decrease in energy consumption in 2020 due to the COVID-19 pandemic, there was an increase in the consumption of primary energy in biomass in 2020, which is fundamentally due to a rise in biomass use for the production of electricity (+11%). This fact reveals the increased importance of the use of biomass in the national energy mix. Figure 1 presents the evolution of electricity production and power from biomass power plants in Portugal from 2000 to 2021. In 2000, the electricity production was marginal, only 1,037 GWh and, after 20 years, the production is 3,243 GWh. During this period, there was a significant increase of approximately 215 times of electricity production from dedicated biomass power plants. This evolution was made in different ways along this period, starting slowly until 2007 and faster until 2012. This rapid

increase was mainly due to 9 new dedicated biomass power plants that started operation with more 90 MW (see Figure 1 b)). Between 2012 and 2017 the production stabilized, reaching 2,574 GWh.

More recently, from 2017 to 2021, the electricity production from biomass, mainly from forest biomass, increased again due to the Portuguese government incentives above mentioned. Currently, in Portugal, the total installed solid biomass capacity is approximately 5% of the total renewable power.

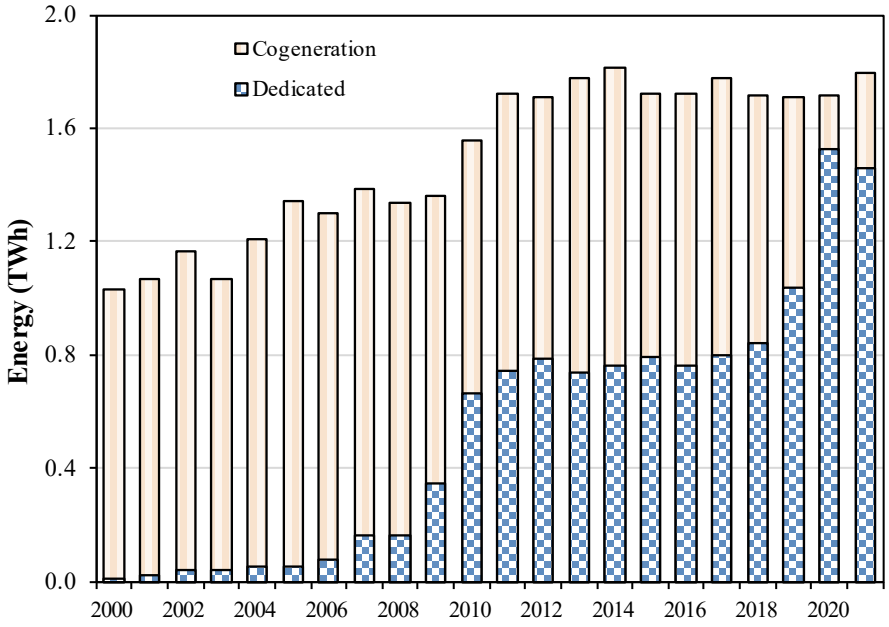

a)

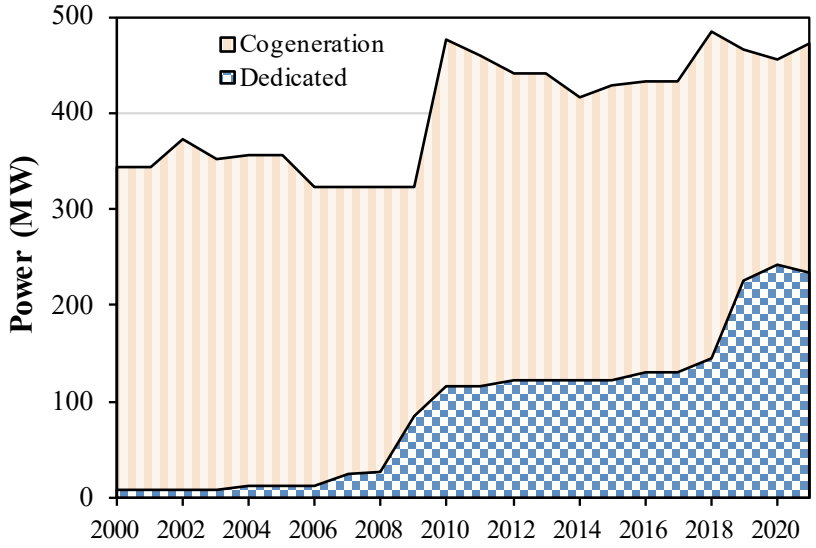

b)

Figure 1: Biomass power plants (dedicated and co-generation) evolution in Portugal from 2000 to 2021: a) Annual production of electricity and b) Installed power. Data source: DGEG [20].

It is important to point out that in Portugal, approximately 6.2 million hectares of land are covered by forestry areas (36.19% of the national territory), making Portugal a country with great potential for the exploitation of forest biomass [21]. Viana et al. [22] estimated that in Portugal the total amount of available biomass averages around 1.097 million dry tons/year, with 579.91 thousand dry tons/year from maritime pine and 517.23 thousand dry tons/year from eucalyptus resulting from forest logging. Figure 2 a) presents an overview of the distribution of land use, and Figure 2 b) the occupation of the different species in the Portuguese forest in 2015 [21]. Regarding the occupation of the forest area by the different species, eucalyptus is in fact the most common species in Portugal. The interest in this material in the paper and pulp industry, along with its invasive character and fast growth, explains the interest in this fuel.

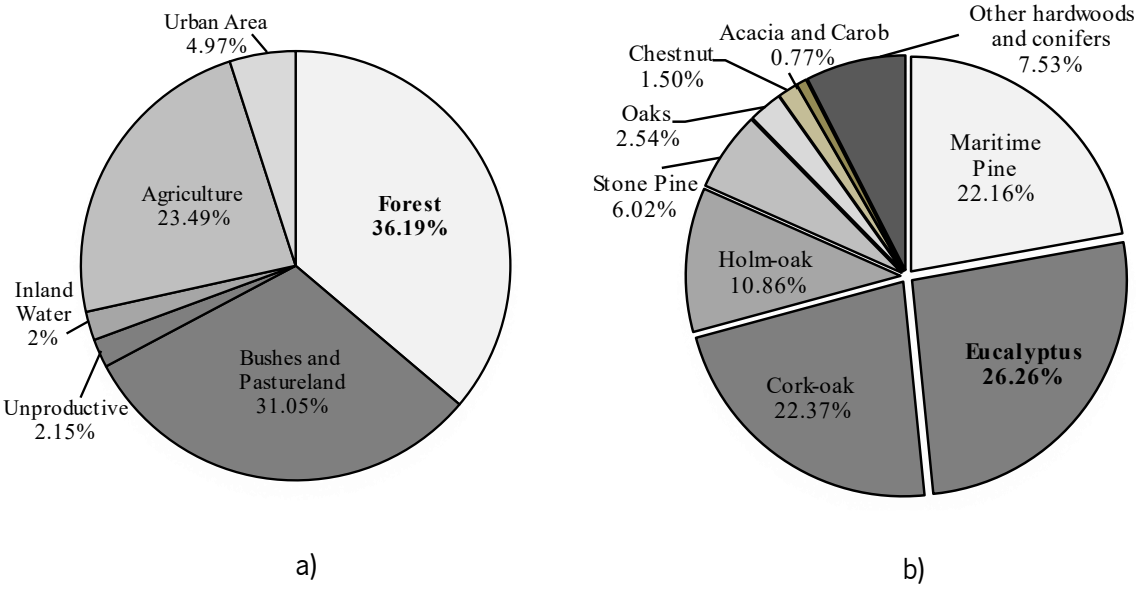

Figure 2: Portuguese mainland: a) distribution of land use and b) percentage of forest area by species. Data source: ICNF [21].

Regarding the European context, Figure 3 presents the status of the biomass energy sector. In 2020, the different EU countries presented different contributions of biomass energy in the renewable energy mix. The total biomass installed capacity in 2020 in the EU-27 Member States amounts to 15,560 MW, and the electricity generated was approximately 82.953 TWh [23]. According to the latest data from 2020, the three EU-27 countries with the largest amounts of installed biomass capacity are Sweden (2,942 MW), Finland (2,442 MW), and Germany (1,597 MW). The share of the national renewable electricity generation in different EU countries varies greatly from almost 66% (Estonia) to 0 (Cyprus and Malta).

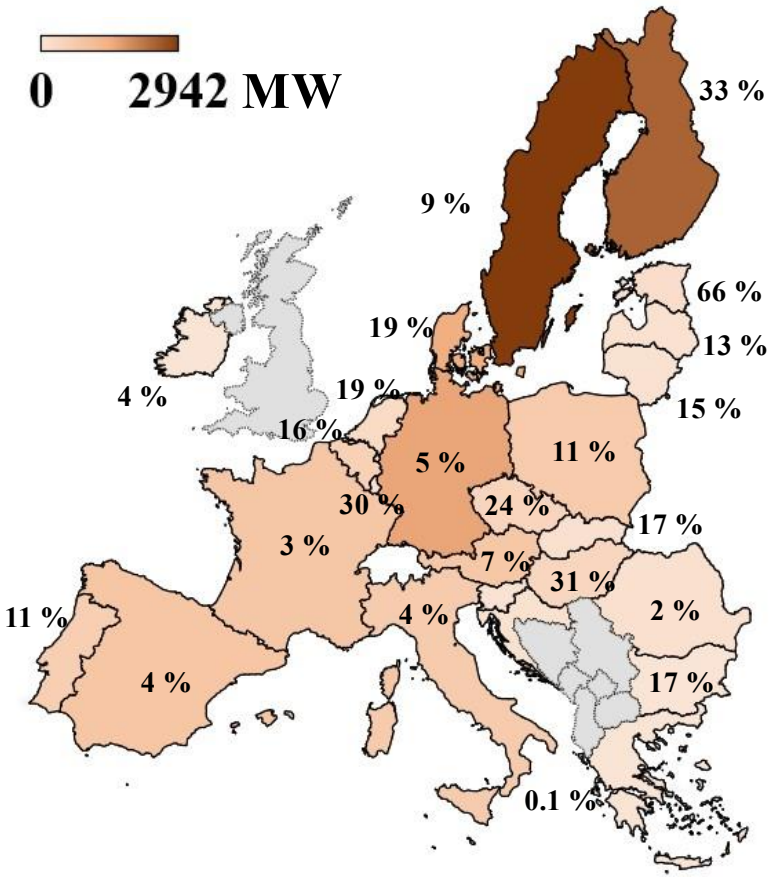

Figure 3: Overview of the solid biomass contribution in terms of biomass capacity (power) in the EU-27 Member States in 2020 including the share in renewable electricity generation (%). Data source: Eurostat [23].

Furthermore, there are countries like the United States of America, India, Brazil, and China where solid biomass energy has a major role in renewable energy production. The last two counties are becoming progressively important producers, benefiting from national support programs for biomass electricity generation [12,24]. In its turn, India was the country where the installed solid biomass power increased more, around 27 times from 2000 to 2019 [25]. At the same time, in the United States of America, no significant investments in this sector have been identified except for the conversion of 545 MW from coal plants to biomass [12]. Table 1 summarizes the solid biomass contribution to the renewable electricity production of these main countries and its installed power. The contribution in Europe as well in the World is also provided.

Table 1: Overview of the solid biomass contribution worldwide in 2019. Data source: IRENA [25].

	USA	Brazil	China	India	Europe	World
Installed Power (MW)	9,841	14,981	15,738	10,212	25,501	102,055
Share in RE (%)	6.54	10.40	3.95	7.37	11.74	6.57

After the first ambitious climate and energy targets of the EU in 2007 (Directive 2009/28/EC), recent climate targets for 2020, 2030, and 2050 have been set to progressively reduce gas emissions up to 80% by increasing the share of renewable energy in the energy mix [26]. Taking into account this policy, the Portuguese Government in a recent report that defines the climate and energy strategy between 2020 and 2030 states that only small co-generation biomass plants (up to 15 MW [27]) will be promoted. Furthermore, the evolution of dedicated biomass power plants capacity (including biogas and urban solid wastes) is expected to be 500 MW in 2030 (currently there is 407 MW) [28]. Furthermore, the strategy of carbon neutrality only predicts an increase in the installed capacity of biomass (including biogas, urban solid wastes, and co-generation plants) up to 1.8 GW in 2050 [29]. At this time there are already 891 MW and, therefore, significant developments in this sector are expected [30]. The reason to disregard projects of new dedicated biomass power plants could be due to its quite low efficiency.

The low efficiency is related to the complexity of the biomass combustion process, its instability, and due to non-utilization of the available thermal energy for other purposes. Biomass combustion involves simultaneous multiphase fluid flow, chemical reactions, heat (convection and radiation), and mass transfer [31]. Due to this complex and irregular process, there are various operational problems inside an industrial boiler. Besides, the pollutant emission limit is often exceeded. Figure 4 presents the combustion process inside a grate-fired boiler, the main technology that is currently used for heat and power generation from biomass combustion [32].

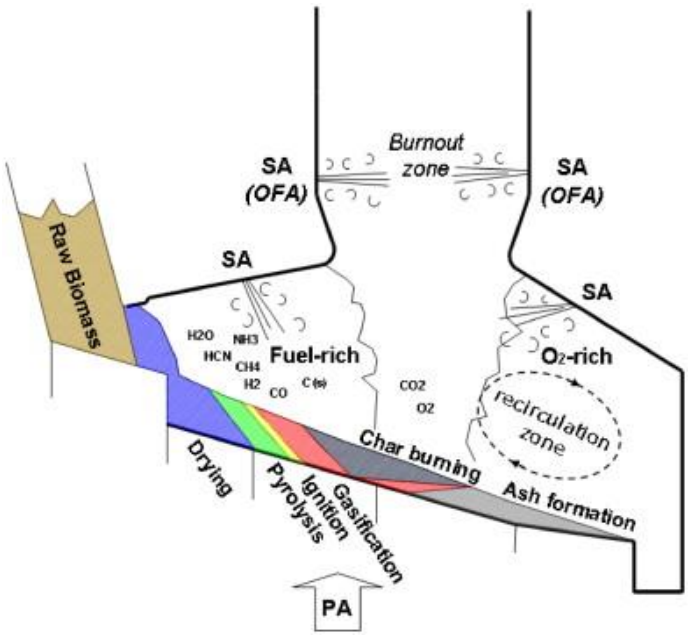

Figure 4: Representation of the different reaction zones in a grate-fired boiler burning biomass. PA: primary air; SA: secondary air; OFA: over fire air. Adapted from Yin et al. [32].

The fuel enters from the left side typically fed in by a traveling grate. Then, the moist fuel falls to the grate, where it is moved to the right by grate movements. The fuel undergoes a thermal conversion process initiated by a drying process and followed by devolatilization and char burning.

In this regard, in order to give scientific explanations to this identified phenomenon, CFD modeling is a powerful tool for predicting flow and biomass conversion, being possible to anticipate problems that can occur during the combustion phase. The comprehension of the processes in the bed area is rather limited, as it is difficult to obtain information through measurements because of the limited physical and optical accessibility inside a grate-fired boiler. Therefore, CFD modeling of the entire process inside a boiler is a promising alternative to meet economic and environmental demands on the operation of grate furnaces allowing a better understanding of the combustion process.

1.2 Objectives

This project aims to understand and predict the biomass combustion inside an industrial grate-fired boiler. In a power plant that uses biomass as fuel, it is important to control the efficiency of the combustion process since the combustion process is very unstable. The general purpose of this work is to develop a numerical model to simulate the biomass combustion behavior in industrial boilers that use forest residues as fuel. To achieve this general purpose two specific objectives were defined:

1) Characterization of the combustion behavior of the main forest residues used in the thermal power plants of Portugal. The kinetic parameters (activation energy, and pre-exponential factor) will be determined as they are necessary to calculate the reaction rates that occur during the conversion of the biomass particles.

2) Development of a numerical model for the combustion of biomass particles on the grate considering the experimental results. This numerical model will be integrated with a CFD model that could be used to optimize the combustion in industrial boilers using forest residues.

Following the contextualization, the research opportunity previously detailed, and the main specific objectives, the research question of this project can be formulated as follows:

"How is it possible to model, in a realistic way, the biomass combustion in an industrial boiler?"

In order to answer effectively to this issue, it is necessary to break down the problem and define which steps should be followed. For this, auxiliary questions are defined that lead to the answer to the research question formulated. These are:

- How can biomass combustion analysis be carried out efficiently and realistically in an industrial boiler?
- Which methodologies currently exist to predict biomass combustion?
- How to properly define biomass combustion inside an industrial boiler?
- What is the combustion behavior of the different main forest residues?
- What are the main difficulties in solving the solid phase conversion problem and its combination with the gas phase?
- What technologies/models currently exist to solve the proposed problem?

The combination of the answers to each question presented here leads to a response to the research question, which is more comprehensive, and its solution does not correspond to a simple exercise. With this deconstruction of the research question, the researcher can more easily understand if the topic proposed contains the necessary attributes.

1.3 Research Methodology

This project intends to be an added value not just for the power industry but also for the academic community. In this way, to develop an outstanding research project, it is essential to develop the design research that is a general plan that ensures to answer the research question. Figure 5 presents an overview of the methodological approach framed under the MIT Portugal PhD Program in Leaders for Technical Industries (LTI).

Throughout the last years, the MIT Portugal Program has supported new mechanisms to drive innovative research and foster academic-industry collaboration at an international and national level. Most of the knowledge leaves the University for different contexts but, there is also the knowledge that is provided by the outside and that is not learned at the University. This ultimately results in knowledge-based manufacturing and competitive product design, delivering high-level research in engineering systems with an emphasis on the promotion of interactive collaboration with industry.

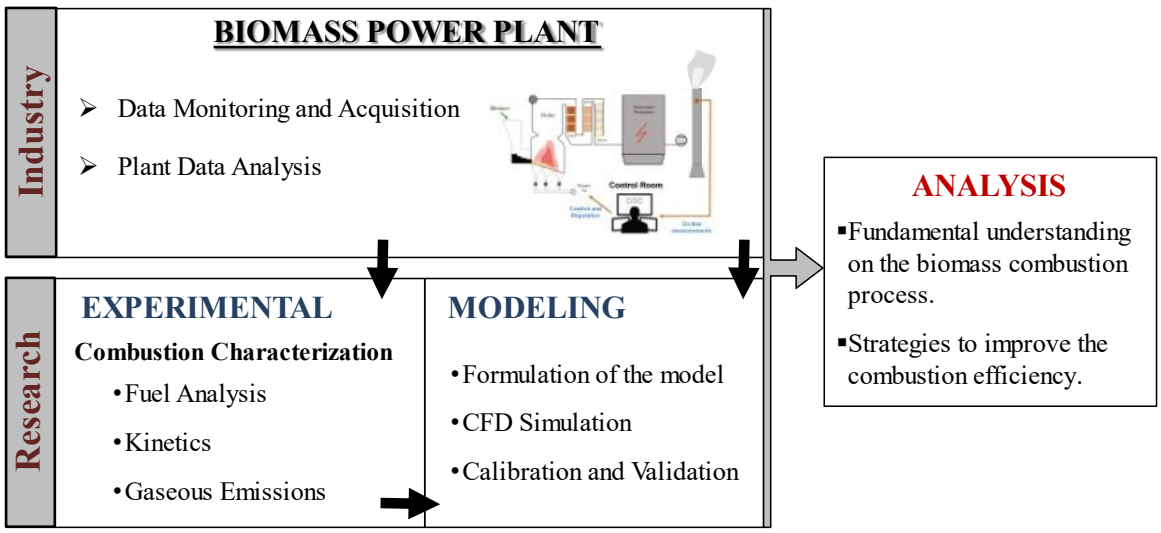

Figure 5: Overview of the methodological research approach to be used in this work.

This is a research-based doctoral program, aimed to explore solutions for complex industrial problems through problem-oriented and project-based activities, and it is strongly anchored in an engineering system approach that couples education and research. In that sense, the LTI will provide the knowledge and methods necessary to combine the research and advanced processes, in order to obtain results worthy to be implemented in technologically advanced industries like the power plant in Mortágua.

The research design reflects the organization of all the ideas and thoughts related to the project and presents all the research decisions. In order to answer the research questions, the investigation will follow two essential methodologies, experimentation, and numerical modeling coupled with field research in a biomass power plant. These methodologies are complementary, and the main results of the experimentation will be used in the numerical model which, in its turn, is developed considering the knowledge obtained in the industry and the limitations in the numerical modeling. Furthermore, this methodology is oriented to provide the answer to the main research question: "How is it possible to model, in a realistic way, the biomass combustion in an industrial boiler?" To achieve the answer to this question, the eXtended Discrete Element Method (XDEM), a code developed at the University of Luxembourg, is used together with the parameters determined by the experimentation work to first address the conversion of particles in similar conditions to the environment inside industrial power plants. Then, a CFD model, based on the conditions provided by an empirical bed conversion model, of the industrial boiler of Mortágua Power Plant is developed to predict the gas flow and combustion. Then, after a previous calibration and validation of the numerical model with data collected in the boiler, parametric

studies to investigate the influence of some relevant parameters in the combustion process are performed in order to understand how it is possible to improve the combustion efficiency.

The project aims to eliminate the industrial paradigms around the energy conversion by combustion of biomass, giving scientific explanations to the phenomena identified in the process, being possible to anticipate errors and defects that can occur during the combustion inside an industrial boiler. Through the combination between experimental research and numerical simulation tools, one is expected to reduce pollutant emissions and costs, leading to the improvement of the process that is used in biomass power plants.

1.4 Contributions of this Work

The application of computer simulation approaches to the design and improvement of combustion systems has grown during the past two decades. The market competitiveness highly demands the optimization of processes and products in order to minimize the invested resources, time, financial or human. This philosophy comprises a broad range of areas, particularly in the power energy field, where CFD plays a crucial role in the development of new technologies and products.

This PhD work provides a comprehensive methodology, from experimentation and numerical modeling to field research in a power plant, to model the biomass combustion in the context of the grate-fired boilers simulation. Consequently, several aspects relevant to biomass combustion modeling in an industrial boiler are investigated, namely its composition, thermophysical properties, combustion behavior of small particles, the kinetics of the reaction, and gaseous emissions which their knowledge are fundamental to the accuracy, reliability, and efficiency of the model. In this way, this study helps to understand and develop knowledge underlying biomass combustion and its implementation in a vibrating grate-fired boiler by providing a numerical model calibrated using the experimental and operational experience.

Although some investigations have been published in this area, it is observed a need for studies in biomass combustion involving thermal conversion analysis, kinetics, and gaseous emissions. Until now, few works have been succeeded in analyzing these three issues from micro to macro scales. In that sense, this work addresses the biomass conversion process on the grate of industrial boilers with the main objective to properly represent the biomass decomposition and release of volatiles. To fulfill, with success, this requirement, a one-step scheme for the devolatilization with kinetic data obtained from a

traditional thermogravimetric analysis (TGA) is proposed, and the volatiles released are investigated using a purpose-built small-scale reactor.

This is an ambitious project, framed under the MIT Portugal PhD Program, that, even though it will focus on a specific industry, it is also expected to provide relevant answers for other applications that use biomass as fuel to produce energy. In that sense, the knowledge obtained with the numerical tool developed in this project will be implemented in technically advanced industries like the power plant in Mortágua (Portugal). Apart from the contribution to the enhancement of scientific knowledge, the result of the application of this tool enables to reveal comprehensively the fundamental phenomena occurring inside an industrial grate-fired boiler, the reduction of pollutant emissions, and the improvement of the combustion efficiency.

1.5 Thesis Outline

This PhD thesis aims to present the framework for the development of a computational tool for trustworthy simulation of biomass combustion in industrial grate-fired boilers, in which the main focus relies on fuel conversion. To achieve this aim, this Thesis was divided into ten chapters.

Chapter 1 presents the contextualization of this work within the current challenges of biomass combustion in industrial grate-fired boilers to produce energy. The main motivation and contributions of this PhD work are also addressed. The research questions and the objectives of this investigation are established as well as the context of this proposal from the LTI perspective is explained. To fulfill the objectives proposed in this thesis plan, the research design and methodology are detailed.

Chapter 2 summarizes a literature review on the research subject, and also the most important issues related to the biomass combustion modeling in industrial grate-fired boilers. Firstly, biomass as a fuel is introduced, exploring its physicochemical properties, the conversion process, and its characterization. Then, an analysis of the existing CFD modeling methodologies is presented and discussed. In addition to the different modeling approaches, the different mathematical models used to model the different phenomena occurring inside the combustion system are described. This literature review establishes the comprehensiveness and significance and credibility of this research work.

In Chapter 3, the object of study, the biomass power plant of Mortágua, and the main results obtained from an experimental campaign to evaluate the combustion performance are presented. Initially, the power production process at the power plant is described, compromising mainly details of the fuel and

the conversion process. Regarding the experimental campaign, an investigation through an analysis of the historical and monitored data, and a set of experiments to study the influence of some key parameters are presented. Furthermore, the study of the possibility to reduce the flue gas temperature, as a measure to increase the efficiency, is analyzed.

Chapter 4 introduces the research methods used to perform the experimental work involved in this thesis. The main forest residues that are being used as fuel in biomass power plants are presented and, the preparation procedures for the experiments using the thermogravimetric and macro thermogravimetric reactors are presented. Detailed features, as well as the operation procedure of both equipment, are described.

Chapter 5 is devoted to the numerical methodology implemented to develop two numerical models. The first one represents the conversion of the biomass particles in the setup designed for macro thermogravimetric experiments, and the second one is the grate-fired boiler from the Mortágua Power Plant. The main theory and methodology behind the numerical model are described, from the governing equations to the gas-phase models applied to describe the fluid flow and chemical reactions. All the details regarding the numerical domain, boundary conditions, mesh, and solver configuration are presented in this chapter.

The next four chapters are dedicated to the presentation of the experimental and numerical results. Chapter 6 presents an assessment of the physicochemical properties of the fuels selected for this work. Each fuel is fully characterized in terms of chemical composition by proximate and ultimate analysis and its calorific value. Furthermore, this chapter examines the variation in terms of the thermal properties (thermal conductivity, thermal diffusivity, and heat capacity) and ash elements of the different types of biomass fuel.

In Chapter 7, a comprehensive analysis of the thermal decomposition behavior of different forest biomass samples using a thermal analysis technique. This technique is extremely useful and essential to study combustion behavior under controlled conditions. Posteriorly, an analysis of the reaction kinetics using different mathematical models is presented in order to further propose a mathematical model to describe the main reactions during the combustion process.

In Chapter 8, and in contrast to those presented in the previous chapter, the results of the experiments in a purpose-built small-scale reactor using larger particles are presented. These experiments are complementary since the transport phenomena have an influence on heat and mass transfer, and the gas emissions during the devolatilization are collected. Consequently, the thermal decomposition behavior

and gas emissions are evaluated using different reactor temperatures. This chapter is further complemented with the comparison between the experimental results and the predictions obtained from the mathematical model presented in Chapter 5 to compute the mass loss of biomass particles.

Chapter 9 focuses on the presentation and discussion of the numerical results obtained through the CFD simulations. The knowledge acquired by the experimental work performed in this research (Chapters 6, 7, and 8) is used to recognize fundamental aspects for obtaining an appropriate grate conversion of the biomass and this information is used to define the baseline case considering the nominal operating conditions of the Mortágua power plant. This model provides the basis for parametric studies that are also presented to investigate the influence of the combustion air system and the temperature of primary air.

Finally, Chapter 10 presents the most significant conclusions of the present work. A suggestion of selected research lines for future investigation on the main subject of biomass combustion, and CFD simulation, are also presented.

CHAPTER 2

BACKGROUND AND LITERATURE REVIEW

To understand the phenomena concerned in this work, it is necessary not only to understand the biomass combustion process but also to understand specifically what CFD is, and how it can be applied to study and to predict the biomass combustion process inside an industrial grate-fired boiler. The following sections present an overview of the existing literature on several topics related to the biomass combustion process, its characterization, as well as the strategies to develop a CFD model to predict the biomass combustion process inside an industrial scale boiler. Since the focus of this work is the development of a numerical model, a summary and identification of the different model assumptions and problems involved in particles/bed modeling are presented. This literature review establishes the significance and credibility of the research work, providing an overview of the main theories with a critique comment on their validity. Furthermore, the main contributions of the present work to the literature are highlighted.

2.1 Biomass as Fuel

Biomass is generally defined as any type of organic substance whose origin is due to a biological process. According to Directive 2009/28/EC of the European Parliament of 23 April 2009, on the promotion of the use of energy from renewable sources [33], biomass is defined as *"the biodegradable fraction of products, waste, and waste of biological origin from agricultural activities (including substances of plant and animal origin), forestry and related industries, including fishing and aquaculture, as well as the biodegradable fraction of industrial and municipal waste".* As it can be seen, biomass is included within the Directives for the promotion of the use of renewable energies. The reason is the closed carbon cycle where biomass is inserted, i.e., despite the emission of pollutant gases to the atmosphere during the conversion of biomass, the carbon content of these emissions has been previously removed from the same atmosphere by the photosynthesis process while the tree/plant grows, hence net carbon emissions are considered zero [34,35].

Thus, there are several types of biomass fuels available ranging from woody to municipal wastes materials. Due to this variability, biomass fuels can be classified into three categories depending on their origin [36]. The first one, primary residues, includes biomass fuels obtained from by-products of forest materials and food crops such as wood, straw, and cereals. The second one, secondary residues, are derived from processing materials for industrial and food production, including for instance paper mills, food and beverage industries, and apricot seed. Finally, in the third category, there are tertiary residues which include waste and demolition wood derived from other used biomass materials. Furthermore, from another point of view, biomass fuels can be classified into five categories based on the knowledge of their properties: woody biomass, herbaceous and agricultural biomass, aquatic biomass, animal and human wastes, and contaminated and industrial biomass wastes [37].

This makes for a significant variability in terms of properties. Considering the main product of biomass in this work (power/heat generation), and that amongst the different options for energy conversion, the most usual, and also inexpensive, combustion, requires a thorough understanding of the fuel properties (physical, chemical, and thermal) [38]. The composition of biomass is usually obtained by proximate, ultimate, and structural analysis techniques. The first two analyses are fundamental to determine the chemical properties for combustion. It is particularly important because the composition of biomass is considered a unique fundamental information that characterizes and determines its properties, quality, potential applications, and environmental problems [37]. Regarding the physical properties, values may vary significantly and there are properties that depend on the fuel preparation methods, such as particle

size, shape, and bulk density, and other properties that are intrinsically dependent on the biomass fuel (density and porosity) [39]. In its turn, thermal properties have an important role to play the biomass thermal degradation. This group of fuel properties includes heat capacity, thermal conductivity, and emissivity. These properties are dependent on the temperature, moisture content, and the degree of thermal degradation of biomass [40]. Moisture, volatiles, char, and ash are products of the thermal degradation of biomass, and as its formation and/or consumption vary with time, this conversion process will define the thermal properties.

One of the most important deciding factors is the moisture content of the fuel since it provides information concerning the applicability in a combustion process and its storability [41]. The moisture content of biomass fuels can reach 60% (wet basis), which is a major disadvantage compared with other solid fuels like peat and coal which have a more narrow range, close to 20% [42]. Although difficulties in the preparation and grinding of the biomass are associated with high moisture contents, the major problem is related to the decreasing of the heating value, a critical property of biomass fuels, which is frequently expressed either as a Higher Heating Value (HHV) or Lower Heating Value (LHV). The difference between LHV and HHV is related to the contribution or not of the heat of evaporation of the water from the moisture and hydrogen from the fuel. Because of the low heating values, biomass is accompanied by poor ignition, flame stability problems, lower combustion temperature, delayed release of volatiles, and, consequently, longer residence time in combustion units, and therefore, reduced combustion efficiency [42]. This is why Jenkins et al. [43] state that for most biomass fuels the autothermal limit is around 65% (wet basis) which means that above this value, insufficient energy is released during the combustion to fulfill the energy necessary for heating and evaporation. To overcome this problem, it is recommended the installation of a storage facility next to the place where biomass is converted [6].

The volatile matter content is the part of the fuel that is released as combustible gases due to heating. Various hydrocarbons, hydrogen, oxygen, carbon monoxide, and carbon dioxide are the main composition of the volatile gas [44]. The amount of volatile matter released is strongly dependent on the material and the conversion conditions (temperature and heating rate) [45–47]. Vassilev et al. [37] analyzed the chemical composition of 86 varieties of biomass and, typically, the volatile fraction varies between 48 to 86% (dry basis), which is significative higher than peat and coal (12-68%).

After the volatile release, the remaining part of the fuel is the fixed carbon, and after the fuel is completely burned, ash is the remaining inorganic residue. Generally, biomass has a ratio of volatile matter to fixed carbon (VM/FC) higher than 4 while, for instance, coal is always lower than 1. Consequently, when

biomass facilities are designed, it is required a higher volume to achieve complete combustion [42]. Furthermore, during the design phase, the knowledge about the ash composition, mainly information about the ash forming elements, is important since phenomena like fouling, slagging and deposits are related to the ash composition [6,48]. Some elements and their compounds, like potassium, sodium, sulfur, and chlorine need attention due to their association with corrosion problems in biomass combustion devices [48].

In addition to these minor elements, the principal component of biomass is carbon, oxygen, and hydrogen, in decreasing order of abundance. Comparing the variation of these three elements in biomass fuels with their content in peat and coal, the carbon and hydrogen content are approximately in the same range, although biomass fuels have a wider range with a lowest lower limit, while the oxygen content is higher. This means that biomass fuels have a higher thermal reactivity [49]. Nitrogen and sulfur might also be found in biomass fuels, but in small quantities, usually around 1% or lower. Nonetheless, these elements are of special relevance concerning NOx and SOx emissions [41]. Therefore, in general, biomass fuels when compared with coal have a lower bulk density, higher volatile content, lower calorific value, and higher moisture content. Furthermore, its chemical composition is more variable [6]. Table 2 presents the results of proximate and ultimate analyses of some of the most relevant solid fuels used for heat and power generation, from a large database on the properties of conventional fuels. The values are on a dry basis to avoid large variations due to the different moisture content of the fuels.

Table 2: Typical proximate and ultimate analyses (wt%, dry basis) and higher heating values (MJ/kg, dry basis) for different biomass types. Source: Phyllis2 database [50].

	Eucalyptus	Bagasse	Wheat straw	Forest residues	RDF	MSW	Peat	Coal
Proximate Analysis								
Carbon	48.80	45.90	43.92	50.31	40.75	49.23	53.30	63.54
Oxygen*	44.41	42.91	44.36	39.95	38.59	23.73	33.15	28.95
Nitrogen	0.17	1.73	0.80	1.03	0.28	1.82	1.43	0.70
Hydrogen	6.00	5.68	6.07	4.59	7.57	8.15	5.60	4.52
Sulfur	0.02	-	0.25	0.11	0.53	0.25	0.16	0.31
Ultimate Analysis								
Volatile matter	86.00	84.22	73.40	82.41	76.00	72.60	68.10	49.20
Fixed Carbon	13.20	12.00	17.65	13.62	12.25	10.58	25.60	46.97
Ash Content	0.80	3.78	8.95	3.97	11.75	16.82	6.30	3.83
VM/FC	6.52	7.02	4.16	6.05	6.20	6.86	2.66	1.05
Heating Value								
HHV	19.62	18.23	17.65	20.17	20.22	20.48	21.22	24.63
LHV	18.31	16.99	16.45	19.16	18.57	18.70	20.00	23.64

MSW – Municipal Solid Wastes RDF – Refuse-Derived Fuel

As referred before biomass includes a wide range of materials, but only a few types are appropriated for use in heat and power production. In this work, the term biomass is used to refer to biomass that comes from the forest.

2.2 Biomass Combustion for Power Generation

2.2.1 Combustion Phenomenon at the Particle Scale

Nowadays, the oldest and most mature technology for the production of heat and power, and the main source for providing renewable heat is solid biomass combustion. The applications of biomass combustion involve a wide range from domestic equipment with dozens of kW to district heating, dedicated, or combined heat and power plants up to hundreds of MW of installed capacity.

Biomass combustion involves several decomposition reactions that present an important role in overall performance in grate-fired boilers, and also in domestic boilers, like for instance: pollutant emissions, unburnt formation, and formation of high amounts of fly ash [51]. According to the literature, the process of biomass combustion may be divided into four successive or overlapping sub-processes: heating and evaporation of moisture, volatile release to the freeboard due to thermal decomposition and char formation, combustion of volatiles in the freeboard, and char oxidation [52]. All processes, heating, devolatilization, and char combustion, are governed essentially by heat and mass transfer. Figure 6 presents a schematic representation of the different conversion steps and the relevant heat and mass fluxes for a biomass particle.

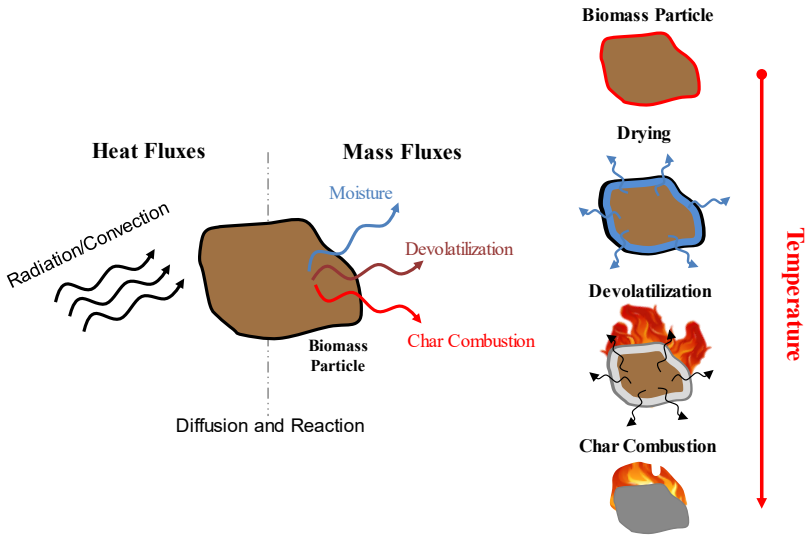

Figure 6: Representation of the biomass combustion stages.

It is generally assumed that the combustion starts with the ignition on the surface. When a fuel particle is inserted in a furnace, it dries, and devolatilizes, firstly mainly through thermal radiation heat transfer from the environment to the particle surface followed by internal transfer of heat inside the particle. Drying is considered when the temperature of the particles reaches approximately 100 °C and, in its turn, devolatilization only starts after the moisture evaporation is completed [53]. The devolatilization process is the fundamental process of combustion because biomass contains a large proportion of volatile matter. Once the volatiles leaves the fuel through the pores of the particle and mix with the surrounding air, combustion occurs in the gas phase. This step is usually quite fast but depends always on the environment outside of the particle which will impose the total conversion as well as the emissions [43]. Finally, the char is oxidized, and at the end, only ash remains on the grate. Here, during this stage, the combustion starts occurring heterogeneously in the solid phase. Factors such as the final temperature and the heating rate are parameters that influence the char concentration [54]. It should also be mentioned that volatile gases after the first mix with the primary air or surrounding air, usually, in combustion equipment, will further react with secondary air to promote complete combustion.

In the past decades, a considerable advance was achieved in understanding the homogenous reactions that take place above the particle conversion, whereas investigations and knowledge have been progressing concerning the particle conversion and the heterogeneous reactions of solid-gas. Based on the previous principle of particle conversion, heat and mass transfer play a key role in the combustion process. The heat transfer to the particle leads to a chain of sequential physical and chemical transformations of the particle due to the conversion processes described previously. In parallel to the heat transfer to the particle, an external and intraparticle mass transfer of oxygen to the surface occurs as well as the release of volatiles out from the particle occurs. The rate of convective and radiative heat transfer to the particle will impose which mechanism occurs first. If the radiative and convective terms are high enough to heat the surface to the ignition temperature and swept away the volatiles, the ignition will start at the surface by the heat transfer mechanism. In contrast, if the heat transfer is low, the volatiles may ignite and form a flame around the particle and the ignition will start due to the mass transfer mechanism. However, the chain of conversion processes may overlap in space and time, and their mechanism depends largely on the thermal and physical properties of the biomass particles and on the heat and mass transfer conditions. Hence, the thermal behavior and the conversion of the particle can be assessed by the thermal thickness of the particle. This judgment can be based on the Biot number which defines if the particle is thermally thin or thick if it is lower or higher than 0.1, respectively [55]. The first hypothesis means that temperature gradients in the particle are negligible and, consequently,

the reactions occur sequentially. On the other hand, if the particle is thermally thick, the reactions occur simultaneously, and it is important, mainly for mathematical models that describe the particle conversion, to differentiate the regions where the different processes take place [56]. Therefore, the Biot number identifies the uniformity of the temperature distribution inside a particle based on the heat transfer resistance inside and on the surface of the particle. The Biot number (Bi) is usually defined as Equation (1):

$$\mathrm{Bi} = \frac{h\,D}{k} \tag{1}$$

where D represents the characteristic length considering a sphere particle, h the effective heat transfer coefficient also considering the radiative effect and k the thermal conductivity of the particle.

These two different thermal regimes appear due to the fundamental heat transfer theories earlier introduced by Çengel and Incropera for the study of transient heat transfer [57,58]. In biomass combustion systems the Biot number is usually higher than 0.1 [59]. The literature suggests that in a packed bed, particles undergoing heating by convection and radiation can be considered as thermally thin if their diameter is lower than 30 mm [60]. Furthermore, Bryden et al. [61] studied the pyrolysis of a thermally thick particle, and suggested that instead of two thermal regimes there should be considered a third separate regime, called a thermal wave, for Biot numbers higher than 10. Here drying and pyrolysis regions move through the particle like a wave where pyrolysis and char exist simultaneously. Since most of the facilities of biomass combustion involve particles of larger sizes, this regime is of particular importance. Still considering larger particles, Johansson et al. [62] studied the impact of neglecting the intra-particle gradients in the combustion modeling. Differences between thermally thin and thermally thick models in the prediction of the flue gas release and temperature profiles for particles larger than 5 mm were observed by the authors. However, the ignition rate and maximum temperature in the bed predictions are not significant, even for particles with 40 mm.

2.2.2 Large-Scale Conversion Technologies of Biomass

This is the fundamental process that occurs at the particle level in specific facilities to produce heat and power. In Portugal, fluidized bed and grate furnaces are the main technologies used for forest biomass combustion. It should also be mentioned that there is also another technology, suspension, or pulverized fuel combustion. However, is not so common in biomass combustion facilities because it is compromised due to the difficulty in grinding biomass fuels to sufficiently fine particle sizes that are required by this

technology [63]. Therefore, pulverized fuel boilers are the most commonly built systems to burn coal [64]. A precise record of the existing biomass power plants is presented in Annex A [65,66].

In the fluidized bed technology, the biomass is fed to a hot turbulent bed composed mostly of sand and the primary combustion air and is introduced from the bottom of the furnace in order to promote the bed fluidization (Figure 7 a)). This technology can be characterized as either Bubbling Fluidized Bed (BFB) or Circulating Fluidized Bed (CFB) combustion systems. In the former, the material remains in the bubbling bed while in the CFB it entrains in the flow and circulates in the equipment.

Regarding the grate furnace technology (Figure 7 b)), this has been used for forest biomass combustion for heat and electricity production for several years [32]. Basically, the biomass is fed from the top of the furnace, and it is burned and moved from one side (inlet) to the other of the furnace (ashtray). Grate-fired boilers are known for their flexibility to burn a wide range of fuels in terms of moisture, ash content, and particle size, and require less fuel preparation and handling [32].

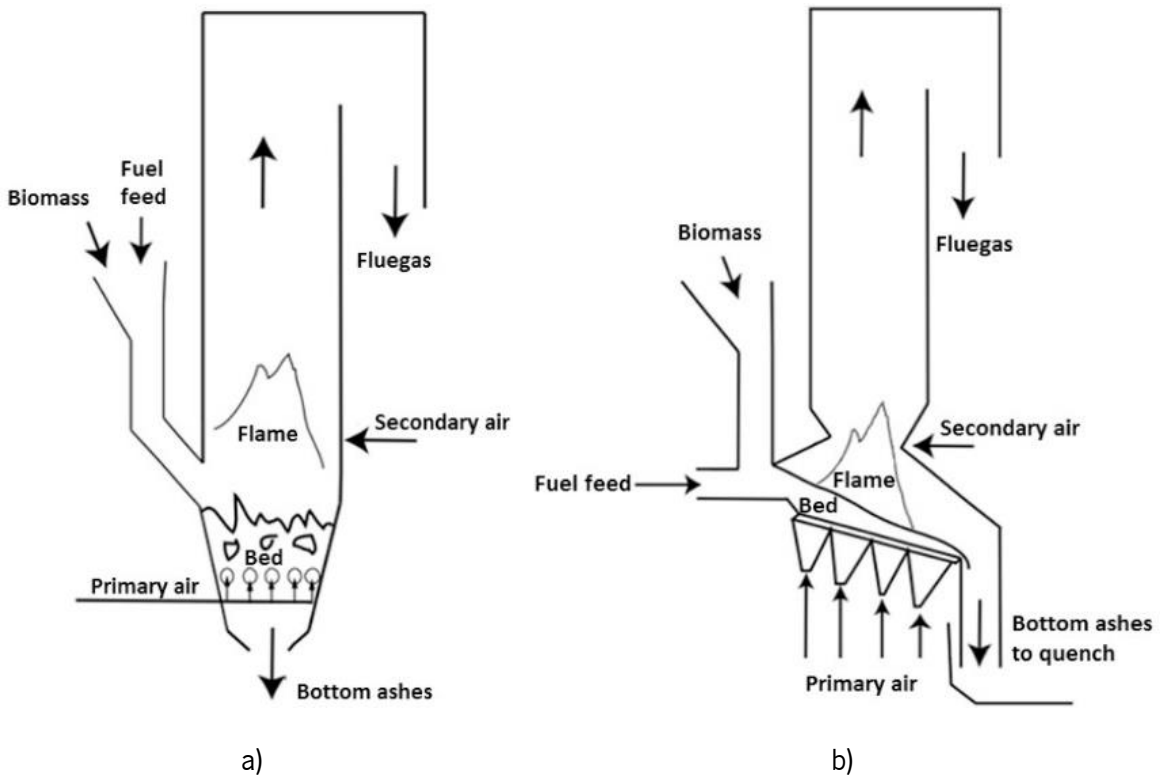

Figure 7: The different conversion technologies of biomass to energy: a) fluidized bed and b) grate furnace. Source: Costa et al. [67].

Furthermore, this technology is an attractive system thanks to its low investment cost, simplicity, and capability to efficiently burn wet and untreated fuels of different qualities. Grate furnaces are one of the most deployed technologies in the world, even if Costa et al. [67] had demonstrated that a fluidized bed presents a smaller environmental impact than a grate furnace. However, to meet the stringent legislation on pollutant emissions, the design of grate-fired biomass furnaces and their operating conditions have been the subject of several investigations. Table 3 presents a summary of the solid biomass combustion technologies considering the main differences in their fuel specifications, the characteristics of each boiler type, gas flow conditions, temperatures, and environmental as well as economic aspects.

Table 3: Overview of the main parameters of the Grate and Fluidized bed technologies for solid fuels combustion. Source: Adapted from [63,64,68].

Parameter	Grate-fired	Fluidized bed
Capacity/Size (MWel)	5-100	30-350
Fuel	Biomass, MSW, Straw	Biomass, RDF, Coal
Ash content (%)	<10	<10
Moisture content (%)	10-60	5-60
Particle Size (mm)	>10	1-10
Excess O_2 (%)	5-8%	3-4%
Gas velocity (m/s)	2-8	4-12
Heating rate (K/s)	1-100	1,000-10,000
Devolatilization time (s)	~100	10-50
Char combustion time (s)	>1,000	100-500
Temperature, Turbulence, and Time	Intermediate temperature, poor mixing, very long residence time	Low temperature, very good mixing, long residence time
Environmental impacts	Low NOx emissions need special technology or advanced air systems	Low NOx emissions due to low temperature
Economics	Low investment and operation cost	High investment and operation cost

2.2.3 Combustion Phenomenon at the Bed Scale

In grate-fired boilers, because of the four sub-processes above mentioned, the thermo-chemical conversion of biomass on the grate is considered a complex process as it involves various aspects of thermodynamics, fluid dynamics, chemistry, and physics [69]. Solid biomass is fed periodically mainly as a function of fuel quality and power. Uniform load is required to ensure homogeneous combustion conditions over the grate area as fuel-rich combustion leads to incomplete combustion [70]. Usually, grates are divided into different zones in order to provide different primary air mass flow rates that will allow complete combustion on the grate. This is an important point together with the grate movement because it affects significantly the air-fuel mixing and biomass conversion [32]. The combustion gases

leaving the fuel bed will be further oxidized by the secondary air. Proper mixing between the flue gases and the air is also a crucial point to ensure complete combustion and, therefore, higher thermal efficiency and reduced pollutant emissions.

Peters and Raupenstrauch [71] analyzed the phenomenological description of the main processes during biomass combustion in a grate-fired boiler, and considered that a comprehensive analysis can be focused on the following three major processes:

1. Thermo-chemical conversion of biomass particles.
2. The flow of the flue gas between the particles.
3. The overall motion of an ensemble of particles.

The understanding of the entire process is challenging and needs a description of the relevant physical mechanisms of these sub-processes and establishing relations between them. Hence, due to the complex nature of the thermo and fluid dynamic processes involved inside the furnace, there are different time and length scales that can be differentiated during the bed conversion [72]. The reaction process of the bed can be analyzed by the reactants available and their conversion. However, the presence of a reactant depends on the transport rate, either diffusive or convective. Thus, the time scales of the overall process are determined by the slowest of transport and reaction rates. If there is a significant difference between both rates, a kinetically controlled reaction regime is introduced, which may prevail for a single particle and a bed. Peters [73] analyzed the combustion regimes of a single particle and a packed bed, representing its conversion as a sum of the conversion of all the particles in the packed bed. The analysis introduced two dimensionless parameters, the Damkohler number (Da), and the Thiele modulus (Th). The first is introduced to evaluate if the bed can be modeled as a well-stirred reactor ($\mathrm{Da} < 1$) or as a stratified bed ($\mathrm{Da} > 1$). In the first case, the reacting agents are present everywhere, where all particles have the same reaction conditions, and reactions occur in any place of the bed at the same time. However, if $\mathrm{Da} > 1$, the combustion moves along the bed as the reacting agents are available and flow through the particles being consumed during the reactions. The Th number is employed to subdivide the previous two regimes taking into account if the conversion is dominated by a reaction kinetics or diffusion on particle scale. In poor transport of the reacting agents compared to the reactive terms within the particle, where $\mathrm{Th} > 1$, the shrinking core approach prevails, and the conversion front achieved the center of the particle. In contrast, when $\mathrm{Th} < 1$, the entire particle reacts, and the increased conversion leads to the reacting core approach.

2.2.4 Strategies for Combustion Performance Improvement

Even though grate-fired boilers are a mature technology, there are still some problems associated with this technology. For instance, the mixing between the volatile gas and the air in the freeboard and the pollutant formation should be analyzed for a better understanding and improvement. This, along with the tightening of the environmental regulations, has motivated in the last decades the improvement of accurate design techniques to optimize the combustion process, and simultaneously include new technologies to control pollutant emissions to the environment. Increasing the efficiency of the combustion process leads to savings on fuel costs, and cheaper production of sustainable energy, with successful reduction of pollutant emissions due to a good combustion performance. Additionally, and taking into account that a significant fraction of the costs in grate-fired plants is related to the operation, it is obvious that a thorough understanding of the combustion process is required for reducing costs without relying on empirical rules of thumb. In this sense, the requirement for the implementation of strategies to keep flue gas emissions as low as possible resulted in the development of primary emission reduction techniques, which are only concerned with combustion modifications. Therefore, these measures aim to modify the operational or design parameters of the combustion equipment in such a way that the formation of pollutants is reduced at the source.

In this regard, combustion air systems are an essential aspect of the performance of the industrial boiler, and they are being increasingly used to reduce emissions [74]. Generally, as stated by Nussbaumer et al. [75] and Yin et al. [76] improvements in boiler performance and emissions can be achieved by modifying the air system. Air systems are used to provide oxidants to the fuel and control the combustion process inside the combustion equipment. In this way, an improperly designed combustion air system results in poor mixing of air and fuel. As a result, boilers operate with a high excess of air, particularly with a high airflow under the grate leading to an increase in the number of particles transported into the equipment, as well as an increase in the emission of pollutants. Recent developments modified the air system in terms of the split ratio of secondary air to primary air by increasing the secondary air to more than 40% of the total air, when compared to older facilities [63].

In modern grate-fired boilers, biomass combustion in the fuel bed occurs in sub-stoichiometric conditions, rich in fuel, because biomass fuels have a higher content of volatile matter on a dry basis. Therefore, it also means a slower conversion of the fuel, which results in a lower combustion temperature on the grate and, therefore, longer fuel residence time. On the other hand, a smaller amount of primary air reduces the number of fuel particles blown out of the grate, and, in this way, the amount of unburned material

dragged from the grate is reduced. Consequently, there is a certain minimum primary air ratio, and if it is decreased, stable combustion cannot be maintained. This minimum value depends on several factors, such as fuel moisture, combustion air temperature, and excess air ratio [77]. The excess air for moist biomass fuel is set to 25% [78]. However, a low excess air ratio is the key to burn biomass at high boiler efficiency and low CO and NOx emissions. In addition, the grate movement significantly affects the conversion and distribution of biomass in the fuel bed, avoiding fuel piles. The fuel characteristics are determinant properties to adjust the vibration and dwell time. Furthermore, it is essential to point out that periodic oscillations increase fly ash emissions and higher CO emissions due to incomplete oxidation resulting from a decrease in oxygen supply during the vibration period. These findings were also reported by Yang et al. [79] in analyzing the operation of a 12 t/h MSW incinerator.

The optimization of the overfire air system concerns the injection location and velocity as the two main design parameters for the secondary air system. This air system must oxidize all CO released over the grate [76–78]. To date, there are some investigations on the literature reporting the influence of air systems on biomass combustion behavior. Yin and Li [80] presented an overview of all the key technologies currently used to improve efficiency and reduce the environmental impacts of direct biomass combustion. Amongst the various technologies, the possibility to use advanced secondary air systems to optimize mixing, temperature, residence time, and local stoichiometry in the freeboard is an attractive option. The flue gas recirculation (FGR) is another technique to reduce NOx emissions. However, the resulting lower temperature inside the combustion chamber promotes ash agglomeration on the wall of the boiler [81]. Although up to 80%, or more, of the NOx emissions, are generated due to the fuel mechanism [82], there are some investigations that prove this approach effective in reducing NOx emissions [81,83–85].

Other interesting options to improve the combustion performance are the adjustment of the frequency and amplitude of the grate, a better undergrate primary air distribution, and the preheat of the primary air. Yang et al. [79] investigated the influence of the grate movement and concluded that fluctuations in the gas emissions are related to this parameter. The influence of the primary air supply was studied by different authors considering different firing systems and their influence on various phenomena. For instance, Lamberg et al. [86] showed that reduction of the gas emissions can be achieved when the amount of the primary air is reduced. Wiinika and Gebart [87] studied the influence of the primary air on the fine particle emissions, and the authors achieved a reduction of the particle emissions with lower primary air flow rates. However, the reduction of the primary air flow rate is limited by the fuel quality (mainly its moisture content) as stated by Staiger et al. [88]. In experiments carried out in a large firing

system, as reported, for instance, by Markovic et al. [89], it was verified that an increase in the primary air intensifies the volatile release, as well as char burning up to a critical point. After that, a further increase in the primary air results in slowing down the combustion process and reduces the char burned. Furthermore, Jorgensen et al. [90] demonstrated the benefits of using numerical simulation to design new concepts for air systems and analyze and optimize an existing air system. Considering three case studies, the authors proved that numerical simulation is a cost-effective method of evaluating air systems and design improved modifications.

Concerning the preheat of the primary air, this technique can optimize the drying and devolatilization of the bed [91]. Saidur et al. [92] and Barma et al. [93] suggested that the high temperature of the flue gas stream can be used as the source of the heat energy to transfer the energy in a heat exchanger to the primary air. The combustion air will gain a large portion of sensible heat required to accelerate the combustion process rather than only drying the fuel. This approach proved to be effective to evaporate moisture while keeping within limits the local maximum temperature in the furnace [94]. Examples of investigations focusing the air preheating include the works from van Kessel et al. [95] and Van Der Lans et al. [96]. Table 4 synthesizes the studies assessed to evaluate the biomass combustion process based on the various strategies used to improve the combustion performance.

However, although this technique allows the improvement of the combustion performance and also the increase of the overall efficiency of a biomass-fired boiler since heat losses via the chimney will be reduced, problems related to corrosion can occur [30]. The corrosion in air preheaters is due to the acid condensation present in the flue gas composition [97]. Since failures due to corrosion will cause a reduction in the heat exchangers lifetime, to prevent this problem, it is essential to study the lowest admissible temperature limit. There are two different possibilities reported in the literature to study the reduction of the flue gas temperature. The first one is the use of empirical relations available to calculate the dew point of some acids. This approach was recently used by Brandelet et al. [98] to estimate the dew point temperature in a biomass grate-fired boiler. The other possibility is the utilization of probes inserted into the flue gas stream at different controlled temperatures. Then, on the probe, the morphology, and composition of the deposits can be analyzed through different microscopic techniques. For instance, Frandsen et al. [99] used the scanning electron microscopic, while Zhang et al. [100] used X-ray diffraction, and X-ray fluorescence techniques. Table 5 presents more details about the state of the art to evaluate the lower temperature limits that the flue gas can achieve without condensation.

Table 4: A review of the studies assessing the influence of the air system on the biomass combustion process.

Author	Type of work	Fuel	Firing system	Parameter evaluated	Main Results
Meng et al. [101] 2019	Experimental	Pine woodchips	Laboratory fixed bed furnace, ~10 kW	Air flow rate, preheating, ignition, and burning rate	Higher flame propagation and mass burning rate with a higher flow rate or temperature.
Caposciutti and Antonelli [102] 2018	Experimental	Pine and chestnut woodchips	Commercial fixed bed boiler, 140 kW	Air staging and air excess	Air excess has the main influence on emissions. Air split ratio control the combustion.
Khodaei et al. [53, 54] 2012	Experimental	Wood pellets	15 kW Laboratory boiler	Air staging	50% CO reduction and lower particle emissions than non staged combustion.
Markovic et al. [89] 2014	Experimental	MSW	Laboratory fixed bed furnace	Air flow rate, fuel moisture, and inert content	An increase in the primary air speed leads to higher conversion rates.
Houshfar et al. [82,83,105,106] 2012 and 2011	Experimental	Wood pellets	Laboratory reactor	Excess air, FGR, and air staging	Primary excess air ratio of 0.8-0.95 minimize NOx emissions. FGR reduces NOx emissions.
Lamberg et al. [86] 2011	Experimental	Wood pellets	Small-scale pellet boiler	Air staging and load operation	Lower emissions with low primary air flow.
Zhao et al. [107] 2008	Experimental	Corn stalks	Laboratory fixed bed furnace	Preheating and fuel moisture content	For higher fuel moisture, burning rate and ignition propagation decreased. Opposite trend with higher air temperature.
Strempek and Jorgensen [108] 2008	Numerical	Biomass	Industrial grate-fired boiler	Air supply	New overfire air system reduced CO and NOx
Staiger et al. [88] 2005	Experimental	Woodchips	Grate-fired boiler, 450 kW	Thermal load, Excess air ratio	CO emission is a function of fuel quality. The fuel quality limits the primary air reduction.
Wiinika and Gebart [87] 2005	Experimental	Wood pellets	Laboratory reactor, 10 kW	Air supply	Fine particles decrease with lower air supply.
Yang et al. [109] 2004	Experimental and Numerical	MSW	Laboratory fixed bed furnace	Primary air flow rate and fuel moisture content	Same as Zhao et al. [107]
Yang et al. [79] 2004	Experimental and Numerical	MSW	Grate-fired boiler, 12 t/h	Primary air flow rate, fuel moisture content, devolatilization, channeling, and transient behavior	Fluctuations have a significant impact on emissions. Shorter grate movement reduces O_2.
van Kessel et al. [95] 2004	Experimental	Biomass	Laboratory fixed bed furnace	Primary air preheating	Preheating of the primary air acts as a catalyst for the ignition rather than only drying.
Jorgensen et al. [90] 2002	Numerical	Biomass	Industrial grate-fired boiler	Air supply	More effective mixing with a low number of parts and higher flow is obtained. Staging the combustion reduces NOx emissions.
Thunman [110] 2001	Experimental	Woodchips	Laboratory furnace and Grate-fired boiler, 31 MW	Ignition and propagation	The ignition propagation depends on the fuel moisture and air flow rate.
Saastammoinen et al. [78, 79] 2001 and 2000	Experimental and Numerical	Biomass	Laboratory fixed bed furnace	Ignition front propagation	Higher fuel moisture decreases ignition velocity, volatiles, and power. Less amount of air is required to achieve the maximum rate.
Van Der Lans et al. [96] 2000	Experimental and Numerical	Wheat straw	Laboratory fixed bed furnace	Air flow rate and preheating	Higher air temperature resulted in lower maximum bed temperatures. NO emission decreased with higher air flow during ignition.

Table 5: Studies from the literature evaluating the reduction of the flue gas temperature. Numerical works considering empirical correlations.

Author	Type of work	Fuel	Firing system	Species tested / Experimental technique	Limit temperature
Zhang et al. [100] 2020	Experimental	MSW	Grate-fired boiler, 400 t/h	EDS, SEM, XRD	65 °C (inlet water temperature)
Brandelet et al. [98] 2020	Numerical	Biomass	Grate-fired boiler, 180 kW	Ashes and H_2O	< 75 °C
Wei et al [113] 2017	Numerical	Coal	-	H_2SO_4	> 80 °C (material temperature)
Chen et al. [114] 2017	Experimental and Numerical	Coal	Grate-fired boiler, 29 MW	H_2SO_4 and H_2O / EDS, SEM, XRD and XRF	101.4 °C / > 80-90 °C (material temperature)
Xiang et al. [115] and [116] 2016	Numerical	-	-	H_2SO_4 and H_2O	20–120 °C
Vainio et al. [117] 2016	Numerical	Biomass and RDF	BFB boiler, 107 MW	SEM-EDX and XRF	100 °C (material temperature)
Wang et al. [118] 2016	Experimental and Numerical	Biomass	CFB boiler, 65 t/h	H_2O / SEM, XRD, and XRF	52.3 °C / > 90 °C (inlet water temperature)
Retschitzegger et al. [119] 2015	Numerical	Biomass	Grate-fired boiler	HCl, HNO_3, H_2SO_3, and H_2SO_4	75–110 °C (inlet water temperature)
Frandsen et al. [99] 2002	Experimental	Biomass	Grate-fired boiler, 33 MW	SEM	> 60 °C (material temperature)

EDS – Energy Dispersive Spectrometer
SEM – Scanning Electron Microscope
XRD – X-ray Diffraction
XRF – X-ray Fluorescence Spectroscopy

2.3 Characterization of Biomass Combustion

As it is impossible to maintain repeatable and fully controlled environments, and to monitor all the dynamics involved in field-scale experiments, it becomes necessary to perform investigations at a small scale. This should be sufficient to provide a controlled environment, and large enough to define realistic conditions. Moreover, biomass combustion in grate-fired boilers can be described as a series of reactions, which begins at a relatively small scale. Furthermore, from the design and operation of industrial biomass boilers, there is a need to model the combustion to further determine their key operating and design parameters. As represented in Figure 8, a comprehensive understanding of the devolatilization is fundamental to the conversion process. In order to completely characterize this stage, the kinetics of the reaction and the determination of the volatiles released are essential. The study of the biomass combustion behavior and the kinetics of the solid-state reactions have been developed through fundamental thermal analysis methods. According to the International Confederation for Thermal Analysis and Calorimetry (ICTAC), thermal analysis is addressed as a group of techniques where a property of the sample is monitored against time and/or temperature and, consequently, the change of the sample in

terms of its weight is measured as a result of an imposed temperature program in a specified atmosphere [120]. In the literature, TGA is the most usual thermoanalytical technique used for solid-phase thermal degradation studies and for kinetic measurements [121,122], while the gaseous release process analysis and the heat and mass transfer effects can be evaluated using the same technique but at a larger scale which is commonly known as Macro TGA [123].

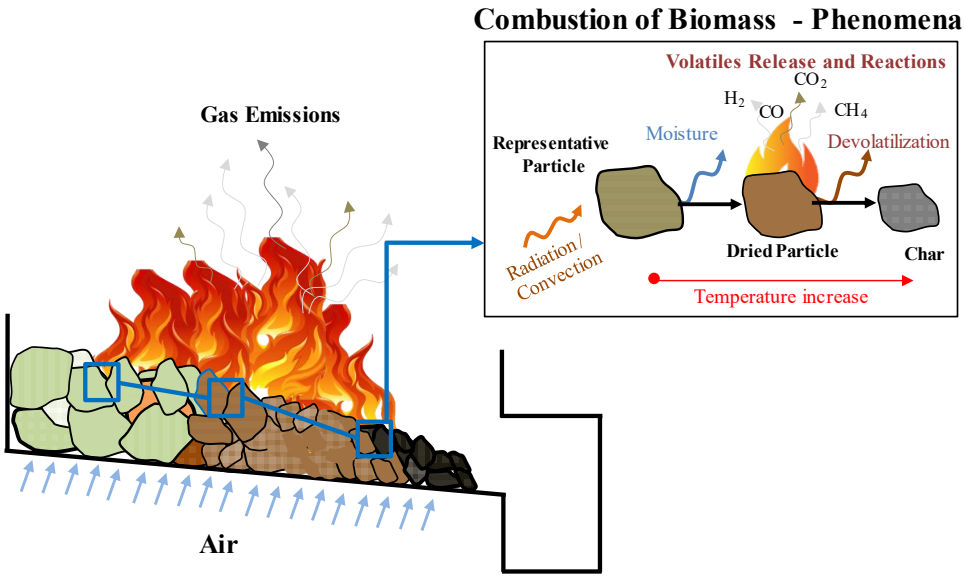

Figure 8: An overview of the phenomena occurring during the multi-scale biomass combustion process.

2.3.1 Thermogravimetric Analysis

As biomass combustion is a complex process [124], it is important to understand the physical and chemical processes involved at the particle level to enable proper understanding [125,126]. TGA is a powerful tool to study the devolatilization rate during the biomass combustion process and obtain important parameters which are essential in characterizing and understanding its behavior [127,128]. TGA is widely implemented to investigate and compare thermal degradation events and kinetics during the combustion of solid materials such as coal and biomass [129]. The decrease in mass is measured under controlled conditions while the thermal process is taking place, as the temperature increases with time. Consequently, information about the thermal conversion dependency with temperature will be obtained at the particle scale. According to the search results from the Web of Science Database considering the keywords “thermogravimetric analysis” and “biomass”, there is a growing trend about biomass and the application of TGA to biomass in scientific journals since 2000. Figure 9 presents the

annual number of publications from 2000 to 2021, which highlights the use and importance of TGA to investigate the thermal decomposition of biomass.

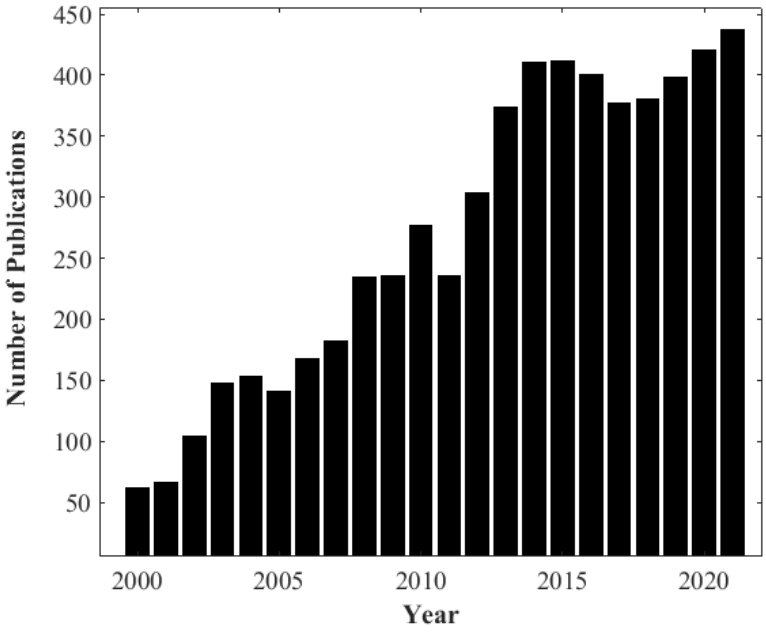

Figure 9: Number of annual publications from 2000 to present on thermogravimetric analysis, TGA, and biomass: Data Source: Results from Web of Knowledge Database.

A thermogravimetric analyzer consists of a sample pan that is supported by a precision balance placed in a furnace where the heating rate and environment can be controlled. Time, temperature, and weight are the three variables continuously measured and recorded during the TGA experiment. Taking the first derivative of such recorded data, known as derivative thermogravimetry (DTG), important parameters to thermal behavior characterization are provided. These key parameters are initial decomposition (T_{in}), peak ($T_{\max}$), and (T_b) burnout temperatures. T_{in} corresponds to the beginning of the weight loss, and it is defined as the temperature at which the rate of weight loss reaches 1%/min after the initial moisture loss peak in the DTG profile. T_{max} is the point at which the maximum reaction rate occurs. T_b is identified when the last peak comes to the end and the temperature at which the sample is completely oxidized. It is taken as the point immediately before the reaction ceases when the rate of weight loss is down to 1%/min [130]. All this information allows the thermal decomposition characterization of biomass samples and, in particular, the last two characteristic temperatures are important to fuel parameters, especially in establishing the residence time in the combustion chamber. The experimental procedure and the most important points are illustrated in Figure 10.

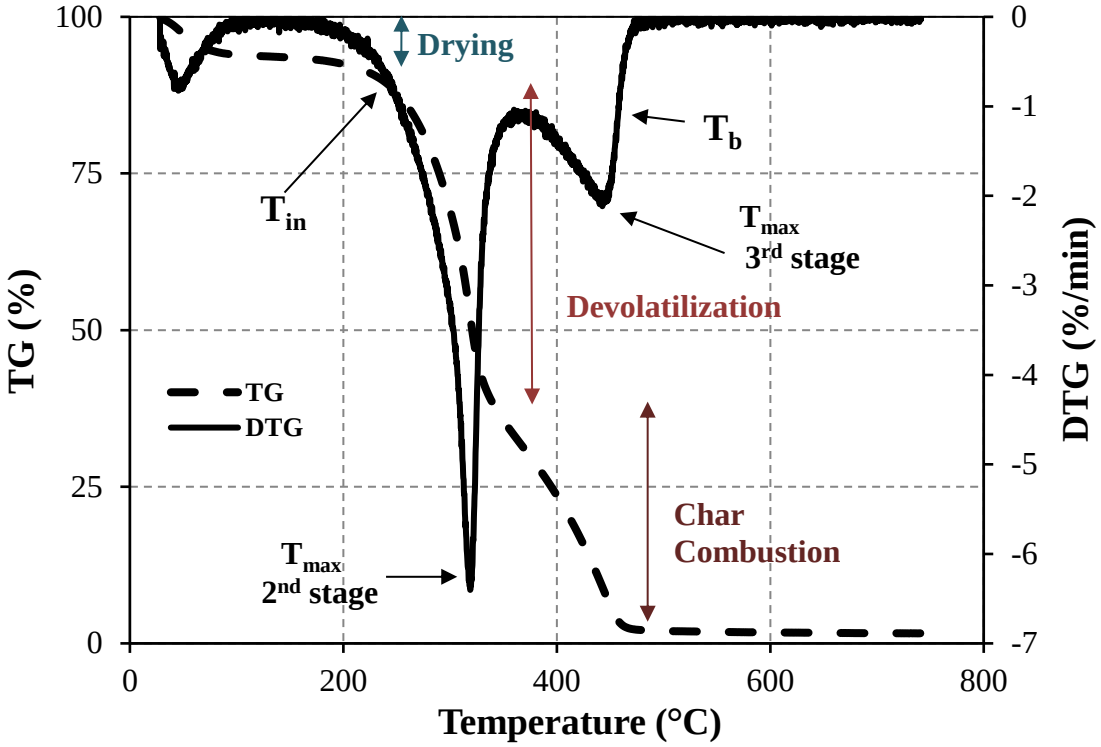

Figure 10: Mass loss as a function of time (above) and temperature (below) during the combustion of biomass [131].

The shape of the thermogravimetric curves (TG) and DTG curves is dependent on several factors, including the type of biomass, atmosphere and its flow rate, the heating program which includes the heating rate and the final temperature, initial mass, and the particle size of the fuel [43]. These constitute several factors that affect the TG, and that will determine the characteristic thermal decomposition behavior. The initial mass and particle size should be as small as possible to avoid the effect of heat and mass transfer limitations [132,133]. Regarding the atmosphere, two options can be considered, oxidative or inert. An oxidative atmosphere greatly affects the devolatilization behavior [134]. The final temperature must be enough for the complete decomposition of the carbonaceous materials. Finally, the heating rate is an important parameter as it greatly affects the rate of release of volatiles due to the thermal inertia of the particles and, in this way, different heating rates should be applied in order to study its influence [135].

Non-isothermal experiments are generally adopted for the determination of kinetic parameters as they are considered more reliable and less time-consuming when compared with isothermal experiments [136]. Moreover, TGA is very useful in studying the kinetics of biomass combustion because it is a simple and effective way to obtain information on the processes taking place for determining the kinetic parameters [137–140]. In this way, non-isothermal experiments include information on the temperature

dependence of the reaction rate, and it is commonly believed that would be sufficient to derive Arrhenius parameters and the reaction model of a process [141]. Consequently, the heating rate is one of the most relevant parameters in TGA as it affects thermal decomposition and, usually, experiments need to be performed with several heating rates to solve possible compensation effects [142]. In this way, the Kinetics Committee of the ICTAC recommends that no less than three different temperature programs should be applied to obtain quality kinetic data [143].

The TGA results depend on several factors, but studies with a low heating rate are privileged to determine more precisely the temperatures from which the pyrolytic reactions start and to avoid transport effects [144]. In addition to factors such as final temperature and heating rate, first stated by Williams et al. [145] as parameters that influence thermal decomposition and the composition of the final products, the atmosphere is also a factor that influences the thermal behavior of biomass. According to Vamvuka et al. [146], decreasing the oxygen concentration and increasing the particle size and moisture content will cause the ignition and burnout temperature to increase. Consequently, these variations will increase the residence time in the combustion chamber. Furthermore, Vamvuka et al. [146] reported that the composition of the gases, tars, and chars derived from biomass combustion depends on the heating rate and final temperature among other factors. Mani et al. [147] also investigated the influence of different parameters and found that the curves corresponding to the third stage of pyrolysis differ for variations in the particle size, initial weight, and heating rate of the pyrolysis process. Furthermore, an increase in the particle size and heating rate increases the char yield at the end of the experiments. Boriouchkine et al. [148] investigated the combustion of different particle sizes of spruce bark and wood residues. This study revealed that larger particles produced the highest mass loss rate when compared to smaller particles. Regarding the heating rate effect, Yorulmaz et al. [149] analyzed the combustion kinetics of treated and untreated waste wood using TGA under three different heating rates. This study revealed that by increasing the heating rate, the peak and burnout temperatures for all the samples were also increased, and higher temperatures were detected for the same weight loss. Shen et al. [150] examined the effect of the heating rate of four different biomass species, and the experimental results were used to develop a two-step reaction kinetic scheme with activation energy values from different heating rate experiments. Some studies have also analyzed the effect of different heating rates on biomass decomposition under inert atmospheres [136,151–156]. However, as reported by Shen et al. [157] and Anca-Couce et al. [158], the presence of oxygen enhances biomass decomposition and promotes char combustion. Furthermore, the kinetic parameters derived from oxidative environments differ remarkably from experiments in the absence of oxygen [71]. Therefore, in order to simulate combustion conditions, it is

important to study thermal behavior and kinetics in an oxygen atmosphere. In this sense, Kok and Özgür [159], Garcia-Maraver et al. [142], and Álvarez et al. [160] have studied the combustion behavior and kinetics of agricultural residues.

Furthermore, in a real application of biomass combustion to produce power, for instance in an industrial grate-fired boiler, the temperature of the biomass increases and volatiles are released quickly due to the high heating rate that they are exposed (around 1 to 100 K/s) [64]. This fast reaction results in insufficient air diffusing into biomass, and ambient oxygen concentration varies along the time which means that the reaction will change from pyrolysis to combustion [161]. Nevertheless, although modern boilers operate in oxygen-limited combustion under a low primary air flow rate, it is important to point out that most of the time this equipment operates in reaction-limited combustion due to a high primary air supply [76]. However, most of the studies in the literature have investigated pyrolysis using inert atmospheres [147,151,168–170,153,154,162–167]. This is due to the fact that pyrolysis is the first process in thermochemical processes such as combustion and gasification [171].

Few results have been generated from experiments with air [149,150,172–176]. Shen et al. [157] and Anca-Couce et al. [158] reported that the presence of oxygen enhances biomass decomposition and promotes char combustion. Furthermore, the kinetic parameters resulting from oxidative atmospheres differ significantly from experiments in the absence of oxygen [158]. Therefore, to simulate combustion conditions, it is important to study thermal behavior and kinetics in an oxygen atmosphere. In this way, in order to understand these differences, the influence of both oxidative and non-oxidative atmospheres on the biomass thermal conversion have been studied by different authors [157,177–179]. Munir et al. [177] analyze the thermal characteristics of four waste biomass materials and the results showed that it is a complex phenomenon due to different microstructural and elemental characteristics along with the type of atmosphere. The authors found that the weight loss rate in an inert atmosphere was slower, and its reactivity is 52% to 77% less than in oxidative conditions. Similar results were reported more recently by Sher et al. [179] who assessed the thermal and kinetics of diverse biomass fuels to provide valuable information for the power generation industry.

Yuzbasi et al. [178] compared the pyrolysis and combustion of co-firing biomass and coal with the individual behavior of each solid material. Regarding pyrolysis, a similar trend was obtained up to 700 °C. Furthermore, the oxygen levels shift the combustion profile to lower temperatures and an increase in the weight loss rate.

Shen et al. [157] investigated the thermal degradation of pine and birch and applied a new kinetic model, the distributed activation energy model (DAEM). DAEM was found not suitable to describe the thermal decomposition of biomass under oxidative conditions due to the capacity of oxygen to accelerate the mass loss in the first stage and promote complex reactions in the second stage. Furthermore, some works analyzed the influence of the effect of the oxidative and non-oxidative environment through experiments with different oxygen concentrations [134,161,180–182].

Fang et al. [161] studied the effects of oxygen concentration on the mass loss rate and kinetics of pyrolysis and combustion of wood. The author stated that the mass loss rates of wood were independent of oxygen concentration when the temperature was below 250 °C. Furthermore, it was found that the activation energy varied linearly with oxygen concentration at the first stage. Moreno et al. [182] also studied the kinetics of wood wastes and solid wood under different conditions considering three or four reactions depending if the reaction occurs under oxidative or non-oxidative conditions. In its turn, Amutio et al. [181] proposed a kinetic model consisting of six simultaneous reactions.

Chouchene et al. [180] studied the effect of three different atmospheres with different oxygen content on the thermal degradation of solid waste. It was verified that pyrolysis under inert conditions takes place according to two different stages (drying and devolatilization) while under oxidative conditions a third stage, char oxidation, occurs. On the other hand, Su et al. [134] analyzed the effect of oxygen content on the thermal degradation of pine and similar results were obtained. The oxygen promoted the degradation of biomass, and a third stage was observed.

As the previous literature has thrown light on the TGA under different conditions, only a few works have succeeded in analyzing thermal conversion, and determining all the kinetic parameters of experiments covering the possibility of oxidative and non-oxidative conditions with different flow rates. To date, several studies have considered these different parameters, including particle size [146–148] and heating rate [136,142,157–159,183–188,149–156], to study their influence on thermal degradation behavior and kinetics. Additionally, in the literature, there are several kinetic data derived from the weight loss curves of biomass fuels in inert [135,147,189–195,148,152–154,156,163,164,166] and air [133,142,174,175,196–199] atmospheres. There are also other investigations that studied the influence of the atmosphere and applied both atmospheres [130,134,157,161,177,179,182]. This extensive literature review culminated with the selection and analysis of works that analyzed the same fuels (eucalyptus, acacia, and pine) considered in the present work, which is summarized in Table 6.

Hence, considering the current state-of-the-art in this subject, many factors can affect the kinetic parameters, including not only the process conditions, heterogeneity of the sample, heat and mass transfer limitations, and systematic errors, but also the processing and method for the analysis of the TGA results [122]. Consequently, a wide range of kinetic parameters has been reported in the literature and, therefore, direct comparisons are not possible. As evidence of this inconsistency, Figure 11 presents the different activation energy values reported in the literature for Pine devolatilization and char oxidation.

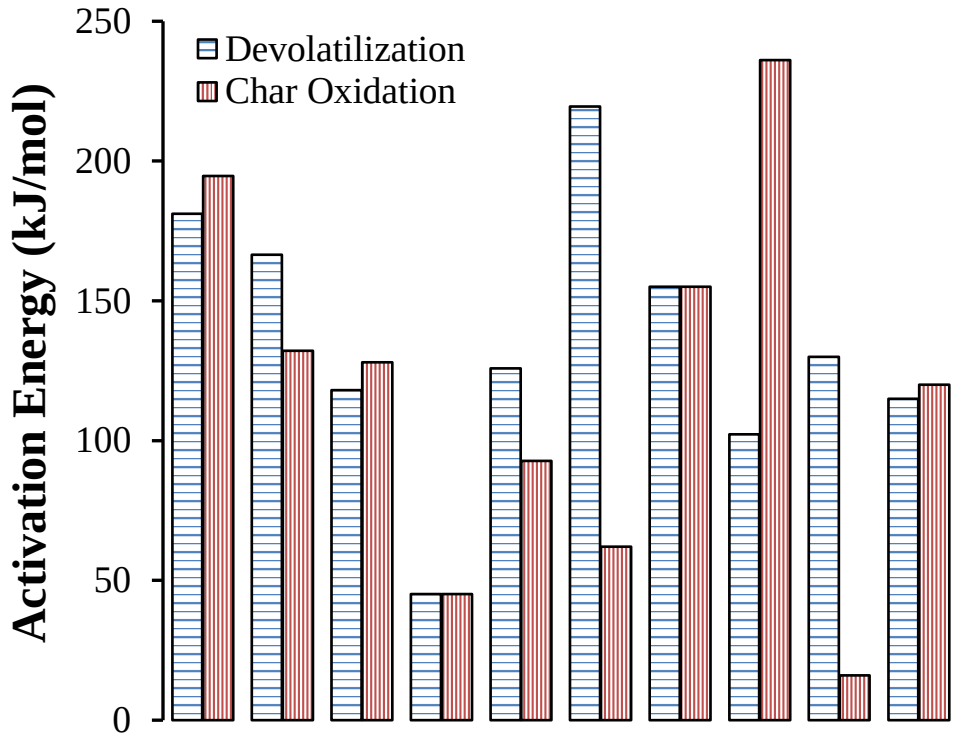

Figure 11: Activation Energy values reported in the literature for Pine devolatilization and char oxidation using two-step sequential models. The red bars are results considering a global reaction. Data Source: [149,150,157,160,181,200–203].

Table 6: Literature review of experimental works that used pine, acacia, and eucalyptus samples.

Author	Country	Reactor Model	Biomass Type	Surrounding Environment	Mass (mg)	Size (μm)	Final Temperature (K)	Heating Rate (K/min)	Kinetic Method
Xu et al. [204] 2021	China	SDTA851E	Pine	Air 60 mL/min	NA	<200	873	5, 10, 15, 40	2-stage mechanism and OFW, Starink, DAEM, and CR
Chen et al. [201] 2020	China	SDTA851E	Pine needle	Air 100 mL/min	1.6	75-150	870	5, 10, 20, 40	3-stage mechanism and OFW, KAS, and CR
Fu et al. [205] 2019	China	TA Instrument SDT Q600	Eucalyptus bark	N_2 100 mL/min	5–10	150–300	1073	10, 15, 20, 25 and 30	Model-fitting
Vega et al. [206] 2019	Colombia	LINSEIS, STA PT-1600	Pine and Acacia	N_2/O_2 mixture 50/13 mL/min	10	mesh 30 and mesh 60	1173	5, 10, and 15	OFW
Mishra et al. [136] 2018	India	Hitachi, TA-7000	Pine and sal sawdust and areca nut husk	N_2 50 mL/min	8	< 1000	1173	5, 10, 15, 20, and 25	1-global, KAS, OFW, CR, FR and DAEM
Wadhwani et al. [168] 2017	Australia	Mettler Toledo TGA/DSC 1	Pine and eucalyptus	N_2 20 mL/min	7.5	1–4000	1173	5, 7.5, 10, 20, 50 and 100	1-global, KAS and OFW
Cai et al. [207] 2016	China	NETZSCH STA 409 PC	Eucalyptus and paper mill sludge	Air 200 mL/min	6	< 200	1223	10, 20 and 40	KAS and Starink
Álvarez et al. [160] 2016	Spain	Perkin Elmer STA 6000	28 different biomass samples	Air 40 mL/min	10	250–500	1173	5, 10, 15 and 20	2-stage reaction and KAS, OFW, CR
Yu et al. [184] 2016	China	TA Instruments, SDT Q-600	Eucalyptus bark	Air 100 mL/min	10	200–600	1223	10, 15 and 20	2-stage reaction and OFW and CR
Soria-Verdugo et al. [185] 2015	Spain	TA Instruments Q-500	Pine, olive kernel, thistle flower, and corncob	N_2 60 mL/min	10	< 100	1073	10, 13, 16, 19, 22, 25, 30, 35 or 40	DAEM
Mishra et al. [155] 2015	India	DTG-60 unit	Pine	N_2 100 mL/min	10	50	973	5, 10, 15, 20, 30 and 40	OFW, KAS, FR, Vyazovkin, Vyazovkin AIC, and z(α) master plots
Chen et al. [186] 2015	China	Pyris1 TGA instrument	Eucalyptus leaves, bark, and sawdust	Ar 100 mL/min	5	74	1073	5, 10, 15, 25, and 50	DAEM

Table 6: (continued).

Author	Country	Reactor Model	Biomass Type	Surrounding Environment	Mass (mg)	Size (μm)	Final Temperature (K)	Heating Rate (K/min)	Kinetic Method/Model
Saldarriaga et al. [167] 2015	Spain	TA Instruments Q-500	Pine	N_2 60 mL/min	10	<100	873	3, 5, 10, 15, 20, 30, 50, 80, 100, 150, 200	DAEM
Soria-Verdugo et al. [187] 2014	Spain	TA Instruments Q-500	Pine	N_2 60 mL/min	10	< 100	873	3, 5, 10, 15, 20, 30, 50, 80, 100, 150 and 200	DAEM
Fang et al. [203] 2013	China	Mettler Toledo TGA/SDTA851	Pine	Air 60 mL/min	10	< 2000	773	30	1-global, CR
Anca-Couce et al. [158] 2012	Germany	Linseis Thermal Analysis, L81/1000	Pine	N_2 and O_2	2-4	200	873	2.5, 5 and 10	FR, KAS, and Fitting algorithm
Amutio et al. [181] 2012	Spain	TA Instruments Q5000	Pine	N_2 and O_2 100 mL/min	10	< 200	1073	15	Optimization model
Shen et al. [157] 2011	United Kingdom	TGA Mettler Toledo TGA/SDTA 8951E	Pine	N_2/Air 50 mL/min	< 5	< 300	1173	5, 10, 20, and 30	1-global, CR and DAEM
Kim et al. [151] 2010	Republic of Korea	TA Instruments, Q-50	Pine	N_2 20 mL/min	25	600 and 850	1073	5, 10, 25 and 50	Differential method
Shen et al. [150] 2009	United Kingdom	TGA Mettler Toledo TGA/SDTA 8951E	Pine	Air 60 mL/min	< 5	500	1073	5, 10, 15, 25, and 50	2-stage reaction, CR
Lapuerta et al. [208] 2007	Spain	TGA Seiko Instruments 6200	Pine	N_2 100 mL/min	10	< 50	1100	5, 10, 20, 30 and 40	Fitting algorithm
Lapuerta et al. [209] 2004	Spain	TGA Seiko Instruments 6200	Pine	N_2 50 mL/min	10	< 500	1100	10, 30, 40, 50 and 60	Fitting algorithm
Gronli et al. [210] 2002	Norway	TA Instruments SDT 2960	Pine	N_2 150 mL/min	5	NA	773	5	Optimization model
Bilbao et al. [172] 1997	Spain	SETARAM 92	Pine	Air 100 mL/min	3 and 20	630	≈1023	7 and 12	NA

CR – Coats Redfern
DAEM – Discrete Activation Energy Model
KAS – Kissinger-Akahira-Sunose
NA – Not Available
OFW – Ozawa-Flynn-Wall
TA – Thermogravimetric Analyzer

2.3.2 Devolatilization Mechanism and Reaction Kinetic

As biomass contains a high content of volatile matter, the description of the devolatilization process is essential. Devolatilization often referred to as pyrolysis is a complex chemical process in which the particles decompose into different products including permanent gaseous compounds, tar, and char. Therefore, currently, there are two major issues in describing the devolatilization process. The first one is concerned with how the progress of the biomass conversion can be represented, and the second one is related to how to properly determine the permanent gas released during the devolatilization.

Regarding the first issue, there are different methods in the literature for describing this step of biomass combustion. The kinetics of biomass combustion depends on many different factors, but the reaction mechanism/kinetic model influences the final result and the way the conversion of the biomass is considered to take place. According to the earlier studies from Di Blasi [211] the kinetics of biomass conversion can be classified into three groups: *i)* one-step global models, *ii)* one-stage, multi-reaction models, and *iii)* two-stage, semi-global models. However, in the last decades, as plenty of research has been published in the field of biomass combustion and pyrolysis, a kinetic description of the devolatilization mechanism has been provided for a better understanding. Thus, for the sake of simplicity and clarity, devolatilization and pyrolysis mechanisms can be classified basically into four groups:

1. One-step global mechanism;
2. Multi-component parallel single reaction mechanism;
3. One-component competitive mechanism;
4. Detailed mechanisms.

These mechanisms assume two particular initial conditions, if biomass is considered as one component or a mixture of components, and if the devolatilization reaction is considered as a single reaction or a set of multiple competitive reactions. Consequently, the group is arranged from the simplest, the one-step global mechanism, to the more sophisticated and complex, the detailed mechanisms. The number of steps in each model refers to the number of kinetic pathways that the reaction can take.

The one-step global mechanism is the simplest decomposition mechanism, acceptable for most engineering applications requiring only mass loss rate predictions [107, 133, 128, 176], and can

be easily obtained from traditional TGA analysis [212]. Secondary reactions are not included and the reaction products, as considered by most of the researchers [122], only consist of char and volatiles. Due to their simplicity, it is used in CFD models to represent and describe the coupled chemical kinetic and physical phenomena of the devolatilization process [175]. Equation (2) presents the form of the single-step mechanism. A second step is commonly added for char oxidation, as referred in [151,154,155,160].

$$\text{Biomass} \rightarrow \text{Volatiles} + \text{Char} \tag{2}$$

The multi-component parallel single reaction mechanism represents biomass by its intrinsic components, and the devolatilization reaction is described as the sum of the contributions of each macromolecule decomposition. Equation (3) shows the main mechanism used in this category. Gronli et al. [210] is one example of the works where the devolatilization of different biomass species was predicted using this mechanism, which is considered more precise to predict the mass loss rate [46].

$$\begin{aligned} &\text{Cellulose} \rightarrow \text{Volatiles} + \text{Char} \\ &\text{Hemicellulose} \rightarrow \text{Volatiles} + \text{Char} \\ &\text{Lignin} \rightarrow \text{Volatiles} + \text{Char} \end{aligned} \tag{3}$$

In order to overcome the limitation of the first mechanism, the one-component competitive mechanism was introduced, and biomass produces competitively volatiles, tar, and char, as represented in Equation (4). As reviewed by Di Blasi [211], Shafizadeh and Chin [213] were the authors who introduced this model, and it is usually applied in fuel bed models [214]. This is a more comprehensive mechanism and requires deeper knowledge of the decomposition of biomass in the different products.

$$\begin{aligned} &\text{Biomass} \rightarrow \text{Volatiles} \\ &\text{Biomass} \rightarrow \text{Tar} \\ &\text{Biomass} \rightarrow \text{Char} \\ &\text{Tar} \rightarrow \text{Volatiles} \\ &\text{Tar} \rightarrow \text{Char} \end{aligned} \tag{4}$$

Detailed mechanisms, e.g., Ranzi Model [215], and Shafizadeh and Bradbury Model [216], are more comprehensive as these models consider competitive and parallel reactions for multiple or intermediate components. In addition, these four types of different reaction schemes are classified as empirical or kinetic models [217]. Kinetic models are global devolatilization models and,

essentially, the mass loss rate is correlated with the temperature of the particle to determine the reaction rate which is expressed by an Arrhenius equation. The reaction rates are only valid for conditions with specific parameters, limiting their general applicability. A detailed description of these and other models used in the literature to describe biomass devolatilization is provided by White et al. [122], Branca et al. [218], and Várhegyi [219].

In addition to this category, there are network models which are very accurate in their predictions of devolatilization behavior, although they are computationally complex. The computational complexity of these network models, as it is considered the physicochemical description of the fuel, directly impacts the amount of time required to run complex simulations [7]. Hence some simulations use simple global devolatilization models instead of complex ones. However, global models generally do not apply to a range of coal types, heating rates, and temperatures as broad as network models, and therefore need to be optimized using trusted data or predictions. Although their origins lie in coal combustion, biomass devolatilization can be considered analogous to the same stage during the coal conversion, the models have been adapted to biomass fuels. Models like the CPD (Chemical Percolation Devolatilization) [220], Bio-FLASHCHAIN [221], FG-DVC (Functional Group Depolymerization Vaporization Crosslinking) [222], and Kobayashi [223] are examples of models developed for coal combustion which were subsequently converted to biomass (Bio-FG-DVC [224], Bio-FLASHCHAIN [225], and Bio-CPD [226]).

The fundamental basis of the kinetic models, that is essential for understanding and modeling the biomass combustion in furnaces, the solid-state transformation rate from biomass to volatile products is generally described by Equation (5):

$$\frac{d\alpha}{dt} = k\ f(\alpha) \tag{5}$$

where t is the time, $f(\alpha)$ is a function called the reaction model which describes the dependence of the reaction model on the conversion rate (α), and k is the thermal dependence term that can be defined by the following Arrhenius Equation (6):

$$k = A\ \exp\left(-\frac{E}{RT}\right) \tag{6}$$

where E is the activation energy (J/mol), T is the absolute temperature (K), R is the universal gas constant (J/mol.K), and A is the pre-exponential factor (s^{-1}). The former parameter means the minimum energy barrier required to break the bonds and change the chemical structure to

another, while A is based on the collision theory and represents the number of collisions per unit of time occurring in the reaction.

Regarding the conversion rate, this term can be defined as a relation between the initial (m_0), final (m_f), and instantaneous (m_t) sample mass. It can be obtained from each thermogravimetric experiment, and it is defined by Equation (7):

$$\alpha = \frac{m_0 - m_t}{m_0 - m_f} \tag{7}$$

For non-isothermal experiments, at a constant heating rate $\left(\beta = dT / dt\right)$, Equation (5) can be expressed as a function of temperature at a constant heating rate, yielding Equation (8):

$$\frac{d\alpha}{dT} = k\ f(\alpha)\frac{1}{\beta} \tag{8}$$

The experimental conditions and the reaction stage considered influence the reaction model. Generally, it is considered a first-order reaction, and this function can be expressed as $(1-\alpha)$ [133,227]. Other functions commonly used if another reaction model is required are presented in Table 7. After all these considerations, Equation (8) can be simplified as:

$$\frac{d\alpha}{(1-\alpha)} = \frac{A}{\beta}\ \exp\left(-\frac{E}{RT}\right)dT \tag{9}$$

The left side of Equation (9) is a function of the conversion rate, and the right side is a function of the temperature. Integrating both sides of Equation (9), the following equation is obtained:

$$g(\alpha) = \int_0^{\alpha} \frac{d\alpha}{(1-\alpha)} = \frac{A}{\beta} \cdot \int_{T_0}^{T} \exp\left(\frac{-E}{RT}\right) \cdot dT \tag{10}$$

Equation (10) has no exact solution and, there are two main mathematical approaches to solve this equation and obtain the kinetics data from the thermogravimetric analysis: 1) model-free methods (isoconversional) and 2) model-based methods [142]. In order to avoid modeling complex reactions, model-free methods can be preferable since the chemical parameters are determined without using any specific reaction model [133].

Table 7: Solid-state rate expressions for the most common reaction mechanism [122].

Model – Name of functions		$f(\alpha)$	$g(\alpha)$
Reaction order controlled	Zero-order	1	α
	First-order	$(1-\alpha)$	$-\ln(1-\alpha)$
	nth-order	$(1-\alpha)^n$	$(n-1)^{-1}(1-\alpha)^{(1-\alpha)}$
Diffusion	1-D	$1/2\alpha$	α^2
	2-D	$-\ln(1-\alpha)^{-1}$	$(1-\alpha)\ln(1-\alpha)+\alpha$
	Jander, 3-D	$1.5(1-\alpha)^{2/3}\left[1-(1-\alpha)^{1/3}\right]^{-1}$	$\left[1-(1-\alpha)^{1/3}\right]^2$
	Ginstiling-Brounshtein, 3-D	$0.5\left[(1-\alpha)^{-1/3}-1\right]^{-1}$	$1-2/3\alpha-(1-\alpha)^{2/3}$
Nucleation	Power law	$n\,\alpha^{(1-n^{-1})}$ n = 2/3, 1, 2, 3, 4	α^n n = 3/2, 1, 1/2, 1/3, 1/4
	Exponential law	$\ln\alpha$	α
	Avrami-Erofeev (n= 1, 2, 3, 4)	$n(1-\alpha)\left[-\ln(1-\alpha)\right]^{(1-n^{-1})}$	$-\ln(1-\alpha)^{n^{-1}}$
	Prout-Tompkins	$\alpha(1-\alpha)$	$\ln\left[\alpha(1-\alpha)^{-1}\right]+C^a$
Geometrical contraction	Contracting area (n=2)	$(1-\alpha)^{(1-n^{-1})}$	$1-(1-\alpha)^{n^{-1}}$
	Contracting volume (n=3)	$(1-\alpha)^{(1-n^{-1})}$	$1-(1-\alpha)^{n^{-1}}$

[a] Integration constant

There are many isoconversional kinetic methods including Friedman (FR) [228], Ozawa-Flynn-Wall (OFW) [229,230], Kissinger-Akahira-Sunose (KAS) [231–233], Starink [234], and Vyazovkin methods [235,236]. The corresponding equations and advantages and disadvantages can be found in Table 8. In model-fitting, different models such as Coats-Redfern (CR) [237], Freeman and Carroll [238], Duvvuri et al. [239], and differential models, can be fitted to the experimental data and which gives the best statistical fit is selected to evaluate the kinetic parameters. An overview of the biomass characterization process to obtain the kinetic parameters is represented in Figure 12.

However, the determination of the kinetic parameters for biomass thermal degradation is particularly complicated considering the presence of complex components and their consecutive and/or parallel reactions. The model-free generates unique kinetic parameters as a function of the conversion rate since they are based on the principle that at each constant conversion, the reaction rate is a function only of the temperature such that [240]:

$$\left[d\ln\left(\frac{d\alpha}{dt}\right)dT\right]_{\alpha} = \left[d\ln\left(k(T)\right)dT\right]_{\alpha} + \left[d\ln\left(f(\alpha)\right)dT\right]_{\alpha} \quad (11)$$

where α and $f(\alpha)$ are constant and, therefore, the second term on the right hand side of Equation (11) is zero. Hence, Equation (11) can be simplified Equation (12):

$$\left[d\ln\left(\frac{d\alpha}{dt}\right)dT\right]_{\alpha} = \frac{-E_{\alpha}}{R} \quad (12)$$

Table 8: Different kinetics methods used in the literature – Equation and advantages and disadvantages. Adapted from: [241,242].

Method	Equation	E_α determination (slope of the plots)	Advantages and Disadvantages
FR	$\ln\left[\beta_i\left(\frac{d\alpha}{dT}\right)_{\alpha,i}\right] = \ln\left[A_\alpha f(\alpha)\right] - \frac{E_\alpha}{RT_{\alpha,i}}$	$\ln\left[\beta_i\left(\frac{d\alpha}{dT}\right)_{\alpha,i}\right]$ vs $\frac{-1}{RT_{\alpha,i}}$	Simple and Accurate; Numerically unstable and sensitive to data noise
OFW	$\ln\beta_i = \ln\left[\frac{A_\alpha E_\alpha}{R\,g(\alpha)}\right] - 5.331 - 1.052\frac{E_\alpha}{RT_{\alpha,i}}$	$\ln\beta_i$ vs $\frac{-1.052}{R\,T_{\alpha,i}}$	Oversimplified temperature integral
KAS	$\ln\left(\frac{\beta_i}{T_{\alpha,i}^2}\right) = \ln\left[\frac{A_\alpha R}{E_\alpha\, g(\alpha)}\right] - \frac{E_\alpha}{RT_{\alpha,i}}$	$\ln\left(\frac{\beta_i}{T_{\alpha,i}^2}\right)$ vs $\frac{-1}{RT_{\alpha,i}}$	More accurate than OFW; Oversimplified temperature integral
Starink	$\ln\left(\frac{\beta_i}{T_{\alpha,i}^{1.92}}\right) = \text{Constant} - 1.008\frac{E_\alpha}{RT_{\alpha,i}}$	$\ln\left(\frac{\beta_i}{T_{\alpha,i}^{1.92}}\right)$ vs $\frac{-1.0008}{RT_{\alpha,i}}$	More accurate temperature integral approximation
CR	$\ln\left[\frac{g(\alpha)}{T^2}\right] = \ln\left[\left(\frac{AR}{\beta E}\right)\left(1-\frac{2RT}{E}\right)\right] - \frac{E}{RT}$	$\ln\left[\frac{g(\alpha)}{T_\alpha^2}\right]$ vs $\frac{-1}{RT_\alpha}$	Forcible fitting to reaction mechanism; Single values of E are obtained

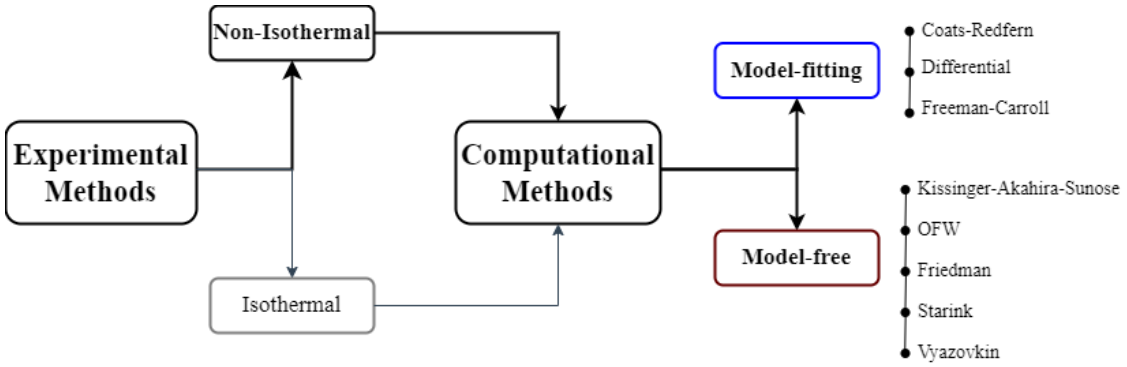

Figure 12: An overview of the methods for solid-state kinetics study [243].

Hence, this kinetic is based on the evaluation of the dependence of the effective E on conversion rate according to the TGA data from multiple heating rates, such as suggested by the ICTAC [143].

The term effective is applied to emphasize a consequence of this dependency, and since in solid-state reactions the kinetic parameters may vary during the reaction progress, it is highly recommended to evaluate if the E values remain constant to rule out the multi-step kinetic mechanism [243]. If E is vary significantly, it means that the reaction process has more than one dominant reaction and a model-free type cannot be used for kinetic analysis. To overcome this problem, the CR method, a model-based method, is frequently applied by different researchers and produces similar E values to those calculated by model-free methods but depending on the selected reaction model considered [142]. The CR model uses the asymptotic series expansion for approximating the exponential integral in Equation (10) According to this model, the kinetic parameters can be determined by the Equation presented in Table 8 and neglecting the term $2RT/E$, which can be considered much lower than one. The A value is then determined from the interception of the plot indicated in Table 8 [244], with the possibility to make this analysis at different stages of the conversion process. Otherwise, to complete the determination of the kinetic parameters A and $f(\alpha)$, usually, the Kissinger or compensation factor methods, and master plots methods have been used to obtain both parameters, respectively [190].

Furthermore, post-processing TGA data is particularly important to obtain correct E values [242]. Consequently, there is a set of steps that should be considered, assessed, and implemented before the kinetic evaluation. Removal of the drying stage, floating points, and smoothing of the derivative conversion rate from the raw TGA data are common practice procedures, in particular, if the FR method will be used. This method is different from the other isoconversional methods since the author uses the differential form of the Arrhenius equation, Equation (9), for the kinetic analysis. In this way, since no approximations or assumptions are used to solve the equation, it is considered more accurate than the other isoconversional methods which are known as integral methods [241]. However, Mishra et al. [155] compared the E values from different isoconversional methods and it was observed higher values at the end of the conversion from the FR method. This means that the FR method is more dependent on the instantaneous conversion rate and more prone to experimental noise. This statement is in line with the Starink finding [245].

2.3.3 Macro TGA and Gas Release Quantification

A devolatilization mechanism and a mass loss kinetic model describes the reaction that occurs during this stage but does not predict the gases released from the particles. Precisely in this regard,

less attention has been paid to predict the gaseous products. Therefore, regarding the second issue of the devolatilization mechanism and description of the devolatilization process, the composition of the volatiles in biomass combustion modeling are often determined from proximate and ultimate analysis data, like the model proposed by Thunman et al. [246] or Neves et al. [247], or based on elemental species and enthalpy conservation equation (e.g. [46]). Thunman et al. [246]. used a chemical balance of the main elements of biomass fuels – carbon, hydrogen, and oxygen elements – to achieve the composition of the products released during the devolatilization. An empirical model composed of three mass balance equations and one energy balance equation, together with two empirical ratios, are proposed to obtain the mass fractions of six chemical compounds (C_6H_6, CO, CO_2, H_2O, H_2, CH_4). Neves et al. [247] present a comprehensive review of the pyrolysis process and the development of an empirical model for the volatiles composition. The focus of this review was on the secondary pyrolysis of gases and the product distribution and composition and the factors influencing them. The permanent gas compounds include a broad range of different species and compounds and can be lumped, mainly, into CO, CO_2, H_2, and CH_4, as well as other light hydrocarbons. This composition is influenced by the heating rate and the main compounds show similar temperature dependencies, although the formation of CO_2 with respect to temperature changes deviates from what is observed in the case of the other compounds [247]. Furthermore, it was found that at temperatures above 500 °C the yields of gaseous products strongly become temperature-dependent, leading to a substantial increase in the CO mass fractions. This was considered a result of secondary reactions, which resulted in the decrease in the tar mass fraction also due to the conversion to CH_4. Furthermore, it is highlighted no significant dependency on CO_2, which means that it is the main product of primary reactions. The same behavior was described by Mehrabian et al. [46] based on dedicated experiments and data collected from the literature. Secondary reactions of the volatiles are negligible at low temperatures, and most of the permanent gases result from biomass thermal degradation. Within the low temperature range, gases like CO, CO_2, and H_2O are the main permanent gas compounds with low quantities of CH_4. As the temperature increases, secondary reactions occur and an increase in CO and CH_4 are attributed to the decrease of tar. Here, due to higher temperatures, the yields of the volatiles have a strong correlation with the temperature, and CO results from the conversion of 2/3 of the tar.

However, the results of this type of approach can produce unrealistic results [248–251], and experimental measurements in a lab-scale reactor are an interesting alternative to address this problem, and also to provide complementary knowledge to the TGA results about the kinetics of

the reaction in the thermal biomass decomposition. This is also particularly interesting because the conditions in biomass industrial boilers are different, and it is important to investigate the thermal decomposition of larger particles and higher biomass quantities than those possible with TGA experiments. This possibility will allow to take into consideration the heat and mass diffusion in the reaction mechanism. Furthermore, using larger samples, the effects of secondary reactions together with the possibility to have higher heating rates can also affect the reaction kinetics. Consequently, due to the complexity of the combustion process inside industrial boilers, together with the motion of the fuel bed, there are several authors that report works in a batch reactor to describe the entire process in a traveling or vibrating grate boiler [89,252–256]. These experiments often include the combustion of a large amount of biomass (in the range of some kilograms). Experiments using batch reactors are also performed to quantify the differences in fuel properties, to study the implications of fuel properties, and to investigate the propagation of a combustion front, i.e., drying, pyrolysis, and char combustion process, in a bed of biomass particles. These types of experiments are useful to develop parametric studies with different operating conditions (primary and secondary air flow rate and temperature) and different fuel properties (moisture content, volatile matter, ash content, chemical composition, heating values, and particle size). Ignition front velocity, ignition rate, conversion rate, and temperature of the reaction zone are the parameters most commonly obtained to evaluate combustion behavior.

Unlike this type of experiment, Macro TGA experiments are a simple and effective technique that allows to study particularly a higher biomass quantity with a particle size representative of the fuel used in industrial facilities in a small reactor. The reactors are then connected to a system to provide insight into the devolatilization products. The volatiles from thermochemical conversion could be detected mainly using gas chromatographs and spectrometers [257]. Gas chromatography (GC) is a novel technique for studying the compounds released and the principle of operation consists of the separation of the individual components of the mixture so that each component can individually be identified and quantified through a detector. First, the sample is inserted into the equipment where it is transported by a carrier gas through a column and, depending on the physical properties of the compounds, the time the sample takes to reach the detector varies. Then an electronic signal is generated based on the interaction with the compound. The main detectors for GC instruments are thermal conductivity detectors (TCD) which are non-destructive and are usually incorporated before another common detector, flame ionizing detectors (FID). Another highly specific GC detector used is the chemiluminescence detector (CLD). More

details about the performance and characteristics of the common GC detectors can be found in Li et al. [258] and in Regmi and Agah [259]. Regarding the other technique, spectrophotometry, it is an analytical technique that also allows to separate, detection and quantify gaseous compounds, but it is based on the absorption of light of the different compounds or on the mass to charge ratio of an ionized molecule. In this technique, there are two different types of spectrometers [260]. The first is referred to as the Infrared Spectroscopy, and Fourier Transform Infrared Spectroscopic (FTIR) and Nondispersive Infrared Sensor (NDIR) are the most common spectroscopic sensors used as a gas detector. The difference lies in the range of wavelengths bands that can be measured [261]. The second technique, Mass Spectrometry, is known in the literature as a sensitive detection technique [262] and the most suitable [263] for gas analysis. In addition, it can overcome the limitation of FTIR in measuring homodiatomic species like H_2 [260]. Table 9 presents an overview of the Macro TGA studies presented in the literature. Only investigations considering combustion and pyrolysis experiments at isothermal conditions were considered in order to approximate to typical operating conditions of a grate furnace. Becidan et al. [264] present the application of chromatography and spectrophotometry to study the gases released during the combustion of biomass residues. A fraction of the exhaust gases is collected and analyzed by an FTIR analyzer and a micro GC. The FTIR was used to quantify CO_2, CO, CH_4, C_2H_2, C_2H_4. The gas samples were also quantified online using a micro-gas chromatograph equipped with two TCD detectors and a double injector connected to two columns to separate and quantify CO_2 and hydrocarbons (CH_4, C_2H_2, C_2H_4, and C_2H_6) and the remaining gases H_2, O_2, CH_4, CO and N_2 in another column. Brunner et al. [265] and Gauthier et al. [266] also applied both techniques to analyze the NOx emissions, the release of ash, and the main gaseous species and tar, respectively. Additionally, Weissinger et al. [267] described the release of nitrogen compounds using FTIR spectroscopy. Both works refer to the importance of the determination of nitrogen gaseous compounds and that may serve as input profiles for CFD simulations. Bennadji et al. [268] and Nikku et al. [269] measured the fractions of light species from pyrolysis at low temperature and compared the reactivity of MSW with biomass and coal samples through the FTIR technique, respectively. Hu et al. [270] analyzed the influence of different atmospheres in the gaseous conversion using a mass spectrometer.

Table 9: Isothermal combustion and pyrolysis studies using the Macro TGA technique.

Author	Fuel	Temperature (ºC)	Flow Rate (L/min)	Mass (g)	Particle Size (mm)	Gas Analysis
Hu et al. [270]	Pellets	600 to 900	Different atmospheres, 0.1	0.4	8	MS
Nikku et al. [269] 2019	MSW, biomass and coal	700, 800, 900	Reduced O_2, 3	0.1	4	FTIR
Baumgarten et al. [271] 2019	Oak and Spruce	250 to 450	Air, NA	1	< 2	Not measured
Samuelsson et al [272] 2017	Spruce	300 to 400	N_2, 7	0.16-0.69	15-24	Not measured
Orang et al. [273] 2015	Cedar, Pine, Poplar, and Oak	400 to 800	Air, 1	1	15	Not measured
Brunner et al. [265] 2013	Beech, Spruce, Poplar and Wilow	450-750	Air, 30	147.4	Random	FTIR, NDIR, FID, CLD
Gauthier et al. [266] 2013	Beech	450 to 1050	N_2, 2	NA	20 x 30	Micro-GC and a FTIR
Bennadji et al. [268] 2013	Poplar	375, 418	N_2, NA	5.5	19 x 40	FTIR
Becidan et al. [264] 2007	Biomass Residues	600 to 900	N_2, 40	75	80-120	Micro-GC and a FTIR
Becidan et al. [274] 2007	Biomass Residues	600 to 900	N_2, 40	75	80-120	Not measured
Weissinger et al. [267]	Fibreboard waste	300 to 800	Air, ≈2,000	NA	NA	FTIR
Bruch et al. [275] 2003	Beech	500	N_2, NA	NA	8, 12 and 17	NA

CLD – Chemiluminescence Detector
FID – Flame Ionization Detector
FTIR – Fourier-transform infrared spectroscopy
GC – Gas Chromatography
MS – Mass Spectrometry
NDIR – Nondispersive Infrared Sensor

Although the quantification of the gaseous compounds released during the thermal conversion of biomass is not addressed, there are works in the literature where the conversion of biomass was analyzed separately through the Macro TGA technique. Baumgarten et al. [271] and Samuelson et al. [272] analyzed the combustion behavior under typical isothermal conditions in the start-up of furnaces. Orang et al. [273] observed the effect of moisture content on combustion behavior. The author highlighted the higher drying and the ignition times due to the increase of the moisture content.

Thus, Macro TGA experiments provide the possibility to control and maintain external heat fluxes, in order to better represent at small-scale the conditions from industrial boilers when compared with horizontal or lamp tube reactors presented in the literature [266].

2.4 CFD Modeling of Biomass Combustion in Industrial Grate-Fired Boilers

2.4.1 Strategies for CFD Modeling

CFD is the science of heat transfer, chemical reactions, and other related phenomena simulation by solving the mathematical equations which govern these processes using a numerical method [276]. All commercial CFD packages include sophisticated user interfaces to input important parameters and to present results. In this sense, basically, all CFD codes contain a pre-processor, a solver, and a post-processor [276]. Unquestionably, CFD simulations are a powerful and cost-effective tool for research, conceptual studies of new designs, detailed product development, troubleshooting, and redesign. However, the reliability of the results is highly dependent on the accuracy of the physical models adopted, as well as the boundary conditions considered. In this way, the numerical results must be carefully evaluated and, when possible, experimental validations should be performed.

In the specific case of combustion applications, CFD simulations allow a deeper analysis of the sub-processes occurring, by computing the local velocity, temperature, gas species concentration, and pressure losses, among other parameters. This analysis enhances the knowledge of sub-processes and allows the design and optimization of boilers, avoiding the trial and error approach usually applied by the power plant operator that offers no guarantee of success and it is time and cost consuming. The outcome of the improved combustion can be lower pollutant emissions, improved efficiency, increased plant capacity or/and reduced maintenance costs.

However, biomass combustion modeling in a boiler is a very complex process and suitable models are required because most of the CFD commercial packages are limited in handling the conversion of biomass as they are mainly designed to simulate the combustion of gaseous fuels. Thus, in most cases, the commercial software has to be complemented by self-written code for the fuel bed conversion. In this sense, CFD-based modeling approaches for biomass combustion systems are mainly composed of a bed model and the gas-phase simulation. Even though various studies concerning numerical investigations of biomass combustion systems are available in the literature, this makes CFD simulations of biomass combustion a niche application. This is why successful biomass combustion modeling in a boiler is considered a challenging task.

Nevertheless, over the last decades, CFD tools have been increasingly used for optimizing the combustion process, and they become essential in the boiler design and operation troubleshooting. Furthermore, CFD modeling can also be helpful to analyze different working conditions and to estimate a multitude of variables inside the whole domain, in particular, the pollutant emissions [277,278].

The bed model describes the thermochemical conversion of the biomass in the fuel bed of the combustion system, and it provides inlet information for the gas-phase simulation in the freeboard. This model includes aspects such as:

- Fuel properties (physical, chemical, and thermal).
- Biomass conversion process (drying, devolatilization, and char combustion).
- Gas-phase reactions inside the fuel bed.
- Physical changes (shrinking, collapsing, and channeling).
- Movement of the particles in the bed model for increased accuracy.

Fuel bed modeling is challenging because solid biomass is a heterogeneous fuel with regard to its properties (mainly its chemical composition, moisture, size, and shape). Therefore, there is no general approach that can be used for a biomass type as well as the combustion system. However, the objective of the simulation and the firing system has a crucial role in the bed model selection, since the products of solid fuel thermo-chemical conversion which have to be predicted by the bed model, will be used as the inlet boundary condition for the gas-phase simulation.

An overview of comprehensive simulations of biomass grate-fired boilers using moving grates is summarized in Table 10. This review was focused on large and industrial-scale biomass combustion boilers over a wide range of power and fuel. The type of biomass mostly used are woodchips, straw, and municipal solid wastes, and the thermal power ranges between 140 kW and 108 MW, including both pilot-scale and industrial firing systems. Different methodologies were used to describe the biomass conversion on the grate. The choice of the methodology for the CFD simulation depends mainly on the research question, the available computational resources, and available information about the process. Therefore, it is difficult to draw a general conclusion about which strategy or models are the most appropriate for biomass combustion simulation [214].

Table 10: Literature review of the numerical models used to model the biomass combustion systems in moving grates.

Author	Firing system	Methodology Biomass conversion	Gas-Phase						Validation
			Turbulence	Combustion mechanism	Turbulence-Chemistry interaction	Radiation	Additional models	Software	
Ruckert et al. [279] 2021	Grate-fired boiler	Eulerian Model	k-ε	2-step global reaction or 4 [280]	EDC	DOM	No	OpenFOAM	Yes
Yan et al. [281] 2021	MSW	2D bed model (FLIC)	Standard k-ε	Simplified mechanism with 4 reactions	FR-ED	DOM	Heat exchanger model	ANSYS Fluent	Yes
Mousavi et al. [282] 2021	Lab-scale boiler	External model [283]	k-ε	Detailed reaction mechanism	EDC	P1	NOx formation	OpenFOAM	Yes
Xia et al. [284,285] 2021 and 2020	MSW incinerator, 750 t/d	2D bed model	RNG k-ε	2-step global reaction	FR-ED	P1	-	ANSYS Fluent	Yes
Zhou et al. [286,287] 2021 and 2020	Grate-fired boiler	1D Dynamic model	Standard k-ε	2-step global reaction	FR-ED	P1, WSGGM	NOx formation	ANSYS Fluent	Yes
Karim et al. [288] 2020	4 MW grate-fired biomass furnace	Porous medium model	Standard k-ε	Simplified mechanism with 5 reactions	EBU	DTRM	-	AVL Fire 2014	Yes
Netzer et al. [289] 2020	230 kWth grate boiler	0D stochastic reactor model	Standard k-ε	Detailed reaction mechanism	EDC	P1	-	OpenFOAM	Yes
Zadravec et al. [290] 2020	13 MWth grate boiler	1D Empirical model	Realizable k-ε	2-step global reaction	FR-ED (A=0.6 and B=0.5)	DOM, WSGGM	-	ANSYS Fluent	Yes
Bermúdez et al. [291] 2020	4 MW grate-fired biomass furnace	Porous medium model	Realizable k-ε with EWT	Simplified mechanism with 6 reactions	FR-ED (A=2.0 and B=0.5) [292]	DOM (modified)	-	ANSYS Fluent	Yes
Jiang et al. [293] 2020	WTE plant	1D Walking-column model	RNG k-ε	Simplified mechanism with 3 reactions	ED	P1 model		ANSYS Fluent	Yes

Table 10: (continued)

Author	Firing system	Methodology Biomass conversion	Gas-Phase						Validation
			Turbulence	Combustion mechanism	Turbulence-Chemistry interaction	Radiation	Additional models	Software	
Somwangt-hanaroj et al. [294] 2019	6.7 MWe power plant	Particle model	Realizable k-ε with EWT	Detailed reaction mechanism	-	DOM	NOx formation	ANSYS Fluent	Yes
Zhou et al. [295–297] 2019 and 2018	Grate-fired boiler	1D Dynamic model [298]	Standard k-ε	Simplified mechanism with 4 reactions	FR-ED	P1 model	-	MFIX [299] and ANSYS Fluent	Yes
Rezeau et al. [300] 2018	250 kWth boiler	Porous medium model	Realizable k-ε	Simplified mechanism with 4 reactions	FR-ED	P1 model, WSGGM	-	ANSYS Fluent	Yes
Tu et al. [301,302] 2018 and 2017	Grate-fired boiler	1D Empirical model	Standard k-ε	Simplified mechanism with 3 reactions	FR-ED	DOM, WSGGM	NOx formation	ANSYS Fluent	Yes
Patronelli et al. [303] 2018	140 kW fixed-bed boiler	Perfectly stirred reactor and Porous medium model	Standard k-ε	2-step global reaction	EDM	P1 model	-	ANSYS Fluent	Yes
Caposciutti et al. [304] 2018	140 kW fixed-bed boiler	Porous media model	Standard k-ε	2-step global reaction	EDM	P1 model	-	ANSYS Fluent	Yes
Mätzing et al. [305] 2018	Pilot-scale grate combustor and WTE plant	1D reactor cascade model	Standard k-ε and SWT	Simplified mechanism with 6 reactions	FR-ED (A=1.0 and B=0.5)	P1 model	-	ANSYS Fluent	Yes
Rajh et al. [306,307] 2018 and 2016	13 MWth grate boiler	2D steady model [308]	Realizable k-ε with EWT	2-step global mechanism	FR-ED (A=0.6 and B=0.5)	DOM	-	ANSYS Fluent	Yes
Ahn et al. [309,310] 2018	230 kWth grate boiler	Empirical conversion	Standard k-ε	2-step global mechanism	FR-ED	DOM	-	ANSYS Fluent	Yes

Table 10: (continued)

Author	Firing system	Methodology Biomass conversion	Gas-Phase						Validation
			Turbulence	Combustion mechanism	Turbulence-Chemistry interaction	Radiation	Additional models	Software	
Karim et al. [311] 2018	4 MW moving grate boiler	Porous medium model	Standard k-ε	Simplified mechanism with 5 reactions	EBU	DTRM	-	AVL Fire 2014	Yes
Costa et al. [312,313] 2018 and 2016	RDF incinerator	Empirical 0D model	SST k-ω	2-step global reaction	EDC	P1 model	-	ANSYS Fluent	Yes
Costa et al. [314–316] 2015, 2012 and 2009	Waste-to-energy plant	2D bed model (FLIC) [317]	k-ε	2-step global reaction	EDM	-	-	ANSYS Fluent	Yes
Wissing et al. [318] 2017	MSW plant	In-house DEM code [319,320]	SST k-ω	-	EDM	P1 model	-	ANSYS Fluent	Yes
Duffy et al. [321,322] 2016 and 2013	Grate furnace	2D porous medium model	Standard k-ε	Mechanism of Westbrook and Dryer [323]	EDM	Not included		ANSYS Fluent	Yes
Mahmoudi et al. [324] 2016	Forward acting grate	DEM model			Not specified			OpenFOAM	Yes
Galleti et al. [325] 2016	Moving grate	Empirical bed model	Standard and Realizable k-ε, and k-ω model	2-step global reaction	EDM	P1, WSGGM	-	ANSYS Fluent	Yes
Chen et al. [326] 2015	500 kW boiler	2D bed model (FLIC) [317]			Not specified			ANSYS Fluent	No
Cordiner et al. [327] 2014	50 MWth furnace	3D bed model	Standard k-ε	-	Partially Stirred Reactor model	P1	NOx formation	OpenFOAM	Yes
Shiehnejadhesar et al. [328] 2013	180 kWth moving grate furnace	1D Empirical model	Realizable k-ε	Simplified mechanism with 3 reactions	EDM	DOM	-	ANSYS Fluent	Yes
Kurz et al. [329,330] 2013 and 2012	240 kW moving grate	Porous medium model	Standard k-ε	Simplified mechanism with 3 reactions	EDM	DOM	-	AIOLOS	Yes

Table 10: (continued)

Author	Firing system	Methodology Biomass conversion	Gas-Phase						Validation
			Turbulence	Combustion mechanism	Turbulence-Chemistry interaction	Radiation	Additional models	Software	
Yin et al. [331] 2012	Vibrating grate, 88 MW	Empirical bed model	Standard k-ε	2-step global reaction	FR-ED (A=0.6 and B=0.5)	DOM	-	ANSYS Fluent	Yes
Jordan et al. [332] 2010	1.5 MW pilot-scale unit	Porous medium model	SST k-ω	Mechanism with 30 reactions [333]	EDC	P1, WSGGM	-	FLUENT	Yes
Zhang et al. [334] 2010	Moving grate	2D bed model (FLIC) [317]	Standard k-ε	-	-	P1 model	NOx formation	FLUENT	Yes
Yu et al. [335] 2010	Vibrating grate	2D bed model (FLIC) [317]	RNG k-ε	-	-	DTRM	NOx formation	FLUENT	Data from Kaer [336]
Venturini et al. [337] 2010	Moving grate	2D bed model based on [338]	Low Reynolds k-ε model	Detailed reaction mechanism	Flamelet approach	-	Particle transport and deposit formation	XENIOS++	Data from Shin and Choi [338]
Simsek et al. [339] 2009	Moving grate	In-house DEM code [319,320]			Not specified			ANSYS CFX	No
Yin et al. [340] 2008	Vibrating grate 108 MWth	Empirical bed model and 2D model [341]	Standard and Realizable k-ε	2-step global reaction	FR-ED	DOM, WSGGM	-	ANSYS Fluent	Yes
Klason et al. [342,343] 2008 and 2006	50 MW grate fired furnace	Semi-empirical bed model	k-ε	Simplified mechanism with 6 reactions	EDC	DTRM	NOx emissions	Own numerical code [344]	Yes
Yang et al. 2007 [345]	Moving grate, 25 MWe	2D bed model (FLIC) [317]	Standard k-ε	Simplified mechanism with 3 reactions	-	DOM	-	FLUENT	No
Yang et al. [346] 2007	Vibrating grate 25 MWe	2D bed model (FLIC) [317]	Standard k-ε	2-step global reaction	EBU	DOM	-	FLUENT	Data from Kaer [336]
Kær et al. [347] 2006	Vibrating grate 33 MWth	2D walking-column model [348]	RNG k-ε	2-step global reaction	EBU	DOM, WSGGM	Deposit formation model	FLUENT	Yes
Goerner et al. [349] 2006	MSW pilot installation and industrial boiler	Empirical bed model	Realizable k-ε	2-step global reaction	EBU	P1 model	-	FLUENT	Yes

Table 10: (continued)

Author	Firing system	Methodology Biomass conversion	Gas-Phase						Validation
			Turbulence	Combustion mechanism	Turbulence-Chemistry interaction	Radiation	Additional models	Software	
Goddard et al. [350] 2005	Forward-reciprocating grate, 25 MWe	2D bed model (FLIC) [317]	SST k-ω	Simplified mechanism with 3 reactions	EDC	DOM, WSGGM	-	FLUENT	Yes
Huttunen et al. [351] 2004	Moving bed, 1 MW	1D bed model	Standard k-ε	2-step simplified reaction	EDC	DOM, WSGGM	-	FLUENT	No
Kær et al. [336] 2004	Vibrating grate 33 MWth	2D bed model, stand-alone code	RNG k-ε	2-step simplified reaction	EBU	DTRM	-	CFX	Yes
Frey et al. [352] 2003	Reciprocating grate, 500 kW	Experimental measurements as input	k-ε	-	EBU	-	-	FLUENT	Yes
Scharler et al. [353,354] 2003 and 2000	Travelling grate furnace	Empirical model	Realizable k-ε	Global methane three-step reaction mechanism	FR-ED (A=0.6 and B=0.5)	DOM	-	FLUENT	Yes
Ryu et al. [355] 2002	Moving bed	1D bed model	RNG k-ε	Simplified mechanism with 3 reactions	EDC	DOM, WSGGM	-	FLUENT	No
Griselin et al. [356] 2000	40 MW grate fired boiler	Empirical bed model and experimental measurements	k-ε	Simplified mechanism with 4 reactions	EDC	DTRM	Particle dynamics	Own numerical code [344]	Yes
Kim et al. [357] 1996	MSW incinerator	Properties from measurements	k-ε model	Not modeled	Not modeled	DTRM	-	FLUENT	No

DEM – Discrete Element Method
DOM – Discrete Ordinates Model
DTRM – Discrete Transfer Radiation Model
EDC – Eddy Dissipation Concept
EDM – Eddy Dissipation Model
EBU – Eddy Break-Up model
EWT – Enhanced Wall Treatment
FLIC – FLuid Incinerator Code
FR-ED – Finite Rate-Eddy Dissipation model
RNG – Re-Normalization Group
SST – Shear Stress Transport
SWT – Standard Wall Treatment
WSGGM – Weight-Sum-of-Gray-Gases Model

After this careful scientific literature review it was found that the current approaches to solid biomass combustion modeling on industrial grate-fired boilers can be assigned to the following groups:

1. Results from experimental measurements defining the boundary conditions to the CFD model [352,356,357].
2. External bed model computing the boundary conditions to the CFD model.
3. Incorporation of a bed model in the CFD model.

The external bed model can be classified as Empirical (e.g. [301,302,360,312,342,343,353,354,356,358,359]), which means that often are experience-based on conversion rates along the grate, or Separate (e.g. [306,307,361–366,315,326,327,337,346,350,351,358]) when there is a mathematical model describing the biomass conversion dependent or not the freeboard conditions. In its turn, the inclusion of the bed model can follow two different categories: Discrete particle method (DPM) based bed models (e.g. [294,324,339,367]) or Eulerian/Porous medium bed models (e.g. [291,300,303,311,321,329,330,368,369]). Thus, the computational effort of the bed model is a challenging issue when a comprehensive simulation of biomass combustion in grate-fired boilers is required, as a gas-phase simulation already demands significant resources. The level of detail of the bed model tends to be lower, and empirical or separate bed models are preferred. However, with the rapid development of computer hardware and numerical methods, the level of detail of bed models increased significantly over the last few years. Consequently, the inclusion of the bed model into the computational domain of the gas-phase simulation has become more common allowing for a significant improvement in the description of chemical and physical processes involved in the grate. A high percentage, around three-quarters, of the literature reviewed used an external bed model to compute the boundary conditions necessary to perform the CFD simulation (e.g. [353,354,361]), and the remaining works used a CFD model with an internal bed model.

Additionally, taking into account the previous groups, from the implementation point of view, there are two main approaches commonly followed in CFD simulation of fixed-bed biomass boilers to account for the conversion of the solid particles in the bed [277,278]. The first approach is to develop a model that predicts the evolution of the thermal conversion of the bed and, in doing so, the inlet conditions for the gas phase modeling in CFD simulations will be computed (e.g. [353,354,361]). With this approach, the combustion process in the bed and in the gas-phase is treated separately. However, due to the empirical nature of these models, they do not allow full capture of important aspects and the influence of physical

phenomena occurring in the boiler, in particular in the bed, cannot be considered. Figure 13 presents two different models used from this first approach.

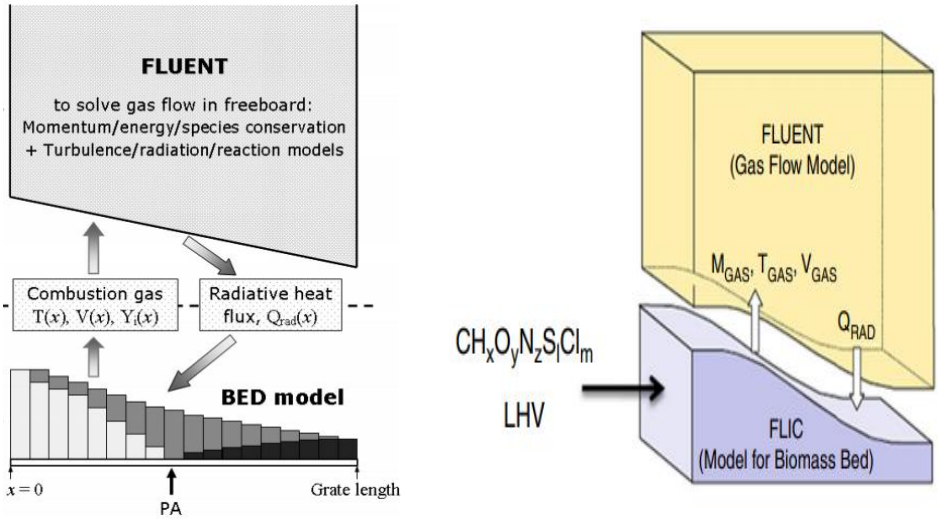

Figure 13: Schematic representation of different modeling methodology for biomass grate-fired boilers: a) One-dimensional "walking-column" transient model [358] and b) FLuid Incinerator Code – 2D bed modeling program [366].

In contrast, the second approach fully integrates the bed region in the CFD simulations (e.g. [291,311,329,368]). This method avoids the separation of the bed and the gas-phase, allowing for the treatment of the interactions between the gas and solid phases on the surface of individual particles and the movement of the bed particles is treated in the same software or separately using a discrete element method [294,324,339,367]. In general, this is the most complex approach and, the solid phase is integrated through the use of User Defined Functions (UDFs), compiled in the CFD codes, which essentially characterize the thermal conversion of the solid particles and the interactions between solid and gas phase within the fuel bed.

Such UDFs describe the drying, devolatilization, and char combustion processes. Figure 14 presents two case studies using the second approach. In Figure 14 a) the aim is to represent every single particle present on the grate, whereas in the other approach, Figure 14 b), the ensemble of particles in the bed region is treated only in average terms [72,370]. The first one, Figure 14 a), is generally referred to as the DPM approach, where the Discrete Element Method (DEM) is extended to predict the particle movement, conversion, and the heat and mass exchange between the solid- and gas-phase. This can be directly obtained from the individual contributions of each particle present in the computational cell. In

the other approach, denoted as the Eulerian model, the exchange between the phases has to be modeled for a representative particle [46,255]. Hence, according to the literature, the simulation of multiphase flow phenomena can be addressed by one of these two different categories which can be defined as pure Eulerian models and the coupling of Eulerian and Lagrangian models.

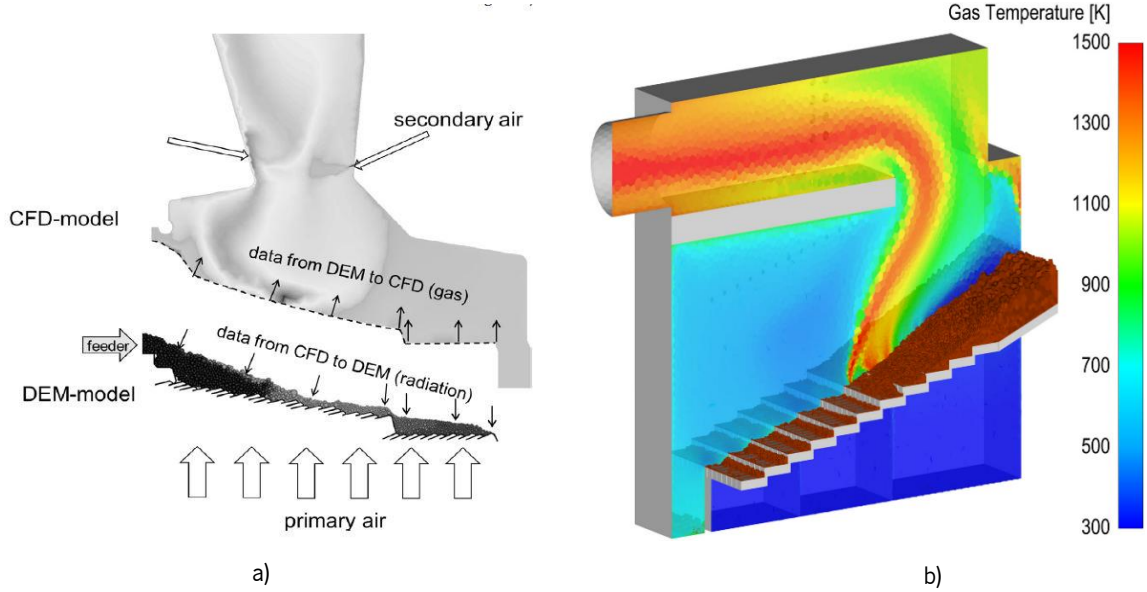

Figure 14: Diagram of a) DEM/CFD coupling [367] and b) Bed model fully integrated into the CFD simulation domain methodology applied by Bérmudez et al. [291].

Therefore, the first category, like the model presented in Figure 14 b), treats all phases as a continuum on a macroscopic level and they are suited for computational efficiency. However, due to the averaging of data as the size, shape, and material properties of individual particles are lost. Furthermore, it avoids the representation of gas streaks since the flow is homogenized [292]. The methods of the second category, in which the model in Figure 14 a) is one this example, include engineering applications where dense beds are presented, such as packed beds from the thermal conversion processes where there is a complex interaction process between the fluid and solid phases due to the thermochemical conversion. This interaction is combined by mass, momentum, and energy transfer between the different phases.

2.4.2 Gas-phase Modeling

For the gas-phase simulation, already well-established by CFD methods, includes turbulence, combustion (chemical reactions and mechanism), and radiation models. Moreover, in many cases, the objective of CFD simulations is the pollutant emissions modeling and additional models need to be added to the CFD simulation. These additional models include mainly NOx formation and particulate emissions models. A majority of the CFD models reported in the literature were developed in the ANSYS Fluent software. Figure

15 presents the overall structure and the key modules of CFD modeling of biomass combustion in grate-fired boilers.

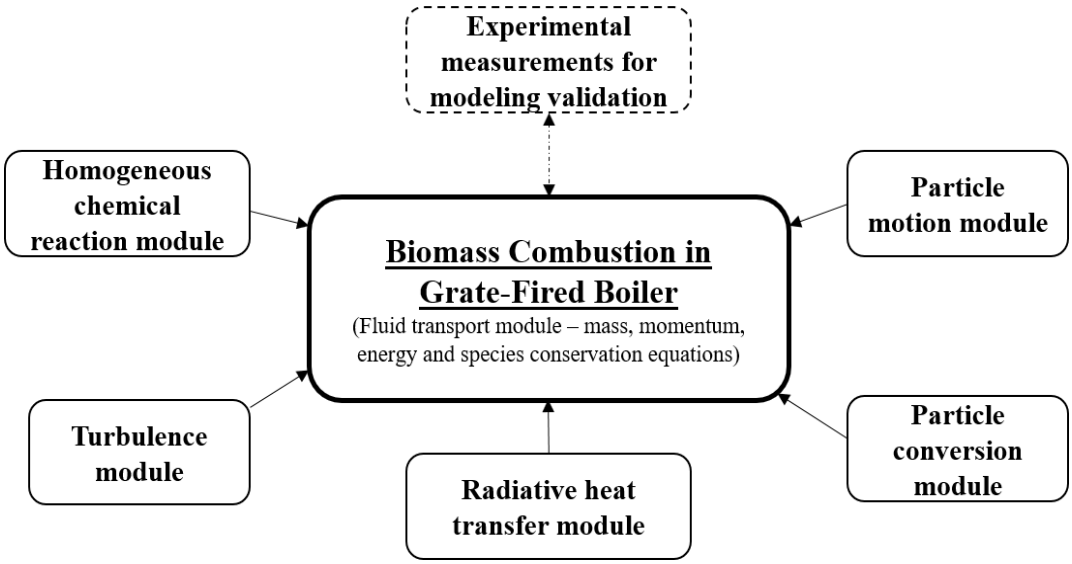

Figure 15: An overview of the basic modules used in CFD modeling of biomass combustion in a grate-fired boiler.

Hence, models for turbulence, radiation, reaction mechanism, and the turbulence-chemistry interaction are included to simulate the all gas-phase phenomenon within the full geometry of the industrial grate-fired boiler.

As with the great majority of flows in industrial processes, turbulence plays an important role in industrial boilers due to their influence on the transport and mixing of the fuel and oxidizer. Although it can be very arguable which turbulence model better handles a real problem, under the Reynolds-Average Navier-Stokes (RANS) modeling framework, the two-equation standard k-ε model is the most commonly used in the literature. In this model, proposed by Launder and Spalding [371], the turbulent velocity and length scales are independently determined with a low computational cost, reasonable accuracy, and robustness when compared with the other two-equation models [214]. Kurz et al. [329,330] and Venturini et al. [337] are examples of works in the literature that modified the standard k-ε model to account for the influence of particles on turbulence and low turbulence regions.

Regarding the radiation, it is often the dominant heat transfer mechanism in industrial furnaces due to the high temperatures present, and, therefore, the radiative intensity should be computed. The Discrete Ordinates and P1 models are widely applied in grate-fired boilers simulation to solve the radiative transfer equation. The former is computationally expensive but applies to all optical thickness whereas P1 is less demanding but only applicable to optically participating medium [214]. However, in the literature, there

are some authors that neglect the effect of thermal radiation. This simplification leads to saving computational costs since the radiation models are computationally costly. Examples of this simplification are common in the simulation of gasifiers. For instance, Lu et al. [372] demonstrated that temperature and volatiles composition predictions with no radiation model are very similar to the results of the simulation with P1 and Discrete Ordinates model.

In addition to the two previous phenomena, in biomass combustion, as already mentioned, volatiles play an important role in the conversion process and pollutant formation. Thus, the accuracy of the CFD model also relies on the details of the combustion mechanism. A usual assumption in the gas-phase combustion modeling is that the reactions are kinetically fast just above the fuel bed, where the temperature is typically high in some parts of the grate and the reactions are fast. Consequently, the combustion is only controlled by the mixing rate of the oxidizer and the volatiles. However, there are areas where the temperature is lower and, the kinetics of gas-phase reactions will become the restricting mechanism. This phenomenon can be addressed by employing the Finite Rate model, where the minimum value between kinetics and mixing is the factor that limits the reaction rate [340,373]. This model is frequently used together with the Eddy Dissipation model, which was developed by Magnussen and Hjertager [374,375] to compute the limiting chemical reaction rate. This model was developed and validated for combustion with strong turbulence. However, as inside industrial boilers, there are some regions with low turbulence, mainly near the bed, the chemical reactions are influenced by the turbulent mixing of the flue gas since due to the high temperatures, kinetic limitations are less significant [376]. Therefore, as the bed affects the gas flow, damping the turbulence, there are some authors that modified the Magnussen parameter to account for the effect of the particles over the turbulence and, consequently, obtain a better turbulence–chemistry interaction [305,306,331,353,377–379].

Considering the combustion reactions, they are highly complex and are commonly simplified into a series of global reactions. There are only a few publications considering detailed chemical reactions. Thus, the most applied reaction scheme is the 2 global reactions. An example is the 2 step hydrocarbon oxidation (Equation (13) and (14)) from Westbrook and Dryer [323].

$$CH_4 + 1.5\,O_2 \rightarrow CO + 2\,H_2O \quad (13)$$

$$CO + 0.5\,O_2 \leftrightarrow CO_2 \quad (14)$$

Another alternative commonly applied is a 4 reaction scheme, and a popular mechanism is from Jones and Lindstedt [280] taking methane as the hydrocarbon (Equation (15) to (18)).

$$CH_4 + 0.5\,O_2 \rightarrow CO + H_2 \quad (15)$$

$$H_2 + 0.5\,O_2 \leftrightarrow H_2O \quad (16)$$

$$CH_4 + H_2O \rightarrow CO + 3\,H_2 \quad (17)$$

$$CO + H_2O \leftrightarrow CO_2 + H_2 \quad (18)$$

These gas-phase reactions can be easily modeled in CFD using the species transport model.

2.5 Overview and General Comment of the Research Status

Biomass combustion for heat and power has seen rapid progress in both research initiatives and in market oriented applications. In the previous sections, details regarding the major issues and achievements in biomass combustion, their characterization, and the current state-of-the-art for the modeling of large-scale grate-fired boilers were explored and presented. As it was noticed, grate firing systems are widely used in combustion due to their capability to burn a broad range of fuels and with the main principle to transport the fuel along the full length of the grate provided by grate movements and being able to have enough space for burning the particles. The difficulties and costs in performing experiments highlight the increase in the interest and necessity for a CFD analysis. Furthermore, the advances and constant improvement of computer performance also contributed to an increased role of CFD applications. Despite this significant attention in this field, improvements are still needed to make large-scale grate-fired boilers modeling affordable. Since various simplifications and assumptions have to be made to simulate a complete combustion system, some recommendations can be identified based on this comprehensive review. Biomass conversion on the grate plays a key role in the overall performance of grate-fired boilers (for instance: combustion efficiency, pollutant emissions, and deposition) and several simplifications are necessary to keep the model numerically efficient. For this purpose, a set of equations describing the heat and mass transfer, and chemical reactions in the fuel bed on the grate, is required. To develop a reliable CFD model for grate-fired boilers, the quality of the inlet boundary conditions, mesh, models, and the numerical methods all play important parts and must be correctly accounted for. The numerical results should be always validated with experimental data. Experimental measurements are an important aspect as they can provide the operating conditions, which cannot deviate from the normal state, and will be important to validate the numerical model [248]. Despite these facts, some details of the grate-firing systems are not readily accessible and uncertainties with the details in biomass-fired grate

boilers challenge the modeling, operation, optimization, and mainly, the validation of the numerical model. Phenomena such as combustion instabilities in the fuel bed (local burnouts, channeling formation, and spatially uneven fuel-bed thickness); non-continuous biomass feeding and grate movement, and irregular deposits on the furnace walls and air nozzles have to be considered when experimental measurements are being conducted to validate the numerical model.

Unquestionably, simplifying premises cannot be avoided due to the computational resources when a reliable model should be obtained, and, consequently, has to include the most important phenomena taking place in an industrial grate-fired boiler. The bed conversion defines the central key problem that should be explored and studied in detail since it plays a key role in the overall performance of a grate-fired boiler. However, there is a strong dependency on the particles conversion, combustion, and their motion on the grate. Due to the complexity of the entire process as there are different and many physical and chemical phenomena occurring at the same time, considering the previous literature survey, further research is required to better understand the complexity of biomass conversion on a vibrating grate.

The main process occurring during the particle conversion is the devolatilization, and it is specifically in this stage where there is the main drawback and stiffness of the main CFD models. It is necessary to know the composition, the amount of pyrolysis products in different thermal conditions of the reactor, and the reaction rate of the particles. A recent investigation mentioned that numerical prediction inside a grate-fired boiler depend on the devolatilization kinetics mechanism and that can significantly affect the outputs from the bed model [293]. Most of the CFD models usually employed biomass elemental composition and enthalpy conservation equation or models like the proposed by Thunman et al. [246] and Neves et al. [380] to determine the composition of pyrolysis products (e.g. [46]). However, the results of this type of approach can produce unrealistic results. Therefore, there is a clear need to use TGA and macro-TGA techniques to gain a full insight into the devolatilization behavior of biomass. Both techniques provide complementary information about kinetic mechanisms involved in the thermal decomposition and volatiles composition. Another alternative to define the composition of the flue gas can be based on the experimental measurements. However, experiments during the operation of industrial boilers are difficult and expensive to carry out and the alternative is to conduct experiments at certain temperatures in a small reactor and use these results for the simulations [267,381,382].

In addition to the contents presented in this chapter, there are five important review articles discussing the state-of-the-art status of process simulations of biomass thermochemical conversion. Dernbecher et al. [214] gave a comprehensive overview of simulations of biomass combustion systems focusing on

systems with fixed bed, and covers various technologies (moving bed, pellet boilers, wood log stoves). Rahdar et al. [248] reviewed the current state-of-the-art literature dealing with numerical modeling and experimental analysis of moving grate biomass combustors. Haberle et al. [53] reviewed the state-of-the-art of numerical models used for thermochemical degradation and combustion of thermally thick woody biomass particles. The focus is on their implementation in numerical simulation tools. Khodaei et al. [383] provided a fundamental overview of the methodologies employed in the modeling of laboratory-scale fixed-bed combustors. The paper also includes treatment of the fundamental thermo-physical fuel characteristics which need to be considered when undertaking macro-scale (bed-level) modeling. Yin et al. [32] summarized the state-of-the-art knowledge on grate-fired boilers burning biomass: the key elements in the firing system and the development, the important combustion mechanism, the recent breakthrough in the technology, the most pressing issues, the current research and development activities, and the critical future problems to be resolved.

In conclusion, from this literature analysis, it can be stated that by having a proper model describing the different phenomena associated with the conversion on the grate, an accurate numerical model can be achieved.

CHAPTER 3

INDUSTRIAL GRATE-FIRED BOILER: CASE STUDY

In this chapter, the object of study, the biomass power plant, and the main results from an experimental campaign to evaluate the combustion performance are presented. The power production process at the power plant is described from the reception of biomass to the combustion gases leaving the chimney. The experimental campaign took place during a 12 days period, and included an analysis of the historical data. During such activity, a detailed physical and chemical analysis of the biomass as well as the monitoring of the flue gas emissions with the boiler control analytical instruments were carried out. Additionally, a set of experiments to study the influence of the primary air distribution on the grate and the time between grate vibrations were performed. This analysis mainly covers the combustion process on the grate. Furthermore, the results of this industry-academic collaboration, with the purpose to understand and improve the power generation led to the analysis of one strategy to increase the overall efficiency of the power plant unity: the identification of the flue gas lower limit temperature. Consequently, the operating conditions and the possibility to reduce the flue gas temperature were explored with promising results to improve the power plant efficiency.

3.1 Plant Description

The fulfillment of energy targets in relation to the use of renewable energy has been a strong incentive for the development of thermal plants that use biomass. Since these facilities operate with low-value waste, this orientation has also received a strong incentive to remove the excess of fuel in the forest and reduce the risk of fire. Although initially, the number of plants planned for Portugal was very large, the actual number of units in operation is small. The first plant of this type entering into production in Portugal was the Mortágua power plant (Figure 16) that uses mainly forest residues. This plant is embedded in the forest, which is an advantage, keeping low the shipping costs of the fuel. Its installed capacity is rated at 10 MW, and it was designed to operate 7,800 h/y and deliver approximately 60 GWh/y to the mains electric power. Fuel is supplied from various sources within approximately a 50 km radius.

This power plant operates according to the Regenerative Rankine Cycle (Figure 17). This thermodynamic cycle is made up of a boiler, a turbine/generator (turbine type: C634AR), a condenser, a deaerator besides various pumps that allow the fluid to move along the thermodynamic cycle. The cycle operates at a pressure of 42 bar and 422 °C superheat, and the condensation pressure is 0.0798 bar.

Figure 16: The Power Plant of Mortágua [384].

Legend:

CT – Cooling Tower
G – Generator
P – Pump
PH – Preheater
T – Turbine

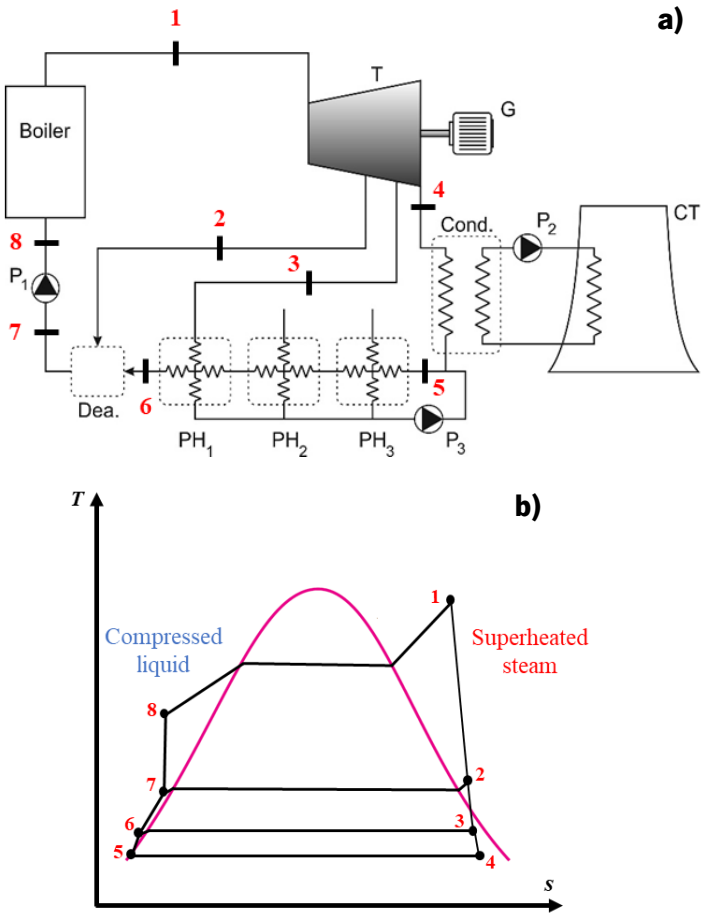

Figure 17: Schematic diagram of the power plant: a) Rankine cycle and b) Temperature-Entropy diagram.

In this plant, firstly, the biomass received is shredded and stored in a specific area where there is a weighing station. Then, the fuel is transported by conveyor belts to a moving grate. Subsequently, the fuel is introduced into the boiler, more specifically, on a vibrating grate, where the conversion of chemical energy of the biomass into heat energy takes place. Furthermore, the ashes, unburnt, and silica agglomerates, with great hardness, are formed during the biomass combustion process, and they are collected in a wet ashtray.

In the boiler, high-pressure steam is generated which is then fed into the condensation turbine (with extractions), directly coupled to a generator (97% efficiency). The boiler also has auxiliary natural gas burners, which are used in start-up situations or if there is a break in the biomass supply.

Flue gases released from the combustion chamber have high temperatures of approximately 1,000 °C. On its way to being released through the chimney to the outside, its energy will be transferred to the water/steam circulating inside the boiler heat exchangers (Figure 18). In brief, the combustion

gases generate the steam through three different heat transfer surfaces before being released into the atmosphere. Preheating before the boiler is carried out in three preheaters (PH) (that draw energy steam from the small streams of steam used in the turbine sealing and drains and form a direct bleed from the turbine at 0.4 bar) and the deaerator (direct bleed turbine at 4 bar). The preheating raises the temperature from the condensing temperature to 143 °C.

The turbine expands the steam to the condenser pressure (0.0798 bar), and just upstream of the turbine, the superheated steam is throttled from 46 down to 42 bar. The steam is then entirely condensed in a condenser, transferring the heat to a cooling tower through a closed water loop. In the turbine, there are two extractions. In the first one, the steam is directed to the deaerator (4 bar, 1.226 kg/s) and, in the second extraction, the steam is used to heat the previously condensed water (0.4 bar; 0.498 kg/s). These values refer to the nominal thermal load.

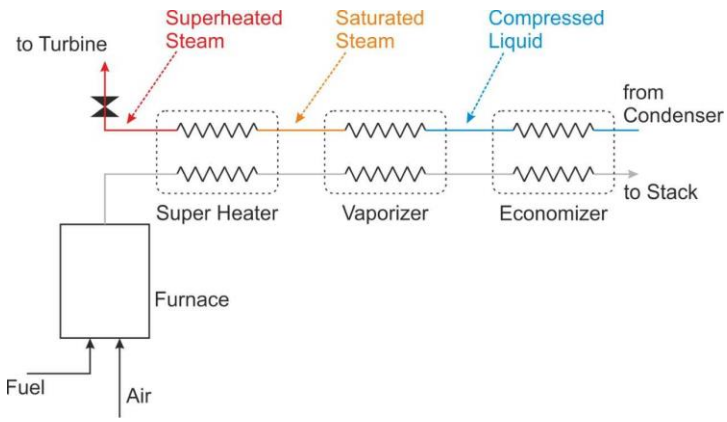

Figure 18: Schematic diagram of the interaction of flue gases and water/steam.

3.2 Experimental Characterization

In addition to the fuel characterization, the boiler's operating conditions, temperatures at the different heat exchangers, and flue gas emissions were monitored for a period of 12 days. This information is available on the plant's computer system, where the operators can view and control any part of the process. The main operating conditions were recorded using this system.

In this regard, to obtain information about the plant's performance, data from meters installed on the combustion chamber and other positions, along with the flue gas and water/steam circuit, were collected. Detailed physical and chemical analysis results on the biomass fed to the power plant in the winter

(February) and summer (June and August) seasons have been carried out. Additionally, the oxygen level, carbon monoxide, and nitrogen oxide concentrations in the flue gases were also measured with the boiler control analytical instruments and recorded by the plant's computer system.

The plant's computer system, where plant information and controls are displayed on graphics screens, consists of programmable logic controllers containing all software to manage and regulate the entire power plant. The plant' operators can view and control any part of the process from the computer screens while retaining a plant overview. This system was used to record the main operating conditions. Tables 11 and 12 present the information about the equipment used to assess the combustion performance and the methodology applied to characterize the fuel composition. The moisture of the fuel was evaluated using the moisture analyzer KERN DBS 60-3 (repeatability – 0.02%).

Table 11: Information about the equipment used to perform the characterization of the combustion performance.

Measurement	Equipment	Range	Accuracy
Gas Emissions	ABB Endura AZ20 O_2 Analyzer	0.01 to 100 % O_2	< ± 0.75 %
	ABB URAS 14 Analyzer (Another flue gas)	20 to 100 liters/h	≤ 1%
Temperature	K Thermocouple	Max: 1200 °C	± 0.004 °C
Air Flowmeter	ITABAR Flow Sensor – IBR-26 (primary air fan)	Max: ≈ 10,040 m^3/h	± 1 %
	ITABAR Flow Sensor – IBR-26 (secondary air fan)	Max: ≈ 6, 336 m^3/h	

Table 12: Methods used to characterize the fuel.

	Parameter	Standard/Methodology
Physical characterization	Moisture	ISO 18134-1:2015
	Ash	ISO 18122:2015
	Particle Size	ISO 17827-1:2016
Chemical characterization	Carbon	ISO 16948:2015
	Hydrogen	ISO 16948:2015
	Nitrogen	ISO 16948:2015
	Oxygen	ISO 16993:2016
	Sulfur	ISO 16994:2016
	Chlorine	ISO 16994:2016
Heating Value		ISO 18125:2017

In addition to the experimental data analysis, a set of experiments to study the influence of some parameters were performed. Typically, in industrial grate-fired boilers, the grate, where the combustion

occurs, is composed of multiple under grate air compartments with separate dampers for the operator to bias the primary air in the area of the furnace where the fuel is concentrated. In this way, the amount of direct air can be adjusted to promote the drying of the fuel, the release of the volatiles, and provide the oxygen necessary for the combustion of the remaining char on the grate. A conventional opening percentage of the dampers in the three different grate sections (60-80-0%) was first assessed. Then, the influence of the supply more air in the first and last part of the grate was evaluated using the configurations of 90-90-0% and 50-90-30%.

The time between grate vibrations is another parameter that the operators can adjust to convey and distribute the fuel evenly and a continuous discharge of fuel ash. Consequently, problems like channeling flow and bed-level instabilities can be prevented with a proper grate vibration cycle. Therefore, these two parameters were studied to understand their influence on combustion behavior. It is also important to point out that the boiler manufacturer recommends the typical cycle of intermittent vibration between approximately 5 to 20 seconds of vibrating up to 30 minutes intervals. This interval depends on the fuel and the thermal load of the grate. Consequently, three different intervals (3, 10, and 15 minutes) between vibration periods are evaluated to understand their influence on combustion performance. Regarding the primary air dampers, since typically more air is supplied in the first sections of the grate, three different configurations of the valve opening percentage are evaluated to understand the influence of the supply less and/or more air in the first and last section of the grate.

3.3 Fuel Characterization

Biomass procurement deals with various forest operators and, consequently, the fuel burnt, and its quality varies enormously through the year. The fuel used consists of approximately 80% of forest residues (mainly eucalyptus) and 20% of non-contaminated wood wastes such as residues from pine and acacia woods. Table 13 presents the composition of the main species, including the moisture content (on a mass basis), used in the power plant. The actual elemental analysis is from a particular batch of fuel that is feeding the plant is also presented.

The fuel used in the power plant is, therefore, highly heterogeneous, being eucalyptus the dominant specie, and the heating value is strongly affected by its moisture content. For this reason, the moisture content and the inert quantity are monitored continuously to adjust the real fuel heating value. Furthermore, natural gas is used as a start-up and a regulation fuel in a co-combustion process with biomass.

The biomass feeding system in the boiler is performed by gravity, from a small silo fed by a hopper. Inside the boiler, a movable grate receives biomass, providing the vibrating grate where combustion takes place. The vibration cycles and their duration are manually fixed, with typical values of 2 minutes and 2.5 seconds. It should also be mentioned that biomass feed control is carried out by two controllers, one for the fuel delivery rate and another for the feed grate speed. The boiler has a thermal power of approximately 35 MW, and its minimum efficiency is 81%. The maximum reference flow of biomass rate is 12.2 t/h for the full load and 40% moisture. The main combustion parameters are presented in Table 14.

Table 13: Composition of the main fuels used in the power plant.

Parameter	Acacia dealbata		Pine		Eucalyptus	
	Chips*	Branches	Chips*	Branches	Chips*	Branches
Moisture (%)	29.40	28.50	51.10	60.40	47.80	41.40
Ashes (% db)	0.60	2.30	0.30	2.20	3.20	0.50
Carbon (%)	48.61	52.33	50.89	51.69	53.49	48.68
Hydrogen (%)	7.06	7.32	7.59	6.90	7.06	6.91
Nitrogen (%)	0.44	2.04	0.27	0.87	1.11	0.26
Sulphur (ppm)				≤100		
HHV (MJ/kg)	18.98	21.85	19.81	20.89	22.74	19.06
LHV (MJ/kg, db)	17.45	20.27	18.17	19.40	21.21	17.55
LHV (MJ/kg, ar)	11.60	13.79	7.65	6.20	11.42	7.99

* without bark
ar – as received
db – dry basis
HHV – Higher Heating Value
LHV – Lower Heating Value

Table 14: Nominal operating conditions.

Parameter	Value
Fuel flow rate (kg/h)	12,200
Primary air flow rate (m^3/h)	33,150
Secondary air flow rate (m^3/h)	13,250
Excess air (%)	40

The monitoring and control of fuel particle size distribution is essential to achieve complete and efficient combustion. Thus, two samples, with around 1 kg and 0.4 kg, were collected to characterize the physical dimension of the biomass. Figure 19 a) and b) present the particle size distribution from the two samples collected. As it is possible to verify, a large percentage of the fuel has more than 100 mm. Bonefacic et al. [385] presented that large particle size implies an ignition delay, and, as investigated by Mason et al.

[386] and Riaza et al. [387], increased the burnout time. The total burnout time is decisive information for the design of grate furnaces since it defines the grate length and the size of the entire furnace [255].

Furthermore, larger particles establish the potential for large internal temperature and composition gradients [388]. Nevertheless, Caposciutti et al. [389] investigated the effect of woodchip size distribution on combustion in a 140 kW underfeed stoker boiler. A more uniform spatial distribution of volatiles was observed when employing larger woodchips. Therefore, since fine particles lead to localized emission of volatiles [386], larger particles can be a more interesting option because their combustion will occur further from the feeding point.

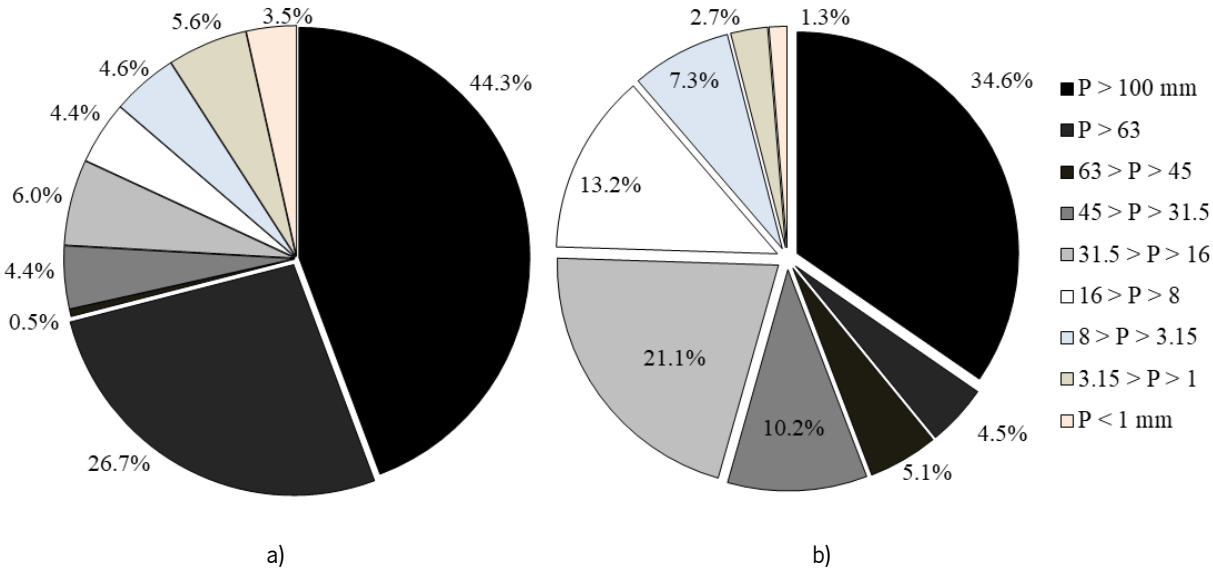

Figure 19: The physical dimension of the biomass used in the power plant: a) sample with 1 kg and b) sample with 0.4 kg of biomass.

In addition to the particle size distribution, moisture and ash content are essential parameters regarding the decision concerning the type of furnace, its design, and its operating conditions [255]. Biomass has a highly variable moisture content and will vary in moisture when in contact with air of variable humidity. Equilibrium moisture in biomass ranges typically above 25% on a wet basis when the ambient relative humidity exceeds 90–95% [390]. In a boiler, the energy efficiency can be increased by 5 to 15% with increased combustion temperature and reduced flue gas temperature using the dried instead of wet biomass [391]. Regarding the ash content, this parameter has to be considered as a higher ash content leads to higher entrainment of ash particles from the fuel bed with the flue gas and, consequently, increased deposits on the furnace wall, erosion of the heat exchanger, and airborne particulate matter

emissions [41]. The ash content can be interpreted as a guiding parameter to the level of ash related operational problems. In this way, several samples from a particular batch of fuel fed the plant, in different seasons, were analyzed. Figure 20 presents the variation of the moisture and ash content of the biomass investigated in the winter (Figure 20 a)) and summer seasons (Figure 20 b)).

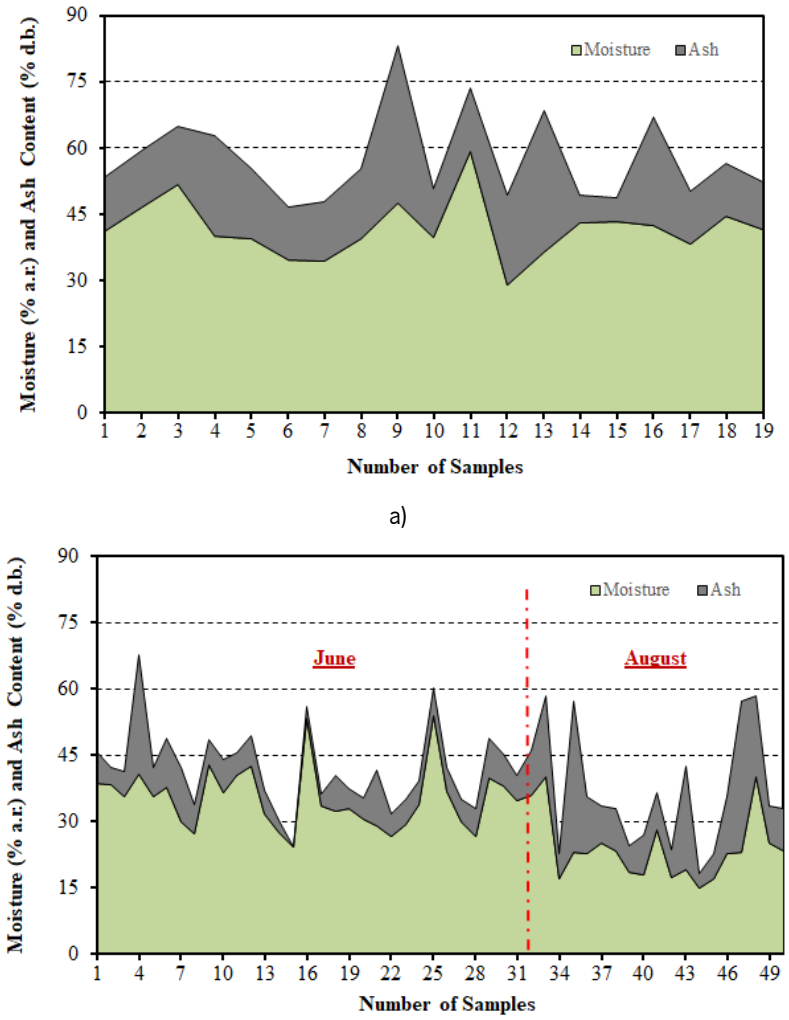

Figure 20: Moisture and ash content of the fuel used at the power plant in different seasons samples: a) from February and b) from June and August.

As the plant fuel is highly heterogeneous, moisture content and inerts quantity monitoring are essential to adjust the operating conditions of the power plant to the fuel quality. The moisture content ranges from an average of 41.64% in February and 23.26% in August. The ash content was higher in February, with an average of 16.02%, and a lower of 7.07% in June. This variation highlights the influence of the time of

year on the physical properties of the fuel. Consequently, the plant operators should pay attention to this information to control the power plant.

Regarding the chemical composition of the biomass, it can also vary concerning both the concentrations of the main elements: Carbon (C), Hydrogen (H), Oxygen (O), and Nitrogen (N). Table 15 presents the chemical properties of the biomass relevant to combustion. These results correspond to the samples collected during the winter season. In addition to the main element analysis, the contents of sulfur (S) and chlorine (Cl) and the heating value were also determined. S and Cl contents are essential to understand the possibility of corrosion. The heating value refers to the energy that can be obtained by burning this type of biomass.

Furthermore, as mentioned by Hupa et al. [392], the fuel's N content is of particular relevance since it is related to NOx emissions when biomass is burned. In this way, considering the values reported by Obernberger et al. [41], NOx emissions are reduced for N content lower than 0.1%. Consequently, considering the average N content presented in Table 15, NOx emissions will not be very significant, and this finding is supported by the NOx level measured.

Table 15: Chemical composition of the biomass and heating value.

	Elemental analysis (%)						**Heating Value (MJ/kg)**		
	C	H	N	O	S	Cl	HHV	$LHV_{db.}$	LHV_{ar}
Average Value	47.96	5.92	0.50	39.37	0.03	0.14	19.08	17.79	10.67
Standard Deviation	1.12	0.25	0.08	1.35	0	0.06	0.47	0.42	1.65

ar – as received

db – dry basis

According to Sommersacher et al. [393], a possible relation to describe the corrosion risk is the molar 2S/Cl ratio. Only minor corrosion risks must be expected when this ratio is higher than 4. Also according to Symonds et al. [394], fuels that have a Cl/S molar ratio higher than 2, where the absence of S enhances the formation of chlorides, have a catalytic effect on the corrosion. In this way, analyzing these two parameters, it was observed that all present samples had a 2S/Cl ratio lower than 4, and only two samples presented values of Cl/S ratio lower than 2. Therefore, according to these indexes, burning this biomass, there are corrosion risks. Figure 21 presents the variation of the fuel indexes for the different samples.

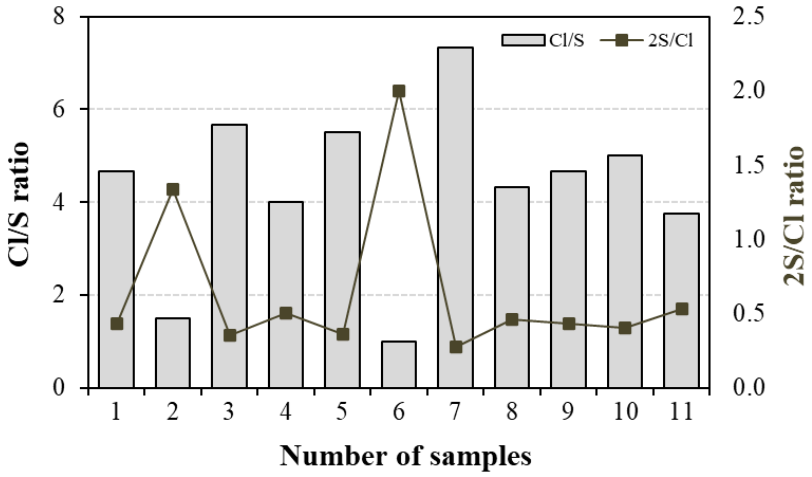

Figure 21: Variation of the fuel indexes to assess the corrosion risk.

3.4 Analysis of the Combustion Process

As far as the combustion performance of the power plant is concerned, the air system has a significant contribution. The primary air, supplied through the moving and vibrating grate, is dependent on the moving grate velocity according to an air stoichiometric operational curve provided by the manufacturer to adjust the primary air according to the emissions. Based on biomass with 35 to 40% moisture content, the operators can modify this curve through the offset level. It is important to note that only a small part of the total primary air flow rate is preheated and delivered through the moving grate. Therefore, a significant amount of the primary air flow rate is supplied through the vibrating grate, which is divided into three sections. The first two parts are where the air is provided for the combustion, with the highest air flow rate for the second section. In the third section, no air is supplied, or only a small amount, because all the fuel has been consumed, and adding air would be harmful to the combustion process. Furthermore, the air flow rate, primary and secondary, is automatically regulated by the boiler control system, but it can also be adjustably manually.

The secondary air system is also controlled based on the grate velocity and oxygen content in the flue gases. The secondary air flow rate, supplied by 117 nozzles located at different height levels, is computed considering these two parameters, and its value will be between 5,000 and 22,000 m^3/h. This value can also be adjusted manually by the operators. Figure 22 presents the primary and secondary air system design to understand its path, division, and location in the boiler.

To improve the combustion performance, there is the possibility for flue gas recycling through 4 holes located on the opposite wall of the biomass feeding. However, problems related to air leakage and particle

accumulation on the valves caused this system to be inactive. Nevertheless, the gaseous emissions of the plant, fundamentally particles, nitrogen oxides (NO_x), and carbon monoxide (CO), are below the emission limits. Table 16 details the flue gas emissions (on a volume basis) obtained during a mandatory measurement.

Table 17 presents the operational parameters that were monitored for one week where the power plant operated under normal conditions. These parameters, temperature, emissions, and flow rate were recorded to support a numerical model that will allow the characterization and optimization of the combustion process.

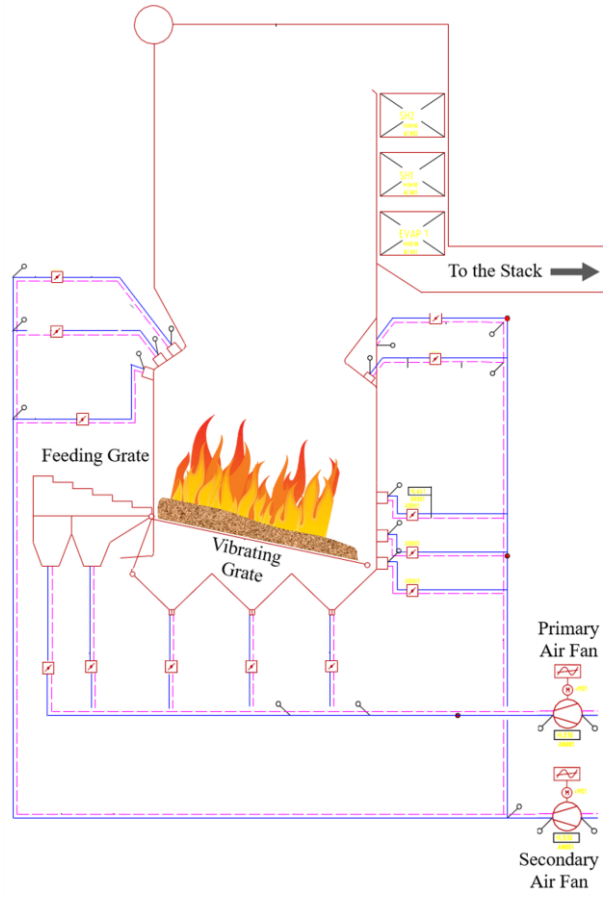

Figure 22: Schematic diagram of the air system and the feeding and vibrating grate.

Table 16: Gaseous emissions and corresponding legal limits.

Parameter	Emissions (mg/m³)	Limit values (mg/m³)
Particles	25	150
CO	120	500
SO_2	5	500
NO_x	125	650

Table 17: Operating parameters recorded for one week of regular operation.

	Average	Minimum	Maximum
Temperature (ºC)			
Primary and Secondary air	19.90	12.41	27.34
Furnace	829.52	705.59	916.57
Superheater	516.56	460.52	550.37
Evaporator	304.91	288.16	322.40
Economizer	199.99	174.08	211.23
Stack	193	184	203
Emissions			
Oxygen (%)	10	6	15
Carbon monoxide (mg/m^3)	516	180	562
Nitrogen oxide (mg/m^3)	170	109	250
Air Flow Rate (m^3/h)			
Primary	49,470	34,970	54,140
Secondary	18,140	10,850	26,000

Due to the highly heterogeneous composition and properties of the fuel, the conversion process is subject to many disturbances, and it is considered unsteady. These disturbances are reflected in process instabilities. This issue can be observed in Figure 23, where the instantaneous value of the flue gas emissions and air flow rate are presented. In this Figure, a 9-h data record had been collected from the control room and shows the O_2 concentration, carbon monoxide emission, and air flow rate during the normal operation of the power plant. It is possible to observe that one of the main characteristics of the recorded data is the fluctuation of O_2 and primary air flow rate values. O_2 varied from 7% to around 10% and the primary air flow rate was between 35,000 to 50,000 m^3/h. This is an interesting point since the fluctuation of the O_2 is also in line with the vibration cycle of the grate, as demonstrated by Yang et al. [395], and also related to the quantity of primary air supplied inside the boiler which appears as a controlling mechanism of the fuel burning on the grate.

3.4.1 Influence of the Primary Air Distribution

Since the vibrating grate has three different sections where the primary air supply can be controlled by opening the valves, three different combinations of the openings were tested for approximately 30 minutes each. During the experimental campaign, the grate vibration cycle was kept for 10 minutes.

Initially, the power plant was operating with an opening percentage in the first, second and third sections of the grate of 60, 80, and 0% respectively. Then, it was modified to 90% in the first two thirds and, in the last third of the grate, remained at 0%. Due to these modifications, there was a slight increase in CO

emissions. The average value of 257.93 mg/m³ was obtained, which increases by 1.8 mg/m³ compared with the previous configuration.

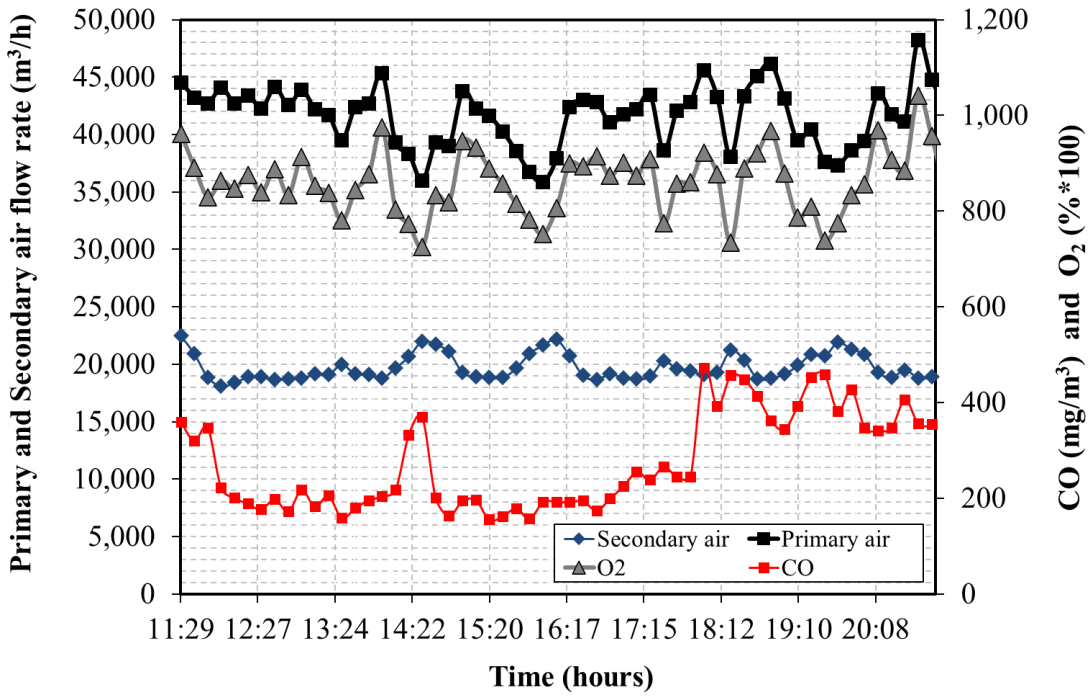

Figure 23: Data collected for one day at the maximum power.

Therefore, the valve opening configuration was changed to 50, 90, and 30%. With this configuration, small flames were observed because of the air supply at the last third of the grate. However, despite the average CO emission were reduced by around 2%, the opening of the previous valve is considered unnecessary since only a small amount of biomass was burned. Furthermore, as the supply of primary air in the last zone reduces the flow in the other zones, it was found that the power generated decreased when compared to the other configurations.

Therefore, with this set of experiments, it was proved that it is unnecessary to supply air to the last section of the grate and, consequently, it was decided to close the valve in the previous third and maintain the percentage of the opening of the valves in the other two-thirds of the grate. With this configuration, an increase in power was possible since more biomass was burned. This happens mainly because there is less fuel in the third part of the grate and the biomass conversion takes place in the first two-thirds. As Markovic et al. [396] stated, if the primary air speed is increased, higher biomass conversion rates will be obtained, and, consequently, more power will be achieved. This explains why the power was higher in the first two set-ups. The result of the tests performed can be observed in Figure 24.

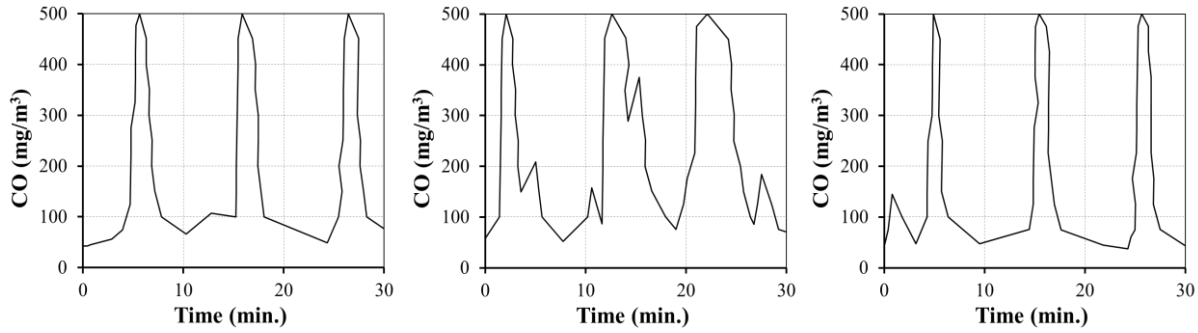

a) b) c)

Figure 24: Variation of the carbon monoxide emissions during different primary air supply conditions: a) 60/80/0%, b) 90/90/0%, and c) 50/90/30%.

3.4.2 Influence of the Grate Vibration

Regarding the influence of the grate vibration cycles, different time intervals between grate vibrations were analyzed. Initially, the time interval between the vibration periods of the grate was defined as 3 minutes and with a vibration period of 3 seconds, which means that there was not enough time to stabilize the combustion process on the grate. Given these circumstances, it was noticed that the time between the vibration periods was insufficient because, when CO emissions reached their lowest level, the grate would vibrate again and, therefore, CO emissions would return to their maximum value. The average CO emission was 271.17 mg/m^3.

Consequently, the combustion period on the grate was extended without vibration, going from 3 to 10 minutes. With this modification, it was possible to observe a long period in which CO emissions were lower and only increased again when another cycle was initiated. This increase in time resulted in a decrease of 6.4% of the average CO emission when compared to the first configuration.

Due to the success of the previous experiment, once again the time interval between grate vibrations to 15 minutes was increased. However, despite a 5% reduction in CO emission, it was noted that there was an accumulation of biomass in the first section of the grate. This agglomeration could lead to the interruption of the power plant. Consequently, it was defined to ensure the correct operation of the power plant, that the maximum time intervals between grate vibration are 10 minutes. Figure 25 presents the variation of the CO emissions during the tests performed with different grate vibration cycles.

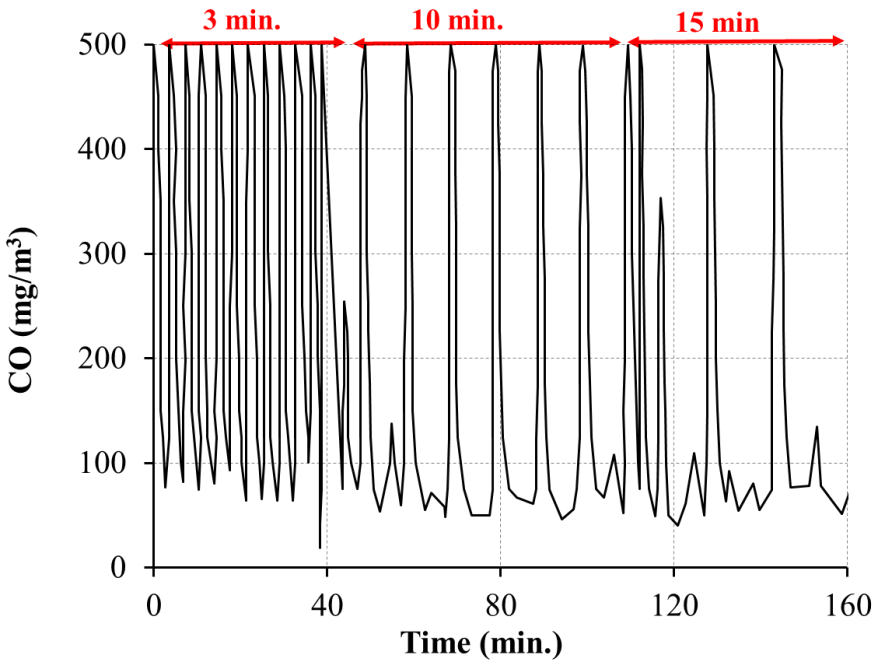

Figure 25: Variation of the carbon monoxide emissions during different grate vibration cycles.

This set of experiments was important since a very significant decrease in CO emissions was achieved. This decrease is quite substantial because the emission of CO means energy that is wasted since there was no oxidation of CO into CO_2, and, therefore, the energy that would be released in this reaction was not used.

It should be noted that the vibration time and the time between vibration periods must be adjusted to suit the fuel characteristics. The vibration action can help improve fuel distribution on the grate, avoiding the formation of agglomerations on the grate and, therefore, exposing the fuel surface to heat and oxygen for complete combustion to occur. The vibration period of the grate promotes the mixing between the fuel. It was verified that with each cycle of grate movement, there is a drop in the oxygen concentration in the flue gases and an increase in CO emissions. However, as investigated by Yang et al. [395] and Sabelstrom [397], the recorded CO emission peaks can be partially avoided by adjusting the secondary air. Furthermore, Yang et al. [395] suggested that during grate vibration, the primary air would be reduced to avoid raising particles, which significantly affects the oxygen and furnace temperature.

An overview of the average results for the different monitored parameters is presented in Table 18.

Table 18: Average results of the monitored parameters during the experimental campaign.

	O_2 (%)	CO (mg/m³)	Primary Air (m³/h)	Secondary Air (m³/h)	Power (MW)
Different primary air supply					
60-80-0%	8.57	256.13	43,111	18,598	9.228
90-90-0%	7.84	257.93	38,217	21,036	9.176
50-90-30%	9.06	253.84	41,975	18,985	9.069
Different grate vibration cycles					
3 min.	7.76	271.17	43,026	20,228	9.233
10 min.	8.58	253.74	43,183	18,637	9.226
15 min.	8.78	240.21	41,528	20,163	9.217

In the furnace, the energy released from mixing fuel elements with oxygen depends on the final combustion products. This does not depend on any intermediate combinations that may occur. For instance, one kilogram of carbon reacts with oxygen to produce about 32.8 MJ of heat (Equation (19)). The reaction can occur in one step (Equation 6) to form CO_2, or, under certain conditions, it can occur in two steps (Equations (20 and (21)). In this two-step process, CO is first formed, producing only 9.2 MJ per kilogram of carbon. In the second step, CO reacts with additional oxygen to form CO_2 and releases around 23.6 MJ per kilogram of carbon.

$$C+O_2 \rightarrow CO_2 \quad (19)$$

$$C+0.5O_2 \rightarrow CO \quad (20)$$

$$CO+0.5O_2 \rightarrow CO_2 \quad (21)$$

Therefore, if the CO oxidation reaction does not occur, 23.6 MJ per kilogram of carbon is wasted or approximately 10.1 MJ per kilogram of carbon monoxide [78].

3.5 Evaluation of the Limit to Reduce the FGT

Air preheating is one of the most powerful techniques to improve boiler efficiency [91]. This can be done by applying a heat exchanger for waste heat recovery since the exhaust gas temperatures are usually high. However, to extract heat from the exhaust gas, particular attention to corrosion problems on the heat exchanger is necessary.

When biomass fuels are burned, a small amount of SO_3 can be formed during the combustion process if the sulfur content is significant. Then, this chemical compound can combine with water vapor forming sulfuric acid vapor. Furthermore, other acids like H_2SO_3, H_2SO_4, HCl, HBr, and HNO_3 can also exist in gaseous form in the flue gas. Subsequently, when the surface temperature of the heat exchanger is lower

than the dewpoint temperature of an acid, or the flue gas is cooled to this limit, the acid vapor will condense onto the surface, and corrosion problems will take place. Therefore, before designing a heat exchanger for air preheating, it is necessary to determine the acid dew point temperature of the flue gas. In this study, the empirical relations (Equations (22)-(26)), available in the literature for calculation of the dew point of some acids, are used:

$$1000/T_{DP} = 3.7368 - 0.1591\ln(p_{H_2O}) - 0.0326\ln(p_{HCl}) + 0.00269\ln(p_{H_2O})\cdot\ln(p_{HCl}) \quad (22)$$

$$1000/T_{DP} = 3.5639 - 0.135\ln(p_{H_2O}) - 0.0398\ln(p_{HBr}) + 0.00235\ln(p_{H_2O})\cdot\ln(p_{HBr}) \quad (23)$$

$$1000/T_{DP} = 3.9526 - 0.1863\ln(p_{H_2O}) + 0.000867\ln(p_{SO_3}) - 0.00091\ln(p_{H_2O})\cdot\ln(p_{SO_3}) \quad (24)$$

$$1000/T_{DP} = 2.276 - 0.02943\ln(p_{H_2O}) - 0.0858\ln(p_{SO_3}) + 0.0062\ln(p_{H_2O})\cdot\ln(p_{SO_3}) \quad (25)$$

$$1000/T_{DP} = 3.664 - 0.1446\ln(p_{H_2O}) - 0.0827\ln(p_{NO_2}) + 0.00756\ln(p_{H_2O})\cdot\ln(p_{NO_2}) \quad (26)$$

where T_{DP} is the dew point [K], and p_i is the partial pressure of the gaseous compound i [mmHg]. Equations (22) to (24), to compute the dew point of HCl, HBr, and H_2SO_3, are from Y.H. Kiang [398], and Equation (25), for H_2SO_4 and HNO_3, is from Verhoff and Banchero [399]. Regarding the H_2SO_3 and H_2SO_4 dew point temperature, according to Blanco and Peña [400], SO_3 formation amounts from 1 to 2 vol.% of the sulfur oxides formed in the flue gases.

The empirical correlations presented in Equations (22) to (26) are used since a detailed measurement of the exhaust gases containing these chemical compounds was performed. Table 19 presents the results from an experimental campaign carried out for one hour. This information will be sufficient to compute a first approximation of the dew point temperature, defining the minimum operating temperature on the flue gas heat recovery exchanger.

Table 19: The chemical composition of the main acids on the exhaust gas and operating conditions.

	Emissions (mg/m³)					Temperature	Pressure	Flow rate
	H_2O (%)	SO_2	HBr	HCl	HNO_3	(ºC)	(kPa)	(m³/s)
Value	22.30	50.4	0.09	29.7	319	189	99.48	37.91

Subsequently, considering the operating conditions of the power plant and the lower temperature that can be achieved without reaching the lower dew point, an assessment of the waste heat recovery system payback will be evaluated as a preliminary estimative of the viability to add an air preheating heat exchanger.

Figure 26 shows the calculated dew points of the acids considered. As seen before, the moisture content varies considerably according to the season. In this way, the acid dew points were computed as a function of their value (Figure 26 a)). As SO_3 formation amounts to different percentages of SO_2, to obtain the range of variation of the acid dew point according to their percentage, Figure 26 b) presents the H_2SO_4 dew point temperature to the range of variations suggested in the literature and, to different SO_2 concentrations. This was performed since the SO_3 concentrations in the flue gases of biomass combustion plants firing low sulfur fuels such as wood chips and/or bark are below the detection limit so, the level of confidence in the results of the measurements is low [119].

Considering these results, the limit to reduce the flue gas temperature should be up to 125 °C (Figure 26 b)) to ensure that H_2SO_4 condenses if the biomass combustion plant burns fuels with a high amount of sulfur. Considering this limit and the average flue gas temperature presented in Table 17, with a waste heat recovery exchanger, it is possible to reduce around 70 °C in the flue gas temperature, which represents a saving of 7% of the total energy input.

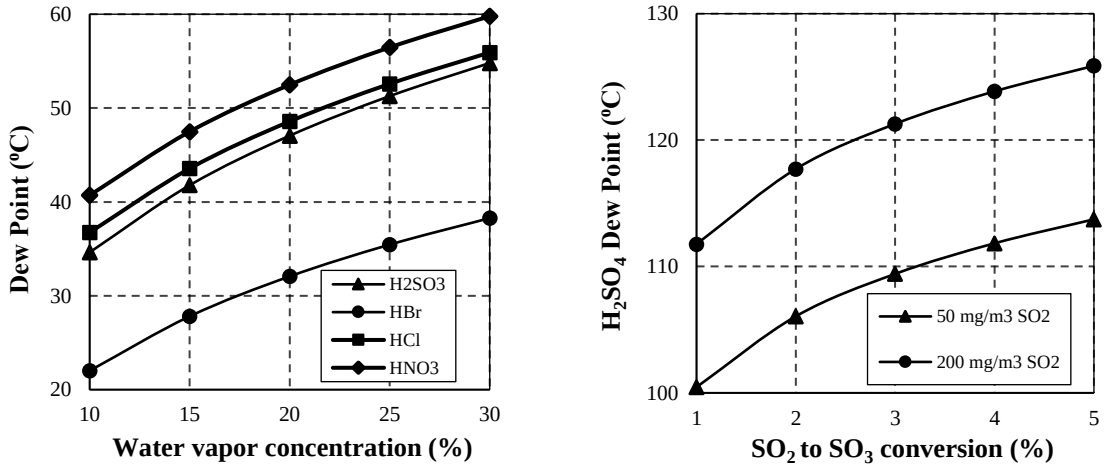

a) b)

Figure 26: Acid dew point temperature as a function of a) water vapor content and b) SO_2 to SO_3 conversion.

In the literature, similar results were presented. For instance, Frandsen [401] reported a full-scale measuring campaign on a straw-fired grate boiler and observed severe corrosion at 60 °C due to the condensation of hydrochloric acid. This author suggests, to avoid Cl-corrosion, the surface temperature should be kept above 80 °C. Furthermore, Retschitzegger et al. [119] also evaluated low temperature corrosion through empirical correlations, and a calculated H_2SO_4 dew point of 118 °C was obtained, which is in line with the present.

Based on this temperature limit, the estimation of energy and cost savings for a boiler can be carried out. The heat recovered by the heat exchanger can be estimated through Equation (27):

$$\dot{Q} = \dot{m}_{fg} c_p \Delta T_{fg} \tag{27}$$

where $\dot{m}_{fg}$ is the mass flow rate of the flue gases for heat recovery, c_p is the specific heat at a constant pressure of the flue gas, and ΔT_{fg} is the temperature drop of the flue gas.

Regarding the cost savings associated with energy and the payback period considering the investment in a waste heat recovery exchanger, these can be determined by Equations (28) and (29):

$$\text{Cost Saved} = \text{Annual Energy Saved} \times \text{Price of Energy} \tag{28}$$

$$\text{Payback} = \frac{\text{Incremental Cost}}{\text{Annual Cost Savings}} \tag{29}$$

To perform this analysis, Table 20 presents the parameters used. In this way, considering the average stack temperature and the maximum dew point temperature, the heat recovered was estimated as around 0.91 MW. Then, considering the range of values of the lower heating value, the fuel price, and the number of hours that boiler can operate, the fuel saving was estimated as 328.79 kg/h, and the cost saving was around 51,291 €/y.

By estimating the investment in the waste heat recovery system at around 6,000 €, the payback period is clearly less than 1 year. The heat recovery system was estimated based on the costs presented by Shah and Sekulic [402]. In order to do this analysis, it was assumed that the primary air temperature should be increased from its average value (presented in Table 10) to 100 °C using a plate heat exchanger. This selection was defined based on the recommendations of Kilkovsky et al. [403]. Consequently, the cost factor was achieved taking into account these considerations.

The benefits calculated make the design of the waste heat recovery exchanger economically attractive, and, therefore, more studies should be carried out to validate this first estimative.

Table 20: Parameters considered to compute the payback period of a waste heat recovery exchanger.

Parameter	Value
c_p	1.1 kJ/kg.K
ρ	0.7 kg/m³
ΔT_{fg}	70 °C
$\dot{m}_{fg}$	61,000 m³/h
LHV	10 MJ/kg
Fuel price	0.02 €/kg
Number of operating hours	7800 h/y
Heat exchanger cost	6,000 €

CHAPTER 4

EXPERIMENTAL MATERIALS AND METHODS

To improve the biomass combustion process, it is fundamental to understand and analyze the influence of the main factors that govern the conversion process. Experimental research plays a key role to obtain reliable details of the combustion developments in a biomass particle. In this sense, this chapter presents and describes the main forest residues that are being used as fuel in biomass power plants. For this purpose, the preparation procedures for the experiments using the thermogravimetric and macro thermogravimetric reactor are presented and, detailed features, as well as the operation procedure of both equipment, are described. Both techniques provide complementary information about the kinetic mechanisms involved in thermal decomposition and gaseous emissions. Furthermore, this analysis is also complemented by performing physical and chemical analyses, whose procedure is also described. The combination of standard and advanced methods, including laboratory experiments, provides a comprehensive knowledge to evaluate the combustion behavior of the fuels and acquire important information to further improve CFD codes.

4.1 Solid Biomass Samples

The selection of biomass was framed by the range of resources typically used in the power plant of Mortágua and considering the main forest species in Portugal. Pine, eucalyptus, and acacia are extensively used in Portugal as fuel for power generation. Pine, here referred to as *Pinus pinaster*, also commonly known as maritime pine, along with Eucalyptus (*Eucalyptus globulus*) are the main Portuguese forest species. The first resource is more abundant in the northern and central regions of the country [21] and provides a significant amount of raw material for the wood-based industry (pellets production, sawmills, paper and pulp, and panels) [404]. However, the impact of wildfires and climatic changes have been reported as important issues reducing the pine forest area [405]. Consequently, an increase in the feedstock price has been verified. The increase in the prices presented an opportunity for dedicated energy crops such as acacia. Acacia – *Acacia dealbata* – is an invasive species, native from Australia, and present in the southern regions of Europe. The weather in these areas favors its growth, which makes this resource an interesting option for suppressing energy requirements. In its turn, eucalyptus is a fast-growing tree species, also invasive, and extensively present in the seaboard region of Portugal. The large extension of eucalyptus is the result of planting, and not of natural dispersion/invasive behavior. The excellent adaption to the soil and national climate, the fast growth, and its wood properties contributed to highlighting eucalyptus as a reference in Portugal, and also allowed an increase in the eucalyptus area [406]. This is a particularly important material to meet the increasing demand for paper, pulp, and timber industries, and its residues due to these activities are further collected to generate electricity and heat. According to Duncker et al. [407], in Portugal, its growth is subject to one of the most intensive forest management regimes in Europe, commonly 10 to 12-year intervals for three rotations. Additionally, eucalyptus is a highly valued forest resource often connected to the fire phenomenon since it is in fire-prone environments [408]. This concern, combined with the reduction of the pine availability, led to looking for alternatives. Since Portugal is a reference in modern olive production, and it is expected that during the next decade to be the third largest producer of olive oil in the world, olive tree pruning should be a very interesting alternative for power generation. According to Nunes et al. [409], Portugal has 361 thousand hectares of olive groves. Hence, residues from olive grove maintenance or from the olive oil production process can become an important energy resource. For instance, it was estimated that approximately 50% of the biomass potential in Mediterranean regions where this agricultural residue is available residues is from olive grove maintenance [142].

Therefore, these four distinct species were selected to study their combustion behavior. Furthermore, considering the information collected in the Power Plant of Mortágua, presented in Chapter 3, different

parts of the different species are used as fuel to produce energy. In this way, in order to understand the influence of the different parts of the trees in the combustion, different parts of the species were taken into account. Thus, all parts of the eucalyptus tree were collected, while pine and acacia branches and the central part of the trees (trunk) were considered. From the olive trees, only the branches, without leaves and olives, were harvested.

The biomass residues were collected in a local forest in the north region of Portugal. Figure 27 presents the raw biomass samples at the collection time and the localization where the samples were harvested. Then, the samples were stored in a closed room in the Mechanical Engineering Department of the University of Minho. After being stored, the biomass residues were ground up to a specific particle size distribution depending on the experiment it was used for. After this process, the residues were spread on a room floor in order to be air-dried, and to achieve a moisture content that prevents organic decomposition (10 to 15%).

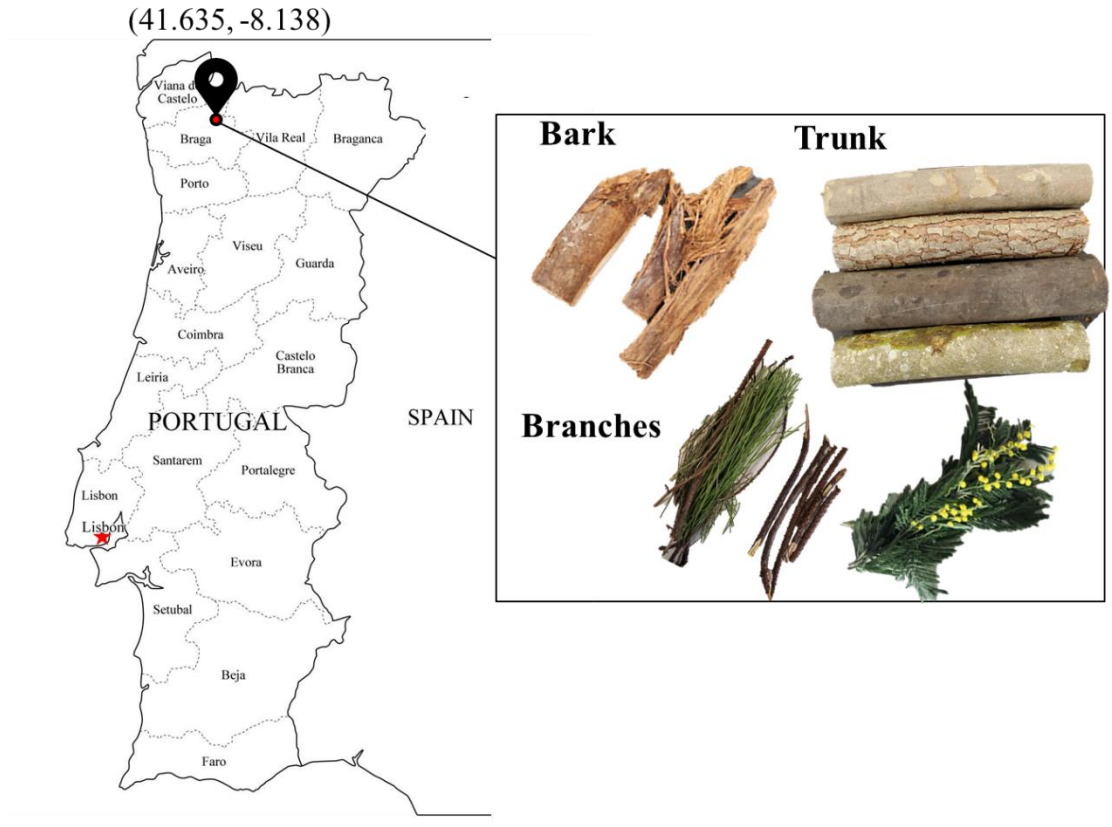

Figure 27: Localization of the collection point of the samples and the raw biomass samples selected.

In the present work, the physicochemical properties, the mass loss rate, the thermal conversion kinetic, and the volatiles composition are evaluated. By doing this, an effective strategy for evaluating combustion behavior was developed. The methodology presented in the next subsections is useful to characterize the thermal conversion of forest biomass samples taking into consideration the physical and chemical characterization of the raw materials. These studies are decisive to obtain a deep and reliable knowledge of the thermal conversion of the biomass particles in industrial furnaces. Consequently, experiments are conducted in a controlled environment, providing repeatable conditions, precise measurements for the different fuels, and ambient conditions to quantify the influence of different key parameters. Figure 28 presents an overview of the different analyses carried out in this work.

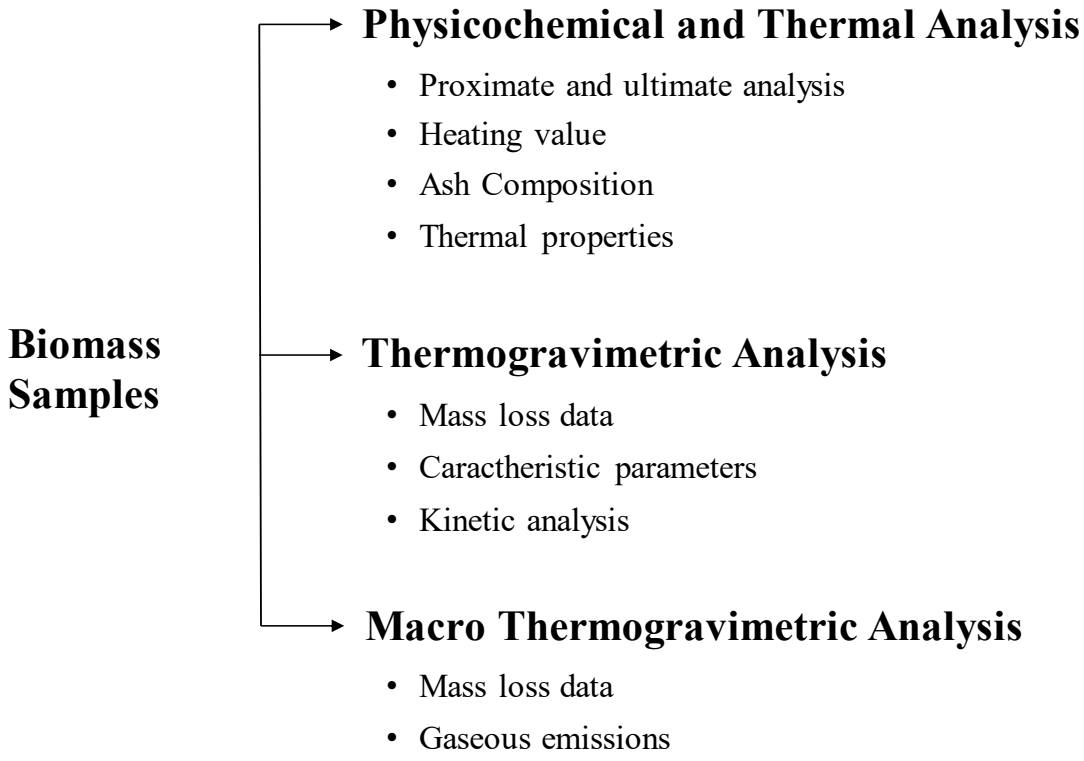

Figure 28: Outline of the different analyses considered to characterize the biomass combustion behavior.

4.2 Physicochemical and Thermal Properties Analysis

The physicochemical characterization of the raw materials involves the development of the proximate and chemical analysis, and the determination of its heating value. The proximate analysis is the determination of fuel in terms of moisture, volatile matter, ash, and fixed carbon constituents. This analysis was carried out using a scale and a muffle furnace. The ultimate analysis corresponds to the determination of the

main elements in the composition of the samples. The analysis was performed in two complementary equipment, to determine the relative amount of carbon, hydrogen, nitrogen, and sulfur, while the heating value was measured by using a calorimetric bomb, LECO model AC500. In addition to the main chemical elements previously mentioned, the elements present in the ash content of the samples were also determined. Lastly, the thermal properties, thermal conductivity (k), diffusivity (α), and heat capacity (c), were determined simultaneously using the Hot Disk Thermal Constants Analyzer. Table 21 presents the technical details of the equipment used to measure the different parameters and the different methods used to characterize the different properties. All properties were measured according to procedures described in the standards, which are mentioned in the following sections.

Table 21: Equipment and methods used to characterize the different fuels.

Property	Parameter	Equipment	Standard/Methodology
Proximate Analysis	Moisture Volatile matter Ash content Fixed Carbon	Scale: KERN ABJ 220-4NM Oven: Venticell 111 Muffle furnace: Termolab MLR	CEN/TS 15414:2006 CEN/TS 15402:2006 CEN/TS 15403:2006 Calculated as: (1- Volatile matter- Ash content)
Ultimate Analysis	Carbon Hydrogen Nitrogen Oxygen Sulfur	LECO TruSpec CHN Macro and LECO CS-200	CEN/TS 15104:2005 Calculated by difference CEN/TS 15408:2006
Heating Value	HHV and LHV	LECO Automatic Calorimeter AC500	DIN-51900-2
Ash Analysis	Composition	Bruker D8 Discover XRD and EDX - Pegasus X4M (EDS/EBSD)	
Thermal Properties	k, α, and c	Hot Disk Thermal Constant Analyzer TPS 2500S	ISO 22007-2:2015

4.2.1 Measurement Techniques

Physicochemical Properties

All analyses were processed according to specific standards and performed in the waste characterization laboratory of CVR (*Centro para a Valorização de Resíduos*). The proximate analysis was performed according to the procedures specified in the standards CEN/TS 15414:2006, CEN/TS 15402:2006, and CEN/TS 15403:2006. These international standards specify the methods for the determination of moisture, volatile matter, and ash content of milled samples of solid biofuels, respectively. The fixed

carbon, referred to the quantity of material remaining in the sample, excluding the ash content, after the devolatilization stage and is then computed based on the values previously determined. These methods can be described as a gravimetric analysis where a quantitative procedure is defined. The moisture content of the sample is determined after an extended period in the oven at 105 °C and the mass loss is determined considering the initial and final mass. The method to determine the volatile matter already entails rapid heating to 900 °C of the fuel in a furnace. Then, the volatile matter in the sample is obtained through the mass loss adjusted to the moisture content. In its turn, the method to determine the ash content also involves the heating of a sample in a furnace until 550 °C for a long period of time. Subsequently, the mass of ash is then measured on a scale and represents the sample of the remaining residue in the crucible.

The ultimate analysis was performed according to CEN/TS 15104 standard and the sulfur content was measured according to CEN/TS 15408 standard. The composition of the main chemical elements is derived from controlled combustion at 900 °C in an oxygen atmosphere to complete the reaction and obtain products like CO_2, H_2O, NO_2, and SO_2. Then, the gaseous compounds pass through a column and the relative volume fraction of each is measured in the outlet based on the thermal conductivity of the gas. The absolute masses of carbon, hydrogen, nitrogen, and sulfur in the original sample can then be estimated. The remaining percentage to complete the 100% is estimated as the oxygen content in the sample.

The heating value measurement was performed according to the procedures specified in the CEN/TS 14918:2005 standard. Its value is determined by the combustion of the samples in a controlled environment. In the AC500 Automatic Calorimeter, the sample is placed in the combustion vessel, a high-pressure oxygen rich atmospheric environment, which is surrounded by water. The temperature of the water is measured by an electronic thermometer, and the difference in water temperature between pre-fire and post-fire is processed by the software of the equipment in order to determine the heating value of the fuel. The gross (HHV) and net calorific value (LHV) are then computed according to the DIN standard 51900-2.

Regarding the ash analysis, the ash compounds, or the inorganic constituents, were determined using X-ray Diffraction Spectroscopy (XRD) and Energy Dispersive X-ray spectroscopy (EDX) techniques. The first technique is used for the analysis of the crystalline structure of the sample rather than the elemental content present in the material. The interaction of the incident rays in the sample produces diffracted X-rays that are then detected, processed, and counted. By scanning a specific range of the sample, all

possible diffraction directions should be achieved, and they are then converted to identify the different compounds. This identification is performed using EVA analytical software where the phase identifications can be made by comparing the experimental pattern with the International Center for Diffraction Data database, using a search matching algorithm. Based on the diffractograms obtained using a specific sweep, and integration time, and with the knowledge of the expected compounds, it is possible to carry out a structural characterization, although it is not always possible to carry out a precise and complete identification of the crystalline phases. However, the chemical composition of the different elements in the samples can be observed with a scanning electron microscope (SEM). The SEM is equipped with an EDX spectroscopy detector that allows to quantify the required chemical elements. In this way, by irradiating the sample with a ray of electrons each element in the sample can be identified by its characteristic spectra and relative concentrations from their respective emission intensities.

Thermal Properties Characterization

The thermal properties of the samples are determined using the Transient Plane Source (TPS) technique to perform simultaneous measurements of thermal conductivity and diffusivity, in accordance with ISO 22007-2. The TPS method is based on a transiently heated plane sensor hot disk which should be placed between two pieces of the sample material to be tested. The Hot Disk sensor consists of an electrically conducting pattern in a double spiral, which has been etched out of a 10 μm thick Nickel foil. This spiral is sandwiched between two thin sheets of insulating material. In this way, when performing a measurement, a plane Hot Disk sensor is fitted between two pieces of identical samples, each with a plane surface facing the sensor. By running an electrical current strong enough to increase the temperature of the sensor between a fraction of a degree up to several degrees, and at the same time recording the temperature increase as a function of time. Hence, the Hot Disk sensor is used both as a heat source and as a dynamic temperature sensor. The solution of the thermal conductivity equation assumes that the Hot Disk sensor is located in an infinite medium, which means that the transient recording must be interrupted as soon as any influence from the outside boundaries of the two sample pieces is recorded by the sensor [410].

The inexistence of the contact resistance during the analysis of the experimental data is considered the main advantage of TPS when compared to the traditional steady-state thermal properties methods [411]. Table 22 presents the most important specifications and the operating parameters of the thermal analyzer used in this work.

To determine both the thermal conductivity and thermal diffusivity with good accuracy, the dimensions of the sample and the operating conditions of the experiment (time and power) should follow the recommendations presented in Table 23 [412]. A quick estimative of the sample dimensions, time, and power, for materials with low thermal conductivity, such as wood materials, can be calculated using the expressions presented in Table 23 and an optimum sample size (thickness and diameter) can be estimated based on the sensor radius.

Table 22: Specification and operating parameters of the thermal analyzer.

Parameter	Value
Temperature range	Up to 300 °C
Sample size	Depends on the diameter of the Disk elements
Thermal conductivity range	0.005 W/m/K to 1500 W/m/K
Reproducibility	Thermal Conductivity ±2% Thermal Diffusivity ±5% Heat Capacity (per unit Volume) ±7 %
Kapton sensor – 5501 model	6.4 mm radius

Table 23: Recommendations of the thermal analyzer operating conditions [412].

Parameter	Value/Expression
Thickness and diameter of the sample (mm)	Thickness: $r \leq h \leq 4r$ Diameter: $4r \leq D \leq 8r$
Time (s)	$t = \frac{r^2}{\alpha}$
Power (W)	$P = 50\, r\, k$

4.2.2 Experimental Procedure

The different fuels were prepared using similar processing methods to provide consistent samples for subsequent analyses by the methods described previously. For the proximate and ultimate analyses, approximately 500 g of each fuel with specific granulometry is necessary. Hence, the raw materials were milled in a knife mill into powdered samples until they achieve a size lower than 0.5 mm. After the milling process, the samples were sieved in a vibratory sieve shaker to collect only particles with a size between 0.125 and 0.250 mm. Figure 29 presents both equipment used to prepare the samples while Figure 30 shows the samples obtained through this preparation process. As can be observed, there is a transition in the color of the lighter trunk samples (inner part) to the darker bark and branches (outer part). This is commonly associated with the increase of the extractive content in the outer part of the tree [206].

a) b)

Figure 29: Equipment used to prepare the samples: a) Knife mill and b) Vibratory sieve shaker.

a) b) c)

d) e) f)

g) h)

Figure 30: Samples used in the experiments: a) Pine trunk, b) Pine branches, c) Eucalyptus trunk, d) Eucalyptus bark, e) Eucalyptus branches, f) Acacia trunk, g) Acacia branches, and h) Olive branches.

Ash Composition Analysis

Since the results depend on the production method of the ash sample, (basically the combustion temperature, heating rate, and atmosphere in the muffle will influence the final content of the sample), it is important to maintain as much as possible the experimental conditions and for that, the EN 14775:2009 standard was followed. Hence, the samples for the ash composition analysis were derived from the previous process using particles larger than 0.25 mm, were collected. Then, the raw materials were further heated in a muffle using the heating program mentioned in the standard. Posteriorly, the samples were introduced in the SEM and XRD equipment and three measurements in different places of the sample and the final result is the average of the three measurements. Figure 31 presents the equipment used to produce the ash.

Thermal Properties Determination

The samples for measuring the thermal properties were prepared according to the recommendations provided by the Hot Disk Thermal Constants Analyzer. Consequently, to ensure good thermal contact, in the experimental apparatus, the sensor is clamped between two identical cylinder-shaped samples, each one with 40 mm in diameter and 20 mm in thickness. These dimensions were defined according to the recommendations presented in Table 23.

Figure 31: Equipment used to produce the ash and the result after the heating program.

In order to prepare similar samples, an experimental procedure was established. Figure 32 presents the main operations necessary to produce the cylindrical samples, which consist of the following steps:

1. Machine the wood logs to obtain 40 mm diameter samples and sand the side;
2. Cut the sample into pieces of 23 mm thickness;
3. Mill all samples to obtain 20 mm thickness;
4. Sand the remaining faces again.

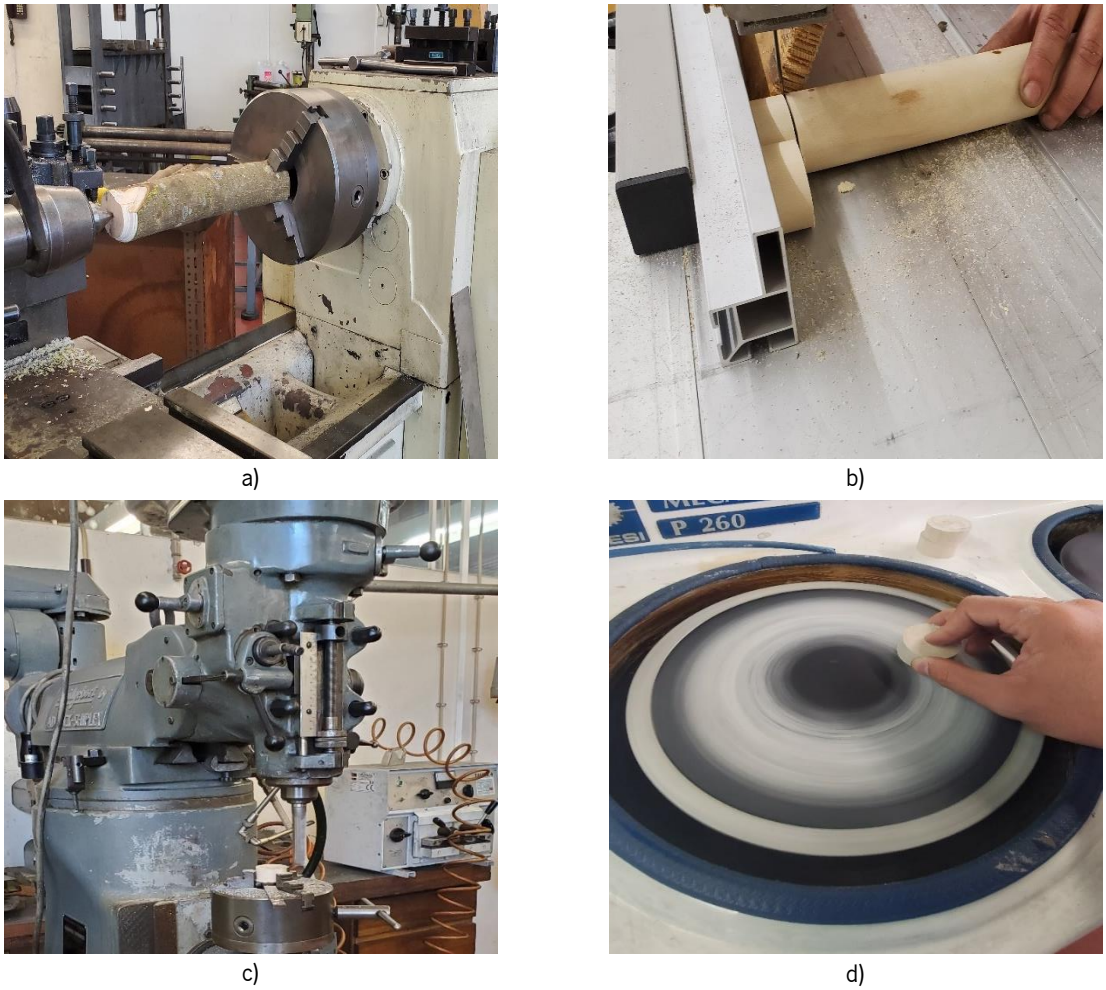

a) b) c) d)

Figure 32: Procedure to obtain the cylindrical samples: a) machining, b) cutting, c) milling, and d) sanding.

After this process, a random sample of each fuel was measured to verify the moisture content. The samples were placed in a muffle furnace at 105 °C for 24h, and the moisture content was found to be very variable, from 10.30% to 51.56%. Since the moisture content of the samples is different, it was decided to ensure a constant and equal moisture content in the different samples, in order to avoid the

influence of the moisture content in the final result of the thermal properties. To achieve this requirement, the samples were stored in a desiccator with a potassium sulfate solution for a minimum of two weeks, with a known target relative humidity, in order to ensure 20% of moisture content in the samples. The relative humidity inside the desiccators was continuously monitored by using humidity sensors, SHT31 Smart Gadget with an accuracy of ± 2%, allowing to monitor its stability over time. The effectiveness of this procedure was previously verified using the samples prepared for the Macro Thermogravimetric experiments, and more details are presented in Annex B. Figure 33 presents the samples and their storage container with the salt solution in the lower part. Then, after a minimum period of time in the desiccator, the first part of the experiment involved the measurement of three thermal properties (thermal conductivity, specific heat capacity, and diffusivity) at room temperature and for 20 % of moisture content. Measurements were carried out for two samples of each test sample, and it was repeated three times for each sample. Then, mean values of thermal conductivity were obtained by averaging. Once the experiments have been completed, new experiments are performed but the samples are completely dried after 24 h in a muffle furnace at approximately 105 °C. Figure 34 presents the experimental apparatus for the thermal properties determination.

a) b)

Figure 33: Samples prepared for the thermal properties determination experiment (a)) and the desiccator where the particles were stored (b)).

The heat capacity value resulting from the experiment is based on the volume of the sample. Hence, the density of the sample is necessary to be determined to define the heat capacity on a mass basis.

Figure 34: Experimental apparatus for the thermal properties determination.

The density was simply computed by dividing the mass of the sample by its volume. The former was measured by a precision scale with a resolution of 0.001 g, and the volume was calculated once the diameter, and thickness were measured of the sample by using a steel caliper with a resolution of 0.1 mm. Table 24 presents the average geometrical dimensions and the corresponding weight.

In addition, power and time were also calculated and inserted into the program that controls the test based on the equations presented in Table 24. Furthermore, the isotropic measurement module was selected to carry out each experiment. This module allows the measurement of the geometrical mean value of the thermal properties in the sample volume.

Table 24: Geometric and physical characteristics of the samples.

Fuel	Diameter (mm)	Thickness (mm)	Weight (g)
Eucalyptus	39.72 ± 0.14	19.49 ± 0.60	16.54 ± 0.66
Pine	40.05 ± 0.15	19.89 ± 0.18	15.05 ± 0.98
Acacia	39.62 ± 0.14	19.96 ± 0.89	13.51 ± 0.61
Olive	38.62 ± 0.63	19.90 ± 0.14	23.94 ± 0.19

4.3 Thermogravimetric Analysis

To understand transport phenomena at the particle level, TGA is the most useful method. This is a thermo-analytical method widely implemented to investigate and compare thermal degradation events and kinetics during the combustion of solid materials, such as coal and biomass [129]. The decreasing of mass is measured, under controlled conditions, while the thermal process is taking place, as the temperature increases. A simultaneous TGA-DSC (Differential Scanning Calorimetry) equipment, shown in Figure 35, from TA Instruments brand and model SDT 2960, was used to carry out the TGA experiments in an oxidative atmosphere. This equipment combines two thermal analysis techniques. The first one is TGA where the amount and rate of change of the sample mass as a function of temperature and time is measured, and the second is calorimetry which corresponds to the measurement of the heat flow as a sample is subject to a user defined temperature ramp. Hence, a simultaneous measurement of temperature, time, mass, and heat flux of a sample in a controlled atmosphere is carried out. However, two operating conditions are available to characterize any material that exhibits weight loss or phase changes as a result of thermal decomposition, dehydration, and oxidation. The most usual operating condition when biomass is studied is the dynamic behavior, in which the temperature is increased at a linear rate. Additionally, the equipment allows the operation in an isothermal mode, in which the temperature is kept constant during the experiment. Table 25 presents the specifications in terms of the possible temperature and heating rate of operation as well as the precision and accuracy of the different devices used. Heat flow and temperature accuracy, and validated with standard metal samples.

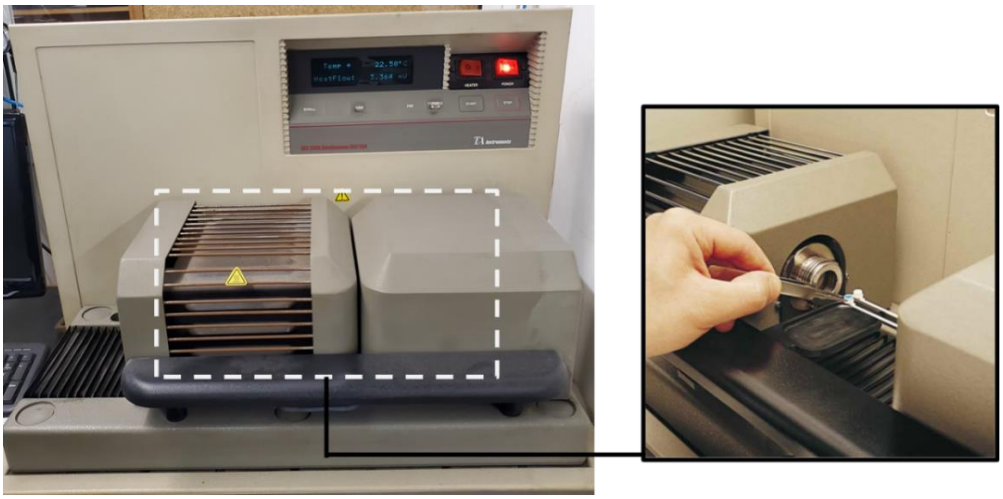

Figure 35: TGA-DSC equipment used to perform the thermogravimetric experiments.

Table 25: Specification and Operating Parameters of the Thermogravimetric Equipment.

Parameter	Value
Temperature range	Ambient to 1,500 °C
Sample and reference control thermocouple	Platinum-Platinum – 13% Rhodium Type R
Heating rate	100 °C/min to 1,000 °C
Heat Flow Accuracy	Better than ± 2%
Heat Flow Precision	Better than ± 2%
Temperature Accuracy	± 1 °C
Temperature Precision	± 0.5 °C
Weight Sensitivity	0.1 µg
Weight Accuracy	± 1 %
Sample Cups	90 µL Alumina
Furnace atmosphere purge gases	Helium, Nitrogen, Oxygen, Air, Argon

4.3.1 Measurement Techniques

In the TGA, the sample is inserted into a sample pan. Inside the electric furnace, as the temperature is increased, a reduction of the sample mass and the weight loss is measured using a microscale. This is connected to the sample holder which is derived from a taut band meter movement located at the rear of each balance arm. The scale arm is maintained by an optically activated servo loop in the horizontal position by adjusting the zero position. Hence, the weight variation is indirectly measured by the amount of restoring current necessary [413].

Figure 36 illustrates the various components of the TGA apparatus to measure the temperature and weight. The DSC module is based on the principle that when a sample and an inert reference sample are heated at a specific condition in a controlled environment, the increase in the temperature of the sample and reference material will be the same unless a reaction occurs in the sample.

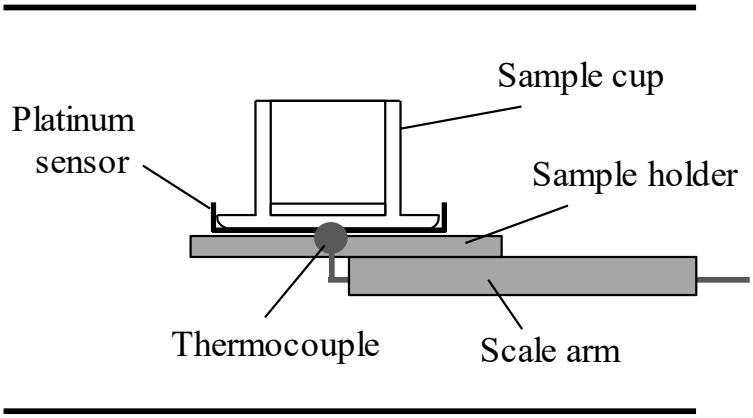

Figure 36: The different components of the TGA equipment.

4.3.2 Experimental Procedure

The raw materials previously milled for the physicochemical analysis were also used to perform the thermogravimetric experiments. Then, the samples were stored in a desiccator, and before each experiment, approximately 10 mg were measured on a high accuracy scale (precision of 0.0001 g). Figure 37 presents both operations. Thereafter, the sample was introduced inside TG equipment, in the crucible where it was properly spread to avoid diffusion problems. Non-isothermal heating with in situ drying was defined as the heating program defined for the thermal decomposition analysis. Figure 38 shows the heating curve defined for all experiments.

a) b)

Figure 37: The different stages after the milling process of the raw materials: a) Storage in the desiccator, and b) weighing of the sample before the thermogravimetric experiment.

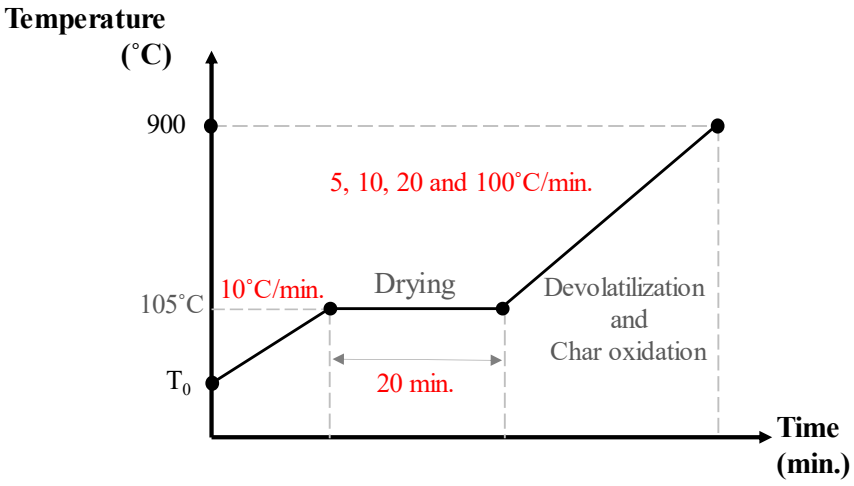

Figure 38: Heating program defined for the thermogravimetric experiments.

Non-isothermal experiments are generally adopted for the determination of kinetic parameters as they are considered more reliable and less time-consuming than isothermal analysis [136]. After the drying stage, low heating rates were defined to avoid transport effects, and to ensure that reaction is only temperature dependent and, consequently, the experiments are performed in a pure kinetic regime. Table 26 summarizes the operating conditions defined to perform the thermogravimetric experiments. In Annex C more details regarding the selection of these operating conditions are presented.

Table 26: Operating conditions of the thermogravimetric experiments.

Parameter	Value
Initial mass (mg)	10
Particle size (mm)	0.125-0.250
Flow rate (mL/min)	100
Temperature (°C)	Ambient to 900
Heating Rate (°C/min)	5, 10, 20, and 100

4.4 Macro Thermogravimetric Analysis

A small-scale reactor was developed with the purpose to study the mass loss and gas release characteristics of intrinsic chemical reactions from the selected fuels. This in-house designed Macro TGA equipment is essential to complement the knowledge acquired with the previous equipment. A considerably higher quantity of biomass and larger particles can be used to analyze the heat and mass transfer effects that affect the overall decomposition since the TGA experiments are performed in a kinetically controlled condition. Because of the sample size, the TGA sample is at an uniform temperature with no internal gradients.

The lab-scale reactor has been designed to mimic the combustion conditions (including drying, devolatilization, and char combustion) of a layer of biomass particles inside a grate-fired boiler as well as possible. During the design stage, some important constraints were addressed. The first issue is related to the possible biomass quantity in each experiment and the easiness of access to the interior of the reactor to introduce the sample. This is particularly important to consider secondary reactions in the fuel bed appropriately, and also to consider high heating rates of the fuel comparable to real-scale grate-fired boilers. Secondly, high flexibility regarding analytical equipment connected with the reactor, and easy

handling during the experiment without any disturbances. Finally, the possibility of online recording of relevant operation data.

The reactor can replicate the behavior of a fuel portion moving along the grate and, thereby, passing through the different reaction zones (drying, devolatilization, and char combustion). The reactor is 200 mm in diameter and 350 mm in height, the walls are made of refractory material to reduce heat losses and contain a 2 kW electrical heater. In the upper part of the reactor, there is a rotating lid with a rip of 10 mm to allow the support of the sample holder which is connected to a scale. Hence, the mass loss during the experiment is measured along time. Figure 39 presents the 3D CAD model of the Macro TGA reactor, and in Figure 40 is presented a schematic diagram of the air supply line to the reactor through the valve on the lower left part of the equipment.

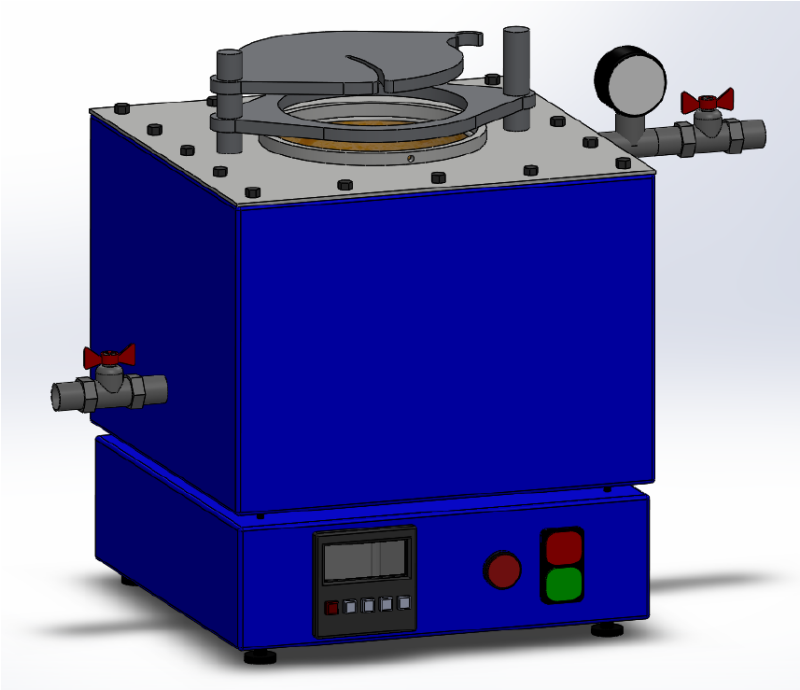

Figure 39: 3D Model developed of the Macro TGA equipment.

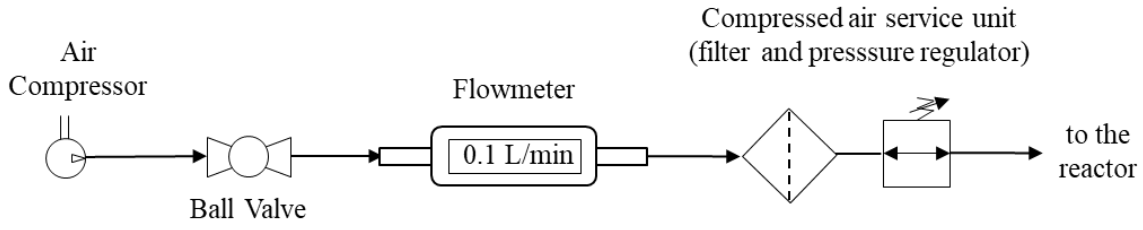

Figure 40: Schematic representation of the setup used to control the volumetric flow rate supplied to the reactor.

4.4.1 Measurement Techniques

The small-scale reactor has two type K thermocouples connected to a digital temperature controller, Eurotherm brand, that controls its operation. The desired temperature can be defined as the setpoint temperature but there is no possibility to monitor and acquire their variation over time. Furthermore, there are other external devices necessary to develop the experiment. An external flowmeter was used to control the gas flow rate supplied to the reactor and a digital scale to measure the mass loss variation of the sample. Table 27 presents the main specifications of both equipment.

Table 27: Characteristics of the flowmeter and scale used in the experiments.

Equipment	Specification
Flowmeter TSI 400series Model 4043	Max: 200 L/min Precision: ± 2%
Scale Vibra AJ 620 CE	Max: 620 g Error: 0.01 g Deviation: 0.001 g

To measure the weight, the sample is introduced into a perforated cylindrical basket of 60 mm in diameter and 50 mm in height suspended from the scale inside the reactor by using a stainless steel wire, 2 mm in diameter. An acquisition and monitoring program based on the LabVIEW platform was developed to record continuously all the data from the three devices. Figure 41 presents an overview of the apparatus involved in the Macro TGA experiments.

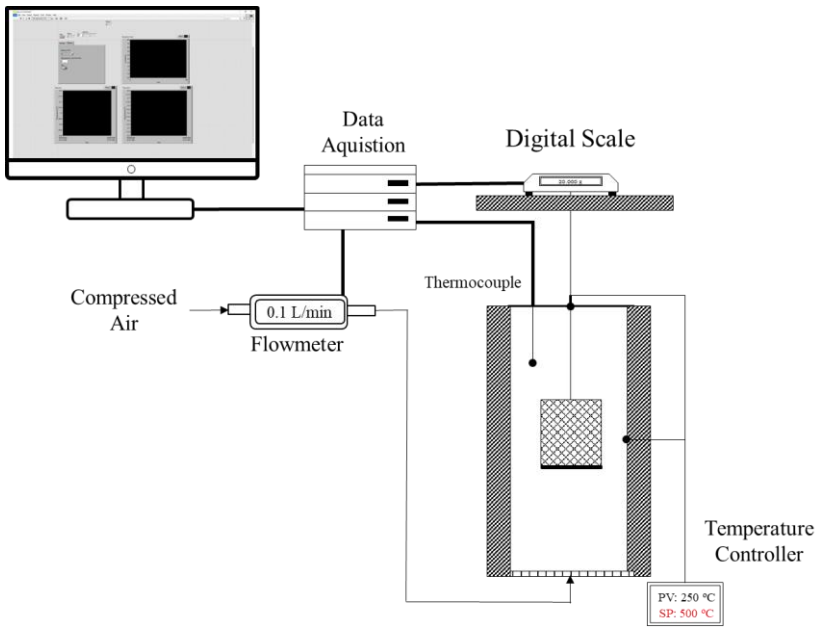

Figure 41: Schematic diagram of Macro TGA system.

4.4.2 Experimental Procedure

The whole idea behind the Macro Thermogravimetric experiments is to use larger particles whose dimensions are close to those observed in biomass power plants. The methodology used to produce the particles for the physicochemical characterization and the thermogravimetric experiments was disregarded as only particles around 6 and 8 mm were obtained. Hence, the alternative technique was to mill the particles in a knife chipper driven by an agricultural tractor. Particles with larger dimensions, ranging from a few millimeters up to hundreds of millimeters can be obtained by this technique. The particles were then spread in a room in order to be air-dried and to reduce the moisture content. After this, the particles were then sieved, and the particle size distribution was assessed by horizontal screening according to the standard EN 15149-1:2010 Part 2 using sieves with square holes apertures of 3.15, 8, 16, and 50 mm.

Figures 42, 43, and 44 present the two equipment used to produce the samples and the appearance of the different particles with different sizes obtained with this procedure, respectively.

Moisture content analysis and Bulk density analysis

From each batch of the different particle sizes, three samples with approximately 100 g were collected to obtain an estimation of their moisture content and bulk density. Figure 45 presents the experimental apparatus used to measure the moisture content and the bulk density, respectively. The moisture content in the different fuels was determined by using a muffle furnace with a temperature setpoint of 105 °C.

Figure 42: Knife chipper used to produce the woodchips.

Figure 43: Vibratory sieve shaker and the sieves (8, 16, and 50 mm apertures) used to separate the particles according to their size.

3.15 – 8 mm 8 – 16 mm 16 – 50 mm

Figure 44: The appearance of the different particles produced with different sizes.

a) b)

Figure 45: Apparatus used to measure the moisture content (a)) and the bulk density (b)).

The maximum moisture content of 30 % was measured, and the samples were spread out again and left in the room for more than two weeks. After this period, following the procedure used for the moisture control of the particles prepared to determine the thermal properties, the samples were stored in a desiccator with a potassium sulfate solution for a minimum of two weeks before being used.

Regarding the bulk density determination, a similar procedure to the EN 15103 standard was followed. A set of particles are introduced in a container with a known volume, the filled container is then shock exposed and subsequently, the weight of the filled container is measured on a scale. Finally, the bulk density is calculated considering the volume of the container and the weight of the empty and filled container.

Procedure

Before each experiment, the small-scale reactor, shown in Figure 46, is turned on and preheated up to a specific temperature. In the interior, the walls radiate heat to the surface of the basket which is in the middle of the reactor. The perforated basket (Figure 47) enables the gas (air or other) to interact with the biomass particles and there is in the upper part a connection to the scale in order to continuously monitor the mass loss of the particles. After reaching a steady temperature in the reactor, the basket is removed, the sample is quickly introduced, and the basket is then introduced back into the reactor.

During each experiment, the air flow was controlled at 0.1 L/min and, because the air flow remains the same during the whole experiment, the excess air ratios vary depending on the combustion stage. The air-fuel equivalence ratio changes from high values during drying to under stoichiometric conditions during the devolatilization and again to high values during the char oxidation stage. This approach is similar to the different stoichiometric conditions in the different zones of an industrial boiler. Furthermore, this process is similar to the conditions in a full-scale grate-fired boiler where the flames and the refractory walls suddenly transfer heat to the fuel. In Annex D more details regarding the selection of these operating conditions and the procedures and the results of the experimental debugging are presented.

Figure 46: The small-scale reactor used for the macro thermogravimetric experiments.

Figure 47: The basket where the biomass particles are introduced for the macro thermogravimetric experiments.

Regarding the analysis of the gas compounds released during all the devolatilization stage, different strategies were tested, but the most effective was using a probe with a heat exchanger connected to a vacuum pump where a Tedlar sample bag is connected. To do this, a reduced air flow rate is necessary in order to avoid any disturbance in the sample collection, and this is why the air flow was kept at 0.1 L/min. The gas sample was then analyzed in the gas chromatograph Bruker Scion 456-GC with a thermal conductivity detector and equipped with two columns: a BR-QPLOT column (30 m length, 0.53

mm internal diameter; film thickness, 20 μm) and a Molsieve packed column (13 × 80/100, 2 m length, 2.1 mm internal diameter). The Molsieve column was used to measure H_2, O_2, N_2, and CO, and argon was used as carrier gas at a flow rate of 60 mL/min. The temperatures in the injector, oven, and detector were 100, 35, and 130 °C, respectively. The BR-QPLOT was used to measure CO_2 and CH_4, and helium was used as a carrier gas at a flow rate of 4 mL/min. Here, the temperatures in the injector, oven, and detector were 80, 35, and 130 °C, respectively. Three samples are removed from the bag and the final composition is averaged. The experiments were run in triplicate and the average values were computed and reported as well as the standard deviation.

4.5 Data Analysis

There is a significant amount of data either generated during the experiments or derived from their results. Data analysis appears as an important task to present the results. This section details the data collection and treatment process, and the mathematical operations considered for subsequent presentation in the results section. The different studies were performed using Microsoft Excel 2019 and MATLAB 2020b.

Regarding the physicochemical properties, the combustion performance is evaluated starting by analyzing the chemical composition and the different proportions of the different biomass elements. This is essential to understand the combustion behavior of the different fuels and establish a relationship between them. The ratio between the volatile matter and fixed carbon, the hydrogen and carbon, and oxygen and carbon content are three examples of useful indicators and characteristic parameters. In addition to the chemical characterization, the heating value based on the experiment in the calorimeter is compared to Equation (30), derived empirically with detailed statistical analysis and presented by Friedl et al. [414]:

$$\mathrm{HHV} = 355\,\mathrm{C}^2 - 232\,\mathrm{C} - 2230\,\mathrm{H} + 5120\,\mathrm{C}\times\mathrm{H} + 131\,\mathrm{N} + 20.600 \quad (30)$$

To complete the chemical evaluation, the ash analyses from SEM and XRD are important to predict phenomena like fouling and slagging. The fouling and slagging phenomena are of great importance for the proper operation of biomass facilities. They are responsible for the generation of undesired material deposits on the surfaces of the equipment and the main difference between both lies in the fact that these deposits are subjected to radiant heat from combustion (slagging) or are given on the heat exchange surfaces by convection (fouling). In large biomass combustion boilers slagging takes place on the main walls of the combustion chamber. Meanwhile, the fouling phenomenon takes place in the first rows of the economizers or preheaters. Usually, these phenomena are estimated for combustion systems using

indexes based on the composition of the ash. They have been developed for the combustion of coal and the composition of the ash is expressed in terms of the oxides for the correlations [415]. Table 28 presents the main indexes that can be considered a predictive tool for the behavior of different fuels. These indexes are generally regarded as a simple and effective method to estimate the ash deposition and agglomeration tendency as demonstrated by Teixeira et al. [416] where the values are consistent with real observations during the combustion of woody and agricultural waste.

Table 28: Ash predictive tendency indexes of slagging, fouling, and agglomeration based on the chemical compounds.

Index	Parameter	Equation	Description	Reference
Deposition	Base to Acid oxides ($R_{B/A}$)	$\frac{Fe_2O_3+CaO+MgO+K_2O+Na_2O}{SiO_2+Al_2O_3+TiO_2}$	<0.5 - low 0.5-1 - medium >1 - high	
	Alkali Index (AI)	$\frac{K_2O+Na_2O}{HHV}\times\%Ash$	<0.17 kg/GJ - low 0.17-0.34 kg/GJ - medium >0.34 kg/GJ - high	[417]
	Total Alkalis (TA)	K_2O+Na_2O	<0.3 - low 0.3-0.4 - medium >0.4 - high	
	Fouling Index (FI)	$R_{b/a}\times TA$	<0.6 – low 0.6-1.6 - medium 1.6-40 - high >40 - extremely high	[416]
Slagging	Slag viscosity Index (SI)	$\frac{SiO_2}{SiO_2+Fe_2O_3+MgO+CaO}$	<0.6 – low 0.6-40 - high >40 – extremely high	[415]

From TGA experiments, the TG and DTG curves allow the identification of different key parameters and indexes. On this basis, the analysis consists of the identification of the ignition, peak, and burnout temperature, the maximum, average, and mass loss rate in the different stages of the biomass conversion, as well as the characteristic times where the biomass is ignited and completely oxidized. Furthermore, also to assess the combustion performance of the different biomass samples, considering the previous parameters, there are four indexes that can be calculated according to formulas presented by Yu et al. [184]. Hence, indexes for each stage of the biomass conversion, i.e., for ignition, volatile matter release, burnout, and also an overall index are calculated. All this information enables the thermal decomposition characterization of the different fuels. Table 29 presents all the parameters considered for

the characterization of the TGA experiments and a correspondent brief description of the meaning of each one.

From the TGA experiments, it is possible to obtain the kinetic parameters. Computational tools to derive this information are convenient, easier, and faster to better handle the large number of data acquired during the experiments. In the present work, a MATLAB code was developed with mathematical functions and inbuilt functions to easily smooth, filter, and fit the data. Figure 48 presents the main steps involved in the determination of the kinetic triplet parameters using different isoconversional methods and the Coats-Redfern equation.

Table 29: Characteristic parameters considered for thermal analysis evaluation and comparison.

Property	Parameter	Description
Temperature	T_{ig}	Ignition temperature (°C). Corresponds to the beginning of the weight loss and is defined as the temperature at which the rate of weight loss reaches 1%/min after the initial moisture loss peak in the DTG profile.
	T_b	Burnout temperature (°C). It is identified when the last peak comes to the end and is the temperature at which the sample is completely oxidized. It is taken as the point immediately before the reaction ceases when the rate of weight loss is down to 1%/min.
	T_1	Peak temperature in devolatilization (°C). It is the point at which the maximum reaction rate occurs during devolatilization.
	T_2	Peak temperature in char combustion (°C). It is the point at which the maximum reaction rate occurs during char combustion.
	$T_{\max}$	Temperature at the maximum weight loss (°C). It is the point at which the maximum reaction rate occurs.
Mass Loss	DTG_{mean}	Average weight loss rate, wt.%/min
	$DTG_{\max}$	Maximum weight loss rate, wt.%/min
	R_1	Weight loss during devolatilization, wt.%
	R_2	Weight loss during char combustion, wt.%
	m_b	Residual weight, mg
Time	t_{ig}	Ignition time, min.
	t_b	Burnout time, min.
Indexes	$I = \frac{DTG_{\max}}{t_b \cdot t_{ig}}$	Indicates the ignition performance. This means how fast or slow the fuel gets ignited. wt.%/min^3
	$V = \frac{DTG_{\max}}{T_P \cdot T_{ig} \cdot \Delta T_{1/2}}$	Reflects the volatile matter release performance. wt.%/min.T^3
	$B = \frac{\Delta T_b}{\Delta T_{1/2}}$	Expresses the burnout performance. It is inversely proportional to how fast the char burn. (-)
	$C = \frac{DTG_{\max} \cdot DTG_{\text{mean}}}{T_b \cdot T_{ig}^2}$	Presents the comprehensive characteristics. The higher the value, the more significantly the samples are burned. wt.%/min^2.T^3

Figure 48: Flowchart of the different stages involved in the kinetic analysis.

This set of stages is very important to obtain the effective kinetic parameters for the combustion of the selected fuels. After each experiment, there are more than 3,000 data points and due to the sensitivity of the devices, it is normal that some noise is present in the data. The noise causes a discontinuity in the normal trend of the data and, consequently, leads to mathematical problems in the differentiation. Additionally, during the heating of the biomass sample, there is an amount of water and volatiles that are released and each data point in the curve of the mass versus time should be lower than the previous one. Hence, these points are removed as well as the initial mass loss due to the drying of the fuel, where the weight loss data before 150 °C was not considered. The problem of the noise is resolved using a local regression applying a weighted linear least square method that smooths the data points and avoids points of inflection in the mass loss curve. Subsequently, the conversion values and their numerical

differentiation were easily computed in MATLAB and the number of data points was reduced according to the ICTAC recommendations [143]. Then, the kinetic parameters are determined by the slope of the numerical plots which is obtained by the different methods presented in Chapter 2.3 through an inbuilt function for linear fitting

Regarding the Macro TGA experiments, a MATLAB code was developed for post-processing the results. The mass loss curves are determined taking into account the average results from three separate experiments at each temperature and the standard deviation for each time. To achieve this, firstly the repeated data are deleted, and a cycle was developed to compute for each time an average mass value. Then, the results are averaged considering the three different runs and the standard deviation is computed. Subsequently, the conversion value is determined, and the means values are plotted with the standard deviation as a shaded area to represent the variability of the mass loss. Figure 49 shows a flowchart representing the different stages of the MATLAB code.

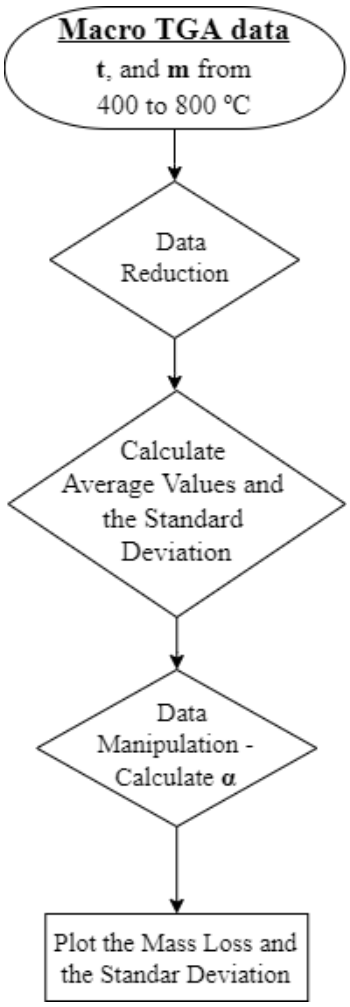

Figure 49: Flowchart of the different stages involved in the analysis of the Macro TGA experiments.

CHAPTER 5

DEVELOPMENT OF THE NUMERICAL MODEL

In the modern world, it is increasingly common to use computational power in research, as well as in problem solving. The fast development of powerful computers and algorithms has made numerical simulation less expensive and time-effective than experimental methods. In the last two decades, the interest in the use of solid biomass as a fuel for power generation, together with the continuous tightening of regulations, has motivated the improvement of accurate design techniques which are required to optimize the combustion process, new technologies, and simultaneously control pollutant emissions to the environment. A better understanding of the entire process occurring in the biomass furnace helps designers to improve the conversion efficiency and better control the equipment. This chapter presents the mathematical formulation behind a dense particle system to study and analyze in large detail the highly multi-scale and interconnected phenomena.

5.1 Software and Modeling Approach

The biomass combustion process in dedicated or cogeneration power plants is of an extremely complex nature due to many involved physical and chemical phenomena. To meet environmental restrictions there are different approaches to predict several phenomena and, therefore, prevent harmful emissions in a cost effective manner. Since the different phenomena involve physical complexities, the mathematical modeling of the gas flow, combustion, and a detailed description of the biomass particles conversion and their movement have been a challenge in the past decades. Comprehensive models have the capability to include the microscale phenomena to study and quantify interactions between particles, between particles and fluid, and as well particle conversion phenomenon, up to macroscale phenomena which are focused on the general theory to connect particles scale information (discrete) and the fluid flow (continuum). Thus, the coupling of these features highly enhances the development of numerical simulations of multiphase flow phenomena.

In this work, this type of overall model of the biomass conversion in a grate-fired boiler, as represented in Figure 50, is decomposed into two different numerical models in order to thoroughly study the different interconnected phenomena. The first one is a mathematical model developed to predict the biomass particles conversion in the burning conditions of the boiler. This model was developed considering the setup designed for Macro TGA experiments, in order to be analyzed previously its accuracy and further be coupled with CFD models. The analysis of the particle conversion is performed through an in-house simulation platform, called XDEM. This program is a multi-physics and multi-scale code developed at the University of Luxembourg to establish an advanced simulation technology.

The second one is a CFD model where the gas flow and combustion are predicted based on an empirical bed that is based on the biomass conversion into the different grate sections of the industrial boiler of Mortágua Power Plant. CFD modeling is an effective tool able to indicate the most relevant phenomena that occur inside an industrial boiler. The CFD analysis is here based on the ANSYS Fluent 2020 R1 software. This software is used for fluid flow and heat transfer problems and is structured with numerical algorithms capable of solving them as well as chemical reactions that occur in the freeboard of the equipment. In the following sections, more details about the two different tools and numerical models are described.

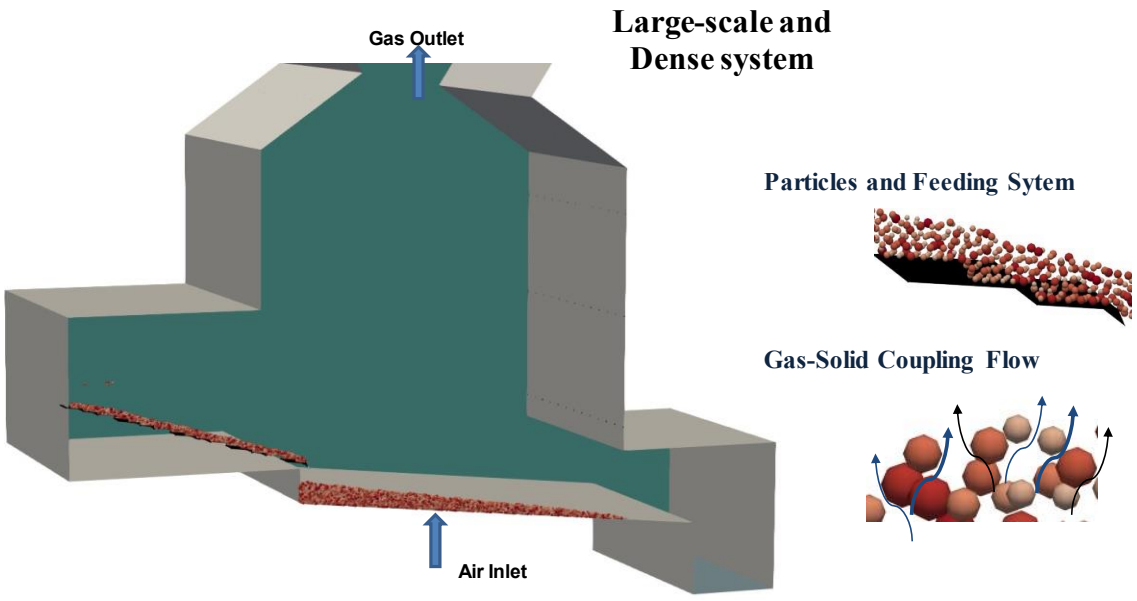

Figure 50: An overall model representing the multi-scale problem involved in the simulation of a biomass combustion boiler.

5.1.1 ANSYS Fluent

ANSYS Fluent is a leading commercial CFD software for the prediction of a wide variety of flows. This simulation program solves the fundamental differential governing equations for the mass, momentum, and energy conservation through the Finite Volume Method. With this method, the computational domain is first split into a set of control volumes, which are known as cells, and convert a general scalar transport equation to an algebraic equation that can be further solved numerically. The discrete values of any of these variables, represented by a scalar quantity ϕ, are stored at the center of the grid cells [418]. On a representative cell, after integrating the transport equation that expresses the conservation law in a cell volume, the general form of the discretized equation solved by ANSYS Fluent, considering an unsteady case, is expressed by Equation (31):

$$\frac{\partial \rho \phi}{\partial t} V + \sum_{f}^{N_{faces}} \phi_f \rho_f \vec{v}_f \vec{A}_f = \sum_{f}^{N_{faces}} \Gamma_\phi \nabla \phi_f \vec{A}_f + S_\phi V \tag{31}$$

where V represents the cell volume, N_{faces} the number of faces of each cell, ϕ_f represents the value of ϕ convected through face f, ρ the density, $\vec{v}$ the velocity vector, t the time, $\vec{A}$ the area vector of face f, Γ_ϕ the diffusion coefficient for ϕ, $\nabla \phi_f$ the gradient of ϕ at face f. Hence, the first term of the equation, $\frac{\partial \rho \phi}{\partial t}$, is defined as the transient term which accounts for the accumulation of ϕ in

the cell volume, and the second term represents the convection through the faces, where the product $\rho_f \vec{v}_f \vec{A}_f$ is the mass flux through the face of the cell. On the right side of the equation, there is a diffusion term, $\Gamma_\phi \nabla \phi_f \vec{A}_f$ which considers the gradient of ϕ and, at last, S_ϕ represents the source term of ϕ per unit volume, which means any source or sink that either generates or consumes ϕ.

In this way, the discretization procedure allows to solve numerically Equation (31) ensuring the conservation of the different physical parameters over the entire domain. Hence, as a result of the discretization, the unknown scalar variable ϕ at the cell center as well as unknown values in the neighbor cells, a linearized equation of the Equation (31) can be written using the form of Equation (32):

$$a_p \phi = \sum_{nb} a_{nb} \phi_{nb} + b \tag{32}$$

where the subscript nb refers to neighbor cells, and a_p and a_{nb} variables are the linearized coefficients for ϕ and ϕ_{nb}. Depending on the number of cells, similar equations are solved for each cell, resulting in a set of equations. Then, ANSYS Fluent solves this set of equations as a linear system using a Gauss-Seidel linear equation solver in conjunction with an algebraic multigrid method [418].

For reactive flows such as combustion phenomena, ANSYS Fluent solves additional transport equations for each species involved in the chemical reactions. However, while the fluid flow and gas-phase reaction modeling are entirely computed by the built-in algorithms of ANSYS Fluent, this software presents a drawback regarding the predictions of the biomass particles conversion. The heat and mass transfer in and with the solid phase should be externally modeled. As already mentioned in the literature review in Chapter 2, modeling combustion in biomass grate-fired boilers requires modeling the thermal decomposition of biomass on the grate. Consequently, in this work, to study the performance of the grate-fired boiler from Mortágua Power Plant, the domain to be simulated is divided into two main regions: the bed (a set of biomass particles present in the vibrating grate of the boiler) and the freeboard (interior region of the furnace above the bed). The bed model provides the temperature, the mass fraction of the different species, and the velocity of the gas that leaves the fuel bed into the freeboard and, therefore, defines the inlet conditions for the CFD simulation. Figure 51 presents an overview of the approach used in this work. The next subsections present all the equations involved in the mathematical modeling approach for the numerical model developed using ANSYS Fluent software.

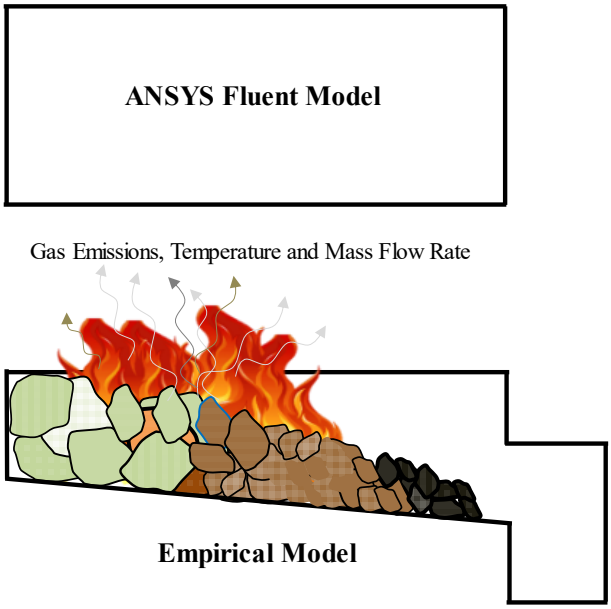

Figure 51: Overview of the strategy to develop the numerical model to simulate the combustion process.

5.1.2 XDEM Software

XDEM was developed for multiphysics simulation in which the dynamics of granular material or particles can be described by the utilization of DEM with the extension of additional thermodynamic properties. This platform combines the flexibility and versatility to address a wide range of problems in the most different applications. For instance, biomass particles can be defined as discrete entities with an internal temperature, composition, and the thermal conversion progress can be further estimated based on the surrounding conditions. Additionally, the position and orientation in time and space are predicted for each particle. Particles are assumed to be homogenous, and, inside each particle, associated transport phenomena are modeled using a set of one-dimensional conservation equations in the radial direction. As presented previously for ANSYS Fluent, a general form of the discretized equation solved by XDEM is expressed by Equation (33):

$$\frac{\partial \rho \phi}{\partial t} V = \sum_{A} \left[\Gamma \frac{\partial \phi}{\partial r} - \rho_g \vec{v}_g \, \phi \right] A + S_\phi V \tag{33}$$

where ϕ represents a volume averaged quantity derived from the phase averaged quantity with the local value of the particle porosity. Consequently, for each particle, a number of one-dimensional and transient equations are solved to estimate temperature, the different phases that constitute the particles, and the species released from the particle. Therefore, a detailed and suitable characterization of the reaction progress in a set of particles can be obtained with this approach.

This tool is commonly coupled with a CFD model to perform a comprehensive multi-phase approach [419]. The model involves various phenomena from the different scales of the particle conversion to the physics involved including the bed motion, turbulence, and chemical reactions. The movement of the particles and the thermal conversion process predicted from XDEM are then coupled to open source libraries from OpenFOAM-Extend 3.2 to solve the governing equations, species transport, and turbulence equations of the gas phase. The coupling between CFD and DEM is a common strategy for addressing relevant complex problems from the industrial sector. Figure 52 represents an overall outline to represent and highlight the main idea behind XDEM. The details of the implementation of the model, as well as the particulate and continuous phase governing equations, are presented in [254,420]. Peters [69] presents also more details about the numeric resolution of the conservation equations.

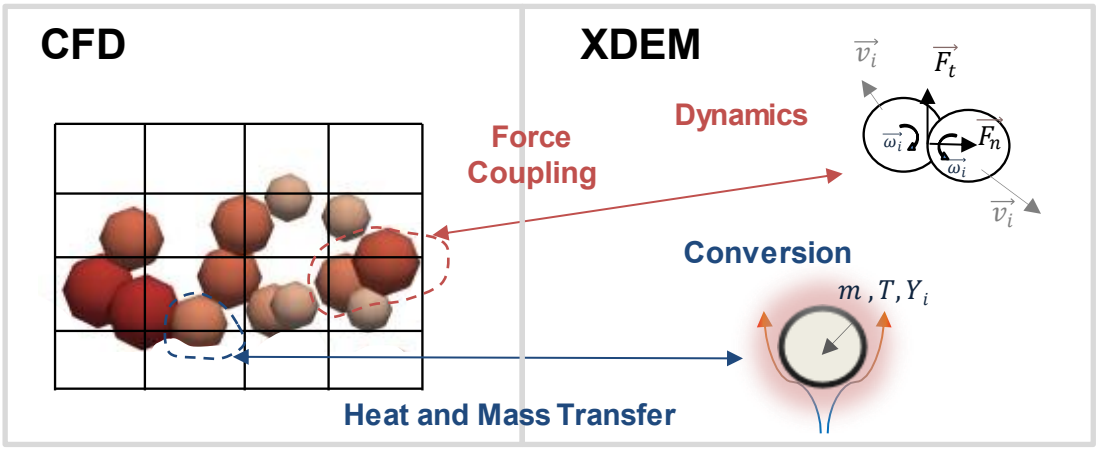

Figure 52: Representation of the XDEM application.

5.2 Mathematical Formulation

Considering the different programs used, this section aims to introduce the mathematical equations solved by each tool, which govern the flow, gas phase reactions, and the conversion of biomass particles. First, the mathematical formulation behind the CFD model is presented considering the nature of the flow field studied in this work, an incompressible reactive and turbulent flow.

5.2.1 CFD Model

The general governing transport equation expressed in Equation (31) is applied to express the conservation laws of mass, momentum, energy, and species.

Mass conservation

A mass balance over a volume element implies that the mass entering is equal to mass flowing out. Equation (34) expresses mathematically the general form of the mass conservation equation, or continuity equation, valid in both compressible and incompressible flows.

$$\frac{\partial \rho}{\partial t} + \nabla \cdot \left(\rho \vec{v} \right) = S_m \tag{34}$$

The source term, S_m, is the mass added to the continuous phase, for instance, through the reactions of the discrete phase like vaporization of water, and from any user-defined sources or sinks. The term $\nabla \cdot \left(\rho \vec{v} \right)$ represents the mass flux rate per unit volume.

Momentum conservation

The equation of motion is derived by applying a momentum balance over a cell element. Momentum conservation, also known as the Navier-Stokes equation, in an inertial reference frame, is given by Equation (35):

$$\frac{\partial}{\partial t}\left(\rho \vec{v} \right) + \nabla \cdot \left(\rho \vec{v} \vec{v} \right) = -\nabla p + \nabla \cdot \left(\bar{\bar{\tau}} \right) + \rho \vec{g} + \vec{F} \tag{35}$$

where $\vec{F}$ represents the force resulting from the interaction of the continuous with external body force which is accounted for when there is the interaction with the dispersed phase or a porous zone, $\rho \vec{g}$ corresponds to gravitational force and p the static pressure. In its turn, $\bar{\bar{\tau}}$ identifies the stress tensor, and its determination can be obtained through Equation (36):

$$\bar{\bar{\tau}} = \mu \left[\left(\nabla \vec{v} + \nabla \vec{v}^T \right) - \frac{2}{3} \nabla \cdot \vec{v} I \right] \tag{36}$$

where μ is the molecular viscosity, I the unit tensor, and the second term on the right hand side of the equation is the effect of volume dilation.

Energy conservation

Equation (37) represents mathematically the energy conservation and can be interpreted as the motion of heat. The first three terms on the right-hand side represent the energy transfer due to conduction,

species diffusion, and viscous dissipation, respectively. The source term S_h includes the heat generated by the chemical reactions and radiation.

$$\frac{\partial}{\partial t}(\rho E)+\nabla\cdot\left(\vec{v}\left(\rho E+p\right)\right)=\nabla\cdot\left(k_{eff}\nabla T-\sum_j h_j\vec{J}_j+\left(\overline{\overline{\tau}}_{eff}\cdot\vec{v}\right)\right)+S_h \tag{37}$$

where k_{eff} is the effective thermal conductivity which means that the turbulent is added, according to the turbulence model, $\vec{J}_j$ is the diffusion flux of specie, h the sensible enthalpy, E the total energy and can be obtained through Equation (38):

$$E=h+\frac{p}{\rho}+\frac{v^2}{2} \tag{38}$$

The enthalpy for an ideal incompressible flow is computed through Equation (39):

$$h=\sum_j Y_j h_j+\frac{p}{\rho} \tag{39}$$

where Y_j is the mass fraction of species j and its enthalpy is obtained through Equation (40):

$$h_j=\int_{T_{ref}}^{T} c_{p,j}dT \tag{40}$$

T_{ref} was defined in this work as 298.15 K.

Species Transport

To predict the local mass fractions of the different chemical species involved in the gas-phase flow, the conservation equation taking the general form of Equation (41) needs to be solved. Since the sum of the mass fractions must be equal to the unity, to minimize numerical error, the local mass fraction of the bulk specie N_2 (specie with the overall largest mass fraction) was assumed by subtraction.

$$\frac{\partial}{\partial t}\left(\rho Y_i\right)+\nabla\cdot\left(\rho\vec{v}Y_i\right)=-\nabla\cdot\vec{J}_i+R_i+S_i \tag{41}$$

It is important to see that Equation (41), S_i is the rate of creation by addition from the dispersed phase combined with any user-defined sources. In this work, this term was not considered. The term R_i represents the production or consumption of species i due to chemical reactions.

Turbulence Modeling

Apart from solving the fundamental transport equations described previously, there is the need to use other submodels to fully describe the fluid flow inside the grate-fired boiler. This requires the modeling of turbulence, radiation, and combustion.

Turbulence occurs when the inertial forces controlling the fluid motion are higher than the damping effect induced by the viscosity of the fluid that represents the viscous force. Hence, turbulent flows are characterized by randomly fluctuating velocity values which affect the heat and mass transfer conditions while laminar flows tend to be steady or to be less random. The Reynolds number, the ratio between the inertia and viscous forces, has been used to identify if a flow is laminar or turbulent. Accordingly, a flow is defined to be turbulent if the Reynolds number is higher than a critical value (typically 2,300 for a flow inside a circular pipe), representing that the inertial forces are most significant when compared to the viscous forces. In this sense, the issue of turbulence becomes important for numerical simulation since the flow becomes unstable due to the random modification of velocity direction, generation of vortices, and transitions from the steady to the transient state [421].

A large proportion of the flows that occur in nature and most of the engineering problems, including in industrial furnaces, are turbulent. However, turbulence depends on the furnace geometry and the design of the air supply. If all details of the fluid flow are necessary to be predicted, the previous unsteady Navier-Stokes equations should be solved by applying a Direct Numerical Simulation (DNS) and, consequently, any turbulence model is required. This allows to solve the whole range of temporal and spatial scales. However, simulations following this strategy require a cell and a time step size smaller than the smallest scales in a turbulent flow, denominated as the Kolmogorov microscale. Consequently, the computational demand is very large for industrial scale problems, and a common engineering approach is to average the unsteadiness of the turbulence. Hence, the governing equation is replaced by the time-averaged equations, the so-called Reynolds-Averaged Navier-Stokes (RANS) equations, and to close the equation a turbulence model should be introduced. With RANS formulation larger cells and time steps can be used, since the length scales of the variations of the mean values are larger when compared to the instantaneous ones. These advantages make the RANS equations more attractive for the study of industrial flows and, therefore, the quality of the numerical results will be a function of the selected turbulence model. Thus, the correct choice of the turbulence model is crucial to obtain accurate and reliable results. Afterward, the basic approach employed to compute the turbulent flow is presented.

Reynolds-Averaged Navier-Stokes Formulation

The turbulence, in this work, was modeled through the RANS approach, and using the two-equation model, more specifically the $k-\varepsilon$ model. In Reynolds averaging approach, the instantaneous velocities are composed by the mean velocity which is time averaged, and the fluctuating components, as represented by Equation (42):

$$v_i = \overline{v}_i + v_i' \tag{42}$$

Hence, likewise, this formulation accounting for mean and fluctuating components is applicable for pressure and the other scalar quantities considered in the previous conservation equations (pressure, energy, and species concentration). Consequently, the final mathematical expressions for the fundamental conservation equations are formulated by applying Equations (34), (35), (37), and (41), this form for the flow variables into the instantaneous component. However, as a result of averaging, new terms are added to the equations to represent the effects of turbulence. The new terms are the Reynolds stresses tensor, in the momentum equation, and turbulent transport fluxes in the energy and species equation and requires its modeling in order to close the fundamental conservation equations. ANSYS Fluent uses a common method, the Boussinesq hypothesis to relate the Reynolds stresses to the mean velocity gradients. Additional information regarding the numerical formulation behind the Boussinesq hypothesis may be found in the manual provided by ANSYS Fluent [418].

Realizable k-ε model

Within the RANS approach, ANSYS Fluent has several turbulence models, each one with its capabilities, its own mathematical expressions, and near-wall options. The available options range from simpler turbulence models, such as the Spalart-Allmaras, which is a one-equation model, to more advanced and accurate turbulence models such as the five-equation Reynolds Stress model. The most popular RANS models are the two-equation models where the solution of two different transport equations allows independently the calculation of the turbulent velocity and length scales. According to the literature review presented in Chapter 2, within the two-equation models, the k-ε models are the most common, in particular, the standard k-ε and the realizable k-ε models. The k-ε models evaluate the transport equations for the turbulent kinetic energy (k) and its dissipation rate (ε).

The realizable k-ε model is an improvement of the standard k - ε model, the default model from Fluent software. The realizable model was proposed by Shih et al. [422] with the intention to address the

deficiencies of the traditional standard k-ε model. Thus, the former model presents a reasonable compromise between calculation accuracy and numerical effort, and, particularly, the spreading rate of round jets is predicted more accurately than with the standard model. Hence, to model turbulence, it was used the Realizable $k-\varepsilon$ model, in which k and ε are obtained from the following transport Equations (43) and (44):

$$\frac{\partial}{\partial t}(\rho k)+\nabla(\rho k u_j)=\nabla\left[\left(\mu+\frac{\mu_t}{\sigma_k}\right)\nabla k\right]+G_k+G_B-\rho\varepsilon-Y_M+S_k \tag{43}$$

$$\frac{\partial}{\partial t}(\rho\varepsilon)+\nabla(\rho\varepsilon u_j)=\nabla\left[\left(\mu+\frac{\mu_t}{\sigma_\varepsilon}\right)\nabla\varepsilon\right]+\rho C_1 S\varepsilon-\rho C_2\frac{\varepsilon^2}{k+\sqrt{\nu\varepsilon}}+C_{1\varepsilon}\frac{\varepsilon}{k}C_{3\varepsilon}G_b+S_\varepsilon \tag{44}$$

where Y_M represents the contribution of the fluctuating dilatation incompressible turbulence to the overall dissipation rate and is neglected in the modeling of incompressible flows. C_2 and $C_{1\varepsilon}$ are constants of the model, σ_k and σ_ε are turbulent Prandtl numbers for k and ε, respectively. S_k and S_ε represents the user-defined source terms, and the constant parameter C_1 and the scalar that measure the deformation tensor, S, are determined according to Equations (45) and (46), respectively:

$$C_1=\max\left[0.43,\frac{\eta}{\eta+5}\right] \tag{45}$$

$$S=\sqrt{2S_{ij}S_{ij}} \tag{46}$$

where the parameter η is computed through Equation (47):

$$\eta=S\frac{k}{\varepsilon} \tag{47}$$

The turbulent viscosity, μ_t, is computed by combining k and ε as expressed in Equation (48):

$$\mu_t=\rho C_\mu\frac{k^2}{\varepsilon} \tag{48}$$

In its turn, G_k represents the generation of turbulence kinetic energy due to the mean velocity gradients and is calculated as:

$$G_k=-\rho\overline{u_i'u_j'}\frac{\partial u_j}{\partial x_i} \tag{48}$$

Considering a non-zero gravity field and a non-zero temperature gradient, the effects of buoyancy on the generation of k are included. Thus, the generation of turbulent kinetic energy due to the buoyancy G_b is calculated through Equation (49) for ideal gases:

$$G_b = -g_i \frac{\mu_t}{\rho \mathrm{Pr}_t} \frac{\partial p}{\partial x_i} \tag{49}$$

where Pr_t represents the turbulent Prandtl number for energy and g is the gravitational force vector in the i direction.

The model constants, $C_{1\varepsilon}$, C_2, σ_k, and σ_ε have been established by Fluent software to ensure that the model performs well for certain canonical flows. The model constants are defined as 1.44, 1.9, 1.0, and 1.2, respectively. The coefficient C_μ, here, in contrast to the standard k-ε is no longer a constant value. Equation (50) expresses the proposed mathematical expression to determine the parameter C_μ:

$$C_\mu = \frac{1}{A_0 + A_s U^* \frac{k}{\varepsilon}} \tag{50}$$

A full description of the mathematical equations to compute the remaining constants A_0, A_s, and U^* can be found in the manual provided by ANSYS Fluent [418].

Wall Boundary Turbulence Treatment

Since turbulent flows are significantly affected by the presence of walls, and as the no-slip condition at the walls has to be satisfied, particular attention should be addressed to correctly compute the velocity gradient close to this region. Furthermore, the turbulence varies according to the distance to the wall. When close to the wall region, viscous damping occurs reducing the tangential and normal velocities fluctuations. In the opposite direction, as the distance from the wall increases, the turbulence rapidly increases by the production of kinetic energy.

In ANSYS Fluent there is the possibility to select a wall function, which means that a set of semi-empirical functions are used to connect the near-wall region to the fully turbulent region and model adequately the wall influence. Consequently, turbulence models will receive modified terms due to the presence of the wall. Hence, this approach requires only an adequate mesh with a reduced refinement in the wall region. The Standard Wall Function, a logarithmic law to compute the mean velocity and temperature is applied

in this work. This model has been widely used in industrial flows and is one of the main options used to predict the fluid flow in a biomass grate-furnace, as indicated in Chapter 2. Further details of the model are presented in the ANSYS Fluent theory guide [418].

Radiation Modeling

The heat transfer mechanism through radiation plays a significant role in the heat transfer analysis in combustion processes. At high temperatures, as in combustion that occurs in biomass boilers, radiation is the dominant heat transfer mechanism from the sidewalls of the boiler to the bed. Radiation is included in the calculation through the source term in the energy equation, and ANSYS Fluent software disposes of several Radiation models to describe heat transfer in CFD simulations. However, some radiation models are more appropriate to solve certain phenomena than others and they differ significantly in their accuracy and computational time requirements. Considering the phenomena inside an industrial biomass boiler, the Discrete Ordinates Model (DOM) is suitable and allows an accurate solution for this problem. Furthermore, this model is commonly applied to combustion cases as discussed in Chapter 2.

The DOM considers and solves the Radiative Transfer Equation (RTE) (Equation (51)) for a finite number of discrete solid angles, each related with a vector direction $\vec{s}$ considering the global Cartesian system (*x, y, z*). Consequently, RTE is transformed into a transport equation for the radiation intensity in the spatial coordinates whereby it is possible to control the fineness of the angular discretization.

$$\nabla \cdot \left(I(\vec{r},\vec{s})\vec{s} \right) + (a+\sigma_s) I(\vec{r},\vec{s}) = an^2 \frac{\sigma T^4}{\pi} + \frac{\sigma_s}{4\pi} \int_0^{4\pi} I(\vec{r},\vec{s}') \Phi(\vec{s},\vec{s}') d\Omega' \tag{51}$$

In Equation (51), I is the radiant intensity, $\vec{r}$ the position vector, α the gas absorption coefficient, σ_s the scattering coefficient, r the refractive index, Φ the phase function, and Ω' the solid angle.

Regarding the gas mixture absorption coefficient (a), this parameter is defined through the Weighted Sum of Gray Gases Model (WSGGM), where for a distance (S) less or equal to 10^{-4} m a is defined according to Equation (52), and for S greater than 10^{-4} m according to Equation (53).

$$a = \sum_{i=0}^{I} a_{\varepsilon,i} \kappa_i p \tag{52}$$

$$a = -\frac{\ln(1-\varepsilon)}{s} \tag{53}$$

In the WSGGM the total emissivity over the distance s is calculated as in Equation (54):

$$\varepsilon = \sum_{i=0}^{I} a_{\varepsilon,i}(T)\left(1-e^{-\kappa_i ps}\right) \tag{54}$$

where $a_{\varepsilon,i}$ is the emissivity weighting factor for the i^{th} fictitious gray gas, the bracketed quantity is the i^{th} fictitious gray gas emissivity, κ_i is the absorption coefficient of the i^{th} gray gas, p is the sum of the partial pressures of all absorbing gases, and s is the path length. For $a_{\varepsilon,i}$ and κ_i the WSGGM uses values from the literature, dependent on mixture gas composition and temperature.

By doing so, the DOM was applied to solve the RTE for four polar and azimuthal angles and considering three pixels each as recommended in the ANSYS Fluent Theory Guide [418]

Turbulence-Chemistry Interaction Model

In ANSYS Fluent the mixing and transport of chemical species are modeled by solving conservation equations describing convection, diffusion, and reaction sources for each one. Multiple and simultaneous chemical reactions can be modeled, with reactions occurring in the fluid phase acting as a source of heat and reaction products for the flow.

In fact, the combustion of volatiles compounds released during the biomass conversion produces heat and, consequently, generates instabilities in the flow, due to the gas expansion and related buoyancy effects. A transition to a turbulent regime is observed due to these instabilities. Consequently, turbulence increases the mixing and, therefore, favors the combustion process and promotes the transport of heat and mass. Accordingly, to compute the reaction rate of combustion species, it is necessary to take into account the effects of turbulence. There are several methods to model this turbulence-chemistry interaction, including the Eddy Dissipation Model (EDM), Eddy Dissipation Concept (EDC), and Finite Rate-Eddy Dissipation Model (FR-ED).

The typical approach to gas-phase modeling is to assume that reactions in the gas phase are kinetically fast just above the fuel bed, where the temperature is high and the reactions are fast, forcing combustion to be controlled only by the mixing rate of oxidant and fuel. Nevertheless, in regions where the temperature is lower (for instance, close to the sidewalls), the kinetics of the reactions may become more important than the mixing phenomenon, requiring an alternative approach to accurately predict the temperature dependence for the reaction rates. In ANSYS Fluent it is possible to account for the temperature-limiting

effect through the utilization of the FR-ED model which computes both the Arrhenius and Eddy-Dissipation reaction rates and provides the net reaction rate as the minimum of the two. This is a formulation that values the prediction of gas temperature at a low computational cost. The mathematical formulation of this model is explained in more detail below.

Combustion Model

The gases released during the thermal decomposition of the fuel react in the gaseous phase, releasing most of the energy contained in the biomass. In general, one can express the various homogeneous reactions through the general expression presented in Equation (55) considering only forward reactions (irreversible reactions).

$$\sum_{i=1}^{N_r} v'_{i,r}\,\mathrm{Reactant}_i \xrightarrow{k_{f,r}} \sum_{i=1}^{N_p} v''_{i,r}\,\mathrm{Product}_i \tag{55}$$

where $v'_{i,r}$ and $v''_{i,r}$ represent the stoichiometric coefficients of the reactant and product i from the reaction r, respectively. N_r and N_p are the number of reactants and Products while $k_{f,r}$ is the forward rate constant for reaction r. Thus, for a reaction to take place, a premix is required from the macroscopic scale of transport to the molecular level and then, reacts according to the chemical kinetics of the particular reaction. Therefore, it is necessary to consider both processes, mixing (ED model) and reaction kinetics (FR model) between the different species present in the fluid flow.

Eddy Dissipation Model

The biomass combustion process inside the grate-fired boiler can be defined as a non-premixed flame, where the turbulence slowly mixes the volatiles that comes from biomass particles with the oxidizer. Based on the work of Magnussen and Hjertager [374] the net rate of production of species i due to reaction r, $R_{i,r}$ is obtained through the smaller value computed through Equation (56):

$$R_{i,r} = \mathbf{min}\left[v'_{i,r} M_{w,i} A \rho \frac{\varepsilon}{k} \min_{\Re}\left(\frac{Y_{\Re}}{v'_{\Re,r} M_{w,\Re}} \right); v'_{i,r} M_{w,i} A B \rho \frac{\varepsilon}{k} \frac{\sum_P Y_P}{\sum_j^N v''_{j,r} M_{w,j}} \right] \tag{56}$$

$M_{w,i}$ is the molecular weight of species i, Y_p is the mass fraction of any product species, P, while $Y_{\Re}$ is the mass fraction of a particular reactant, $\Re$. Parameters A and B are empirical constants

which should be conveniently tuned to account for abnormal mixing rates of the gas compounds that leave the biomass particles. These parameters were empirically determined based on experimental data for different flames. A represents a mixing parameter for the reactants and B is designed for the simulation of combustion under premixed conditions. The former parameter should be tuned for different conditions [353]. In general, with the ED model, the gas temperatures tend to be over-predicted due to abnormal higher reaction rates and, consequently, the species concentrations are also often inaccurately estimated [292]. Considering this issue, the value of A was modified to 0.6 for all reactions taking into account the results presented in the literature [290,292,306,307,353,354,359].

In Equation (56), the chemical reaction rate is controlled by the large-eddy mixing time scale, k/ε, and combustion takes place whenever turbulence is present ($k/\varepsilon > 0$).

Finite-Rate Model

Assuming that molecular-level mixing of the reactants has been achieved, the rate of reaction will depend on the frequency of collisions between the reactant molecules. For this purpose, an Arrhenius-type expression is applied to each reaction. The molar rate of creation/destruction of species i in the reaction r is given by Equation (57):

$$\hat{R}_{i,r} = \left(v''_{i,r} - v'_{i,r}\right) k_{f,r} \prod_{j=1}^{N_r} C_{j,r}^{\eta'_{i,r}} \tag{57}$$

where $C_{j,r}$ is the molar concentration of species j in reaction r and $\eta'_{i,r}$ is the rate exponent for reactant species j in the reaction r.

The Arrhenius expression, Equation (58), is used as a mathematical expression to calculate the reaction rate in reaction r in the forward direction, the source term in the individual species transport equation since it is the easiest way to manipulate the combustion modeling phenomena.

$$k_{f,r} = AT^{\beta} \exp\left(\frac{-E}{RT}\right) \tag{58}$$

where β is the temperature exponent.

Finally, the net source of chemical species i due to reaction is computed as the sum of the reaction sources over the N_r reactions that the species participate in:

$$R_i = M_{w,i} \sum_{r=1}^{N_r} \hat{R}_{i,r} \tag{59}$$

Reaction Mechanism

The combustion process is a set of chemical reaction equations that describe the oxidation of the fuel. This mechanism is modeled with some simplification because, to represent a detailed set of chemical reactions, it would be necessary to model a large number of chemical species and sub-reactions. This, in large-scale models, is prohibitive and a non-common practice due to the time required for the simulation. However, the combustion of biomass or any other fuel involves several different species and chemical reactions. For instance, the combustion of methane involves more than a hundred reactions and dozens of different species. Since it is not possible to use a detailed reaction mechanism and a large number of species due to the computational requirement that would be required, the oxidation of the volatiles is often modeled using a global reaction mechanism in which elementary reactions are represented by a global reaction. In this sense, the homogeneous combustion reactions considered in this work for modeling the volatiles combustion are the represented by Equations (60) to (62):

$$CH_4 + \frac{3}{2}O_2 \longrightarrow CO + 2H_2O \tag{60}$$

$$H_2 + \frac{1}{2}O_2 \longrightarrow H_2O \tag{61}$$

$$CO + \frac{1}{2}O_2 \longrightarrow CO_2 \tag{62}$$

The values of the stoichiometric coefficients and reaction exponents, as well as the constants of the various reactions considered in this work to form the combustion mechanism in the gas phase, are presented in Table 30.

Table 30: Kinetic reaction rate data for the combustion mechanism.

Chemical Reaction	A (s^{-1})	β (-)	E (J / kg mol)	Reaction order
Eq. (60)	5.012E11	0	2E8	$[CH_4]^{0.7} + [O_2]^{0.8}$
Eq. (61)	9.87E8	0	3.1E7	$[H_2]^1 + [O_2]^1$
Eq. (62)	2.239E12	0	1.702E8	$[CO]^1 + [O_2]^{0.25}$

Equation of state for incompressible ideal gases

The velocity of the continuous phase inside the grate-fired boiler is much lower than the speed of sound, i.e., the Mach number is less than 1.0, and, consequently, compressibility effects are negligible. Hence, the variation of the gas density with pressure can be neglected and the density of the fluid is obtained through the utilization of Equation (63):

$$\rho = \frac{p_{op}}{\frac{R}{M_w}T} \tag{63}$$

where p_{op} is the absolute operating pressure defined by the CFD software.

Bed Model

In the bed, where the biomass is converted, several decomposition reactions of the solid fuel take place. According to the literature, the biomass combustion process in the bed can be divided into four successive or overlapping subprocesses. Combustion in a grate-fired boiler can be seen as a fixed bed of fuel, which interacts with the interior of the furnace (freeboard). Thus, it becomes important to determine the mass flow rate of the gases released along the grate, as well as their temperature, and mass fraction of the different chemical compounds. Volatiles released from biomass particles typically consist of hydrogen, carbon monoxide, carbon dioxide, and methane, although their composition depends on the type of fuel and their origin.

In this work, an empirical equilibrium model which describes the biomass conversion as a function of the grate length is used to obtain the initial boundary conditions for the region above the grate. This methodology has been successfully used in the literature for similar studies to predict a comprehensive conversion behavior of the biomass combustion in fixed bed [290,301,306,307,358,359]. Moreover, its performance and accuracy were comparable to some other models, and the equilibrium empirical model addresses properly this engineering problem and provides a more reasonable correct boundary condition for the CFD modeling [290,303,308,358].

Hence, taking into account that biomass conversion on the grate is exposed to a radiation heat flux from the flame in the upper part of the boiler, to a primary air flux from beneath the grate. In addition, as the biomass is being converted to water vapor, volatiles, carbon monoxide, and carbon dioxide from the char oxidation are released. The operating conditions for each position on the grate are fuel feeding rate, composition, the temperature of the fuel and air, incoming radiation flux, and biomass conversion rate.

Taking into account those conditions, an overall mass and energy balance can be established to provide the profiles of temperature, species concentrations, and velocity of the gas leaving the fuel bed into the freeboard. Consequently, the bed model will provide an appropriate lengthwise profile of these parameters along the grate and that is based on the experience and the design of the grate-fired boiler.

In this way, the mass flow rate released in each i (1, 2, or 3) section of the grate can be computed by Equation (64):

$$\dot{m}_i = \dot{m}_{H_2O} + \dot{m}_{vol} + \dot{m}_{char} + \dot{m}_{air} \tag{64}$$

where the terms on right hand side of Equation (64) represent the mass flow rate of moisture, volatiles, char and air released. In its turn, an energy balance represented in Equation (65) is defined to compute the gas temperature:

$$T_i = \frac{\dot{Q}_{rad} + \dot{m}_{CO} Q_{CO} + \dot{m}_{CO_2} Q_{CO_2} - \dot{m}_{H_2O} Q_{H_2O} - \dot{m}_{vol.} Q_{vol}}{\dot{m}_i c_{p,i}} + T_0 \tag{65}$$

where the terms $\dot{Q}_{rad}$, Q_{H_2O}, and Q_{vol} represent the radiative heat transfer from the freeboard region to the i^{th} zone of the grate, latent heat of water evaporation (2,250 kJ/kg), and the energy required to start the devolatilization (418 kJ/kg), respectively. The net heat flux received by the fuel bed is assumed to be constant and uniformly distributed in the first two sections of the grate. In the final part of the grate, since most of this section is not exposed to the flame radiation, only a minor contribution of the radiation was considered.

Q_{CO_2} and Q_{CO} are the heat released from char by a complete oxidation and partial oxidation, respectively. Their values are 32,794 kJ/kg and 9,208 kJ/kg, respectively. The last terms, T_0 is the reference temperature, $\dot{m}_i$ the total mass flow rate released in each grate section, and $c_{p,i}$ the specific heat of the flue gases.

The char reaction and its products in the fuel bed are assumed to be oxidized and produces either CO or CO_2, as expressed in Equation (66). To compute the split ratio between these two chemical compounds, Equation (67) expresses a mathematical relation between their mass fractions and the temperature in the grate.

$$\gamma \mathrm{C\,(s)} + \mathrm{O_2} \longrightarrow 2(\gamma - 1)\mathrm{CO} + (2 - \gamma)\mathrm{CO_2} \tag{66}$$

$$\frac{CO}{CO_2} = 2500 \exp\left(\frac{-6240}{T_i}\right) \tag{67}$$

Consequently, according to Equation (68), the mass flow rates of CO and CO_2 from char reaction in the i^{th} zone of the grate can be estimated by Equations (68), and (69), respectively.

$$\dot{m}_{CO} = \frac{2500 \exp\left(\frac{-6240}{T_i}\right)}{1 + 2500 \exp\left(\frac{-6240}{T_i}\right)} \dot{m}_{char} \tag{68}$$

$$\dot{m}_{CO_2} = \frac{1}{1 + 2500 \exp\left(\frac{-6240}{T_i}\right)} \dot{m}_{char} \tag{69}$$

In addition to the species released during the char conversion, an additional quantity of CO, CO_2, CH_4, and H_2, is considered to be released from the fuel bed into the freeboard due to the devolatilization reaction. O_2 is also considered as input to the freeboard, but its amount is related to the remaining fraction after its reaction with the char particles.

5.2.2 Particle Conversion and Motion Model

Motion

The discrete element method applied in the dynamic XDEM module is based on the soft sphere model [419]. The translation movement of each particle is governed by the second law of Newton where the force acting at the center of gravity of the particle i is expressed by Equation (70):

$$\vec{F_i} = m_i \vec{a}_i = m_i \frac{d\vec{u}_i}{dt} \tag{70}$$

where the particle velocity can be determined by:

$$\vec{u}_i = \frac{d\vec{r}_i}{dt} \tag{71}$$

Contact, drag, and gravitational forces are examples of different sources that may act on the particle. However, the drag force can be neglected due to the reduced velocity of the gas flow, and, in this way, the total force can be calculated through Equation (72):

$$\vec{F_i} = \vec{F}_{i,contact} + \vec{F}_{i,gravity} \tag{72}$$

In its turn, the contact force is the sum of all forces acting on the particle resultant from the contact with other particles:

$$\vec{F}_{i,contact} = \sum_{j=1, j\neq i}^{N} \vec{F}_{ij} \tag{73}$$

The occurrence of contacts between the particles promotes the rotational motion and, for particle i this term can be described by the second law of Euler, Equation (74):

$$\vec{T}_{i,contact} = I_i \vec{\alpha}_I = I_i \frac{d\vec{\omega}_i}{dt} \tag{74}$$

where

$$\vec{\omega}_i = \frac{d\vec{\theta}_i}{dt} \tag{75}$$

$$\vec{T}_{i,contact} = \sum_{j=1, j\neq i}^{N} \vec{T}_{ij} = \sum_{j=1, j\neq i}^{N} \vec{d}_{ij} \times \vec{F}_{ij} \tag{76}$$

The integration of Equations (70) and (74) over time and the particle position, orientations, and velocity are updated accordingly during time integration. More information about the details of the model can be found in the literature [423–425].

Particle Conversion

A discrete particle may be considered of different phases as solid, liquid, gas, and inerts in XDEM. At the particle scale, it is important to note that thermodynamic and physical properties vary along with its conversion. This is considered by a system of one-dimensional and transient conservation equations of energy and mass transport within each particle. Considering the pore volume of a porous particle, the gas mass conservation equation is expressed by Equation (77):

$$\frac{\partial}{\partial t}\left(\varepsilon_p \rho_g\right) + \frac{1}{r^n}\frac{\partial}{\partial r}\left(r^n \varepsilon_p \rho_g \vec{u}_g\right) = S_{mass} \tag{77}$$

where S_{mass} is the sum of the individual mass production or consumption rates due to chemical reactions, ε_p is the particle porosity, u_p the advective velocity, and ρ_g the intrinsic density of the fluid, which is the result of partial densities of species present in the gas phase. The particle geometry is defined by the radius, r, and can be chosen to be an infinite plane, cylinder, or sphere according to the definition of the n parameter, which can be 0, 1, or 2, respectively.

The transport of the different gas species that may form the fluid flow within the pore space is considered using the Law of Darcy, Equation (78):

$$-\frac{\partial p}{\partial r} = \frac{\mu_g \varepsilon_p}{K} u_g \tag{78}$$

where p, μ_g, and K are the pressure, dynamic viscosity, and the permeability of the porous particle, respectively. The balance of individual species, i, within the pores can also be expressed by Equation (79), where the concentration of each species in the gas mixtures depends on the convective and diffusive flux and the chemical reactions:

$$\frac{\partial}{\partial t}\left(\varepsilon_p \rho_{i,g}\right) + \frac{1}{r^n}\frac{\partial}{\partial r}\left(r^n \varepsilon_p \rho_{i,g} \vec{u}_g\right) = \frac{1}{r^n}\frac{\partial}{\partial r}\left(r^n D_i \varepsilon_p \frac{\partial}{\partial r}\rho_{i,g}\right) + \varepsilon_p \sum_k \dot{\omega}_{k,i} \tag{79}$$

where D_i is the molecular diffusion coefficient and $\dot{\omega}_{k,i}$ is the source term which accounts for the consumption or generation of the specie i from the reaction k.

For the conservation of solid and liquid fractions of the fuel, transport mechanisms are neglected. Hence, the variation of these components is only dependent on the reaction source term as expressed in Equation (80):

$$\frac{\partial \rho_i}{\partial t} = \dot{\omega}_{k,i} \tag{80}$$

The depletion of solid material has been taken into account by using a solid intrinsic density shrinking approach in which a decreasing particle density and a reduction of particle size occur during the devolatilization and consumption by the char combustion in the outermost cell. The latter causes a decrease in the particle dimension. Hence, it was considered that the particle shrinks uniformly in the radial direction, and its original shape remains unchanged.

To complete the model, the temperature variation in each particle needs to be computed. The dominant heat transfer mechanisms in a set of particles are the conduction between particles in contact, radiative heat transfer between neighboring particles, and also convective heat transfer to a fluid in the spaces between the particles. Equation (81) represents the energy conservation equation used to determine the temperature:

$$\frac{\partial}{\partial t}\left(\rho h\right) = \frac{1}{r^n}\frac{\partial}{\partial t}\left(r^n k_{eff} \frac{\partial T}{\partial r}\right) + \dot{Q} \tag{81}$$

k_{eff} represents the effective thermal conductivity, T the temperature of each particle, and, in the case of chemical reactions, the energy source, $\dot{Q}$, which can be determined by Equation (82):

$$\dot{Q} = \sum_{k=1}^{N} \dot{\omega}_k H_k \tag{82}$$

where H_k is the reaction enthalpy of reaction k. The effective thermal conductivity considers the heat transfer by conduction in the gas, solid, and radiation in the pore, and can be evaluated using Equation (83):

$$k_{eff} = \varepsilon_p k_g + \sum_{i=1}^{k} \eta_i k_{i,solid} + k_{rad} \tag{83}$$

The radiation term is determined by Equation (84):

$$k_{rad} = \frac{\varepsilon_p}{1-\varepsilon_p} \sigma 4.0 T^3 \tag{84}$$

where σ is the Stefan-Boltzmann constant (5.67x10^{-8} W/m^{2}K^4).

Considering a thermodynamic equilibrium between the particle and intra-particle fluid and the fluid as a perfect gas, the gas density, and its enthalpy can be calculated using Equations (85) and (86):

$$\rho_g = \frac{p_g}{RT_g \sum_i \frac{y_i}{M_i}} \tag{85}$$

$$h_g = c_{p,g} T_g \tag{86}$$

Regarding the thermal conversion stages considered in the mathematical model, it is assumed that the conversion is composed of the following sub-processes: drying, devolatilization, and char burnout. The conversion of each subprocess is governed and calculated by separate submodels.

Drying

The process of drying was approximated by an energy balance considering the energy available for evaporation and the amount of water evaporated. An increase of the temperature above the temperature defined for the evaporation means that the moisture fraction of the particle will be consumed by the evaporation process. Hence, the source term for this submodel can be computed by the Equation (87):

$$\dot{\omega}_{H_2O} = \begin{cases} \dfrac{\left(T - T_{evap}\right)\rho c_p}{H_{evap}\Delta t} & \text{if} \quad T \geq T_{evap} \\ 0 & \text{if} \quad T \leq T_{evap} \end{cases} \tag{87}$$

where ρ, c_p, T_{evap}, and H_{evap} are the density and the specific heat of biomass, the evaporation temperature, and its evaporation enthalpy, respectively.

Devolatilization

Devolatilization occurs after the drying stage, and during the heating of the particle. This conversion process leads to a decomposition of the biomass into char (solid) and volatiles (gases). Thus, the reaction is described using a one-step global reaction expressing the decomposition of the biomass in these two products and also considering the presence of ash as a final product. This is a common practice in the literature to reduce the computational time without reducing the accuracy of the mathematical predictions, as was recommended, for instance, by Blasi et al. [426]. Equation (89) presents the reaction considered to express the devolatilization conversion. The gas fraction is represented by the chemical species considered in this work. The presence of tar was not considered because, in addition to its complex composition, it has been estimated that more than a hundred of different hydrocarbons are released during the devolatilization [334], and are assumed to be fully converted into main secondary products in the form of CO or CO_2 [247].

$$\text{Biomass} \longrightarrow \gamma_{\text{CO}}\text{CO} + \gamma_{\text{CO}_2}\text{CO}_2 + \gamma_{\text{H}_2\text{O}}\text{H}_2\text{O} + \gamma_{\text{H}_2}\text{H}_2 + \gamma_{\text{CH}_4}\text{CH}_4 + \text{Char} + \text{Ash} \tag{88}$$

In its turn, Equation (89) expresses the reaction rate of this stage using a simple Arrhenius equation:

$$\dot{\omega}_{biomass} = A\exp\left(\frac{-E}{R\,T}\right)\rho_{biomass} \tag{89}$$

Char

After the devolatilization, the remaining char was considered to react with oxygen, as represented by Equation (90). This heterogeneous reaction was considered dependent only on the particle temperature, and its reaction rate was calculated using the same mathematical expression defined for the devolatilization reaction. The kinetic parameters were adapted to specifically reproduce the mass loss during this conversion stage.

$$\mathrm{C(s)}+\frac{1}{2}\mathrm{O_2}\longrightarrow\mathrm{CO} \tag{90}$$

Initial and Boundary Conditions

To complete the mathematical model for every single particle, and solve the previous conservation equations, boundary conditions are necessary. Considering that the particles are symmetric, a symmetry boundary condition, Equation (91) and (92), is applied to the center of the particle.

$$-k_{eff}\left.\frac{\partial T}{\partial r}\right|_{r=0}=0 \tag{91}$$

$$-D_i\left.\frac{\partial \rho_{i,g}}{\partial r}\right|_{r=0}=0 \tag{92}$$

At the surface of the particle, the boundary conditions for heat and mass transfer are given by Equation (93) and (94):

$$-k_{eff}\left.\frac{\partial T}{\partial r}\right|_{r=R}=\dot{q}_{cv}+\dot{q}_{rad}+\dot{q}_{cd} \tag{93}$$

$$-D_i\left.\frac{\partial \rho_{i,g}}{\partial r}\right|_{r=R}=\beta_i\left(\rho_{i,s}-\rho_{i,\infty}\right)+\dot{m}_{i,g} \tag{94}$$

where β_i is the mass transfer coefficient, and $\rho_{i,\infty}$ is the gas partial density of species *i* in ambient gas. $\rho_{i,s}$ is the partial density of species i at the surface of the particle, and $\dot{m}_{i,g}$ represents the mass fluxes from the environment. Moreover, $\dot{q}_{rad}$ and $\dot{q}_{cd}$ account for radiative heat and conduction transport through physical contact with the wall and/or particles. Convective heat transfer from the environment to the particle is also considered. Equations (95), (96), and (97) express the way the contribution of the different heat transfer mechanisms is taken into account.

$$\dot{q}_{cv}=h(T_p-T_\infty) \tag{95}$$

$$\dot{q}_{rad}=\sum_{j=1}^{M}F_{p\to j}\sigma(T_p^4-T_j) \tag{96}$$

$$\dot{q}_{cd}=\sum_{j=1}^{N}\frac{1}{\frac{1}{k_p}+\frac{1}{k_j}}\frac{T_p-T_j}{\Delta x_{p,j}} \tag{97}$$

Where T_p, h, and $F_{p\to j}$ are the temperature of the particle, the heat transfer coefficient, and the view factor between particle p and its neighbor j, respectively.

Concerning the transfer coefficients, a range of experiments has already been carried out by numerous authors to determine appropriate laws for different particle geometries and flow conditions at the particle surface [427,428]. Different regimes can be characterized by dimensionless numbers such as Nusselt, Sherwood, Reynolds, Schmidt, and Prandtl. Hence, to determine the heat and mass transfer coefficients, the experimental correlation of Wakao and Kaguei [429,430] are used to compute the Nusselt (Equation (98)) and Sherwood (Equation (99)) numbers. The empirical correlations are valid for the heat and mass transfer coefficients determination between particle and gas in a packed bed, and from low Reynolds numbers up to 8,500 and 10,000, respectively.

$$\mathrm{Nu} = 2 + 1.1\left(\mathrm{Pr}^{1/3}\,\mathrm{Re}^{0.6}\right) \tag{98}$$

$$\mathrm{Sh} = 2 + 1.1\left(\mathrm{Sc}^{1/3}\,\mathrm{Re}^{0.6}\right) \tag{99}$$

where the Re, Pr and Sc, are the Reynolds, Prandtl, and Schmidt numbers, defined by Equation (100), (101), and (102), respectively.

$$\mathrm{Re} = \frac{\rho U\, d}{\mu} \tag{100}$$

$$\mathrm{Pr} = \frac{c_p \mu}{k} \tag{101}$$

$$\mathrm{Sc} = \frac{\mu}{\rho D} \tag{102}$$

5.3 Numerical Models

As initially mentioned, two numerical models are developed in this thesis consisting in a CFD model of a grate-fired boiler and a model representing a set of particles that are burned in a small-scale reactor. In this section, the details of both models are presented.

5.3.1 Grate-Fired Boiler

Geometry Definition

For the numerical simulations of the reactive gas phase flow in the ANSYS Fluent software, the first step consists of the definition of the computational domain to be studied. The simulation concerns the grate-fired boiler, presented in Figure 53, from the Mortágua power plant that was described in Chapter 3. The geometric configuration of the boiler presents symmetry since the secondary air jets on the side walls are equally spaced along its width. Thus, it is only necessary to model 1/13 of the full geometry, which corresponds to a slice of 320 mm in thickness. This simplification allowed a significant reduction in the complexity of the geometry modeling, and also for the subsequent mesh generation. The geometry of the boiler was developed using the scripting language from Gmsh software, providing the possibility to automate the generation of the model with a reduced interface for the user and an easy execution of complex geometries. Figure 54 illustrates an overview of the commands applied to develop the 3D model in Gmsh. This configuration was based on the technical drawing of the equipment, which is presented in Annex E.

Figure 53: The grate-fired boiler.

```
Point(15) = {0.0,  1.39759,  0.0};
Point(16) = {0.0,  0.879395,  0.0};
Point(17) = {2.155,  0.65291,  0.0};
Point(18) = { 4.310,  0.42642,  0.0};
Point(19) = {6.464,  0.2000,  0.0};
Point(20) = { 6.464,  -0.93442,  0.0};

Line(1) = {1, 2};
Line(2) = {2, 3};
Line(3) = {3, 4};
Line(4) = {4, 5};
Line(5) = {5, 6};
Line(6) = {6, 7};
Line(7) = {7, 8};
Line(8) = {8, 9};
Line(9) = {9, 10};
Line(10) = {10, 11};
Line(11) = {11, 12};
Line(12) = {12, 13};
Line(13) = {13, 14};
Line(14) = {14, 15};
Line(15) = {15, 16};
Line(16) = {16, 17};
Line(17) = {17, 18};
Line(18) = {18, 19};
Line(19) = {19, 20};
Line(20) = {20, 1};

Line Loop(5) = {1,2,3,4,5,6,7,8,9,10,11,12,13,14,15,16,17,18,19,20};

Plane Surface(6) = {5};

surfaceVector[] = Extrude {0, 0, 3.900} {
  Surface{6};
};

// create the cylinders for intersection
nCylinder=12;
startCylinder=100;
For i In {0 : nCylinder}
   Cylinder(startCylinder+i)={-0.75, 4.24, 0.03+i*0.32, 1, 0, 0, 0.019, 2*Pi};
EndFor

// create the wall with holes
f1() = BooleanDifference{Surface{17};}{Volume{startCylinder:startCylinder+nCylinder};};
// create the cirles
f2() = BooleanIntersection{Surface{17};}{Volume{startCylinder:startCylinder+nCylinder};Delete;};
// clue wall with holes and circles together
BooleanUnion{ Surface{ f1() }; Delete; }{ Surface{ f2() }; Delete; }

// create the cylinders for intersection
nCylinder=12;
startCylinder=100;
For i In {0 : nCylinder}
   Cylinder(startCylinder+i)={-0.75, 5.78081, 0.03+i*0.32, 1, 0, 0, 0.019, 2*Pi};
EndFor

// create the wall with holes
f1() = BooleanDifference{Surface{17};}{Volume{startCylinder:startCylinder+nCylinder};};
// create the cirles
f2() = BooleanIntersection{Surface{17};}{Volume{startCylinder:startCylinder+nCylinder};Delete;};
// clue wall with holes and circles together
BooleanUnion{ Surface{ f1() }; Delete; }{ Surface{ f2() }; Delete; }

// create the cylinders for intersection
nCylinder=12;
startCylinder=100;
For i In {0 : nCylinder}
   Cylinder(startCylinder+i)={5.25385, 1.76118, 0.03+i*0.32, -1, 0, 0, 0.019, 2*Pi};
EndFor

// create the wall with holes
f1() = BooleanDifference{Surface{9};}{Volume{startCylinder:startCylinder+nCylinder};};
// create the cirles
f2() = BooleanIntersection{Surface{9};}{Volume{startCylinder:startCylinder+nCylinder};Delete;};
// clue wall with holes and circles together
BooleanUnion{ Surface{ f1() }; Delete; }{ Surface{ f2() }; Delete; }
```

Points

Lines

Volume

Definition of the Nozzles

Figure 54: An overview of the commands applied to develop the 3D model in Gmsh.

As can be seen in Figure 55, the grate region, in the lower part of the model, was divided into three separate zones in the lengthwise *x*-direction according to the primary air supply division. Hence, it is allowed the introduction of different boundary conditions to better reproduce the biomass thermal conversion. The secondary air is supplied through nine side nozzles located above the grate. With regard to the secondary air injectors, despite making the mesh construction difficult, it was decided to maintain the circular section of 38 mm in diameter. The gases released from the bed will flow upwards and will mix with the secondary air in order to ensure that the combustion of the gases is completed, and are sent to the outside through the upper face of the model.

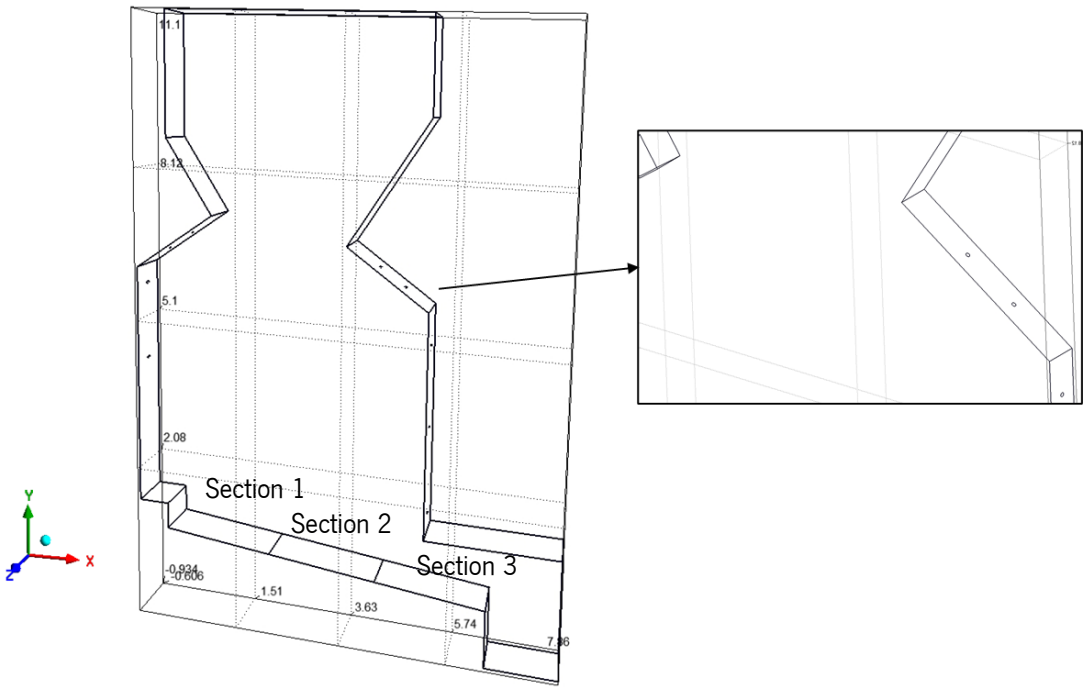

Figure 55: Representation of the 3D model.

Mesh Generation

Time and effort were devoted to the development of the numerical mesh as its quality affects the accuracy of the CFD results. This task required a lot of work since changing the domain division strategy, and locations of the refinement to change the size of elements in the different zones of the domain. All this work was carried out in order to increase the accuracy and reliability of the results.

The OpenFOAM algorithms, in particular, the cartesianMesh option was used to generate a mesh around hexahedral cells, with refinements in specific zones to obtain a suitable resolution of the temperature and velocity field in regions of strong gradients.

Three different meshes were developed to assess the influence of the discretization in the numerical results. Figure 56 presents an outline of one of the meshes developed and focused on some areas where it is possible to observe the refinement that took place in the central area of the furnace and next to the secondary air injectors.

The quality of the results is highly mesh-dependent, so a high-quality mesh is one of the key factors for successful CFD analysis. Thus, Table 31 presents the main values of the parameters that allow the evaluation of the mesh quality.

Table 31: General numerical mesh characteristics from the various meshes produced.

Parameter	Value
Mesh Elements	200k – 900k
Minimum Element Size (mm)	10
Maximum Element Size (mm)	100 – 150
Maximum Skewness	1.25 – 1.44
Maximum Aspect Ratio	7.84 – 9.58
Average Non-Orthogonality	3.68 – 4.84

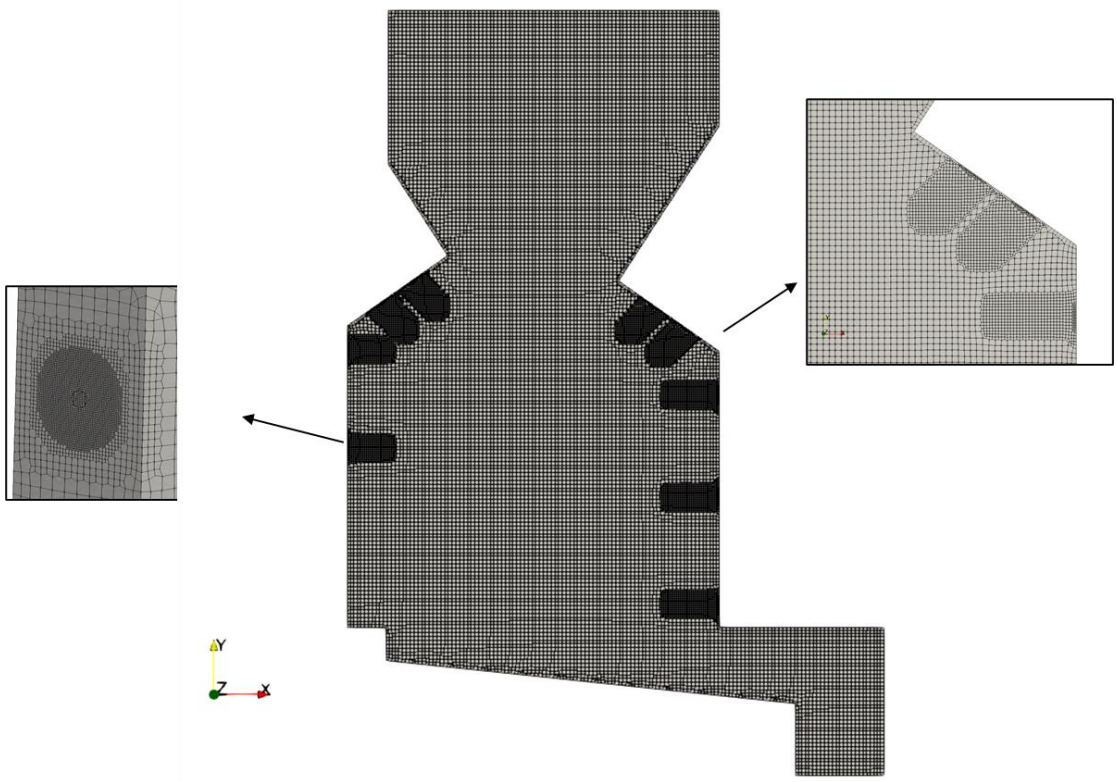

Figure 56: Overview of the mesh and its details in the region of the secondary nozzles.

Boundary Conditions

Boundary conditions describe the fluid flow and thermal variables at the boundaries of the geometric model. These conditions are therefore a critical component of the numerical simulations, and it is important that they are specified correctly.

In this way, the faces corresponding to sections 1, 2, and 3, to the outlet, and secondary air nozzles were selected as boundary conditions. The sidewalls of the model were considered adiabatic and while the front and back faces of the model were defined as a symmetry condition so that there was no influence on the fluid flow.

The values used for the boundary conditions are based on the nominal operating conditions of the boiler presented in Chapter 3, in particular in Tables 13 and 14, along with the results obtained through the empirical bed model.

Regarding the fluid properties, it was considered that the fluid is an incompressible ideal gas.

Solver Configuration

For the CFD simulations performed with ANSYS Fluent software, an incompressible solver, the pressure-based solver, was used. This solver guarantees the mass conservation of the velocity field by solving the pressure equation. Basically, while enforcing mass conservation, the pressure equation is obtained by derivation of the continuity and momentum equations by the pressure. Since the governing equations of the CFD model are non-linear and are relations between them, the solution can only be obtained through an iterative process. To solve these equations in a sequential way, one after the other, the Pressure-Implicit with Splitting of Operators (PISO) algorithm is used in a segregated form. This algorithm was preferred over the Semi-Implicit Method for Pressure-Linked Equations (SIMPLE) to solve the pressure-velocity coupling since it is more efficient, requires a reduced number of iterations to converge, and is useful for unsteady flow simulations, and presents better results for meshes with a reduced quality.

Regarding the spatial discretization, the convection terms of the different transport equations are solved using first-order upwind methods, with the exception of the species transport equations that are solved using second-order upwind method. For the gradient terms, to evaluate diffusive fluxes and velocity, the least-squares cell-based method was selected. Both methods for spatial discretization were selected due to their easier convergence and a less computationally intensive simulation. In addition to the previous interpolation schemes, for pressure PRESTO! was selected due to their suitability for highly swirling flows involving steep pressure gradients.

Furthermore, regarding the transient formulation, the computational model was solved using a first-order implicit method, and the convergence criterion for the iterative calculation was defined as 1E-3 for continuity, momentum, and turbulence equations and 1E-6 for energy and the discrete ordinates equation. An automated method was used to decide the fluid time step accordingly to the convergence rate of the previous step. Nonetheless, the values were limited between 1E-6 seconds and to 0.01 seconds taking into consideration a Courant number of 1.

The contribution of the gravitational acceleration was implemented in a downwards direction along the y-axis, with a magnitude of 9.81 m/s^2.

After defining all models and solver parameters, it is necessary to initialize the simulation. The initialization is necessary to fill the mesh cells with an initial value that is updated along the iterative simulation process. This is perhaps the most critical step of the simulation since a correct initialization facilitates the convergence of the solution, and reduces the computational time. In this way, the domain close to the grate was initialized with 23% oxygen and 77% nitrogen (mass fractions) as an approximation of the air composition and with a high temperature of 1500 K was defined to also promote combustion.

The simulations were computed in a twenty-core (logical) processor, with 128 GB of memory RAM. The results are time-averaged after the boiler reaches a pseudo-steady-state.

5.3.2 Small-scale reactor

The case concerned with the small-scale reactor consists of a basket where the biomass particles are placed with 60 mm diameter and 50 mm height. The number of particles was defined according to the initial mass defined to make the simulations and where average particle size is defined, and automatically the particles are generated in a position inside the basket and considering a variation of 10% in the size dimension. In addition to this configuration, additional information regarding the particles composition in terms of moisture, ash, and volatiles is required.

Figure 57 illustrates the basket geometry including a set of particles with different sizes distributed randomly. The gas phase is specified as hot air that is in direct contact with the particles and although its presence is not simulated, heat transfer conditions are derived to replicate those inside the reactor.

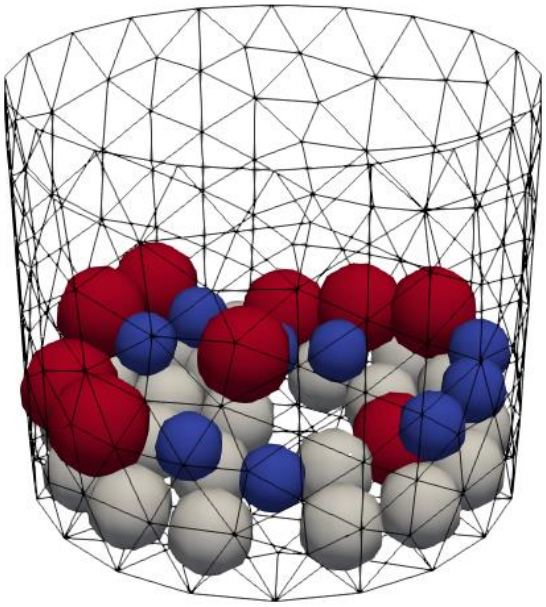

Figure 57: Particles configuration in the basket from the small-scale reactor.

Regarding the boundary conditions necessary to predict the thermal degradation of the biomass particles, an effective heat transfer coefficient has been introduced. In addition to the normal convective heat transfer, as the particles are introduced into a hot environment, the radiative constituent needs to be accounted for. Equations (103) to (105) present the mathematical expressions used to compute the effective heat transfer coefficient. The convective parameter is derived from Equation (98) while the radiation term is obtained by linearization of the Stefan-Boltzmann law for thermal radiation.

$$h_{eff} = h_{rad} + h_{cv} \tag{103}$$

$$h_{cv} = \frac{2\,k_{gas}}{D_p} \tag{104}$$

$$h_{rad} = \varepsilon\sigma\left(T_{wall}^2 + T_p^2\right)\left(T_{wall} + T_p\right) \tag{105}$$

The heat flux received for the particles, was estimated through the calculation of the heat flux provided by the small-scale reactor as defined by Equation (106):

$$q_{eff} = \sigma\left(T_{wall}^4 - T_p^4\right) \tag{106}$$

CHAPTER 6

PHYSICOCHEMICAL CHARACTERIZATION

This chapter presents an assessment of the physicochemical properties of the fuels selected for this work (ET, EB, EBA, PT, AT, AB, and OB). Each fuel is fully characterized in terms of chemical composition by proximate and ultimate analysis and its calorific value. The assessment of the variability of the fuel properties is important to understand the combustion behavior. Furthermore, this chapter examines the variation in terms of the thermal properties and also the ash elements to evaluate the tendency for slagging and fouling. For these experiments, the different parts of the fuels were not considered, and the core of biomass was used. Larger particles of the previous samples were subsequently analyzed in terms of their physical characteristics. All analytical results are presented alongside a discussion and comparison between the fuels.

6.1 Physicochemical Analysis

The results from the physical and chemical characterization of the fuels considered in this work are summarized in Table 32. Based on these results, it is noteworthy that, on a dry basis, all solid biomass samples contain a fixed carbon (FC) and ash content variable in the range of 6.2 to 21.6% and 0.6 to 4.2%, respectively, while the volatile matter (VM) content is considerably high (77.8 to 88.9%). Comparing the different fuels, ET, EB, and EBA samples have the highest VM content along with the highest ash content and lowest FC content. Additionally, from the core part of the fuel to the exterior part, bark, and branches, considering the eucalyptus samples, the ash content increases, and the VM content although does not have a clear trend, the VM content is lower. Saarela et al. [431] also found the same behavior for pine samples and stated that the ash is mainly higher for bark than wood. However, for acacia samples, the results follow the same trend for the VM content, but the ash content is similar. Regarding the moisture content, it was found to range between 2.1 and 11.5%. The presence of water has a negative influence on the combustion behavior and affects the physical properties of the samples. Even for fuels collected at the same time from the same source, the moisture content can vary significantly. If there is a higher moisture value, ignition of the fuel will be difficult, and the heating value will be reduced due to the higher moisture content and the need for more heat to dry the fuel.

Table 32: Physicochemical properties and calorific value of the different biomass fuels.

Property	Parameter	Acacia		Eucalyptus			Pine	Olive
		Trunk*	Branches	Bark	Trunk*	Branches	Trunk*	Branches
Physical Analysis	Moisture (%)	5.0	6.2	3.4	2.1	6.7	11.5	11.2
	Volatile matter (%, db)	81.8	77.8	89.6	88.9	82.9	83.7	81.5
	Ashes (%, db)	1.1	0.7	4.2	1.0	3.2	0.8	1.8
	Fixed Carbon (%, db)	17.1	21.5	6.2	10.1	13.9	15.5	16.7
Chemical Characterization	Carbon (%, db)	45.40	52.40	43.10	47.20	55.90	47.30	49.40
	Hydrogen (%, db)	6.88	7.38	6.46	7.03	7.55	6.40	6.95
	Nitrogen (%, db)	0.77	3.21	0.25	0.11	1.44	0.13	0.24
	Sulfur (%, db)	0.01	0.04	0.01	0.01	0.01	0.99	0.88
	Oxygen (%, db)	46.94	36.97	50.18	45.65	35.10	45.18	42.53
Calorific Value (dry basis)	HHV (MJ/kg)	17.14	20.41	15.20	17.56	22.30	19.10	17.71
	LHV (MJ/kg)	15.66	18.81	13.81	16.05	20.67	18.60	16.22

* without bark

db – dry basis

From the analysis of the VM and FC content, as highlighted in other investigations, the reactivity of the fuel, which means the reaction rate at which the fuel becomes gas, is proportional to the VM content [42,432]. High VM indicates the generation of large amounts of gas (volatiles) during the conversion process facilitating the devolatilization reaction to produce permanent gases. Furthermore, since the fuel fraction that is subject to heterogeneous reactions is the fixed carbon, fuels with high FC content feature a slow combustion condition. Consequently, a VM/FC ratio can be evaluated to establish the ease of ignition or combustibility degree. A high ratio means that the biomass is an adequate fuel and more the biomass is reactive, due to its high VM content. Hence, to allow visual comparison between the different fuels and a better perception of the differences between them, Figure 58 represents the results of the physical analysis. It is possible to state that EBA and ET are the samples more reactive and can be considered more appropriate for combustion processes.

Ashes are closely associated with problems like corrosion, agglomeration, and incrustations, in particular when they include a high content of alkaline oxides and salts [433,434]. From this perspective, despite having a high VM content, the EBA sample may lead to disadvantageous results in the energy conversion process.

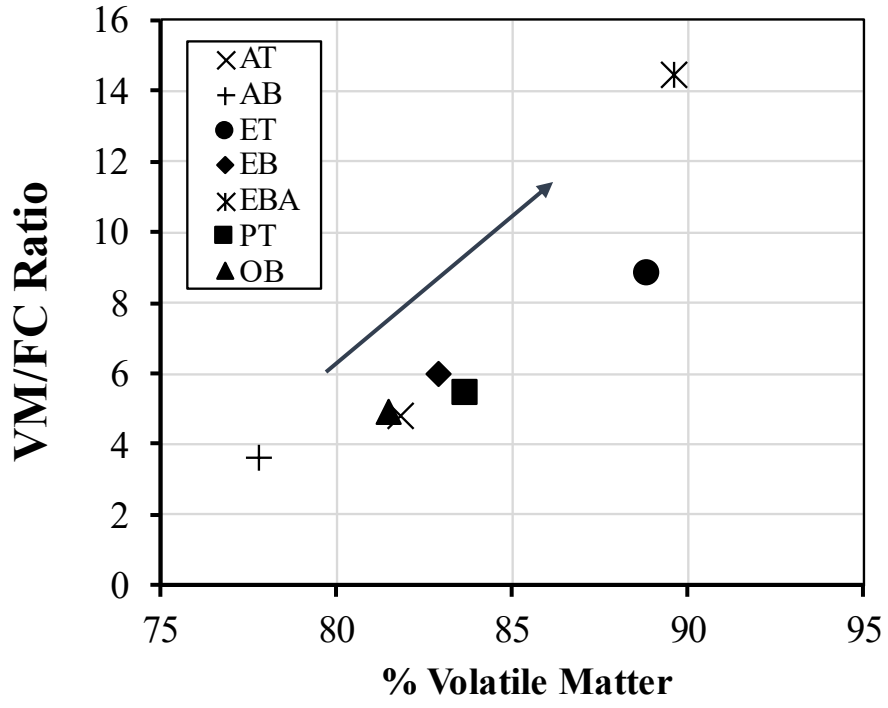

Figure 58: Reactivity of the samples. The arrow symbolizes the direction of the increase in the reactivity of the samples.

The large variations in fuel properties are in line with the range of values presented in the literature and presented in Chapter 2. Furthermore, the differences are important to establish which fuel is more suitable. Regarding the chemical characterization presented in Table 32, it provides the weight percentage of carbon, hydrogen, nitrogen, sulfur, and oxygen on a dry basis. The two chemical elements with higher contributions are carbon and oxygen, ranging from 43.10 to 55.90% and 35.10 to 50.18%, respectively. The content of hydrogen in the samples is very similar at approximately 7. In its turn, nitrogen and sulfur are present in the samples in very low quantity, almost undetectable, and vary between 0.11 to 3.21% and 0.01 to 0.99%. The presence of these two elements is linked to the formation of pollutants. Thus, it is expected that the combustion of pine and olive, with a higher amount of sulfur, will result in higher emissions of SO_2, while acacia presents a significant amount of nitrogen, and NOx emissions are expected to be higher compared with other fuels. A simple and useful approach to compare and classify the different solid fuels is the van Krevelen diagram, which consists of the plot of the hydrogen to carbon ratio (H/C) versus the oxygen to carbon ratio (O/C) [124]. Figure 59 presents the selected solid biomass fuels plotted on a van Krevelen diagram. The premise of this classification method is that solid fuels that fall within groups will have similar properties, regardless of their type. Biomass fuels, typically, present a H/C and O/C ratio between around 1.35 to 1.52 and 0.63 to 1.16, respectively [206]. Therefore, the fuels considered in this work fall in this category.

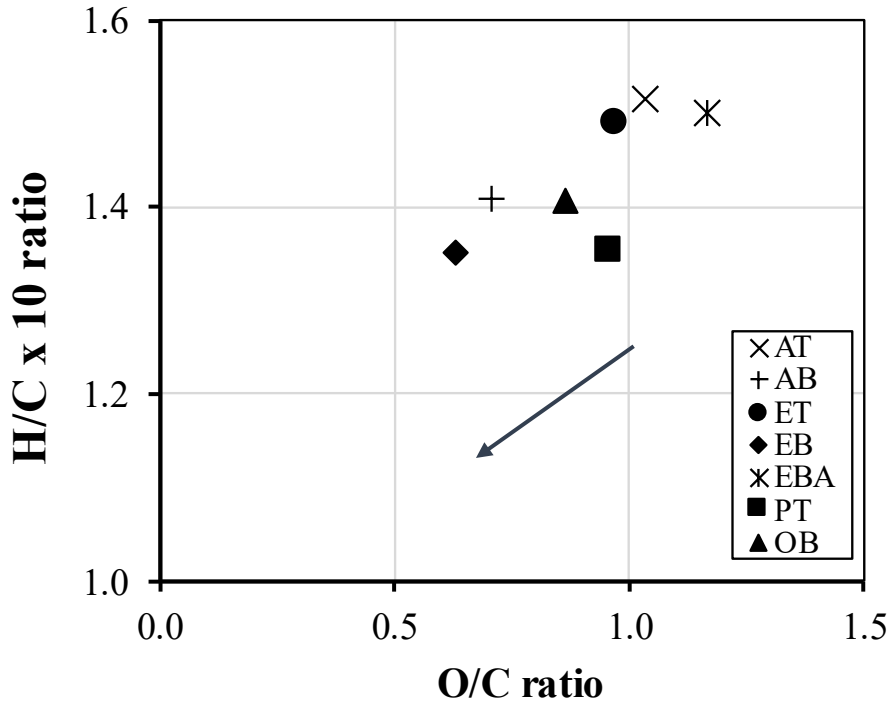

Figure 59: van Krevelen diagram of the selected solid biomass fuels. The arrow symbolizes the direction of increase of the heating value.

This type of information can be correlated to the fuel calorific value and extended to evaluate their reactivity. Lower calorific values are obtained for higher proportions of oxygen and hydrogen, compared with carbon, due to the lower energy contained in carbon-oxygen, and carbon-hydrogen bonds, than in carbon-carbon bonds [432]. Hence, from this diagram, it is possible to verify that AB and EB are the fuels with higher calorific values. Furthermore, taking into account the information presented in Figure 60, these fuels are not so reactive as EBA and ET. Regarding the calorific value measured using the bomb calorimeter equipment, an analysis was performed on a dry basis to make a clear comparison between the different fuels, although, for practical engineering calculations, the dry basis is not useful since the fuel is not supplied to the boiler dry. The measurements were also compared with the estimative given by the correlation proposed by Friedl et al. [414]. As presented in Figure 61 there are discrepancies between the measured values, converted for net calorific value considering the moisture content, and the values predicted by the empirical correlation. The discrepancies vary between 3 and 31%, with an average of 12%. The values from the Friedl equation suggest that there is no significant influence on the chemical composition since the results are around 20.5 MJ/kg. However, it can be observed from Figure 61 that between the measured and calculated values there is a correlation with a coefficient of determination, $R^2 = 0.79$.

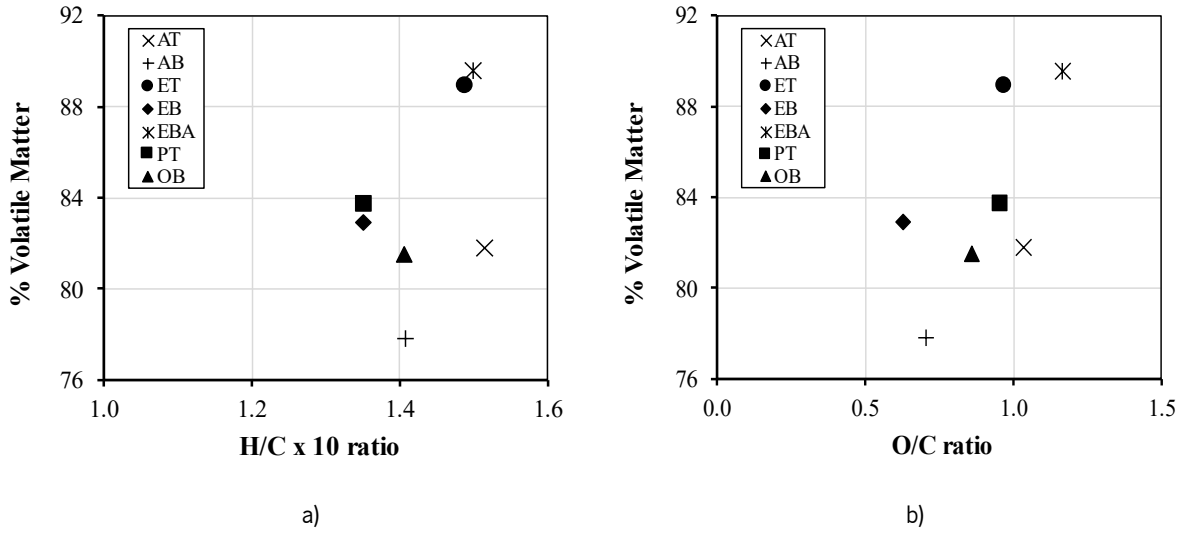

Figure 60: Variation of the volatile matter content of the different samples according to the different ratios: a) hydrogen to carbon, and b) oxygen to carbon.

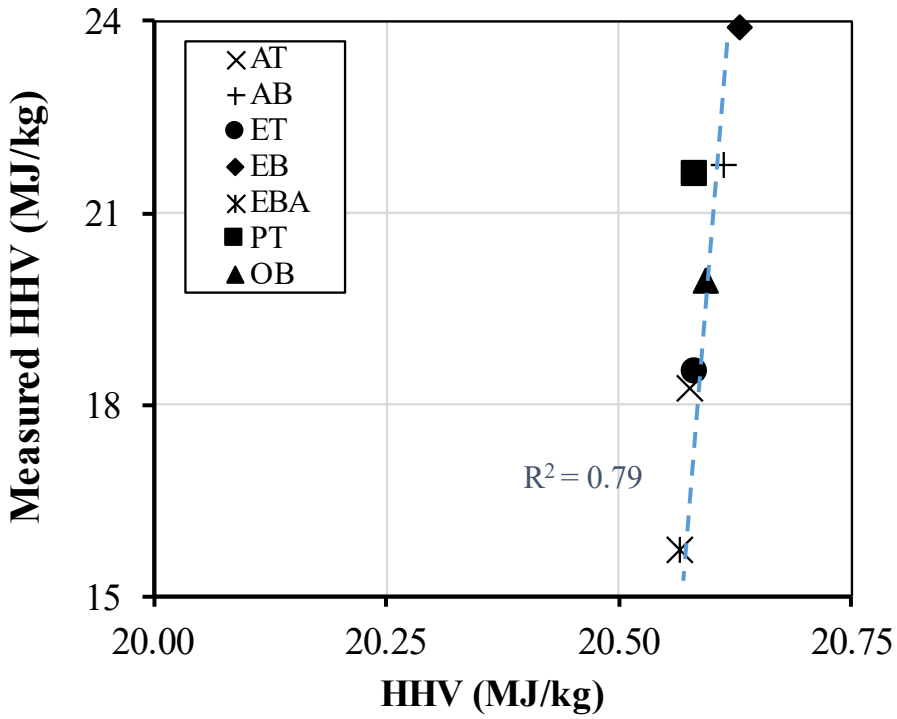

Figure 61: Comparison of the measured and predicted gross calorific value.

6.2 Thermal Properties

Figure 62 presents the average value of three thermal properties as a function of density, resulting from three runs for each sample. The experiments were carried out at an ambient temperature of 21 °C and represent the geometrical mean value of the thermal properties in the probed sample volume. Furthermore, all samples used in the experiments were submitted to the moisture control procedure described in Annex C to achieve a 20% moisture content. As it is possible to observe, the thermal conductivity is strongly correlated with the density. By examining the experimental results, a linear function can represent the relationship between density and thermal conductivity for these fuels. This correlation is the basis of modeling the thermal properties of some solid biomass fuels [40] and can be used for deriving mathematical models used for heat transfer and thermal conversion studies.

The plot in Figure 62 can be used to compare the various solid biomass fuels considered in this study. It is clear from this plot that Olive has a significantly higher thermal conductivity than the other materials. The volumetric heat capacity, along with the thermal conductivity controls the rate of heat dissipation within the bulk of the sample, Olive also presents a significantly high value, although the other fuels present similar values. Mason et al. [435] analyzed the thermal conductivity of fifteen different solid biomass materials, and olive was also the fuel with the highest value.

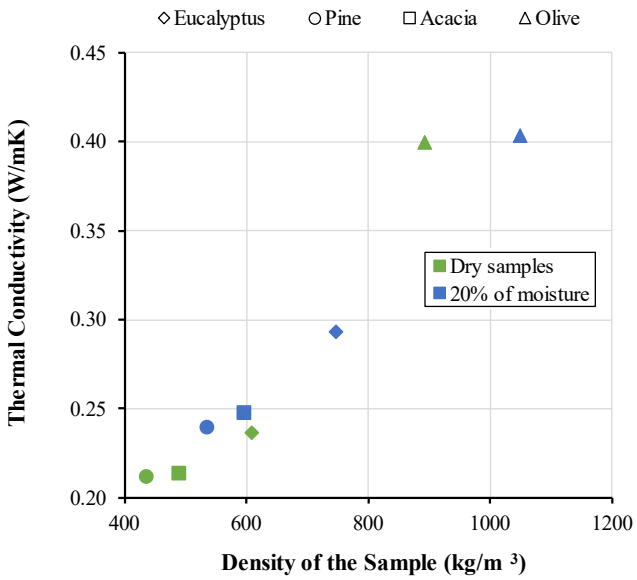

a)

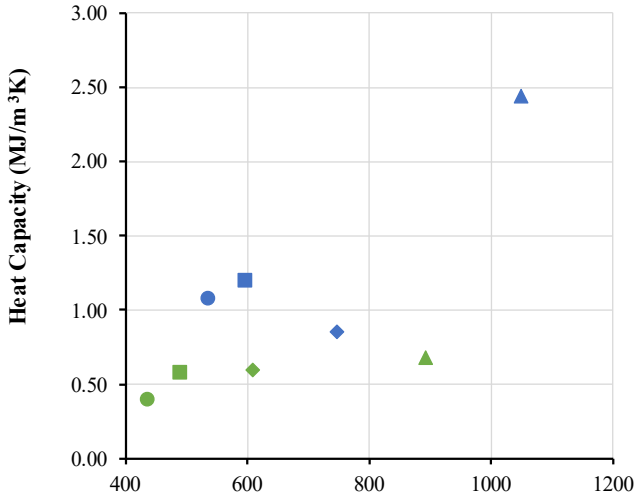

b)

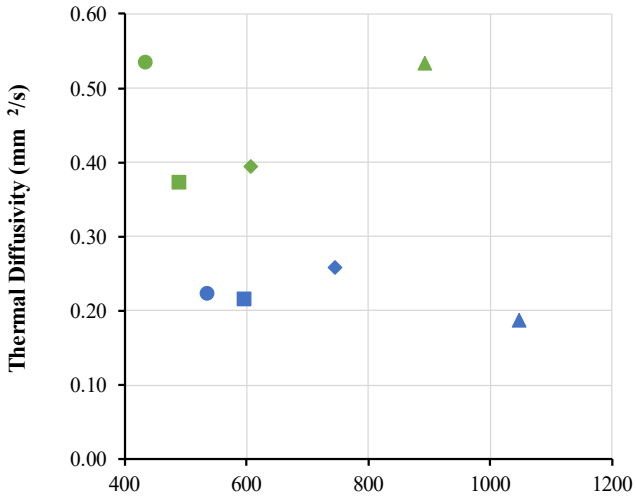

c)

Figure 62: Variation of the thermal properties with the density of the samples: a) thermal conductivity, b) heat capacity, and c) thermal diffusivity.

However, in its turn, the thermal diffusivity, Figure 62 c), present similar values for all fuels. This property controls the transient response of the sample to a thermal perturbation, which may reveal the effect of the structure on heat conduction in the material and the dynamics behind the conduction mechanisms [436]. As reported by Kuznetsov et al. [40], the structure and composition of the samples are important factors that contribute to the difference in the thermophysical properties, and this is why the first two parameters present evident discrepancies. In particular, the density exerts a considerable influence on the transmission of heat through the fibers of the samples [436]. Hence, the thermal conductivity of all investigated fuels, according to the experimental measurements, corresponds to the range of 0.239 to 0.404 W/mK, and the heat capacity is within 0.855 to 2.442 MJ/m^{3}K; and the thermal diffusivity is between 0.187 and 0.258 mm^2/s. These results are within the range of values presented in the literature by Suleiman et al. [436], Guo et al. [437], and Mason et al. [435]. Additionally, a linear regression function for the relation between the thermal conductivity and density can be derived from the results presented in Figure 62 a):

$$k = 0.0003\rho + 0.0534 \tag{107}$$

The mathematical expression presented in Equation (107) has a correlation coefficient of 0.992.

In addition to their dependency on density, k varies considerably with the moisture content. To account for the effect of moisture content in the test samples, after the first experiments, a pair of samples were dried in an oven at 105 °C, for over 24 h, in order to use dry samples in the experiments. Figure 62 also presents the mean thermal properties values for dry samples, and the results show a linear reduction, although the variations are not equal for all fuels.

Thus, several conclusions can be drawn from the analysis of the present results. First, the ranges of the thermal conductivity, heat capacity, and thermal diffusivity for typical solid biomass fuels are particularly wide, presenting values that can vary by a factor of 2. Second, the number of properties that significantly affect the thermal properties results is relatively substantial and involves mainly the physical properties of the samples, although the temperature of the samples is another property that influences the results. In its turn, variation of internal temperatures and heating rates in the particle, which will affect the reaction kinetics, are due to the differences in thermal conductivity [438]. Furthermore, it is important to point out that through the results presented in Figure 62, the heat capacity and thermal diffusivity appear to be dependent on the solid biomass material in terms of chemical properties and structural arrangement of the fibers, while thermal conductivity varies almost linearly with the density of the biomass.

6.3 Ash Composition Analysis

Regarding the ash composition, a preliminary assessment was performed by applying the XRD technique in order to determine the phases that contained the main chemical compounds. For the eucalyptus sample it was calcite, which means there is a significant amount of Calcium (Ca). However, for pine, acacia, and olive samples, it was not possible to detect accurately the different compounds. It was only possible to verify that Magnesium (Mg), Potassium (K), Ca, and Aluminum (Al) elements are constituents of the three samples. In addition to these four chemical elements, Sodium (Na) is also present in olive and acacia, while in the former fuel, Iron (Fe), Silicon (Si), and Titanium (Ti) are also present.

Since the XRD technique was unsuccessful to identify ash compounds, alternative techniques like EDX and X-ray Fluorescence (XRF) were assessed to detect the chemical elements present in the ash samples. Figure 63 presents the differences (in module) in the results of the chemical composition from both experimental techniques. There is a significant difference in the percentage of Al, Si, Phosphorus (P), K, Sulfur (S), and Ca, while the difference in the contents of Ti, Manganese (Mn), and Fe is minor. Furthermore, with EDX it is possible to detect important elements like Carbon (C), Oxygen (O), Mg, and Na but with XRF this was not possible. Table 33 presents the composition of these four elements for the different fuels, and Figure 64 presents the EDX spectrum obtained from one of the three measurements for each solid biomass sample.

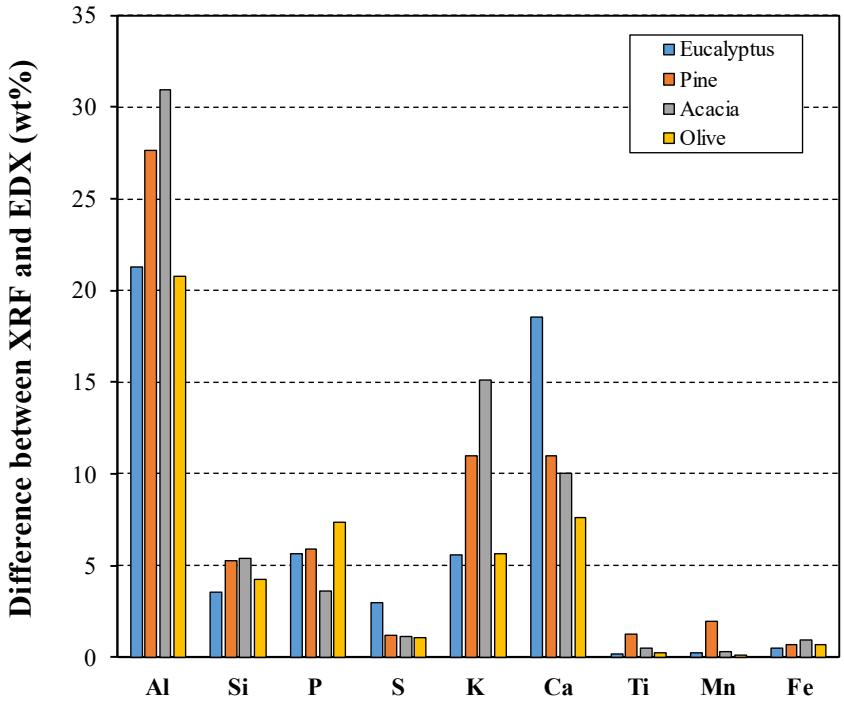

Figure 63: Difference between the results of the two experimental techniques used to determine the chemical composition of the ash.

Table 33: Other elements detected in the ashes using the EDX technique.

	Eucalyptus	Pine	Acacia	Olive
C	9.87	8.84	9.70	8.10
O	37.08	38.91	43.42	36.14
Na	0.43	2.05	8.23	0.32
Mg	5.93	11.11	5.03	1.95

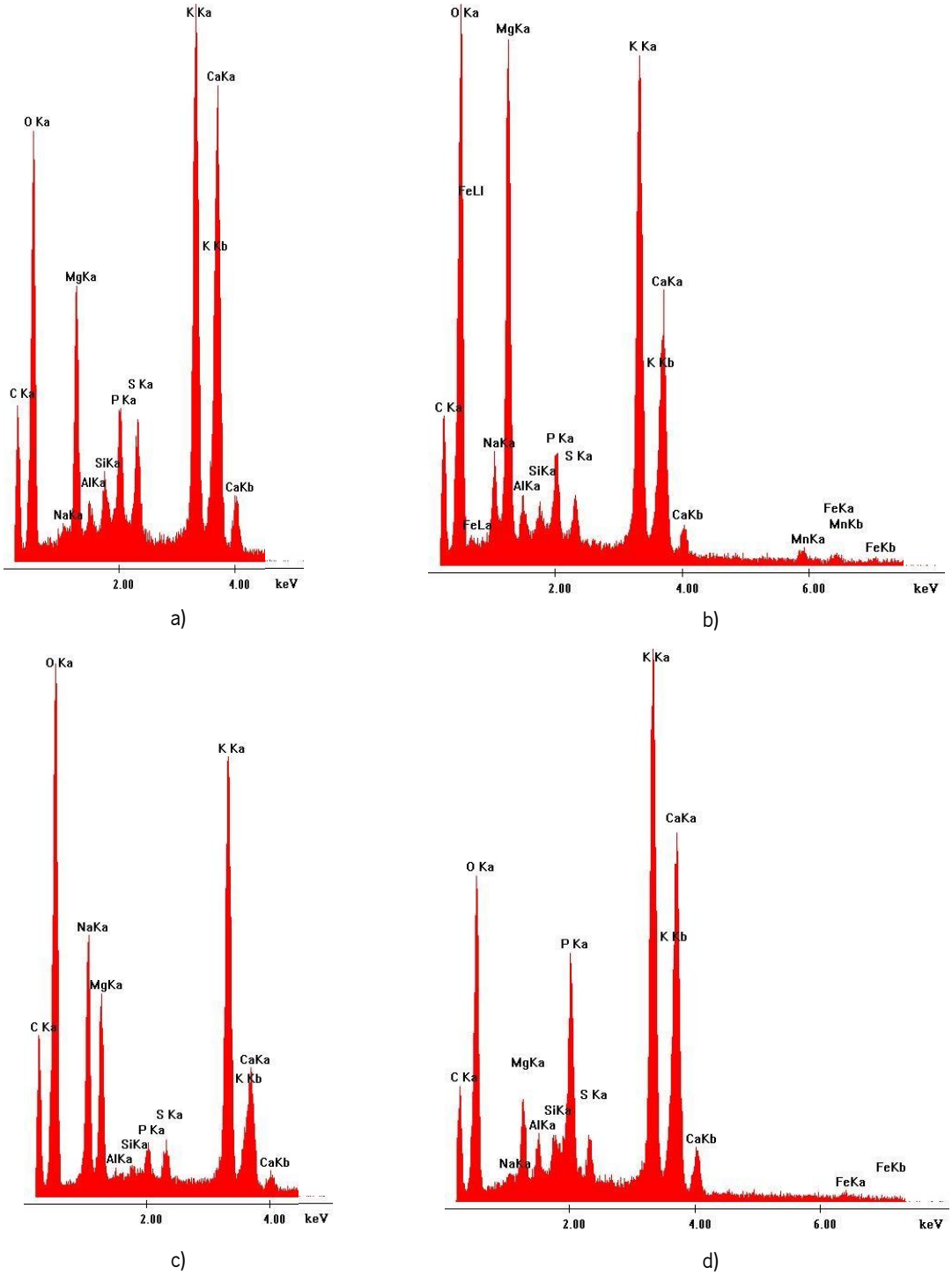

Figure 64: EDX spectrum of one measurement for samples of: a) eucalyptus, b) pine, c) acacia and d) olive.

From Table 33 it is possible to observe that O is the most relevant element in the ash composition, which means that the ash content is composed of oxides. In order to assess the occurrence of undesirable phenomena related to the ash content, an estimative of the ash compounds can be found through an element-to-stoichiometric oxide conversion considering the molecular weight of the element and the compound. Consequently, considering the main elements present in the ash samples, the relative content of the nine main oxides in the ash for the different samples was calculated and is presented in Table 34. The data show a clear contribution of Ca, Mg, Na, K oxides, and compounds like phosphorus pentoxide (P_2O_5). These results are in line with the results from the XRD technique although, in addition to the indications, K_2O and P_2O_5 present a significant presence in eucalyptus and olive ashes, respectively. Furthermore, this data presents some similarities to other reported in the literature. For instance, Vassilev et al. [439] presented an extended overview of the chemical ash composition of 141 varieties of biomass, including eucalyptus and olive samples. The authors identified the Si, Ca, and K oxides as the main compounds present in both samples. Despite fuels having different origins, and the magnitude of the contribution of each compound being different, the samples clearly present the same principal compounds. Additionally, Vassilev et al. [37] in another extended overview, presented data of the chemical ash composition from pine. Nunes et al. [434] analyzed the characteristics of the ashes derived from the combustion of biomass and presented the ash composition of pine samples. In both studies, there is a similarity in the main compounds. Nunes et al. [434] highlighted the contribution of a significant quantity of oxides with low melting points, particularly K, which is associated to critical issues when biomass is burned. This is verified in the four different fuels analyzed in this work.

Table 34: Estimative of the ash compounds based on the results from the EDX technique.

Compounds	Eucalyptus	Pine	Acacia	Olive
Fe_2O_3	0.00	4.54	0.00	3.98
CaO	28.29	21.47	14.60	40.28
MgO	9.83	25.89	11.71	4.55
K_2O	22.85	32.64	38.78	37.45
Na_2O	0.58	3.88	15.59	0.61
SiO_2	2.03	2.52	1.18	4.23
Al_2O_3	0.58	2.43	0.69	4.31
TiO_2	0.00	1.89	0.00	0.00
P_2O_5	7.03	8.81	3.00	18.00

Furthermore, as discussed in Chapter 2, deposition and slagging indexes can be determined to help to predict potential problems in boilers. Taking into account the results presented in Table 34, the slagging and fouling propensity can be evaluated for each biomass fuel and, along with the measurements of the heating value and ash content, the alkali index is also evaluated. The results of this analysis are presented in Table 35 and Figure 65. These indexes provide only an indication of the probability of these problems occurring and do not evaluate the melting behavior of the ash samples.

The results presented by the different indexes show that all solid biomass fuels considered in this work have a higher propensity for of ash deposition. Hence, it is clear from the Fouling index, Figure 8, and $R_{b/a}$ index, that there is a tendency for fouling problems for all biomass fuels, in particular for acacia since their value is substantially higher than that for the other fuels. The occurrence of slagging is estimated through the Slagging index. The data suggests there is no tendency to generate slagging for all the fuels selected. The formula used to compute this index uses, the most important compound to promote agglomeration, silica contribution (SiO_2). Silica, at low combustion temperature, ranging from 700 to 1,000 °C, may easily agglomerate. However, for the four fuels analyzed, their contribution may be negligible.

Table 35: Results of the deposition and slagging predictive indexes based on the chemical compounds.

Indexes	Eucalyptus	Pine	Acacia	Olive
$R_{b/a}$	23.43 (h)	12.91 (h)	43.10 (h)	10.18 (h)
AI	0.19 (m)	0.12 (l)	0.35 (h)	0.39 (h)
TA	0.33 (m)	0.37 (m)	0.54 (h)	0.38 (m)

Propensity: eh: extremely high, h: high, m: medium, l: low.

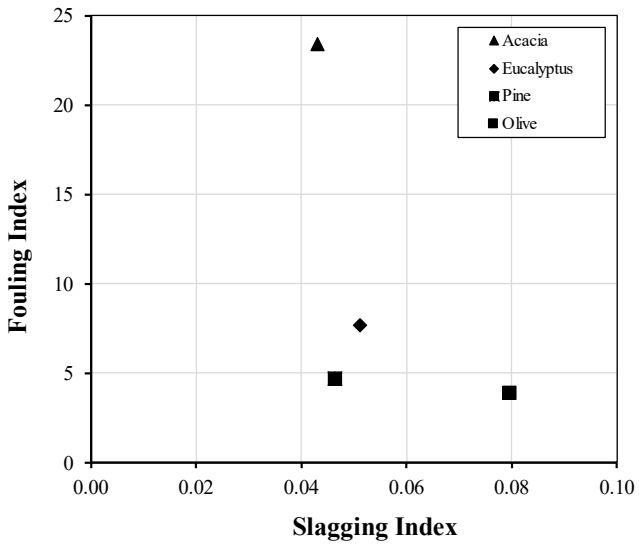

Figure 65: Slagging and fouling propensity for the different fuel samples.

6.4 Physical Properties of Larger Particles

Physical properties of the larger particles produced in this work, which include bulk density and particle size, were determined after the moisture control procedure in order to have a consistent moisture content of 20% for all particles. This procedure had to be performed since the density varies with the moisture content and the accuracy of the measurements is affected by the density differences or inconsistent moisture contents [440]. According to Ragland and Aerts [381], their value and the volume can increase up to the fiber saturation point which is at approximately 30% of moisture. To ensure the accuracy of each measurement, the experiment was repeated three times, and the average and standard deviation values are presented in Table 36 for each particle size class. The different classes of particles were obtained by sieving of eucalyptus particles. It is important to note that woodchips size and shape depend on the chipper equipment use and biomass quality. For this analysis, a large trunk of eucalyptus was used to produce long and narrow chips and, thereby, to obtain particles similar in size to those used in industrial biomass power plants. Particles between 8 and 16 mm were the class more representative. The average bulk density for eucalyptus particles ranges from 185 to 253 kg/m^3. The lower limit was obtained for larger particles since the void volume increases due to the irregular shape of the particles and the thin structure. This analysis is valuable data since information regarding the properties of milled wood provides an estimative of the energy density and is also one of the key parameters for designing boilers and feeding systems. Kuptz et al. [441] and Shrivastava et al. [442] assessed the bulk density of woodchips and similar values were reported. Furthermore, both values, particle size, and density, are a characteristic of the biomass species and type of chipper used [443].

Table 36: Bulk density of the different classes of particles.

Particle Class Size (mm)	Average Bulk Density (kg/m^3)	Standard Deviation
3.15 – 8	253.35	6.28
8 – 16	228.50	6.31
16 – 50	185.29	4.64

It is important to note that particle size determination is not a straightforward procedure due to the irregular shape of the chip. The chips can pass through the sieves if there are two dimensions smaller

than the aperture. Consequently, narrow woodchips can pass the sieve if the with and thickness are smaller than the aperture diameter of the different sieves used in the sieving process. This is an important limitation of the screening method since elongated particles can pass the sieve and thereafter the particle size distribution or the particles contained in particle class size does not correspond to the class limits. Figure 66 presents a batch of the class of particles more representative after the milling process (8 to 16 mm). From this batch of particles, 10 particles were collected, and the three characteristic dimensions were measured with a steel caliper in order to characterize the equivalent diameter of the particle. The average length, height, and thickness are 42.47, 13.48, and 4.32 mm, respectively. Considering these dimensions, the equivalent diameter of a spherical particle was determined, and its value is 16.78 mm. This dimension and the bulk density are important parameters for the development of mathematical models to describe particle conversion.

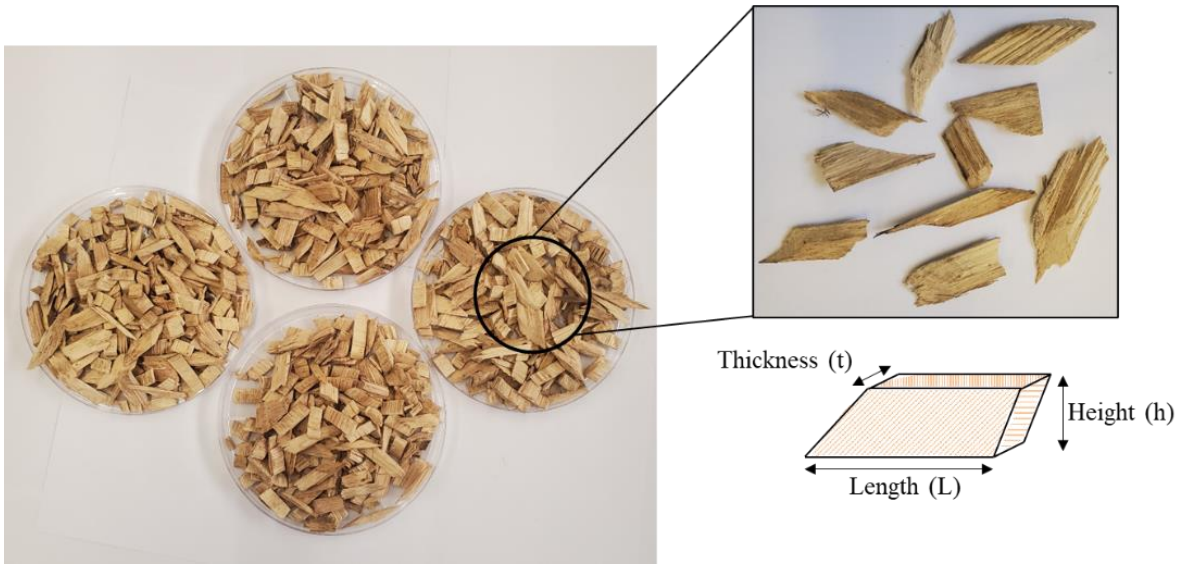

Figure 66: Eucalyptus particles that were obtained from the sieving process for the class 8 to 16 mm.

CHAPTER 7

THERMOGRAVIMETRIC ANALYSIS OF DIFFERENT FUELS

This chapter presents a comprehensive analysis of the thermal decomposition and kinetic of eight biomass fuels (ET, EB, EBA, PT, PB, AT, AB, and OB) in terms of combustion behavior through the TGA technique. The development of experiments in a controlled environment, and repeatable conditions, provide accurate measurements for different fuels and ambient conditions, to quantify the influence of different key parameters. This is fundamental to understand the transport phenomena at the particle level in order to obtain reliable results and information for further proper biomass combustion modeling of large-scale equipment. For this purpose, a global model is evaluated to compute the conversion rate and, consequently, describe the main biomass reactions during the combustion process. Hence, the complexity of the kinetic study is addressed in this chapter.

7.1. Test Conditions

The thermal conversion behavior of the solid biomass fuels considered in this work was analyzed by using the TGA in non-isothermal conditions up to a maximum temperature of 900 °C. The first period of *in-situ* drying was performed to ensure the complete dehydration of the samples. Then, a dynamic heating run, with a steady heat rate from 100 to 900 °C was carried out. But before this, as presented in Annex C, a set of preliminary experiments was developed to guarantee that biomass combustion is only temperature dependent, neglecting transport effects and, therefore, the experiments are performed in a pure kinetic regime. There are several factors affecting thermogravimetric data and, consequently, the kinetic results. Aspects such as the fuel type (physical and chemical composition) and its initial conditions (particle size and weight), reaction conditions (heating rate and atmosphere), as well as the experimental data analysis methodology for post-processing the results are important factors that should be considered before the development of the experiments.

Hence, a parametric analysis was initially developed to understand the influence of the atmosphere, its flow rate, the particle size, and also to evaluate the heating rate [176,244]. These were important experiments to help identify proper conditions for the development of further thermogravimetric experiments. Furthermore, a strategy to avoid the differences in the conversion process due to the different moisture contents of the samples was designed, where a heating program considering an initial drying stage was defined. Moreover, blank experiments were carried out to understand the effect of the gas density variation in the weight measurement, which is commonly denominated as the buoyancy effect. Although the variation of the weight measurement can be reduced, it is important to quantify since the experiments are performed with a small amount of biomass.

Thus, based on the previous experiments, the TGA experiments were developed with particles with a size between 0.125 and 0.25 mm, an initial weight of 10 mg, and an air flow rate of 100 mL/min. Additionally, after the drying stage, heating rates of 5, 10, 20, and 100 °C/min up to 900 °C were considered.

7.2. Thermal Decomposition

The evaluation of combustion performance at the particle scale is important for understanding the phenomena and acquiring accurate data to determine the kinetics of the different reactions. Since the heating rate is one of the significant factors in the thermal decomposition, its influence is firstly analyzed. Then, to deeply understand the conversion of these types of solid fuels, the differences between each

type of fuel and their different parts are analyzed. During each thermogravimetric experiment, the values of the temperature (°C), and weight of the sample (mg) were registered at 1 Hz rate.

7.2.1 Influence of the Heating Rate

Figure 67 presents for each fuel the influence of the heating rate on the variation of the normalized weight loss by the thermogravimetric (TG) curve and shows the first derivative of the TG curve – known as the derivative thermogravimetric (DTG) curve – representing the rate of weight loss profile. All the experiments were carried out in an oxidant atmosphere. The dashed lines represent the DTG curves while the solid lines correspond to the TG profiles. Looking at the different TG and DTG profiles, the conversion of all biomass fuels takes place over a wide range of temperatures and can be divided into three different zones. The first one is related to the drying stage, which during the experiments was performed at 100 °C for 20 minutes mainly to ensure that a large amount of moisture is removed from the sample. Then, there is a progressive mass loss as the temperature increases. In this stage is where the highest amount of matter is released. Hence, the range from around 150 °C to 400 °C is denominated as devolatilization and is due to the decomposition of hemicellulose and cellulose fractions that are present in the biomass fuels [136]. After devolatilization, there is another reaction that can be observed as the slope of the TG curve changes. This third stage occurs at a higher temperature, is associated with the char conversion, and can last up to approximately 680 °C. In this temperature interval, the reaction is endothermic and is due to the decomposition of another polymer present in the biomass, the lignin [190]. The DTG curves help to indicate the components present in the biomass and to distinguish the three different stages of biomass conversion by observing the three different peaks present in these plots. The first peak, not as significant as the other two due to the low moisture content of the samples, takes place due to the moisture release. Subsequently, a second narrow peak is observed within the previously mentioned range of temperatures for devolatilization. However, there are fuels where the conversion shows more than one visible peak in this stage. The last peak appears in a wider range of temperatures and is associated with the slow conversion of lignin. The present results confirm the evidence already reported in the literature [146,160,190,206].

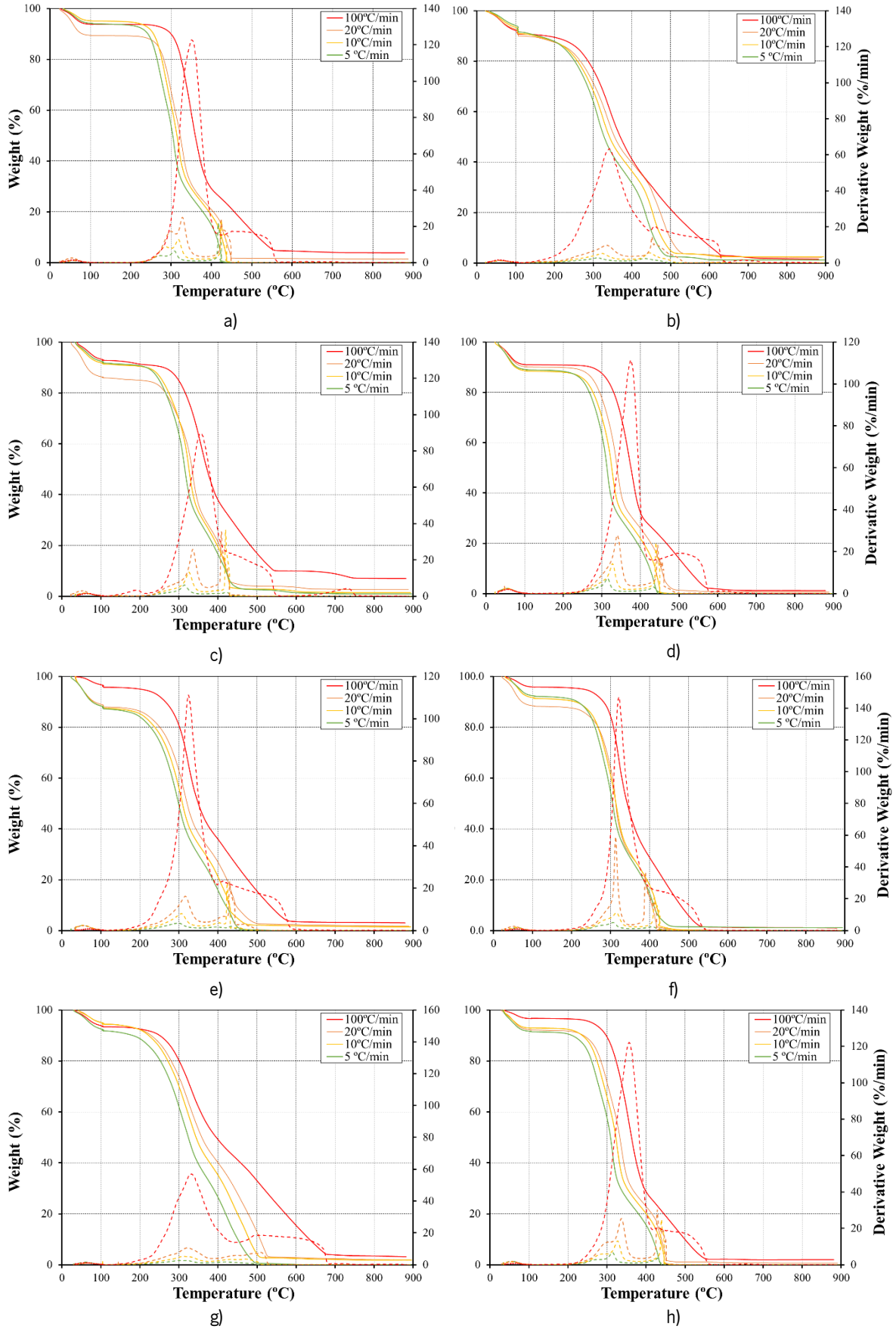

Figure 67: TG and DTG curves of: a)ET, b) EB, c) EBA, d) PT, e) PB, f) AT, g) AB, h)OB.

From Figure 67, it can be observed that the trend is the same for all heating rates, although a shift to higher temperatures is observed when the heating rate is increased. Consequently, the DTG curves also present a similar shift to the right, consequently an increase in the temperature at each peak occurs as higher DTG peaks are associated with higher combustion reactivity associated with the combustion of volatiles. Hence, increasing the heating rate affects the heat transfer in the particle.

According to Chen et al. [186]. this is mainly due to the limitation in the rate of heat conduction into the sample since the thermal conductivity of biomass is reduced which means that higher temperatures are required to set off the decomposition process as the heating rate is increased. Additionally, in agreement with Siddiqi et al. [190], the shifting of the peaks to higher temperatures with higher decomposition rates is due to the increase of heat for the particles and the improvement of transport processes. However, lower heating rates lead to almost complete decomposition, while for higher heating rates, due to the thermal lag in the biomass particles, the residual weight increases.

Another important observation is that the second stage, corresponding to the volatile matter conversion, is significantly enhanced by the increase in the heating rate. Nevertheless, the same phenomenon does not occur in the third stage even though the peak at which it occurs increases with the heating rate. Consequently, the char conversion is higher at lower heating rates, which suggests that due to the higher residence time in the reactor, there are reactions that favor a near complete reaction.

The present results are in agreement with previous works reported in the literature [136,160,186,190,444]. However, some of these works address the biomass conversion in an inert atmosphere, and differ particularly in the last conversion stage due to the presence of oxygen that enhances the conversion of the solid residue by at least in 15% [244]. Mishra et al. [136] also described an effect of an increase of the peak temperature of around 30 °C for pine and more than 1% of volatile matter released when heating rates of 5 and 20 °C/min are compared. Siddiqi et al [190] also described the same findings for waste biomass pyrolysis. In its turn, Álvarez et al. [160] studied the combustion of twenty-eight biomass samples using four different heating rates and it was found the temperature at maximum DTG of the second stage can occur at lower values, while the last stage can occur up to 627 °C.

Thus, the different characteristic parameters like T_{ig}, T_b, T_1, T_2, or m_b are a function of the heating rate at which the particle is exposed. Considering the results from the present work, for instance, T_{ig} was reduced from 4 °C up to around 90 °C when TG results from lower and higher heating rates are compared. t_b is also substantially reduced as the heating rate is increased, achieving values 3 times lower than those

for 5 °C/min. Figure 68 presents an example of the variation of these characteristic parameters, which are not directly observed in TG and DTG curves T_{max}, T_1, and T_2, for the different parts of eucalyptus fuel. Through these data, it is possible to observe that T_{ig}, t_{ig}, and t_b reduced as the heating rate increased, while the opposite effect was observed for T_b. These findings support the previously mentioned findings, where the higher heating rates are responsible for shifting the TG and DTG profile towards higher combustion temperatures.

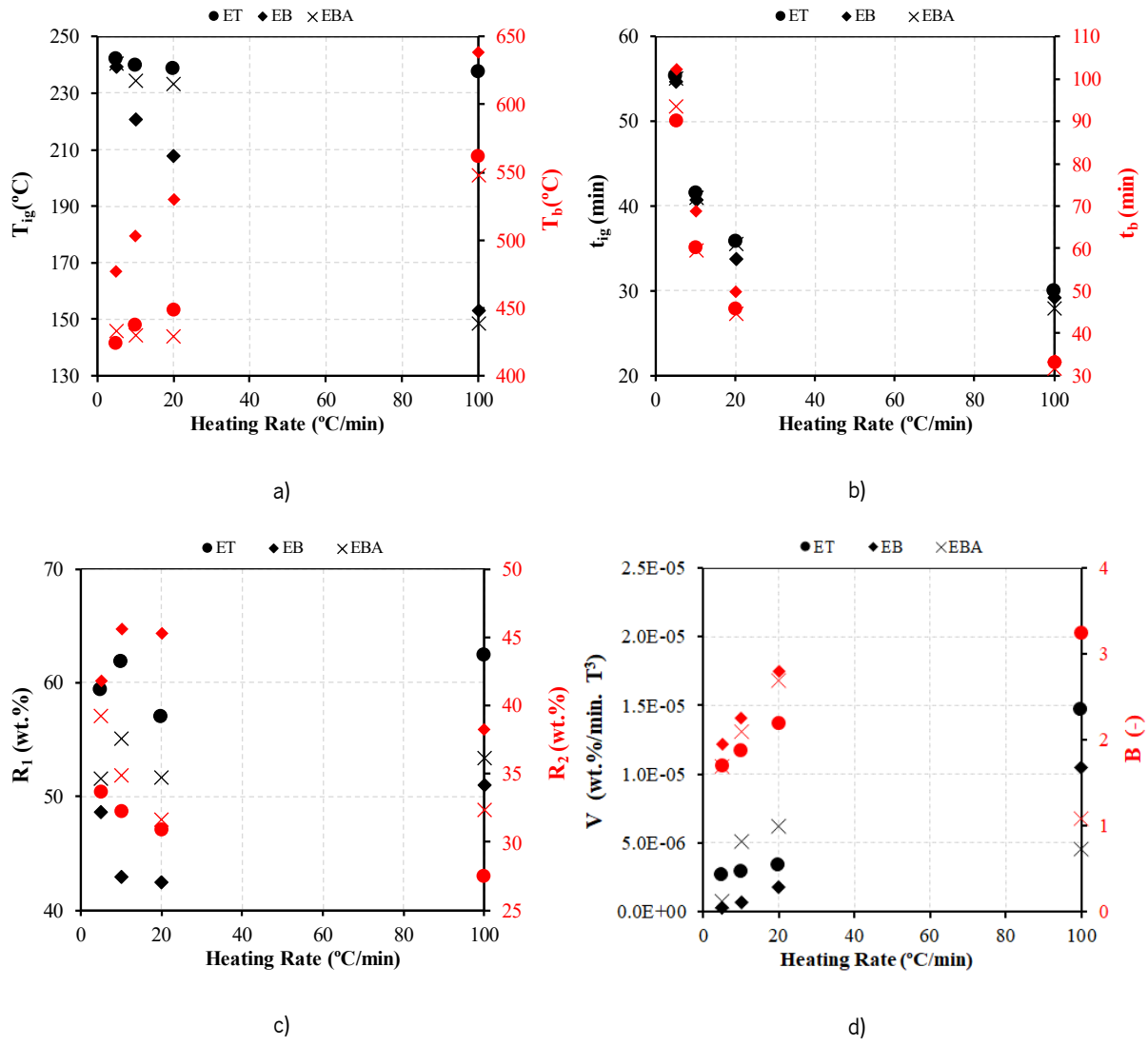

Figure 68: Comparison of the different parts of eucalyptus fuel in terms of characteristic parameters: a) ignition and burnout temperature, b) ignition and burnout time, c) weight loss during devolatilization and char combustion, and d) indexes of volatile matter release and burnout performance.

However, R_1 and R_2 not present a clear influence on the heating rate. Nonetheless, if the small fluctuations observed at intermediate heating rates are neglected, there is an inverse effect of the heating rate in both parameters. As already verified, the weight loss during devolatilization, R_1, tends to increase up to 3%, while the weight loss during the char conversion, R_2, tends to decrease, in particular for EBA, which showed a reduction of 7%. Regarding the volatile matter release (V) and burnout (B) performance indexes, they present a strong correlation with the heating rate since the second and third stages are substantially affected by this parameter. All characteristic parameters for every fuel, at the different heating rates, are summarized in Table 43 in Annex C. Additionally, considering the patterns of the TG and DTG curves between the different fuels, and the characteristic parameters, there are significant differences between the three samples of eucalyptus. For the inner part of the eucalyptus, the trunk sample, a higher mass loss was observed as well as a more effective conversion of the second reaction. Consequently, the combustion of ET is more reactive. According to Vega et al. [206], the thermal conversion of the inner part of biomass fuels is more evident due to their rich cellulosic structure, whereas the outer part is rich in lignin. This is why EBA and EB fuels present a higher conversion of char. EBA conversion in the last region still differs from the other fuels conversion as presents a small peak at lower and higher temperatures, around 180 °C, and 725 °C, respectively. A reduced amount of other constituents like extractives may be responsible for these variations [122,444].

7.2.2 Influence of the Type of Fuel

As previously referred, there are significant differences in the thermal conversion behavior of all different fuels considered in this work, and also between their different parts. It is evident that the discrepancies are related to the intrinsic differences in the chemical and physical composition as well as in the structures and their thermal stability. The different contents of hemicellulose, cellulose, and lignin are important to justify the differences between the TG and DTG curves. For instance, the differences in residual weight at the end of the TGA experiments could be justified by the different contents of lignin, which are also dependent on the fixed carbon content of the different samples. Figure 69 presents the conversion of the biomass samples from the trunk part of the different fuels (ET, PT, and AT), for the lowest and highest heating rates. As demonstrated in Table 32 (Chapter 6) AT has the highest fixed carbon content and at lower heating rates this was the fuel with the higher residual weight. However, for higher heating rates AT presented the lower m_b since the char conversion increased, as opposed to the behavior presented by the other fuels. Furthermore, it is important to point out that the ET conversion in the third stage presents

a high reactivity since there is a higher mass loss rate represented by a slender peak in the DTG thermogram. This feature is observed for lower heating rates, although at the higher heating rate the differences between the fuels in this region are not significant. In contrast, differences in the second stage can be observed. This is another important aspect that should be mentioned as both DTG thermograms present large variations. At 5 °C/min the hemicellulose and cellulose, which should be converted in the range of temperatures of the second zone, are converted at different temperatures while for higher heating rates their degradation overlaps and only one peak is visible. The results presented in Figure 69 a) suggest that hemicellulose reacts at lower temperatures, and the cellulose conversion occurs at a slightly higher temperature [122]. Moreover, the differences between the three fuels could be explained by looking to the volatile matter, but the cellulose content in these samples is another important factor that affects the maximum weight loss rate.

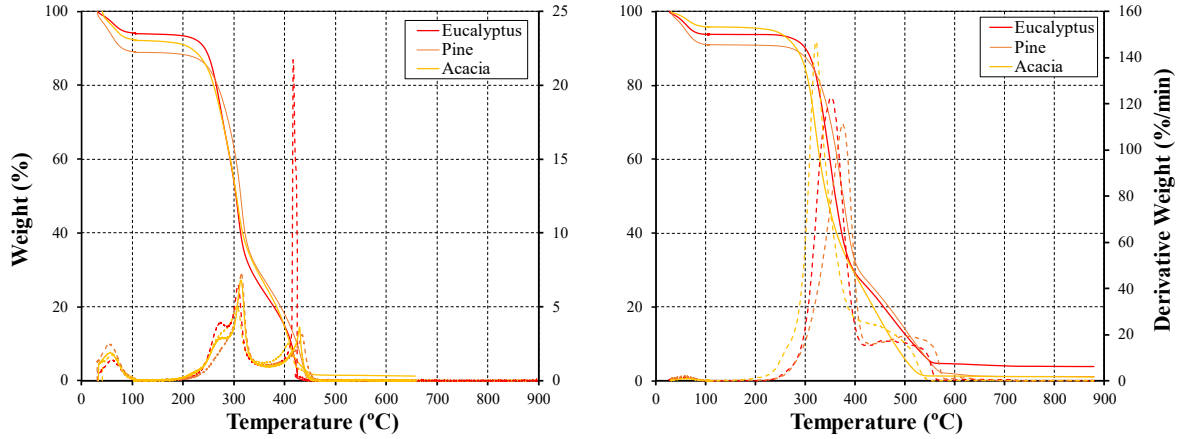

Figure 69: TG and DTG curves for the trunk part of the different samples at: a) lower heating rate – 5°C/min, and b) higher heating rate – 100°C/min.

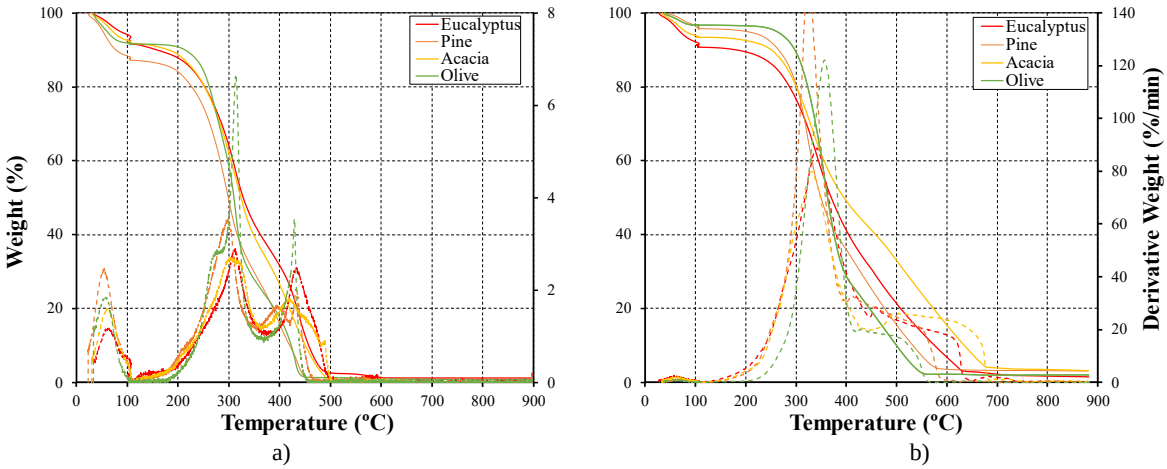

Figure 70: TG and DTG curves for the branch part of the different samples at: a) lower heating rate – 5°C/min, and b) higher heating rate – 100°C/min.

Figure 70 compares the weight loss from the branch part (EB, PB, AB, and OB) of the four biomass samples. For these fuels, there is no separation of the hemicellulose and cellulose conversion in the second stage and the reactivity is lower than in the trunk samples. However, in the third zone, a higher mass loss rate was observed as well as a degradation over a wider range of temperatures. Figure 71 presents a comparison of the characteristic parameters for the different fuels. In agreement with the previous discussion, there are differences between fuels. The OB fuel shows a higher T_{ig} but has the highest value of V since it is the fuel with higher R_1. Regarding the performance in the last stage, EB presents higher R_2 and B for lower heating rates, while at 100 °C/min PB degradation presented higher values. As demonstrated before for the eucalyptus samples, t_{ig} and t_b present the same trend but the differences are reduced when the four fuels are compared, in particular at higher heating rates. This is an indication that thermal conversion is more dependent on the heating rate than the type of fuel.

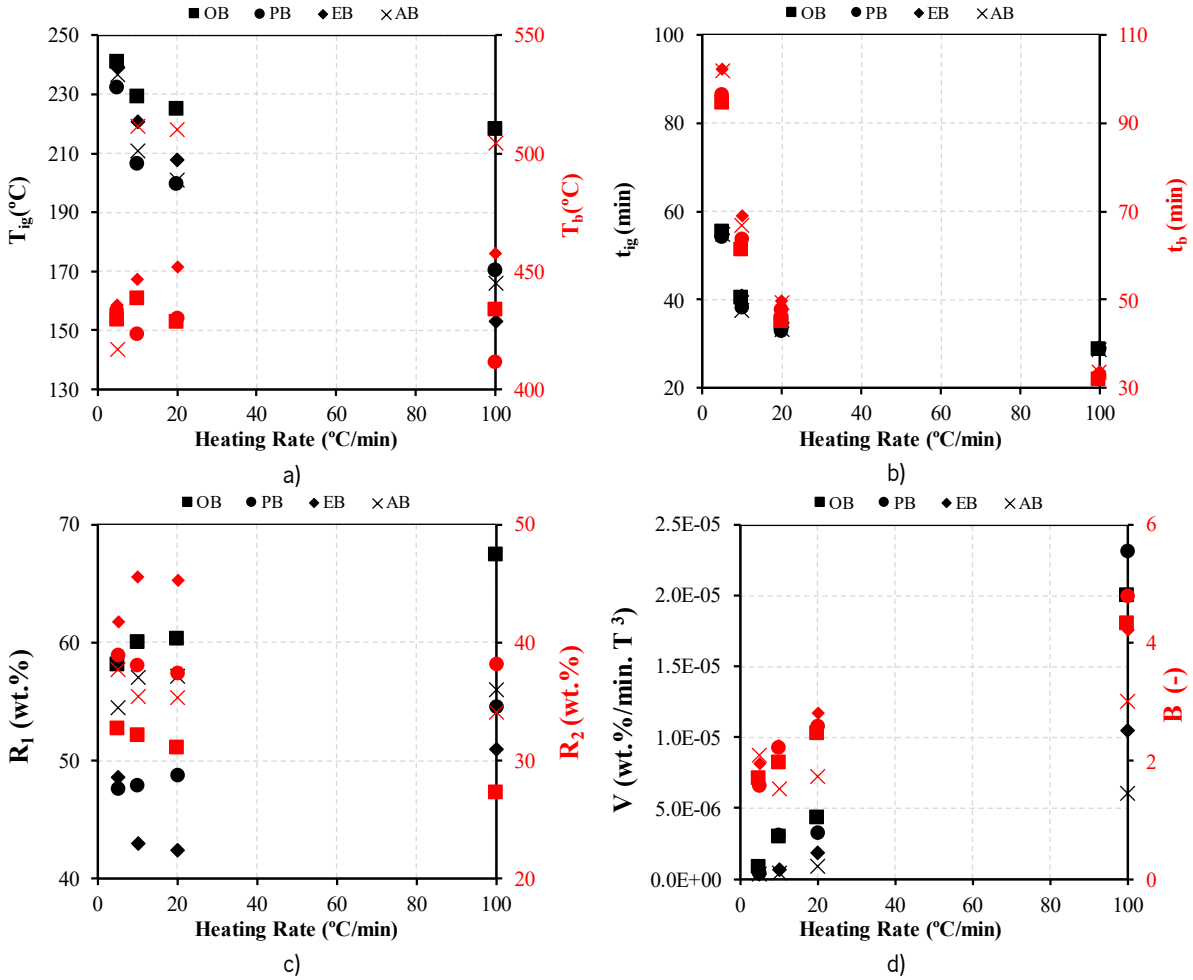

Figure 71: Comparison of the different biomass fuels (from the same part of the tree – branches) in terms of characteristic parameters: a) ignition and burnout temperature, b) ignition and burnout time, c) weight loss during devolatilization and char combustion, and d) indexes of volatile matter release and burnout performance.

7.3. Kinetic Analysis

Based on the data generated from the TGA with the low heating rates, 5, 10, and 20 °C/min, the kinetic parameters for the eight fuels were determined. However, taking into account the comments of Conesa et al. [445] about the significant discrepancies in the kinetic results obtained in the literature due to: a) different experimental methodology, b) data analysis approach, and c) calculation methodology, the procedure described in Chapter 4.5 was firstly assessed. Figure 72 presents an example of the difference between the data obtained by the TG experiment (Figure 72 a)) and the data after the postprocessing developed using a MATLAB code to smooth and filter the weight variations (Figure 72 b)). This process proved to be effective in the smoothing of the weight variation to avoid mathematical problems in the differentiation and to filter the essential data where there is the thermal conversion of biomass for the development of the kinetic analysis.

The activation energy was calculated using four different isoconversional methods, OFW, FR, KAS, and Starink method. Although the overall reaction mechanism with a single first-order reaction model is simpler to implement in a CFD model, as seen in the previous sub-chapter, the biomass conversion has distinct reactions that need to be considered. The thermal oxidation of biomass is a complex process involving a set of physical processes and chemical reactions and a single reaction cannot correctly determine the kinetic parameters of biomass combustion. Consequently, the kinetic analysis relies on a two-step consecutive reaction model, which is composed of the two essential single reactions that more realistic describe the biomass combustion.

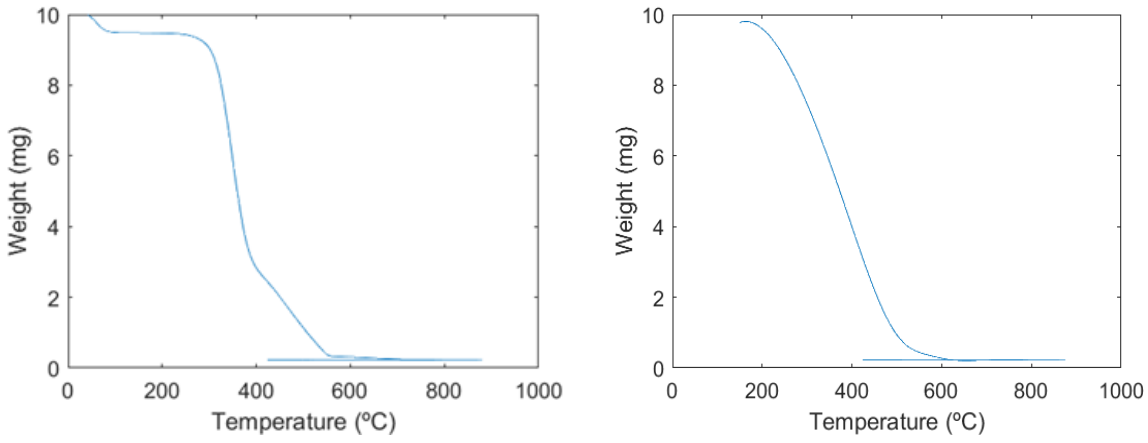

Figure 72: TGA results: a) without preprocessing and b) after the application of the preprocessing methodology for ET at 20 °C/min.

The reaction scheme is hypothesized as represented by Equations (108) and (109):

$$\text{Biomass} \xrightarrow{k_1} \text{Gases} + \text{Char} \tag{108}$$

$$\text{Char} \xrightarrow{k_2} \text{Gases} + \text{Residue} \tag{109}$$

Hence, the two main conversion processes, dealing with the devolatilization and char oxidation are modeled.

7.3.1 Evaluation of the Kinetic Method

The E calculated for all the isoconversional methods considered in this work was obtained by linear regression, as indicated in Table 8 from Chapter 2. The plot of different terms enabled the determination of E for a conversion range between 5% and 95%, using a step size of 5%, as recommended by ICTAC. For example, Figure 73 presents the plots using the different specifications of the four kinetic methods and the corresponding E was determined for each conversion by the linear equation [143].

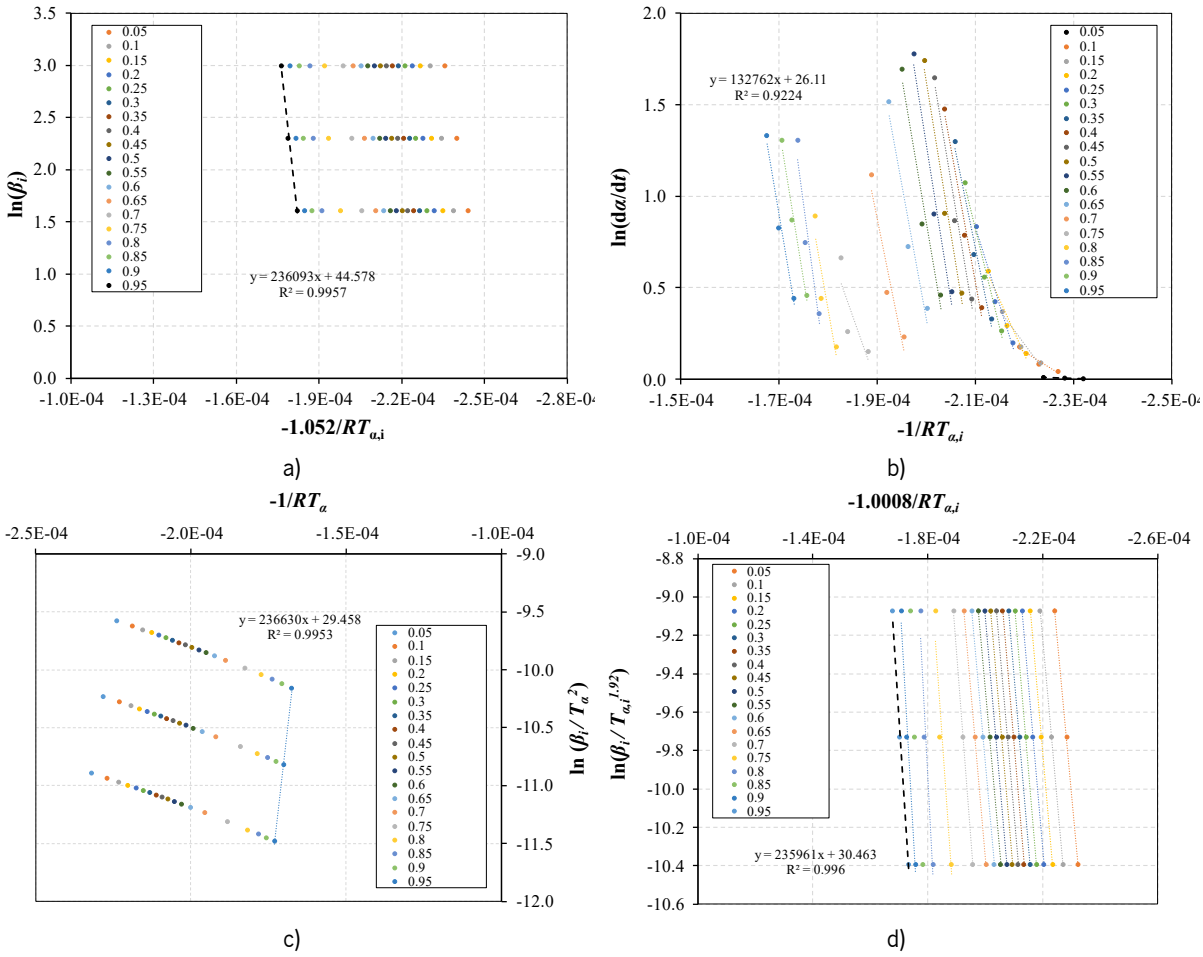

Figure 73: Curves obtained for the different methods: a) OFW, b) FR, c) KAS, and d) Starink for ET sample.

Figure 74 presents an example of the results for E_α as a function of the conversion for the ET sample. It can be observed that OFW, KAS, and Starink methods provide similar results, while using the FR method the results are distinct. The first three methods are based on an integral form and, although there are some approximations associated with the temperature function the results are similar. However, the FR method is based on the differential form of the conversion equation, without assumptions to assess the temperature function. Consequently, this method is sensitive to the experimental results with noise, zones where reaction starts spontaneously, and is known to be more susceptible to inconsistent results [241]. However, the plot for E_α is useful to understand the nature of decomposition reaction and define zones where the different reaction takes place. Table 37 presents the average E values considering the two main reactions during biomass combustion.

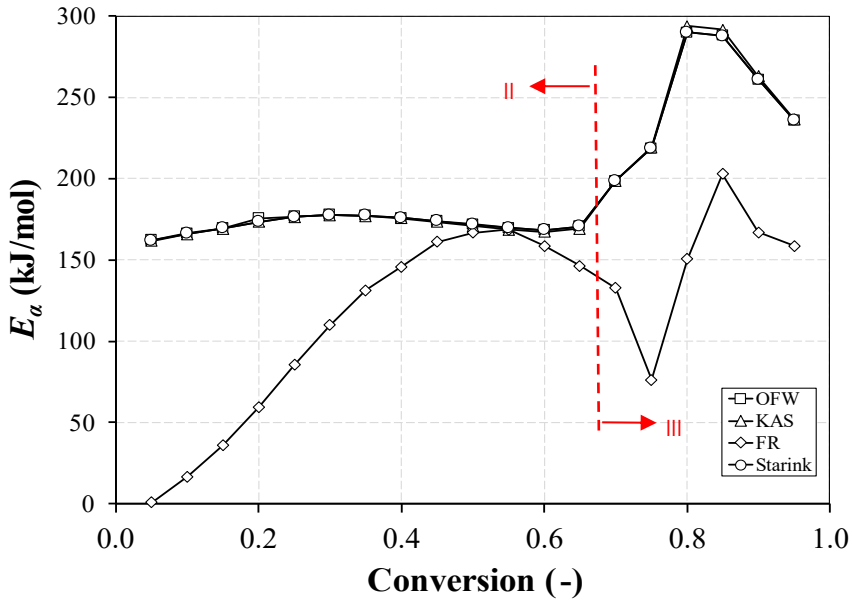

Figure 74: Activation energy value as a function of the conversion for ET. The red dashed line symbolizes the transition from the devolatilization (II) to the char oxidation (III) reaction during the combustion of biomass.

Table 37: Average activation energy values (kJ/mol) obtained by the different kinetic methods for ET, PT, and AT.

	ET	PT	AT
OFW			
Devolatilization	172.01	161.41	177.00
Char Combustion	248.78	211.84	258.46
KAS			
Devolatilization	171.27	160.40	176.68
Char Combustion	250.55	219.37	260.69
FR			
Devolatilization	106.67	87.64	103.09
Char Combustion	148.02	129.16	236.85
Starink			
Devolatilization	171.13	166.35	176.92
Char Combustion	248.69	215.53	260.93

Nevertheless, the dependence of E_α on conversion is an indication that this is made up of independent and consecutive reactions. This is expected since biomass is composed of different components that decompose in different temperature ranges. Hence, since E_α varies significantly with conversion, isoconversional methods are not recommended [143]. This is because isoconversional methods assume that E remains constant throughout the entire biomass conversion process, which can lead to systematic errors [122]. To overcome this limitation, the CR method has been successfully applied to determine the kinetic parameters [129,133,149,150,157,160,203,204,446]. Hence, subsequently, the fitting of the CR method was evaluated using four types of simple reaction models, the 1st and 2nd order reaction model and the 1D and 2D diffusion model. Figure 75 presents an example of the linear regression curves applying the separation based on the two different conversion stages of biomass combustion, which present 65% of conversion. In Table 38, it is possible to verify the reaction mechanism selected to fit the conversion of each fuel and the corresponding kinetic parameters obtained through the linear regression equations. The linear correlation coefficient was higher than 0.906, representing a reasonable and acceptable data fit for all biomass fuels considered in this work.

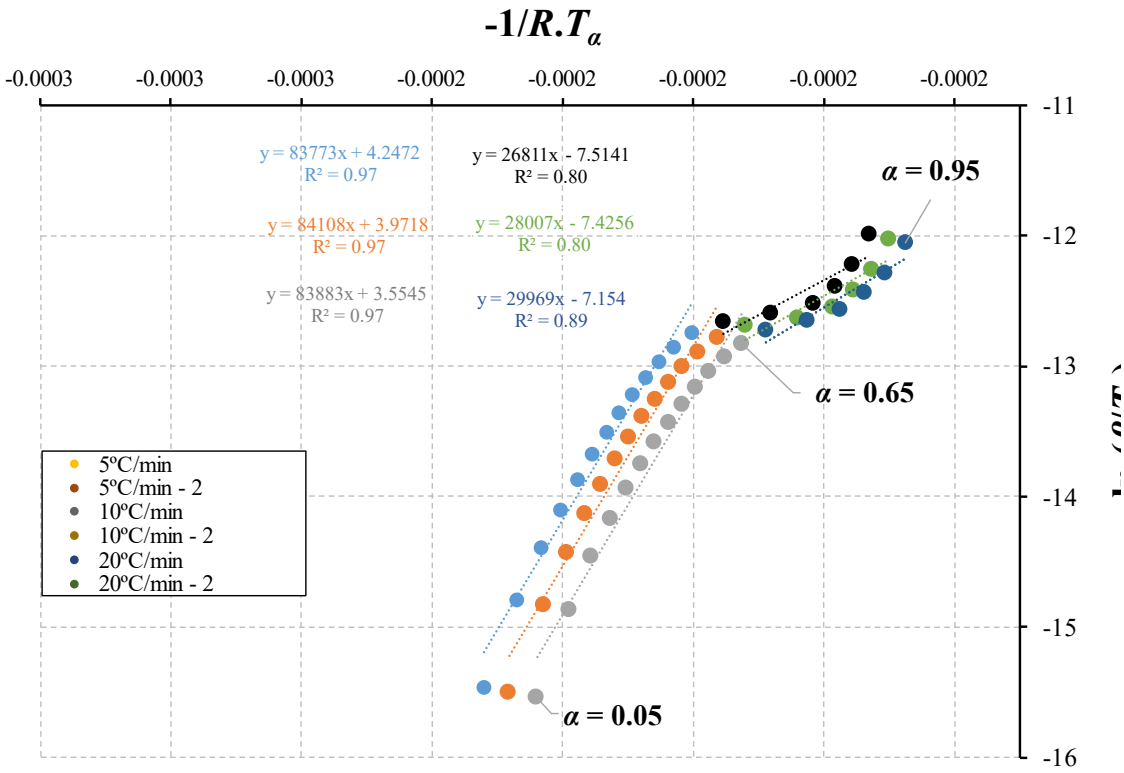

Figure 75: Curves obtained for CR method considering a first-order reaction and for ET sample.

Table 38: Reaction mechanism, linear regression equation, and kinetic parameters obtained through the CR method.

Fuel	Reaction and Mechanism	β (°C/min)	Equation	R^2	E (kJ/mol)	A (min^{-1})
ET	Devolatilization / 2nd order	5	$y = 101295x + 8.2521$	0.992	101.30	2.34E8
		10	$y = 101251x + 7.8343$	0.991	101.25	3.08E8
		20	$y = 100489x + 7.2413$	0.990	100.49	3.37E8
	Char oxidation / 1D diffusion	5	$y = 15839x - 10.5$	0.908	15.84	0.26
		10	$y = 16605x - 10.452$	0.906	16.61	0.58
		20	$y = 17569x - 10.335$	0.973	17.57	1.37
EB	Devolatilization / 2nd order	5	$y = 51765x - 2.7084$	0.997	51.77	2.07E3
		10	$y = 49487x - 3.414$	0.997	49.49	1.96E3
		20	$y = 47922x - 3.9658$	0.996	47.92	2.18E3
	Char oxidation / 1D diffusion	5	$y = 29083x - 8.6433$	0.982	29.08	3.08
		10	$y = 31628x - 8.387$	0.985	31.63	8.67
		20	$y = 31225x - 8.6433$	0.994	31.23	13.24
EBA	Devolatilization / 2nd order	5	$y = 85654x + 4.5529$	0.998	85.65	4.89E6
		10	$y = 86200x + 4.327$	0.999	86.20	7.85E6
		20	$y = 82918x + 3.3558$	0.999	82.92	5.72E6
	Char oxidation / 2D diffusion	5	$y = 30592x - 8.1818$	0.985	35.48	5.15
		10	$y = 30967x - 8.2068$	0.994	30.97	10.16
		20	$y = 35476x - 7.4913$	0.985	35.48	47.61
PT	Devolatilization / 2nd order	5	$y = 98227x + 7.0495$	0.994	98.23	6.81E7
		10	$y = 97665x + 6.498$	0.996	97.67	7.80E7
		20	$y = 95716x + 5.6669$	0.995	95.72	6.66E7
	Char oxidation / 1D diffusion	5	$y = 21532x - 9.6393$	0.968	21.53	0.84
		10	$y = 24184x - 9.2627$	0.947	24.18	2.76
		20	$y = 20082x - 10.082$	0.971	20.08	2.02
PB	Devolatilization / 2nd order	5	$y = 62339x + 0.0238$	0.997	62.34	3.84E4
		10	$y = 63929x + 0.1433$	0.997	63.93	8.87E4
		20	$y = 62681x - 0.4084$	0.997	62.67	1.00E5
	Char oxidation / 1D diffusion	5	$y = 20051x - 9.8785$	0.998	20.05	0.62
		10	$y = 22106x - 9.5897$	0.996	22.11	1.82
		20	$y = 24687x - 9.2734$	0.991	24.69	5.58
AT	Devolatilization / 2nd order	5	$y = 85995x + 4.972$	0.996	85.99	7.46E6
		10	$y = 85790x + 4.5696$	0.996	85.79	9.96E6
		20	$y = 85606x + 4.185$	0.996	85.61	1.35E7
	Char oxidation / 1D diffusion	5	$y = 19874x - 9.7866$	0.989	19.87	0.67
		10	$y = 24213x - 9.1003$	0.990	24.21	3.25
		20	$y = 29230x - 8.3163$	0.968	29.23	17.19
AB	Devolatilization / 2nd order	5	$y = 54053x - 2.1273$	0.999	54.05	3.87E3
		10	$y = 52172x - 2.7972$	0.998	52.17	3.83E3
		20	$y = 49453x - 3.5741$	0.996	49.45	3.34E3
	Char oxidation / 1D diffusion	5	$y = 22176x - 9.7457$	0.994	22.18	0.78
		10	$y = 24926x - 9.4639$	0.997	24.93	2.33
		20	$y = 24551x - 9.7265$	0.995	24.55	3.52
OB	Devolatilization / 2nd order	5	$y = 87737x + 5.2242$	0.999	87.74	9.80E6
		10	$y = 87342x + 4.7329$	0.999	87.34	1.19E7
		20	$y = 86760x + 4.2662$	0.998	86.76	1.49E7
	Char oxidation / 1D diffusion	5	$y = 14977x - 10.721$	0.978	14.97	0.20
		10	$y = 15894x - 10.643$	0.906	15.89	0.46
		20	$y = 19990x - 9.9649$	0.978	19.99	2.26

7.3.2 Influence of the Type of Fuel

Taking into account that E means the minimum quantity of energy required to initiate the chemical reactions, lower values correspond to higher reactivity. According to the kinetic data presented in Table 38, the biomass fuels can be ordered by their reactivity of the devolatilization conversion process as EB > AB > PB > EBA > AT > OB > PT > ET. The values vary between 47.92 to 101.30 kJ/mol while, for char oxidation, E ranges from 14.97 to 35.48 kJ/mol. The devolatilization conversion was best characterized by reaction kinetics, using a second-order reaction model and the char oxidation was successfully described by a diffusion controlled mechanism. The diffusion of oxygen to the char affects the combustion process and should be considered the main mechanism of thermal conversion of biomass in the last stage. The significant difference between the E values for the two stages is due to lower values of E for lignin conversion when compared to cellulose degradation [160]; less energy is required to break the chemical bonds in lignin. Additionally, as there are different thermal conversion behaviors in the last stage of biomass combustion, the reactivity for this stage is defined as: ET > OB > PT > PB > AB> AT > EB > EBA.

These results are in line with the results presented in Chapter 6 since it was demonstrated that Eucalyptus samples present higher reactivity. Hence, the fuel type presented a significant influence on the E values during biomass combustion. Regarding the effect of the heating rate, the dependence of E with the heating rate was less evident and not all fuels presented a consistent trend with the heating rate. According to the previous literature review on the kinetic of the biomass reaction presented in Chapter 2, Magalhães et al. [133] analyzed the effect of the heating rate on the kinetic behavior and a marginal difference was also reported. Álvarez et al. [160] studied the kinetic behavior of different biomass fuels including eucalyptus, olive, and pine and similar results were observed. In this work, the olive fuel also presented a lower reactivity. Fang et al. [203] and Shen et al. [150] determined the E values of pine combustion using a two-stage mechanism and CR method. Both works presented lower energy requirements for char oxidation. Thus, the results from the present study are in the range of the reported results in the literature, although a small variation was detected and can be attributed to the different physiochemical compositions of the biomass fuels.

Regarding A, another observation should be highlighted since this parameter presented a dependence on the heating rate. As the heating rate is increased, A also increased. As suggested by Siddiqi et al. [190] this behavior represents the increase in frequency and intensity of collisions among the molecules.

7.4 Reconstruction and Modeling

Based on the E and A determined for the second and third stage, the conversion rate α can be predicted based on Equations (110) and (111) or (112), respectively.

$$\text{Biomass} \xrightarrow{k_1} \text{Gases} + \text{Char} \qquad \frac{d\alpha_1}{dt} = \frac{1}{\beta} A_1 \cdot \exp\left(\frac{-E_1}{RT}\right) \cdot (1-\alpha)^2 \tag{110}$$

$$\frac{d\alpha_2}{dt} = \frac{1}{\beta} A_2 \cdot \exp\left(\frac{-E_2}{RT}\right) \cdot \frac{1}{2\alpha} \tag{111}$$

$$\text{Char} \xrightarrow{k_2} \text{Gases} + \text{Residue}$$

$$\frac{d\alpha_2}{dt} = \frac{1}{\beta} A_2 \cdot \exp\left(\frac{-E_2}{RT}\right) \cdot \left[-\ln(1-\alpha)\right]^{-1} \tag{112}$$

Two possibilities are considered for the third reaction stage since the best fit to predict the conversion of EBA fuel differs from the other fuels. Hence, the char conversion is computed considering the 2D diffusion mechanism for EBA fuel (Equation (112)), while for the other fuels the conversion is predicted by using the 1D diffusion mechanism (Equation (111)).

Figure 76 illustrates the reconstruction and modeling of conversion as a function of temperature for heating rates 5, 10, and 20 °C/min using parameters derived from the CR method. There are differences, in particular, at the beginning of the conversion, and mainly for trunk samples (ET, PT, and AT). The differences are due to the hemicellulose and cellulose degradation at different temperatures in the second stage, and the average E for the second stage has some difficulties to reproduce the experimental behavior. The difference between the experimental and computed curves is a measure of the applicability of the derived kinetic parameters. To facilitate the comparison of the data, the square of the Pearson product moment correlation coefficient through the experimental and calculated values was determined for each fuel and heating rate. This value is interpreted as the proportion of the variance in the experimental results attributable to the variance in the results. A value above 0.95 was obtained, which corresponds to a good correlation between the experimental and numerical results. Therefore, the differences may be satisfactory from the perspective of engineering calculations and predictions.

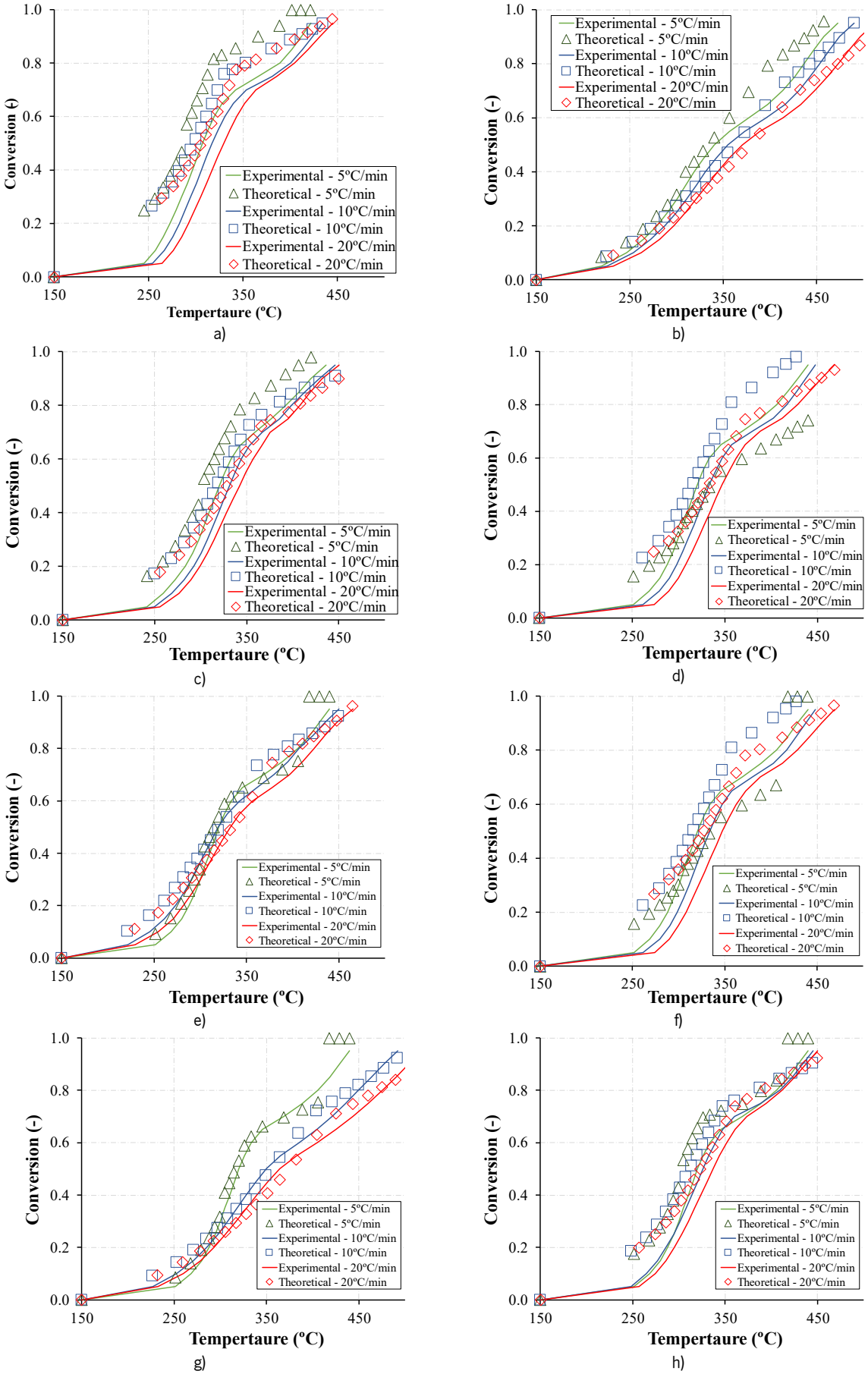

Figure 76: Comparison between experimental and modeled conversion results for the different samples: a) ET, b) EB, c) EBA, d) PT, e) PB, f) AT, g) AB and h) OB.

CHAPTER 8

MASS LOSS AND EMISSION ANALYSIS IN A SMALL-SCALE REACTOR

During the combustion of biomass in a grate-fired boiler, each particle undergoes a sequence of different reactions, and the phenomena differ from the conversion of a single, thermally thin, particle. Hence, this chapter presents the results of isothermal combustion experiments using large particles in a small-scale reactor. Firstly, the weight loss characteristics of eucalyptus, pine, acacia, and olive samples were investigated at different isothermal temperatures. Additionally, the mass loss rate together with the composition of the gases over the devolatilization period was analyzed for the main fuel used in power plants, eucalyptus. This is particularly important to identify the transport phenomena effect and the gaseous products released during the combustion of biomass. Finally, all the information collected in this chapter, and the previous ones, are used in the XDEM to develop an effective numerical model to predict the combustion behavior observed in the experiments from the small-scale reactor.

8.1 Experimental System Debugging

Because of the heat and mass transfer limitations, usually neglected in TGA, a Macro TGA reactor was designed to analyze fast thermochemical reactions. Furthermore, this apparatus enables the testing of more realistic full samples that cannot be regarded by traditional TGA testing. In addition, specific attention was focused to quantify the total products released in the combustion of the samples. However, before the experimental campaign, calibration and verification procedures were carried out. Hence, before the presentation and discussion of the results, this section aims to briefly describe the preparation procedure of the experiments and the calibration experiments.

First, separate blank tests were performed to evaluate the internal heat transfer and to obtain the background of the weight signal before the experiments. Three thermocouples (K type) were introduced in the reactor to record the internal temperature at different positions and to assess temperature gradients in the center of the reactor. This was important to understand which temperature should be defined in the temperature controller in order to obtain the corresponding desired value for each experiment. The runs to evaluate the weight signal were also important since there were disturbances detected due to the interference of the steel wire that connected the basket and scale. After some modifications in the lid and on both connections of the wire, basket, and scale, the gradient of the weight was minimal. Hence, the weight of the basket was appropriately tared, the basket became stable, and deviations below 8 mg were found during long experiments. Consequently, with this set of blank experiments, it was proved that the small-scale reactor had acceptable stability and reproducibility.

Additionally, a set of experiments were concerned with the samples. The initial conditions are an important parameter that should be maintained in each experiment. Neglecting possible variations in the chemical composition of the same batch of particles, the moisture content and the dimension of the particles were considered parameters of particular interest, and their influence should be controlled or quantified. Experiments with random particles and particles from the 16 to 50 mm batch after the sieving process were burnt and the mass loss variation presented slight differences. Since the woodchips present an irregular structure, particles with fixed dimensions were produced to investigate the dimension that influences the mass loss behavior. From the experiments performed, it was possible to observe that the thickness is the key dimension. Although the woodchips present different lengths and/or widths, the thickness is approximately the same and this is the reason for similar profiles of mass loss. Regarding the moisture content, the strategy was to control and obtain similar values for all particles after the experiments. As the moisture content of the particles used in power plants is generally higher, the

maximum value that can be replicated in the laboratory, 20% of moisture, was defined as the setpoint. In this way, the influence of moisture in the mass loss behavior was avoided. Experiments considering the influence of the air flow rate were also considered but due to the limitations of the apparatus to collect the flue gases, the air flow rate needs to be as low as possible to allow that only volatiles are captured. Hence, the air flow rate was set at 0.1 L/min and the initial weight as 20 g, the maximum possible to produce the higher flue gas amount. More details about the procedures and the results of the experimental debugging are presented in Annex B and D.

8.2. Combustion Characteristics

This section presents the results of the combustion experiments using the solid biomass species considered in this work, eucalyptus, pine, acacia, and olive. Figure 77 presents the feedstock burnt, from the batch of particles within the 8 to 16 mm range.

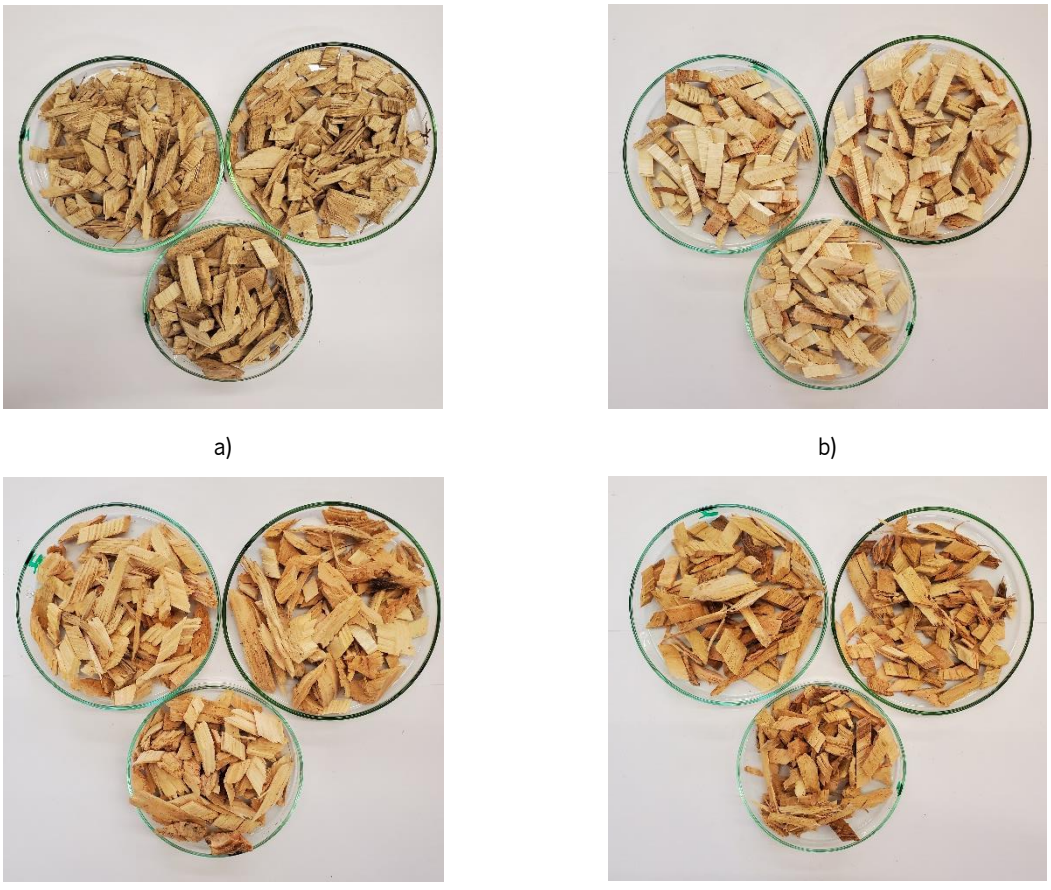

a) b) c) d)

Figure 77: Samples of the different fuels used in the experiments: a) Eucalyptus, b) Acacia, c) Pine and d) Olive.

All experiments were run in triplicate, under identical conditions, and the average values were computed and reported as well as the standard deviation.

8.2.1 Influence of the Temperature

As temperature is one of the most important parameters in the thermal conversion of solid biomass fuels, wide a range of temperatures covering low to high temperatures was performed. Figure 78 presents the normalized sample mass variations for the different reactor temperatures and fuels, where their average value is plotted over time along with the standard deviation as a shaded area. The experiments were run for a long period of time, 30 minutes, in order to ensure the full conversion of biomass.

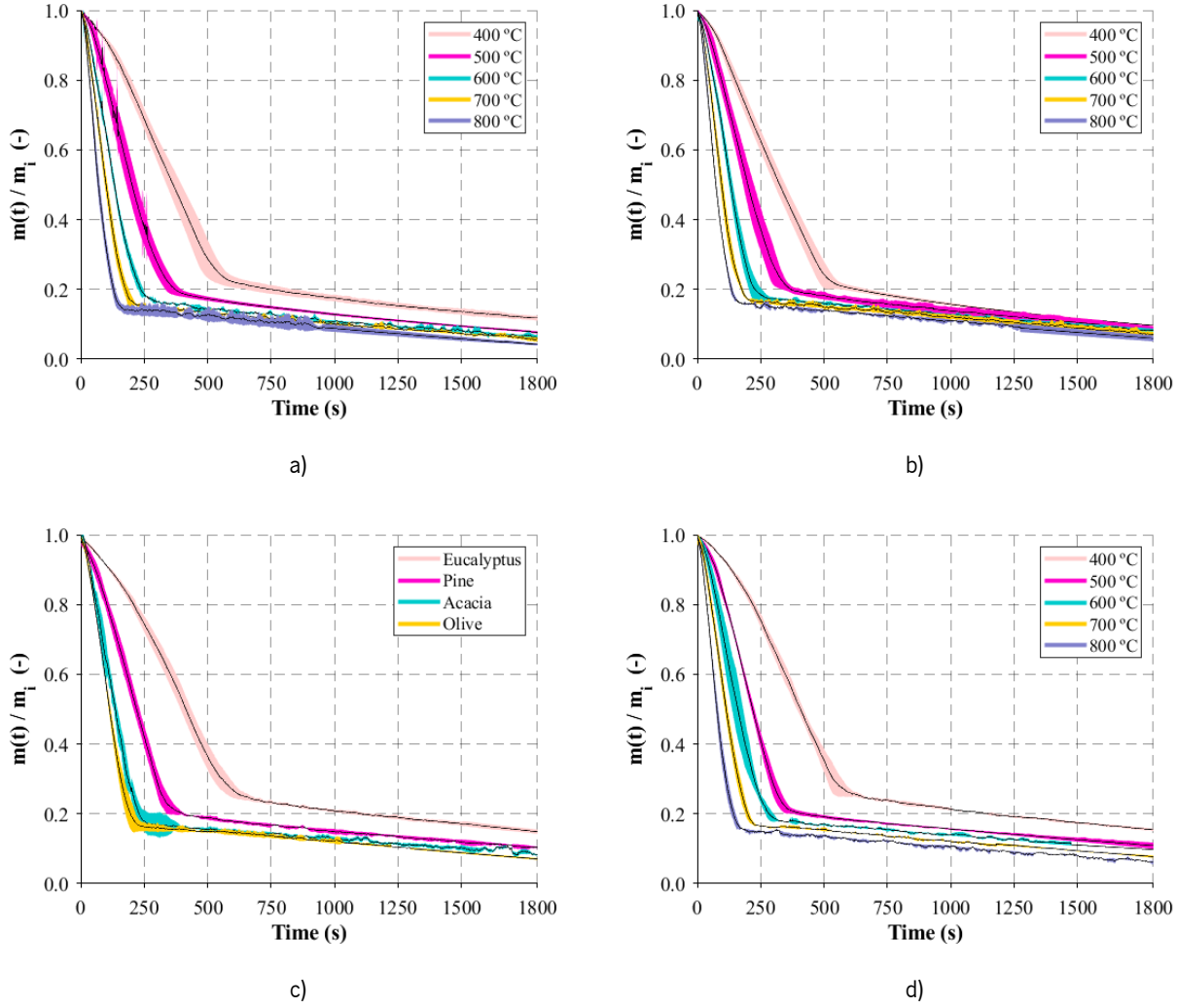

Figure 78: Normalized mass as a function of time and temperature for: a) eucalyptus, b) acacia, c) pine, and d) olive.

The mass loss behavior that can be separated into two different stages, each one showing a linear variation. The first stage of the mass loss profiles presents a uniform slope until a certain point followed by a second stage at a lower slope. The first stage is attributed to the overlapping of drying and devolatilization reactions as they are thermal processes that occur at low temperatures and high rates, while the last stage, which is extended over a long time, is identified with char oxidation. Hence, the combustion behavior is significantly different from the previous conversion profiles analyzed in the TGA, and the direct comparison between both profiles clearly shows that in the combustion process of larger particles it is not possible to identify separate consecutive conversion stages.

The first stage is highly influenced by the reactor temperature and may vary from 650 to 150 s from low to high temperatures. However, the last stage was not influenced by the temperature, suggesting the presence of another predominant phenomenon and conversion mechanism in most of the biomass conversion time. In the literature, for the char combustion phenomenon, it is generally agreed that the conversion reaction is limited by kinetics and diffusion, the latter being normally the limiting factor of the reaction rate [248,278]. Therefore, the results suggest that this conversion step is dependent on the diffusion of oxygen and not dependent on the environment temperature. Hence, the mass loss profile of larger particles combines the kinetic phenomenon and transport processes. Thus, during the combustion of larger particles part of the sample may be in the devolatilization or char stage as well as others can be unreacted.

Furthermore, another important aspect to mention, in line with the independency of the char conversion with temperature, is that as the reactor temperature increases the mass loss profiles are closest. Although the values of the normalized mass are lower for higher temperatures, there was a previous influence of the temperature in the first stage which caused higher mass loss values to be obtained. However, it is important to note that at low temperatures, in particular for 400 and 500 °C, considering the region where there is the transition of the slope of the mass loss profile, approximately 74 to 80% of the initial weight was converted. These values are close to the sum of the moisture content (20%) and the volatile matter of different fuels (65 to 70%), which suggests that a small amount of volatile matter was not released in the first stage.

8.2.2 Influence of the Type of Fuel

As the different solid biomass fuels present different physical, chemical, and thermal properties, the combustion behavior can present differences according to the fuel burnt. Figure 79 presents a comparison of the normalized mass loss between the different fuels at the same temperature.

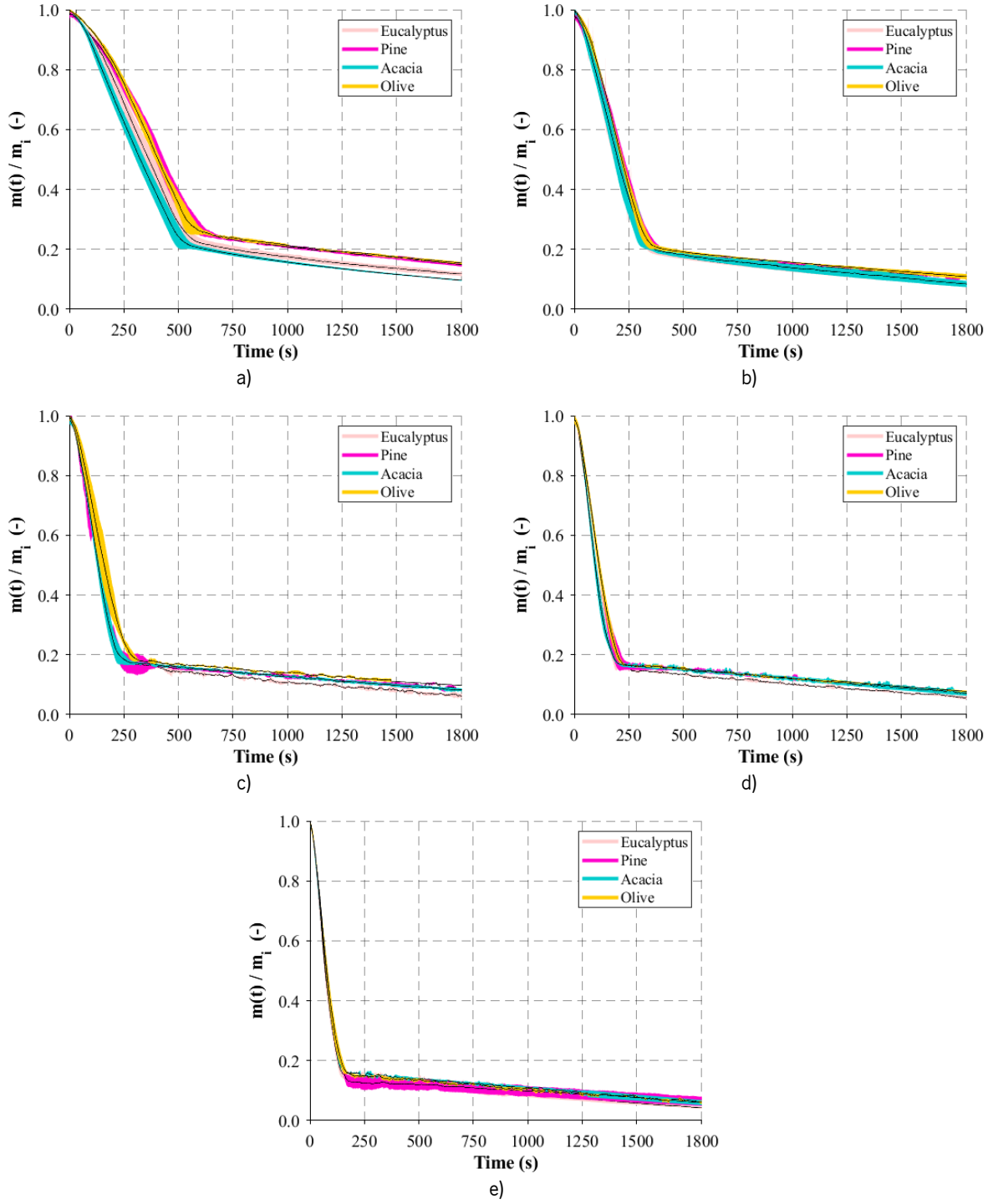

Figure 79: Comparison of the mass loss behavior of the different fuels at different isothermal temperatures: a) 400 °C, b) 500 °C, c) 600 °C, d) 700 °C, and e) 800 °C.

The combustion behavior of the different fuels presents small differences. In particular, the differences are detected at lower reactor temperatures, while at higher temperatures the profiles are almost coincident within the experimental uncertainty. Although some authors, for instance, Becidan et al. [274], argue that factors such as physical, thermal, and chemical properties are known to be relevant in the decomposition of solid biomass fuels the present data suggests that, their influence is only relevant at low temperatures while at high temperatures the combustion behavior is mostly dependent on the reaction kinetics.

To further analyze the mass loss data, Figure 80 shows the difference between the different fuels in terms of the mass loss during the first stage and the time necessary to complete the reaction. As it can be observed, the mass loss during devolatilization increases with temperature for all fuels. The differences between the different fuels become smaller with increasing temperature. However, eucalyptus, which has a higher VM content, presents almost for all reactor temperatures the highest mass loss. This observation is in line with the findings described in Chapter 6, where the reactivity of the fuels was correlated with by the VM content. Hence, based on the data presented in Figure 4 a) the reactivity of the fuels studied can be ordered by descending order of reactivity as follows: eucalyptus, acacia, pine, and olive. Pine and acacia present similar values, although at 800 °C pine was the fuel with the highest mass loss. Another important aspect to note is that pine is the fuel which has a stronger influence of temperature in the conversion rate.

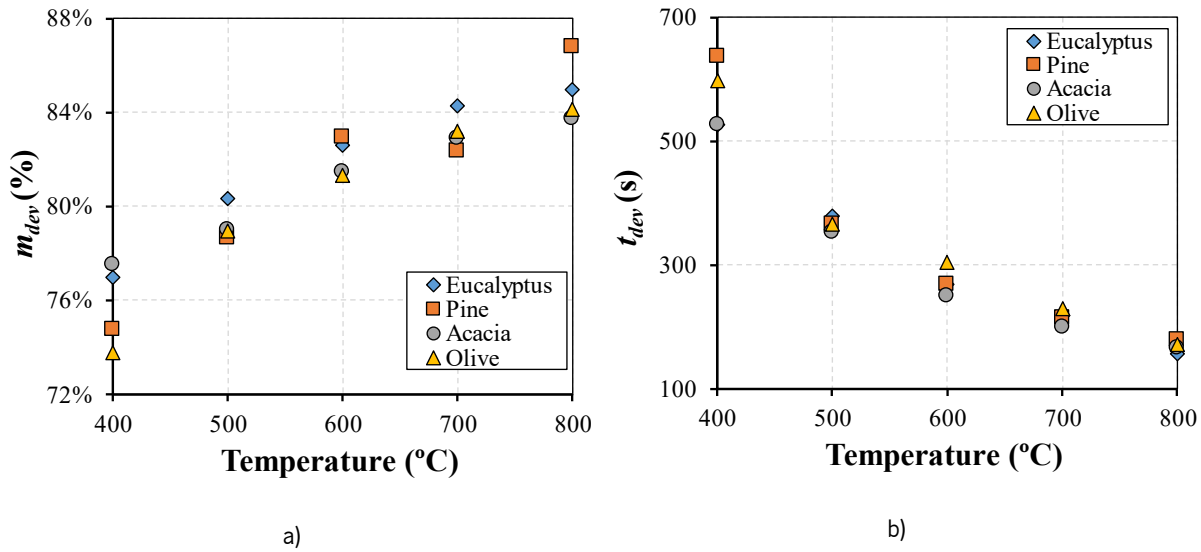

Figure 80: Influence of temperature on: a) the percentage of mass loss during the first stage, and b) corresponding time as a function of temperature.

Hence, for pine, the ratio between the final mass at lower and higher temperatures was 8, while for eucalyptus and olive was 2.8 and for acacia was only 1.6. Therefore, taking into account that at 800 °C the residual mass of pine was close to the ash content (2%), it is possible to state that pine samples present the best combustion performance at higher temperatures. Furthermore, from Figure 80 b) it is possible to observe that the time to complete the first reaction was very similar for all fuels.

Regarding the second conversion stage, Figure 81 presents the percentage of mass loss as a function of temperature. As it can be seen, there is no evident influence of temperature in this reaction. In addition, the differences between the different fuels are within 3%. These results help to support the hypothesis that char conversion is governed by diffusion.

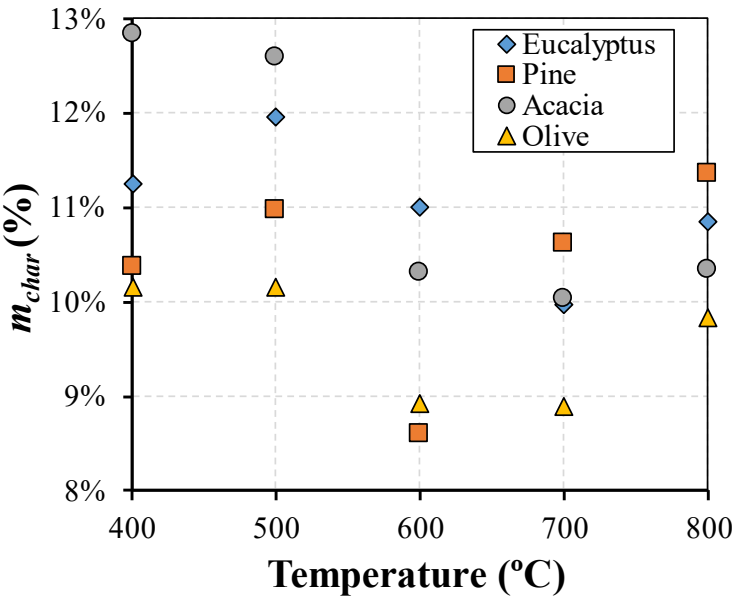

Figure 81: Percentage of mass loss during the second stage as a function of temperature.

8.3. Gaseous Emissions

During the experiments with eucalyptus particles, the gases, which include end-product gases such as H_2, CH_4, CO, and CO_2, released during the devolatilization period were collected in a sample bag. In order to be able to collect the sample during the entire devolatilization period, the flow rate of the sampling pump was adjusted to fill the bag within the time frame of the experiment. Then, the composition of the samples was analyzed in a micro GC where three samples were removed from the bag and inserted into the equipment to detect the concentration of the different compounds. Figure 82 presents the results

from these experiments, and shows, in particular, that gaseous emissions are strongly dependent on the temperature. The remaining volumetric fraction corresponds to the nitrogen content. Consequently, the results reflect that the main gas compounds are produced through thermally favored reactions such as oxidation. CO_2 and CO are always the main pyrolysis products, where CO contribution represents a maximum of 13% and CO_2 12% of the total concentration at 800 °C. The temperature dependence of both compounds shows the same upward trend, although the CO yield is increasing from 8 to 13% between 600 and 800 °C, while the CO_2 yield is only slightly increasing from 11 to 12%. As mentioned by Becidan et al.[264], the trend of CO_2 production tends to stabilize at high temperatures due to their formation through the cellulose and hemicellulose conversion. These are reactions that occur mainly at low temperatures and are not favored by the increase in temperature. In its turn, CH_4 and H_2 are the minor compounds of the flue gas composition. CH_4 ranges from 1% at 500 °C to around 4% at 800 °C.

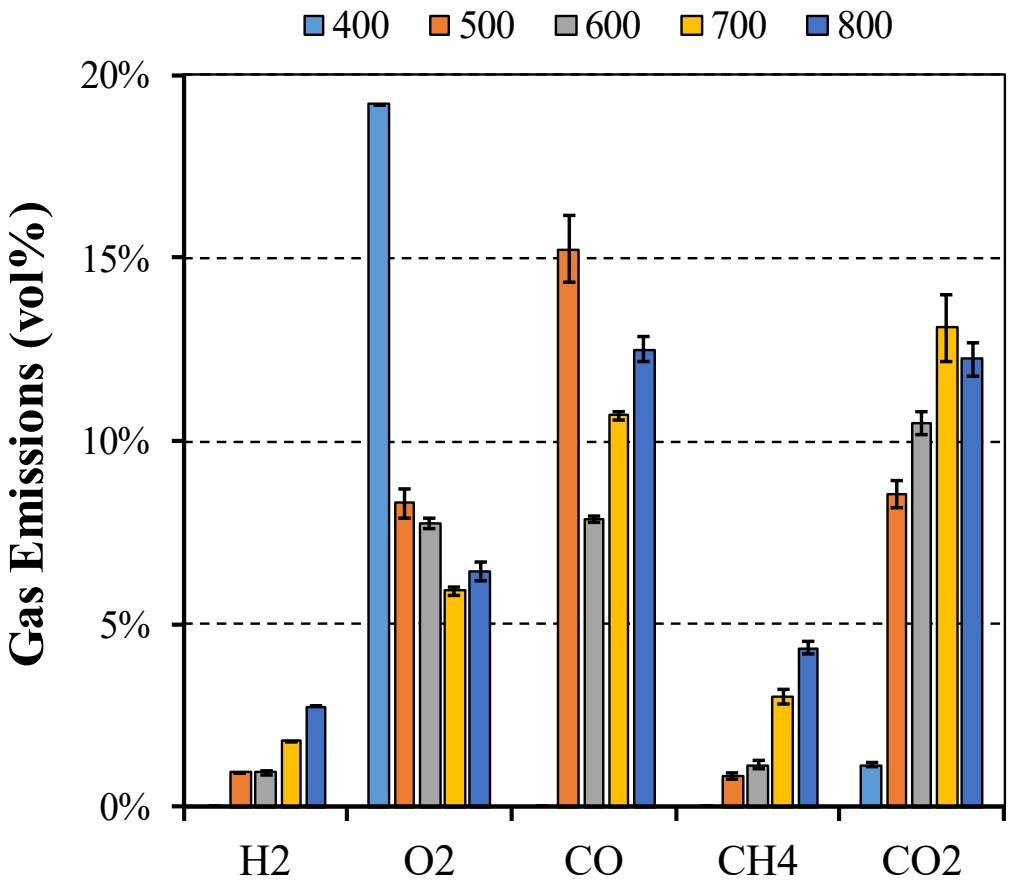

Figure 82: Average gas emissions and standard deviation as a function of reactor temperature.

The H_2 yield, a product mainly attributed to cracking reactions, is slightly increasing with temperature from less than 1% at 500 °C to approximately 2.75% at 800 °C. The O_2 content is not necessarily formed through the biomass conversion and is possibly resulting from the air introduced in the reactor or due to the desorption of air adsorbed in the particles as also mentioned by Figueiredo et al.[447]. Thus, to avoid any disturbance in the sample collection, the air flow was kept at low levels.

Considering the previous results, a general reaction describing the mass fraction of the main compounds released during the devolatilization at the highest temperature, to simulate the hot environment inside an industrial boiler, was established as represented in Equation (113):

$$\text{Biomass} \longrightarrow 0.07CH_4 + 0.56CO_2 + 0.36CO + 0.01H_2 \quad (113)$$

Similar observations have been made elsewhere [46,247,264,266], these results are scarce in the literature and represent extremely useful data for CFD simulation or mathematical purposes to fully describe the biomass conversion. Neves et al. [247] found that at temperatures above 500 °C, the permanent gas compounds strongly become temperature-dependent, leading to a substantial increase in the CO mass fractions. This was considered a product of secondary reactions, which resulted in the decrease in the tar mass fraction also due to the conversion to CH_4. The same behavior was described by Mehrabian et al. [46] based on dedicated experiments and data collected from the literature. Secondary reactions of the volatiles are negligible at low temperatures, and most of the permanent gases result directly from biomass thermal degradation. Within the low temperature range, gases like CO and CO_2 are the main permanent gas compounds, with low quantities of CH_4. As the temperature increases, secondary reactions occur and an increase in CO and CH_4 are associated to the decrease of tar. Here, due to higher temperatures, the yields of the volatiles have a strong correlation with the temperature, and CO is considered responsible for the conversion of two-thirds of the tar. Although the tar was not measured during the experiments, this is in line with the trend presented in the results presented in Figure 82. Becidan et al. [264] investigated the main gas components from pyrolysis of thermally thick biomass residues samples at 600 to 900 °C using an FTIR analyzer and a micro GC. The authors also mentioned a clear dependence of the gas composition with temperature and observed a clear tendency of the hydrocarbons yields to stabilize. Gauthier et al. [266] in the study of pyrolysis of beech wood particles for temperatures ranging between 450 and 1050 °C also found a similar trend. The authors also reported that at low temperatures the emissions are mainly composed of CO_2, whereas pyrolysis above 800 °C was found to produce mainly CO.

8.4. Comparison with XDEM

In order to validate the mathematical model presented in Chapter 5 and verify the suitability of the thermal and kinetic parameters determined in Chapter 7, the conditions of the experiments using eucalyptus particles in the small-scale reactor were simulated. According to the macro TGA experiments, the simulation model was prepared with 41 spherical eucalyptus particles with an average of 10 mm in diameter, with a variation of ± 10%, reproducing the initial weight of the experiments. The variation of the diameter was defined to represent the random variation of the woodchips dimensions and, this arrangement of particles reproduces the experimentally calculated bulk density for particle class between 8 and 16 mm. The VM and ash content of the eucalyptus samples were revised to take into account the 20% of moisture content of the particles used in the experiments. Table 39 summarizes the other necessary parameters to define for the XDEM tool to compute the particles conversion. The values are based on the previous works with biomass particles. Additionally, the heating conditions for the experiment at 800 °C were determined and the heat flux was evaluated as 16.6 kW and the global heat transfer coefficient as 106 W/m^{2}K. These values are important to define the external boundary conditions to the spherical particles.

Hence, considering all the initial conditions mentioned above, Figures 83 and 84 present the overall behavior of the thermal conversion of biomass particles in terms of temperature and mass variation, respectively. This is an interesting approach that allows to visualize the conversion of each particle and evaluate their thermodynamic state over time.

Table 39: Main properties of the biomass particles considered for the simulation.

Parameter	Value
Initial temperature (K)	298
Young's modulus (N/m^2)	10,000
Poisson's ratio (-)	0.45
Restitution coefficient	0.50
Friction coefficient	0.80
Permeability (m^2)	1.97E-14
Pore diameter (m)	5E-5
Particle porosity (-)	0.70

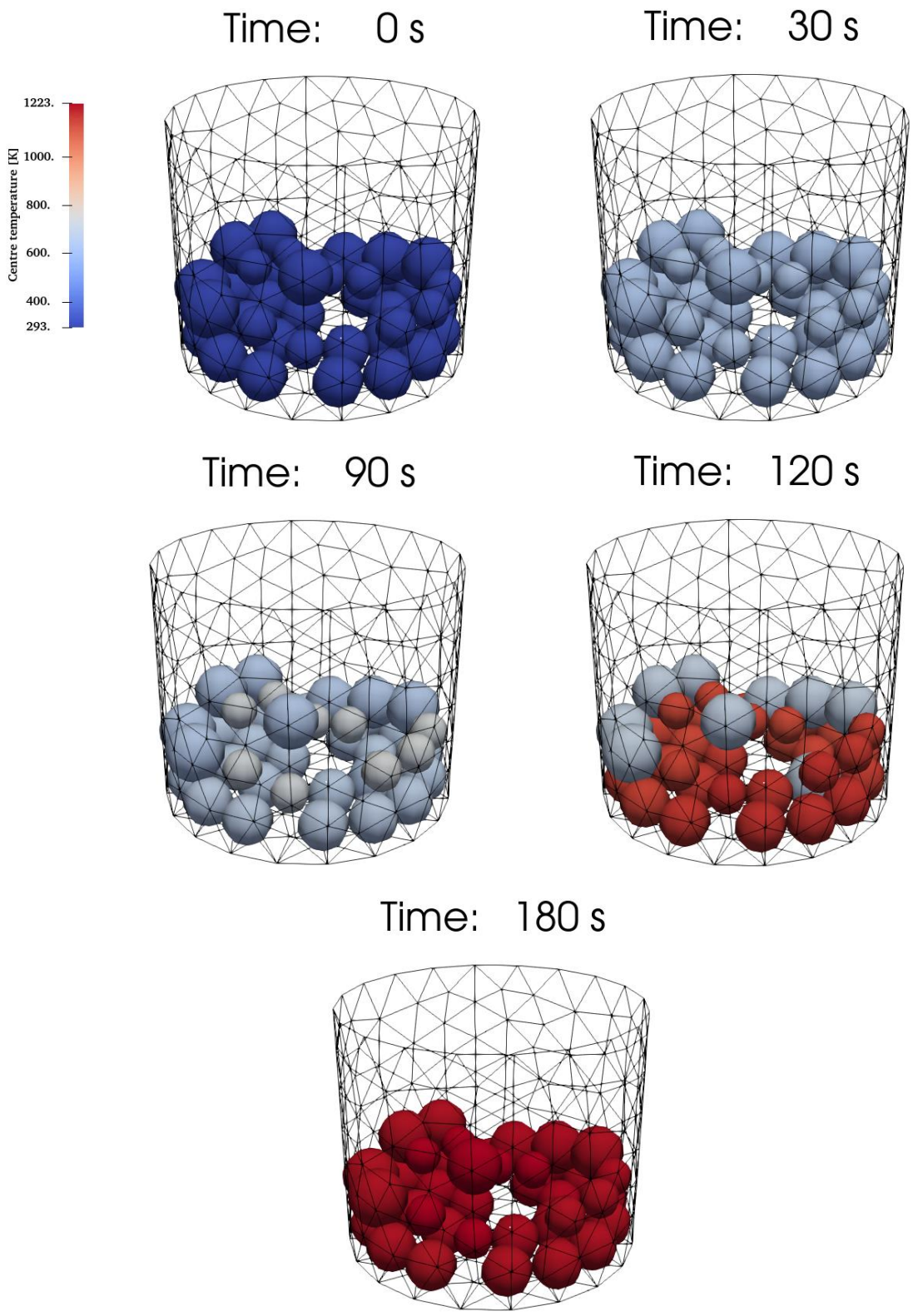

Figure 83: Temperature variation of the particles over time.

The absorbed heat from the surroundings increases the temperature of the particles quickly, and the heat is transferred to particles below by the heat transfer mechanism considered in the model used in this

work. Furthermore, as shown in Figure 83 the particles with lower dimensions are quickly dried, and their temperature suddenly rises to 1223 K, in around 2 minutes, due to the intensive radiative flux from the surroundings and reactions.

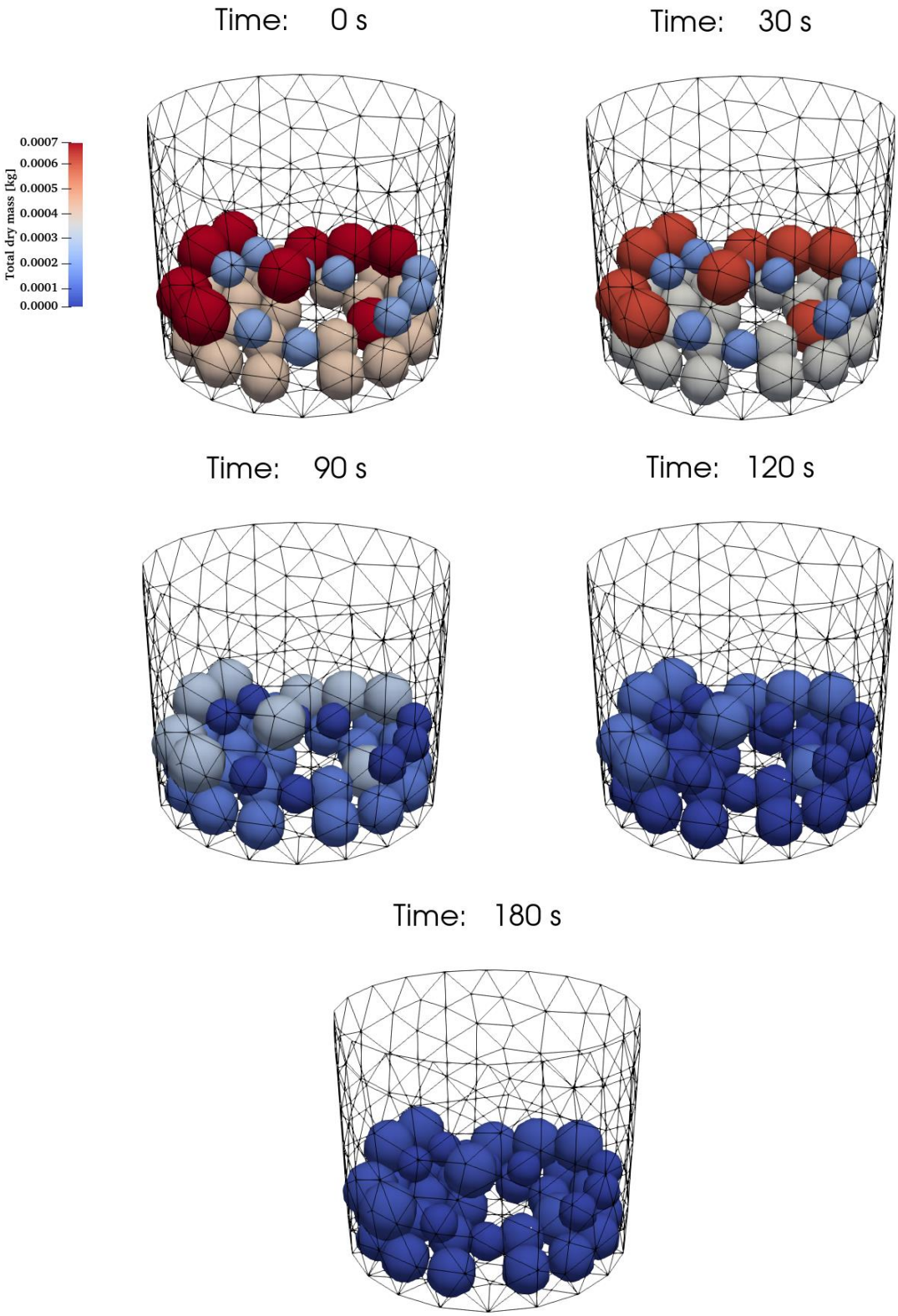

Figure 84: Mass of the particles at different times.

Regarding the mass of the individual particles, as observed in Figure 84, the fast heating of the particles allows complete drying, devolatilization, and char oxidation after 2 minutes. After this time, a reduced amount remains in the basket and is equivalent to the ash content of the eucalyptus.

In Figure 85 a comparison of the mass loss predicted with the simulation model and the experimental average mass loss profile at 800 °C is performed. Despite small differences between the experimental and numerical results, a good agreement between experimental data and the XDEM predictions was achieved, mainly in the first stage of the thermal conversion. Comparing both results, the modeling approach shows that the kinetic model adopted in this work presents some difficulties in predicting the same mass loss behavior as the experiments in the second stage of the reaction. There is a significant discrepancy in the mass loss in this period due to the reaction mechanism. Furthermore, differences occur during the first seconds due to the fast heating and drying of the particles predicted by the mathematical model. The agglomeration and dense arrangement of the particles in the experiments, which prevents a uniform heat flux for all particles, are important factors that may cause a slower mass loss.

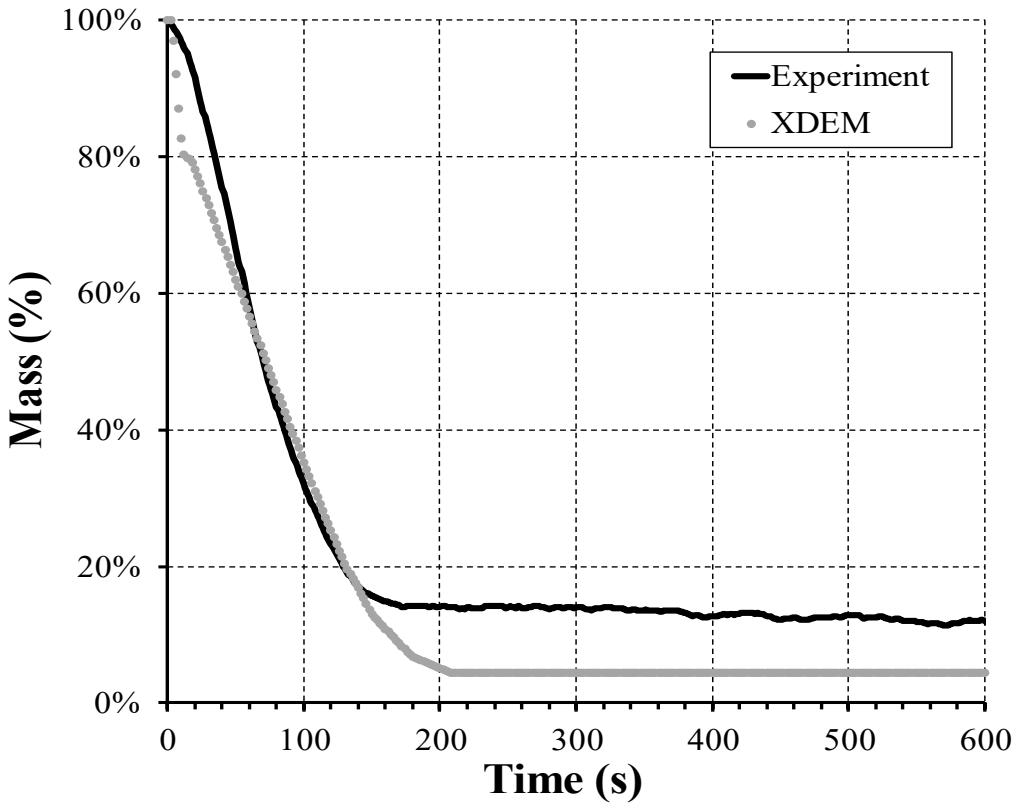

Figure 85: Comparison of the XDEM predictions with the experimental result of the mass loss at 800 °C.

Although the modeling approach does not account for diffusion limitations inside the particles, only the kinetics of the devolatilization and char oxidation reactions, the simplicity and reduced complexity of the mathematical model, and lower computational requirements, make the approach more attractive than more sophisticated models that require various specific parameters that are difficult to estimate.

Therefore, the modeling approach presents a useful option to describe the biomass combustion, and further use of this tool coupled with CFD models to predict the combustion behavior inside biomass boilers.

CHAPTER 9

NUMERICAL RESULTS

This chapter focus on the presentation and discussion of the numerical results from the 3D CFD simulations. These are focused on the analysis of the dependency of the results on the mesh, assessment of the nominal operating conditions, study of the influence of the biomass conversion on the vibrating grate, and analysis of different air supply conditions. The results are presented in terms of the main relevant parameters such as velocity, temperature, and emissions to provide an overall assessment of the biomass combustion process. Numerical models are an outstandingly powerful tool for thermal and fluid dynamics evaluation and prediction of the different phenomena inside the furnace. The model developed can be used to analyze their operation using the nominal conditions and to provide an advanced combustion analysis for improving biomass conversion along the grate and reducing pollutant emissions.

9.1 Grid Independence Analysis

In the freeboard, where the homogeneous combustion takes place, a lot of efforts to generate a high-quality mesh were made. In CFD simulations, mesh plays a vital role in the accuracy of the results and largely affects the convergence and time required to complete the simulation. Hence, firstly, a grid study for estimating the dependency of the numerical results due to the discretization was carried out using the three meshes described in Chapter 5: around 250k, 500k, and 1M cells. The reactive numerical simulations were performed considering the nominal operating conditions. Temperature and velocity were considered the variables of interest to assess the differences in the numerical predictions at two specific locations. Figure 86 represents the two lines selected to analyze the results. The first line, at 3 m is slightly above the first row of secondary air nozzles and the upper line is close to the outlet. More details about the boundary conditions in the grate are provided in the next section.

The effect of the mesh can be seen in Figure 87. The results show some velocity and temperature differences, in particular when the mesh becomes denser, and the number of cells is around 1 million. The differences are higher closer to the grate. Consequently, to achieve reliable CFD results, the mesh with the highest density was preferred and selected for the development of the sensitivity analysis. Meshes denser than mesh 1 were also assessed however, the computational time was substantially higher with no visible gains in accuracy.

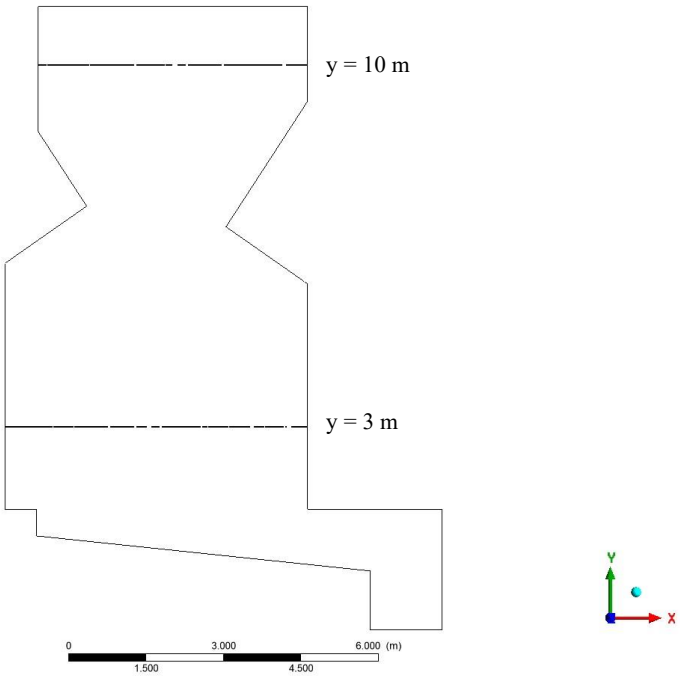

Figure 86: Location of the positions in the middle plane to analyze the grid independence results.

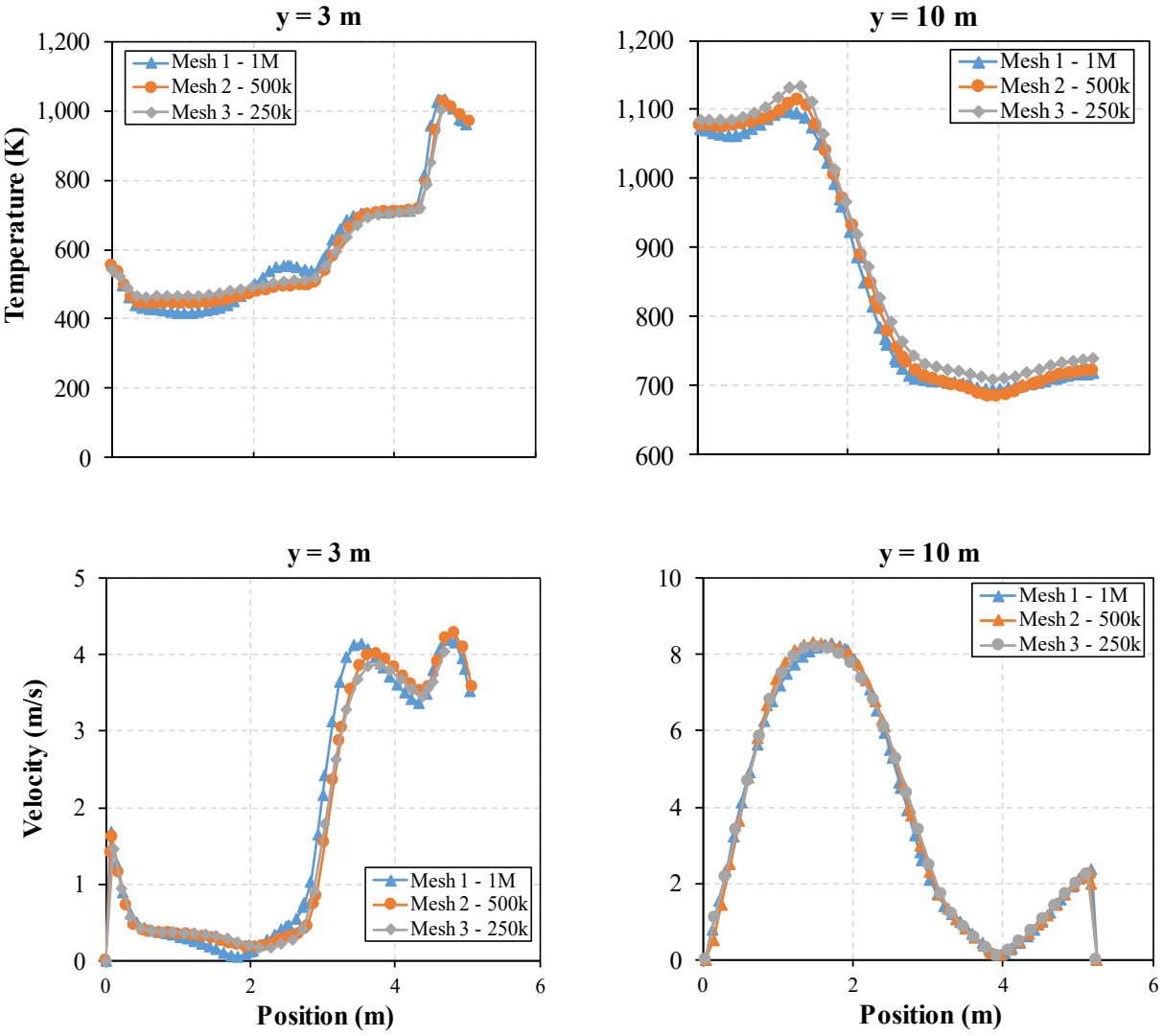

Figure 87: Velocity and temperature profiles for the three grids.

9.2 Nominal Conditions

In this section, the CFD results of the previously selected mesh are presented in more detail. First, regarding the conversion of biomass using the bed model, the different thermal conversion stages of this process, since the primary air supply is split in the vibrating grate, three zones were considered along the grate length. For each zone, biomass conversion rates were specified based on observations in the Power Plant at Mortágua, which agree, in a broad sense, with values found in the literature [301,340,448]. These conversion rates can be found in Figure 88. Through the mass and energy balances presented in Chapter 5, the gas flow rate and the composition of the flue gas that are supplied to the freeboard were estimated. This information was then set as inlet boundary conditions for each zone.

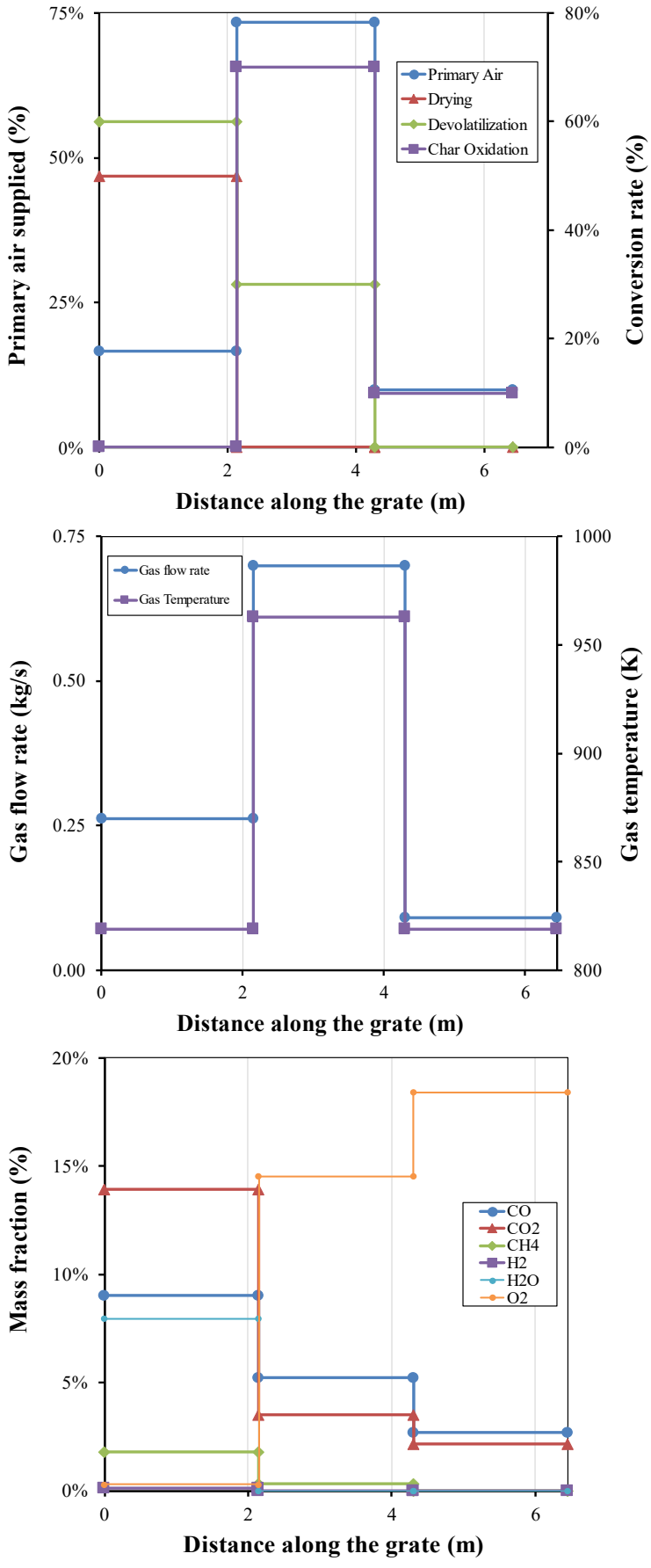

Figure 88: Profiles of the different boundary conditions defined along the grate.

Furthermore, these boundary conditions rely on some assumptions such as the mass fraction of the chemical species CH_4, H_2, CO, and CO_2, based on the results of the experimental measurements carried out in the small-scale reactor presented in the previous chapter. Considering the experience in the Power Plant at Mortágua, there is a significant amount of unburnt fuel in the ashtray and it was considered that only 80% of the char reacts. Furthermore, the radiation incident on the fuel bed top was based on the results presented in the literature and adapted to the size of the boilers studied in this work [301,307]. Additionally, as the entire grate is not equally exposed to flame radiation and wall radiation, it was considered that only 10% of heat flux is transmitted to the last section. Regarding the air supply conditions, for the nominal operating conditions, the primary to secondary air ratio is 79/21 and the excess air is 40%.

Regarding the numerical results, the method by which air is supplied to the boiler is one of the most important parameters in the combustion system. The design of the present boiler consists of two opposing arches to concentrate the flue gas and, to improve the mixing with the secondary air introduced in the side walls through small nozzles. In addition to the introduction of the oxidant in the main flue gas stream, its location is also important to improve the mixing and control the combustion process. The effect of the opposing arches, and the multi-level small nozzles, on the flow in the furnace, can be observed in Figures 89 and 90, where the temperature and velocity contours in the middle plan of the model are presented. This design promotes a concentration in the center zone of the furnace, where the velocity is higher. The fastest reaction rates are found around the ignition air nozzles where high temperature gradients are observed. The design of the boiler was developed by Babcock & Wilcox [78,108] in the late 1970s specifically for biomass combustion and aims to create a controlled combustion zone in the furnace. Secondary air located within and below the arches penetrates and mixes with the volatiles released from the bed. Furthermore, the two arches, present on the opposite walls, define a combustion zone and create a smaller cross-section to promote the mixing of the combustion products. However, the result of inadequate penetration and the presence of arches is that the flow entering the upper furnace is deflected to the center, where the vertical velocity and temperature of the gases are high. This creates large temperature and velocity gradients in the flue gas flow entering the convection section of the furnace (superheater, evaporator, and economizer). The average temperature at the outlet of the domain was 994 °C.

In Figure 91 the velocity field is also illustrated by superimposing velocity vectors to present the dynamic behavior of the flow in the upper part of the furnace. Apart from the secondary air nozzles providing favorable reaction conditions in terms of oxygen, they also provide high turbulence levels in the arch zone.

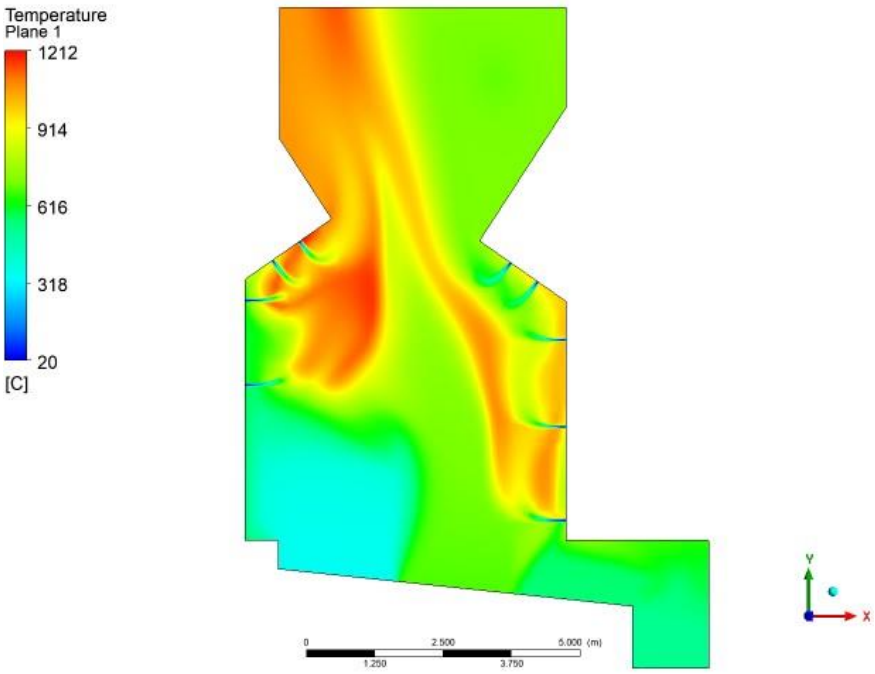

Figure 89: Temperature profile in the middle plane.

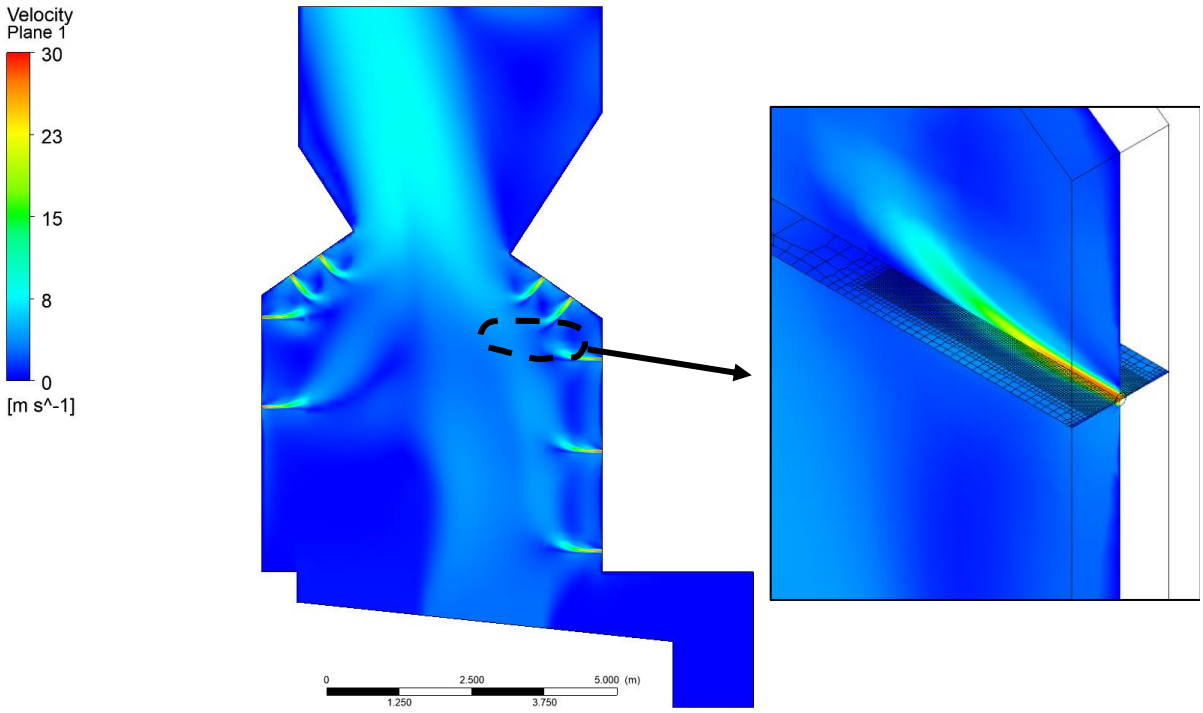

Figure 90: Velocity contour with the detail of the flow in one nozzle.

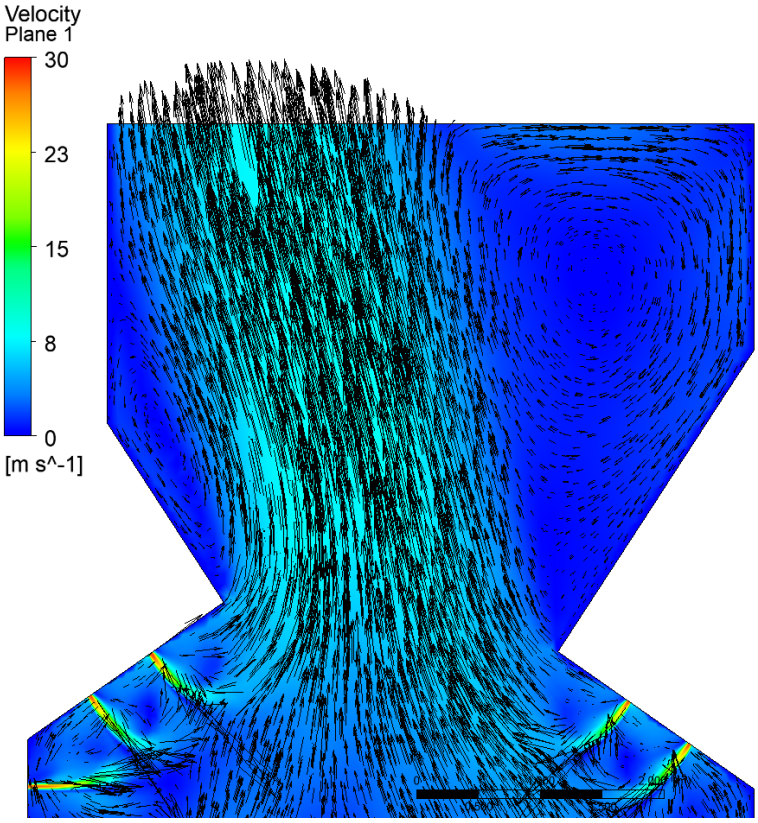

Figure 91: Vorticity inside the boiler.

Figure 92 presents the profiles of the CO_2, CO, and O_2 mass fractions. A general characteristic of oxidation reactions is the occurrence of very fast rates in the secondary air injector regions. Secondary air injectors provide favorable reaction conditions in terms of oxygen and high levels of turbulence, ensuring good mixing of the oxidant with the volatiles. The fastest reaction rates are found around the secondary air jets due to the greater amount of oxygen present for oxidation reactions to take place. Thus, the location and design of these injectors are essential parameters in controlling the combustion process in the furnace. The heat released by the chemical reactions provides the heat transfer by radiation to the surface of the fuel in the grate, thus promoting the initiation of the drying and devolatilization processes. Consequently, these injectors control and maintain the location of the reaction front on the fuel surface at a fixed position. This is important to obtain an acceptable degree of fuel burn. Thus, the secondary air injectors, in the arch of the furnace, supply the necessary oxygen to complete the combustion of volatiles and, in particular, carbon monoxide. This can be observed by the contours of the mass fraction of both species. The small injectors of the air system mix the oxygen supplied by them with the gases released, due to thermal decomposition, thus promoting the rapid oxidation of CO in the lower region of the furnace. The hottest regions in the furnace occur due to the oxidation of CO by the secondary air injectors. The regions

where CO is around 0 and the CO_2 is maximum corresponds to the region where the maximum temperature was obtained. It is also important to mention that the oxidation reaction of CO is controlled not only by its mixing with oxygen but also by temperature. Additionally, CO is almost completely oxidized, and there is only the central region of the furnace containing this specie due to the poor penetration of the secondary air nozzles. However, at the outlet of the furnace, an average mass fraction of CO of 0.009 (779 mg/m³) equivalent to was obtained, which means that a small quantity of energy is lost due to incomplete combustion.

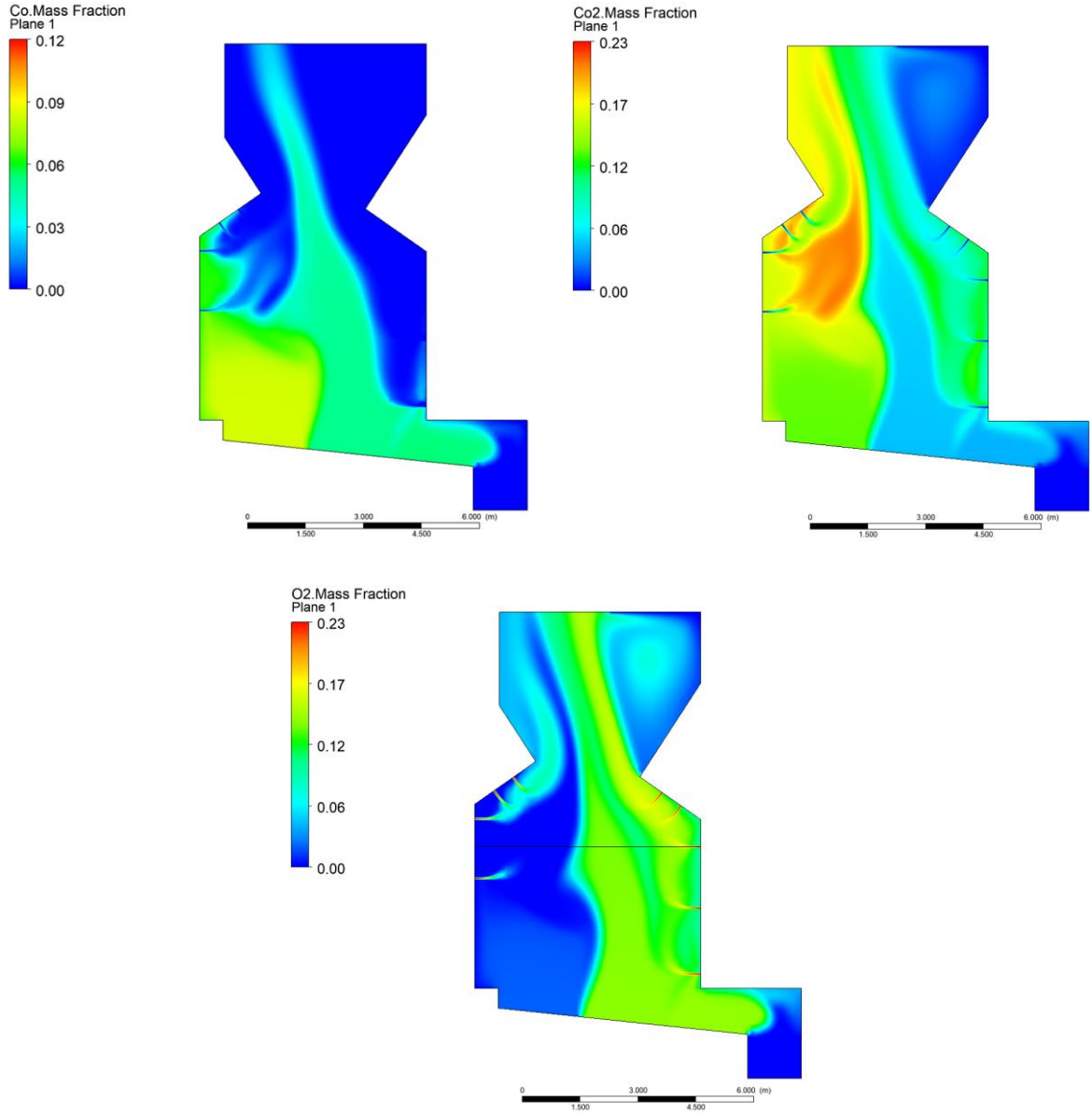

Figure 92: Distribution of the CO, CO_2, and O_2 mass fractions.

Therefore, CO emission is essentially related to the boiler design and the amount of air used in the combustion process. In this way, the mixing of volatiles with the combustion air could be improved if the penetration of the secondary air injectors was higher. Consequently, as can be seen, observed in Figure 92, the CO released in the last sections of the grate does not react completely. Thus, by increasing the penetration of secondary air injectors, the oxidation of combustion products will be improved.

Regarding the CO_2 emissions, the average mass fraction obtained at the exit was 0.12. With this result, it is verified that the secondary air actually allows the oxidation of CO since its input in the simulation had a maximum value of 0.08 (6.87% in volume). In contrast to the CO_2 mass fraction contour, O_2 presents the opposite trend due to its consumption in the CO rection forming CO_2. At the outlet, the simulation pointed out a value of 9.5% (in volume) which is within the range of the data recorded during one week of regular operation in the Power Plant at Mortágua. Furthermore, during one of the monitoring campaigns to determine the emission levels of the Power Plant, the average CO, CO_2, O_2, and temperature in the upper part of the boiler were 719 mg/m^3, 11.7%, 9.1%, and 1080 °C, respectively. The direct comparison of these values presents some discrepancies which may be attributed to the variation of the operating conditions and the results of the bed model. In the grate, combustion instabilities and variations associated with the fuel feeding in terms of properties during the normal operation of the boiler are frequent, and it is difficult to predict the exact conditions for the CFD model. There are different phenomena associated with disturbances in the bed like local burnout and channeling which could be responsible for higher pollutant emissions and uneven consumption of the fuel. Therefore, the discrepancies can be understood but, even though there are some differences between the baseline and the experimental measurements, the baseline model allows to capture of the main flow and combustion features with acceptable accuracy.

Moreover, regarding the supply of air in the furnace, the poor mixing in this type of equipment is often due to the result of the utilization of relatively small diameter of the secondary air nozzles which provide poor penetration into the flue gas flow. Consequently, a relatively simple solution to this problem would be to use fewer injectors but with a larger diameter [78,108,358,361]. However, the distribution of the injectors is also a very important factor in improving the combustion process in the furnace. If the space between injectors is too small, there will be poor mixing between oxygen and combustion products as the flow of air injected through the injectors will be affected. Choi et al. [449] verified the same problem in a grate-type wood waste incinerator. The authors investigated how to reduce CO emissions by simply retrofitting the existing facility without installing any extra equipment, and by changing the existing operating conditions. The reduction of CO emissions was possible through a secondary air nozzle retrofit

based on the jet penetration factor and the momentum flux ratio of a commercial wood waste incinerator and a 3D CFD model was developed to predict how far the CO emissions would be over the limit after the retrofit. Kaer et al [361] also reported the poor mixing experienced in a straw-fired grate boiler as a result of the relatively small diameter of the secondary air nozzles, providing poor penetration into the bulk flow. The author proposed a relatively simple solution with fewer nozzles with a larger diameter. Another strategy was proposed by Jorgensen et al. [90,108]. These authors developed a numerical model to compare a conventional overfire air system design typically used on biomass furnaces to a new advanced design involving the removal of the arches and replacing the numerous small nozzles with a smaller number of controlled penetration nozzles.

9.3 Influence of the Biomass Conversion on the Grate

The purpose of this section is to demonstrate different combustion regimes that can occur during the operation of a biomass power plant. During the normal operation of an industrial boiler, the operating conditions are constantly varying, there are combustion instabilities inside the fuel bed, the movement of the grate affecting the combustion, and variations in the physical and chemical properties of the fuel supply. Thus, it is important to present an overview of different scenarios that can occur in the biomass conversion along the grate. Table 40 presents the cases defined for the evaluation of the combustion behavior inside the furnace as a function of different considerations in the bed conversion model. All the CFD simulations are based on the nominal operating conditions

Table 40: Cases defined for the analysis of the bed conversion model.

Biomass Converstion (%)		**Case 2**	**Case 3**	**Case 4**	**Baseline**
Drying	Section 1	50	40	80	70
	Section 2	0	0	0	0
	Section 3	0	0	0	0
Devolatilization	Section 1	60	80	50	60
	Section 2	40	20	50	40
	Section 3	0	0	0	0
Char Oxidation	Section 1	0	5	0	0
	Section 2	70	75	50	60
	Section 3	10	5	30	20

The differences between the different scenarios can be evaluated in Figures 83 and 94. First, Figure 93 presents the velocity and temperature profiles in the middle plane of the computational domain. The combustion, here evaluated based on the temperature, and velocity field pattern, as observed in the previous results, is governed by the location of secondary air nozzles, and here the fluid flow configuration, although the conditions in the grate are not the same, the flow patterns are similar. Only case 4 presents a higher fluid flow in the last section of the grate since the bed conversion was shifted to this zone. Additionally, the comparison between the three cases indicates that a higher temperature on the left hand side of the boiler was observed for case 3. Higher temperatures can cause severe deposition problems.

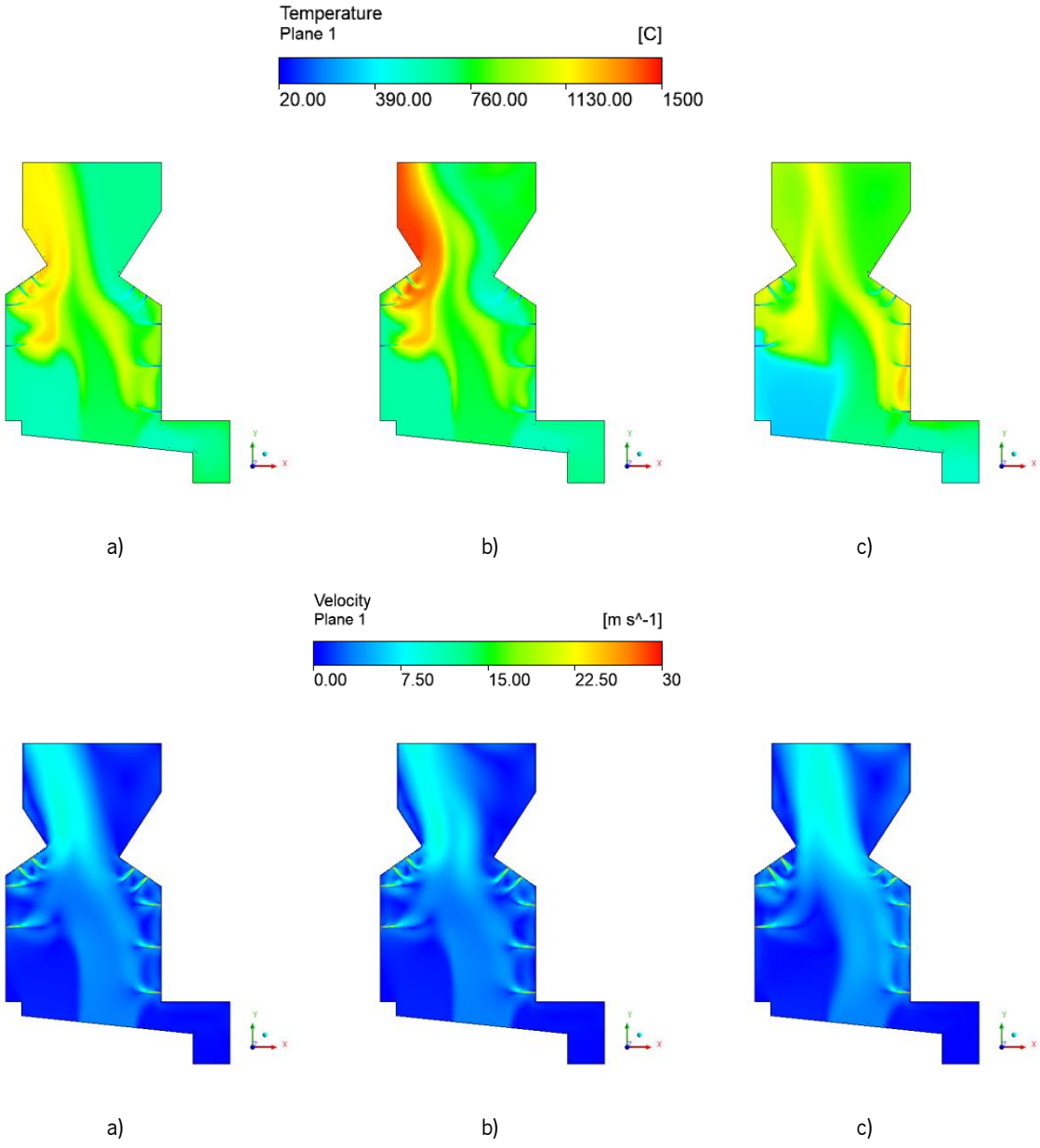

Figure 93: Temperature and velocity contours of: a) case 2, b) case 3, and c) case 4.

In these conditions, secondary air nozzles must push the flame to the furnace center, and this is only possible with a higher flow rate. The result of this increase in temperature is attributed to the biomass conversion mainly in the first section of the grate and the reduction of the amount of energy for drying the fuel.

Consequently, a higher amount of volatiles is released in the left part and, subsequently, their mixing with the air supplied by the secondary air nozzles leads to a different combustion behavior when compared with the other cases. Hence, through the different scenarios, it is possible to verify the modifications in the combustion patterns in the freeboard. In contrast to case 3, as a higher percentage of char conversion in the last part of the grate was considered for case 4, an increase in the temperature in the right wall of the boiler was obtained. Therefore, the bed model apart from playing an important role in the freeboard modeling can capture the dynamic behavior or modifications of the bed conversion in the grate. Through Figure 94 it is possible to observe how the chemical reactions are sensitive to the grate inlet conditions.

The mass fraction contours are a useful tool to understand and evaluate the combustion phenomena. Although case 2 presents the highest CO mass fraction released to the furnace, the design of the boiler allowed to reduce its value considerably to 0.004, the lowest for the different cases tested. Hence, it is essential to highlight that the combustion efficiency is improved when the biomass conversion is in the first two sections of the grate.

In addition, through this analysis, it can be concluded that if the thermal conversion of biomass is moved for the last sections of the grate, higher penetration of the secondary air nozzles is required.

9.4 Sensitivity Analysis of the Air Supply Conditions

Since the design of the air supply system plays a very important role in the efficient and complete combustion of biomass, CFD simulations were developed to investigate the influence of this part of the boiler. The split ratio of primary air to secondary air in a modern grate-fired boiler is 60/40 [32] while in the thermal power plant at Mortágua, considering the nominal operating conditions, is approximately 79/21. Thus, there is considerable potential for improvement since in the previous analyses particular attention was oriented to the need for higher penetration of the secondary air nozzles.

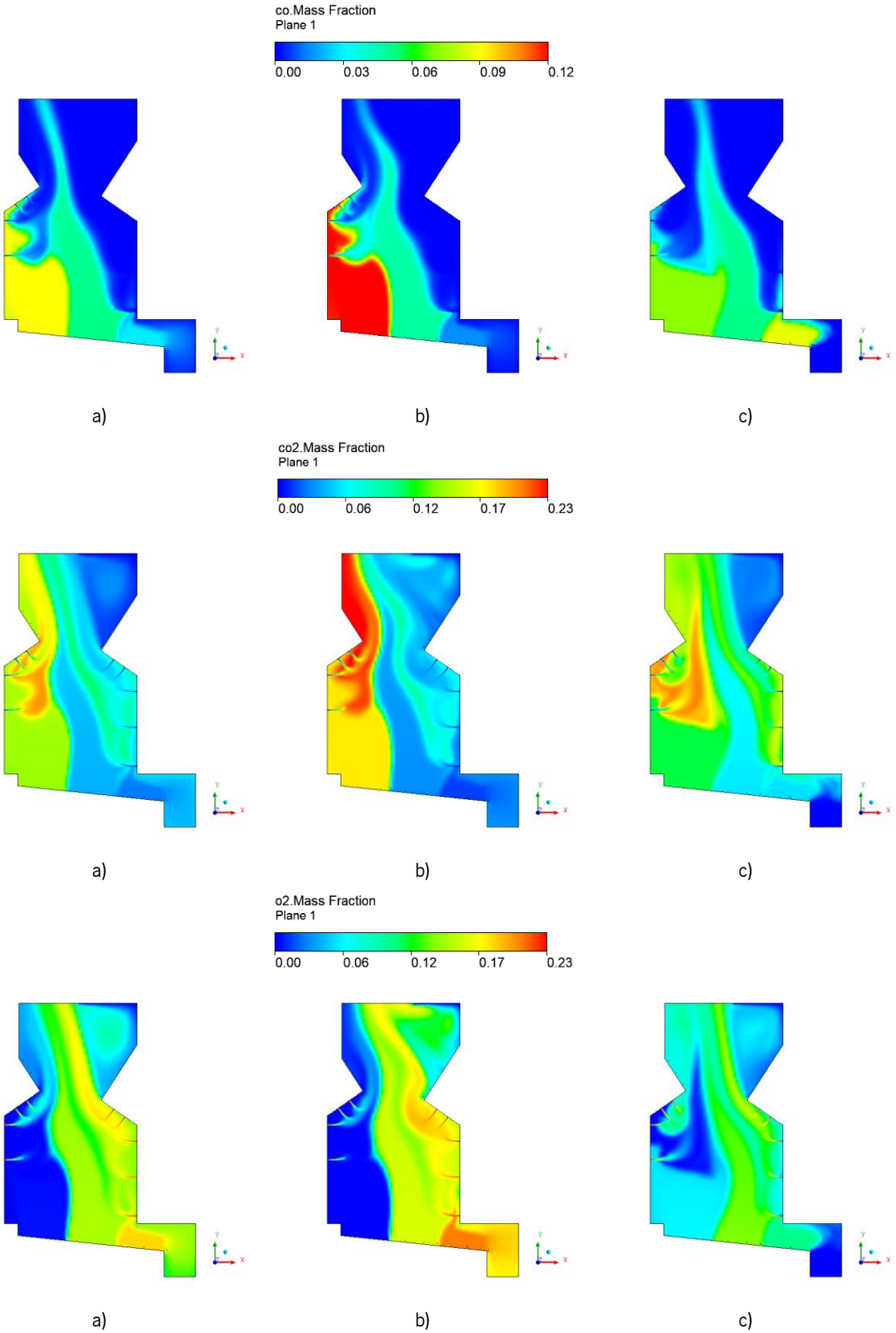

Figure 94: CO, CO_2, and O_2 mass fractions contours for: a) case 2, b) case 3, and c) case 4.

Hence, considering the limitations concerning the air supply and the nominal operating conditions, two different cases were analyzed modifying only the primary and secondary air split ratio. The first case was defined by taking into account the need for more secondary air and a high level of turbulence in the upper part of the furnace, resulting in a 40/60 split ratio. The second case was based on the split ratio value defined by Yin et al. [32] for modern boilers, 60/40.

In the temperature profile illustrated in Figure 95, the highest temperature, around 2,000 °C, was obtained in the first case and occurs due to the mixture of the flue gases with oxygen supplied by the lower secondary air injector present on the right side wall of the boiler. Due to the higher amount of oxygen supplied by the secondary air injectors, the maximum peak temperature was obtained in this case when compared to the others. Providing a higher secondary air flow rate allows more oxygen to be available for the oxidation reactions and, as a result of this retrofitting, a higher amount of energy is released inside the furnace. For this reason, in the case with a 40/60 split ratio, there is an increase in the average temperature inside the furnace to approximately 1,050 °C compared to the 988 °C obtained for the second case.

It is interesting to note that in case 1, due to the supply of a higher secondary air flow rate, the flow dynamics change significantly when compared to the results of the baseline model and 60/40 split ratio. It is possible to verify that due to the higher penetration of the secondary air nozzles and, consequently, higher turbulence generated inside the furnace, the flow is more deflected towards the right wall when compared to the other cases. Hence, through the temperature contour, it is observed that the first injector on the left wall has a relevant role in the determination of the flow and promotes the displacement of the flow to the opposite side. The injectors that are inside the arches also direct the flow towards the lower central part of the boiler, thus promoting a better mixing of the flue gases with the air and increasing the residence time inside the boiler.

The CO reaction rate shows that higher values were observed in regions close to the secondary air nozzles. This fact is essentially due to the higher penetration of the secondary air nozzles and higher availability of oxygen resulting from a higher flow rate of secondary air. Thus, CO is almost completely oxidized to CO_2, and, at the outlet, the average mass fraction of CO is 0.0003, while for the second case its value is ten times higher. This proves that penetration of the secondary air nozzles is a driving factor for promoting higher oxidation of the combustion products.

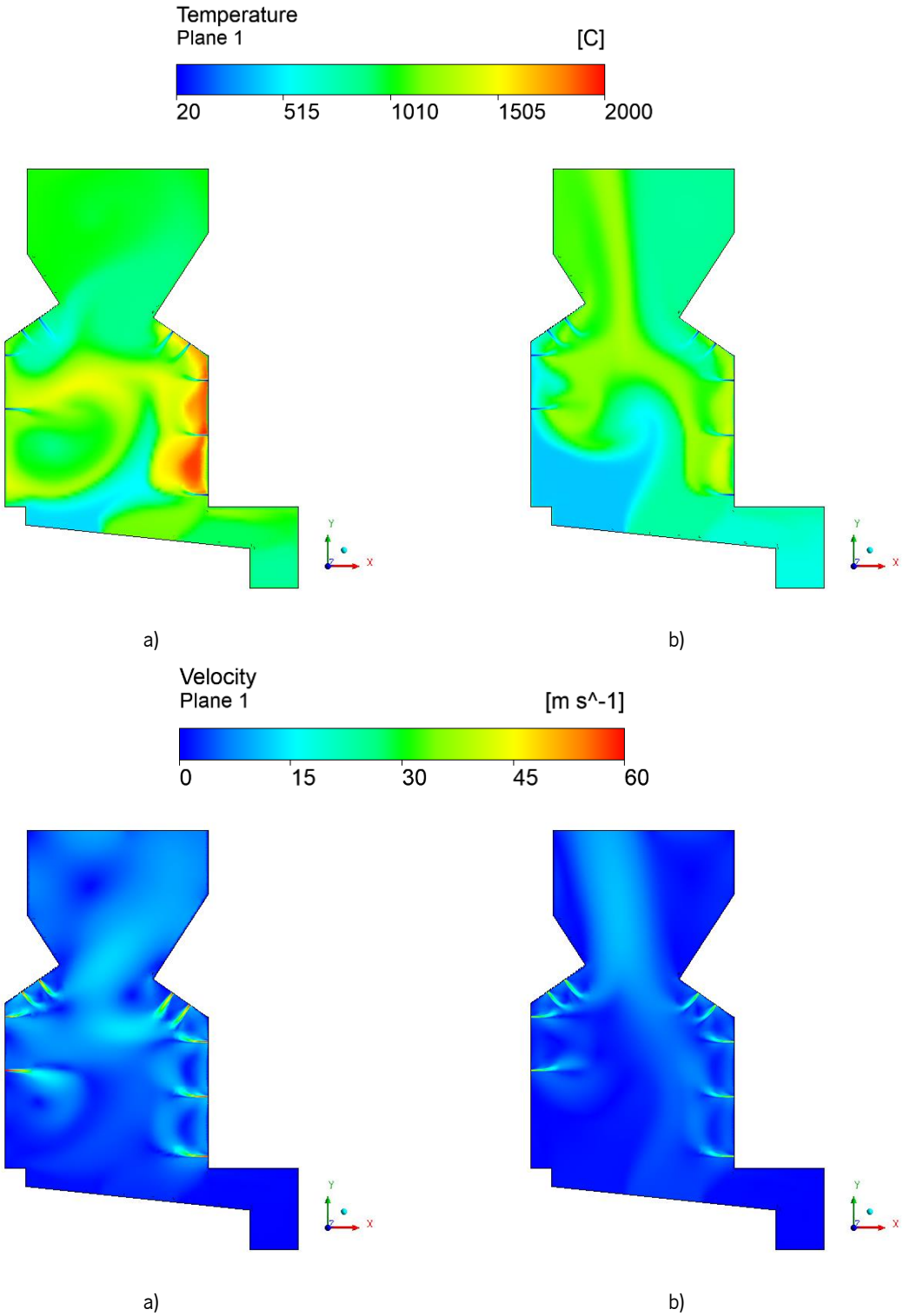

Figure 95: Temperature and velocity contours for the different cases: a) split ratio of 40/60, and b) 60/40

Apart from the influence of primary to secondary air ratio, another interesting variable is the temperature of the primary air. Preheating of primary air is a common practice to improve combustion behavior and to increase the efficiency of the power plant. Hence, considering the previous results, the 40/60 split ratio configuration was selected to analyze the influence of the temperature of the primary air. In general,

the temperature of the primary could reach temperatures up to 200 °C [281]. However, considering the results presented in Chapter 3, temperatures around 100 °C are feasible for in this particular boiler. Hence, a CFD simulation was performed to analyze the effect of preheating the primary air at 100 °C. Figure 96 presents the temperature profile in the middle plane of the boiler, and it is possible to observe that higher temperatures are obtained inside the furnace. The profile is similar to that obtained with a 40/60 split ratio however, the effect of the primary air preheating is visible mainly near the right wall where a region with a higher temperature is observed. Higher primary air temperature also resulted in improving the boiler efficiency in terms of pollutant emissions. Figure 97 presents a comparison of the average mass fractions of CO, CO_2, and O_2 between the previous cases and the present case. Although the CO mass fraction was reduced, the higher temperatures in the furnace can cause negative effects such as the increase in thermal NOx formation and the risk of grate and wall thermal damage. Considering these issues, the increase of the primary air temperature should be verified and carefully assessed for optimal combustion conditions since similar results can be obtained only by retrofitting the air combustion system.

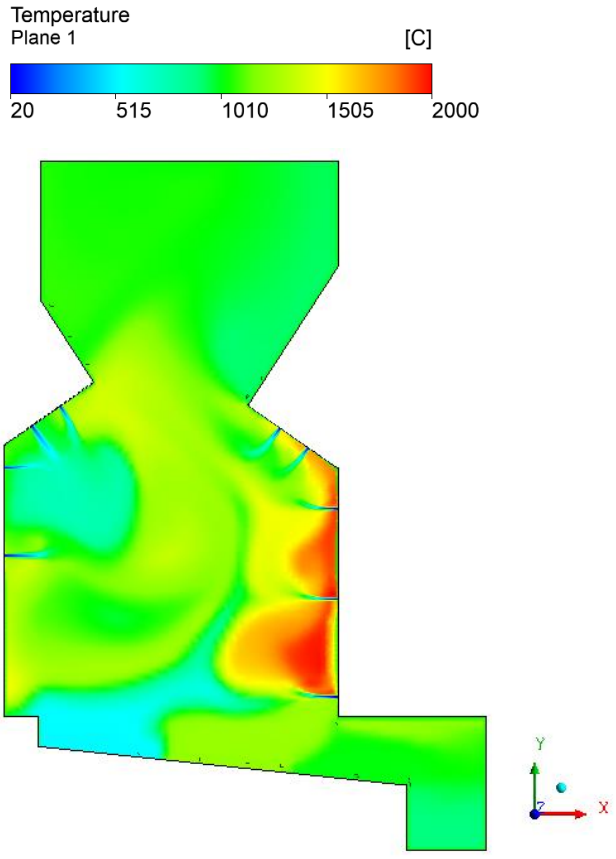

Figure 96: Temperature field for the case with primary air heating.

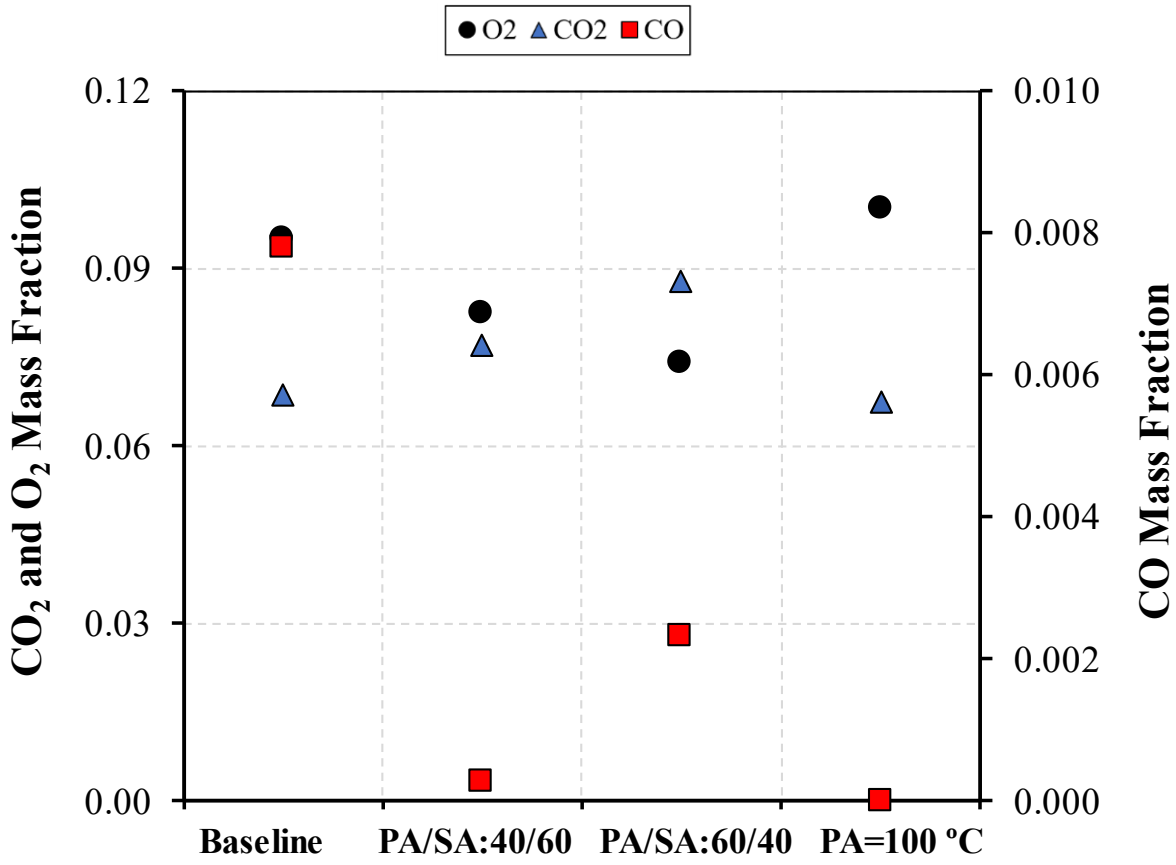

Figure 97: Average CO, CO_2, and O_2 mass fractions at the outlet of the furnace for the different cases.

CHAPTER 10

CONCLUSIONS AND FUTURE WORK

This work represents a comprehensive study addressing the gaps existing in the industry related to the production of electricity from biomass. Hence, this work is intended to be an added value for both the power industry and the academic community with scientific research driven by the close collaboration between academia and industry.

Herein this chapter, the most relevant conclusions resulting from this work are presented. Although the work developed presents some advances in the state-of-the-art, further improvements are identified in order to tackle some of the limitations found in this work. In this sense, suggestions for future research activities are put forward in this section.

10.1 Main Conclusions

This thesis addresses biomass combustion by combining an industrial investigation, experimental activities, and numerical modeling. The conclusions are summarized and highlighted by the assessment of each methodology.

Industrial Investigation

The industrial investigation was focused on the operation of the industrial power plant at Mortágua. The work evaluated the solid biomass fuel used, the overall combustion performance, the influence of the primary air distribution on the grate and the time between grate vibration, and the identification of the flue gas lower limit temperature. The main results and key findings led to the conclusion that:

- The fuel is highly heterogeneous, with the physical and chemical properties at a wide range. The variations of the moisture and the ash content in the fuel highlight the influence of the time of year on the physical properties of the fuel. Thus, the plant operators should pay attention to this information to better control the power plant.
- Increasing the interval between the vibration cycles of the grate results in a significant reduction of CO emissions. However, increasing this period may lead to some agglomeration problems in the grate. The grate vibration promotes the mixing of the fuel particles, and it is also shown that in each vibration cycle, there is a drop in the concentration of oxygen in the flue gases.
- Concerning the primary air supply in the three different sections of the grate, the supply of a more significant amount of air in the first two sections decreases the CO emissions. In the last third of the grate, it is unnecessary to supply air because the fuel present in this location is almost completely burned out.
- The use of empirical correlations for a quick estimation of acid dew point of the flue gas through the heat transfer surface proved to be a reasonable method to improve the plant efficiency. The results revealed that a large amount of energy can be recovered within corrosion free limits, for instance, to preheat the primary air with benefits in the combustion process.
- Based on the previous findings, the installation of one waste heat recovery exchanger was assessed, and the results suggested to be an economically attractive solution.
- The results are very useful to understand the impact of different parameters in biomass combustion on the grate and the impact on gas emissions. The observations were meaningful for the development

of control strategies to increase the efficiency of the combustion process and reduce the pollutants emissions and develop a numerical model of the biomass combustion system.

Biomass Characterization

The experimental work included a systematic evaluation of the physicochemical and thermal properties of different solid biomass fuels, which typically used in biomass power plants. Their combustion behavior was analyzed at scales and conditions relevant to the operation in an industrial environment. The main conclusions can be summarized:

- For the eight solid biomass samples analyzed the VM, FC, and ash content is highly variable. Eucalyptus samples have the highest VM content along with the highest ash content and lowest FC content. Consequently, these samples are considered the most reactive. However, the bark part of the eucalyptus presents a high ash content which is disadvantageous in energy conversion processes.
- Based on the chemical composition, it is expected that the combustion of pine and olive, with a higher amount of sulfur, will result in higher emissions of SO_2, while acacia presents a significant amount of nitrogen, and NOx emissions are expected to be higher compared with other fuels.
- Thermal conductivity is strongly correlated with density. Moisture content also appears to be a parameter that influences the thermal properties. The ranges of the thermal conductivity, heat capacity, and thermal diffusivity are particularly wide, presenting values that can vary 2 times.
- Furthermore, the heat capacity and thermal diffusivity appear to be dependent on the solid biomass material in terms of chemical properties and structural arrangement of the fibers.
- Deposition and slagging indexes were computed through an estimative of the ash compounds based on an element-to-stoichiometric oxide conversion. The results show that all solid biomass fuels have a higher propensity for the appearance of ash deposition, being acacia the most notorious. However, slagging is not expected to be problematic because of their low content of silica.
- The evaluation of combustion performance at the particle scale, by TGA, presented that the conversion of all biomass fuels takes place over a wide range of temperatures, which can be divided into three different zones: drying, devolatilization, and char combustion.
- By increasing the heating rate, it was observed a systematic shift of the mass loss to higher temperatures. Consequently, the second stage was enhanced by this parameter, while the char combustion was not favored, as lower heating rates enable a near complete reaction.
- Regarding the differences between the combustion behavior of the different fuels, a higher mass was observed for the inner part of the fuels as well as a more effective conversion of the second stage

reaction. In its turn, the outer part of the eucalyptus presents a higher conversion of char, which may be associated with a higher lignin content of this fuel. Thus, differences in the chemical and physical composition as well as in the structures and their thermal stability, justify the differences between the TG and DTG curves.

- Based on the TGA data, a kinetic analysis was performed and relies on a two-step consecutive reaction model. The utilization of isoconversional methods proved to be ineffective in the determination of the kinetic parameters since the activation energy is not constant throughout the particle conversion. To overcome this limitation, the CR method was successfully applied to determine the kinetic parameters.
- The devolatilization conversion was best characterized by the reaction kinetics model, using a second-order model, and the char oxidation was successfully described by a diffusion controlled mechanism. The oxygen diffusion to the char affects the combustion process and should be considered the main mechanism of thermal conversion of biomass in the last stage.
- The kinetic parameters during biomass combustion are strongly dependent on the type of fuel, while the effect of the heating rate was less evident and not all fuels presented a consistent trend with the heating rate. According to the results, during the main conversion stage, devolatilization, the branch part of the fuels presented a lower activation energy value and eucalyptus is the most reactive fuel.
- The kinetic parameters were used to estimate the conversion of the different fuels, and the differences between the mathematical and experimental results were satisfactory from the perspective of engineering calculations. In particular, there were differences at the beginning of the conversion, mainly for trunk samples (ET, PT, and AT), and which may be attributed to the complexity of the hemicellulose and cellulose degradation at different temperatures in the second stage.
- For a scale relevant for industrial applications, a purpose built reactor was developed to study the combustion of large particles and determine the mass loss and gas compounds released during the devolatilization.
- Woodchips were assessed in terms of their dimension and bulk density. Being of irregular shape, the equivalent diameter of a spherical particle was determined for the most representative particle size range (8 to 16 mm), at 16.78 mm. In its turn, the bulk density ranges from 185 to 253 kg/m^3.
- Regarding the combustion behavior, the isothermal experiments showed that two distinct stages can be identified for the mass loss, each one with a linear trend. This pattern of the combustion behavior is significantly different from the TGA results and revealed that in the combustion of large particles have the presence of consecutive conversion stages cannot be clearly identified.

- The first stage, which includes drying and devolatilization, presented a dependency on the reactor temperature, while the last stage was not influenced by the temperature. This fact highlighted the influence of the diffusion mechanism, thereby combining the kinetic phenomenon and transport processes in the combustion of large biomass particles.
- The influence of fuel type in the combustion behavior was only detected at lower temperatures, while at higher temperatures the profiles are almost coincident. This fact shows that physical, thermal, and chemical properties are only relevant at lower reactor temperatures, while at higher temperatures the combustion behavior is only dependent on the reaction kinetics.
- Considering the previous findings, the gas compounds released during the combustion of eucalyptus presented a strong correlation to the reactor temperature, being CO_2 and CO always the main devolatilization products.
- Although the experiments were performed at a laboratory scale, it provided insight to understand the transport phenomena at the particle and particles level with different operating conditions and fuels. This was an important task that delivers meaningful and trustworthy data essential to develop a numerical model of biomass combustion systems.

Numerical Work

The numerical work consisted in the development of two different numerical models to thoroughly study the different interconnected phenomena of the biomass conversion in a grate-fired boiler. The most important conclusions can be summarized:

- The developed model using the XDEM tool, considering the setup designed for Macro TGA experiments, which included the physicochemical and thermal properties, and the kinetic parameters determined in the experimental work, provided similar results to the experiments carried out with eucalyptus samples at 800 °C. The model fitted well to the experiments, although in the second stage of the particles conversion, the char combustion, the kinetic model adopted in this work presents some difficulties in predicting the same mass loss behavior.
- Despite the small differences, the numerical model provided an overall view of the thermal conversion behavior of biomass particles in terms of temperature and mass variation. This was an interesting approach that allows to visualize the conversion of each particle and evaluate their thermodynamic state over time, and which demonstrated to be useful to perform coupled simulations with the CFD model of industrial boilers.

- Regarding the numerical model developed to study the biomass combustion in the grate-fired boiler from the Mortágua power plant, the strategy used proved to be effective and a valuable engineering tool to evaluate the design and nominal operating conditions of the present boiler.
- The results highlighted the importance of the contracting section in the middle of the furnace which lead to a concentration in the center zone of the furnace, where the velocity is higher. However, this configuration creates large temperature and velocity gradients in the flue gas flow entering the downstream convection section of the furnace. Furthermore, the CO released in the last sections of the grate does not react completely.
- The development of CFD simulations concerning different combustion regimes that can occur during the operation of the biomass power plant provided interesting results and allowed to define strategies to improve the performance of the boiler. From the different scenarios, it was possible to verify that if a large percentage of char combustion or the combustion of the bed, in general, is moved to the last sections of the grate, an increase in the temperature in the near wall of the boiler is observed and higher penetration of the secondary air nozzles is required. Furthermore, it was verified that the design of the boiler allowed to reduce the CO emissions considerably when the biomass conversion is continued to the first two sections of the grate.
- Therefore, the bed model apart from playing an important role in the freeboard modeling allowed to capture the dynamic behavior or modifications of the fuel bed conversion on the grate.
- In addition to the analysis of the different combustion scenarios at the grate, modifications of the primary and secondary air split ratio to 40/60 and 60/40, and the primary air temperature to 100 °C were evaluated. The CFD simulations showed that due to the supply of a higher secondary air flow rate, the flow dynamics change significantly, resulting in a higher penetration of the secondary air nozzles. This results in lower CO emissions, in particular when the primary and secondary air split ratio to 40/60 is used. This proves that penetration of the secondary air nozzles is a leading factor for higher oxidation of the combustion products.
- The effect of the primary air preheating was also visible mainly in the right wall where a region with a higher temperature and lower CO emissions was observed when compared with the baseline case. However, the higher temperatures in the furnace can cause negative effects such as the increase in thermal NOx formation and the risk of grate and wall damage. Therefore, the primary air temperature increase should be further analyzed in more detail before considering it as a retrofitting solution.

10.2 Suggestion of Future Work

Although the objectives of this work were accomplished, its development opened new opportunities of research that should be complement this thesis. The physical and chemical complexity and the comprehensive nature of biomass conversion in industrial boilers have opened new opportunities for continuing the research and improving the state-of-the-art on biomass combustion and its modeling. For future work, in the field of solid biomass combustion and its modeling, there are two particular issues that seem to be important and that can be explored.

The first one is related to the experimental work using large particles. The development of experiments using an inert atmosphere and an extension of the analysis to the other products of the biomass conversion, in particular, the characterization of the tar, are important aspects that can be further studied to complement this work and improve the particle conversion model. Additionally, the study of the reaction kinetic from oxidative and inert experiments along with the study of the CO and CO_2 mass fractions released during char oxidation are other important aspects that were considered essential to further improve the mathematical model for the particles conversion. The available models in the literature were determined for a certain feedstock, and the applicability to other kinds of biomass char or a different temperature range is limited, and, with this study, the limitations found in this work will be complemented.

Besides the experimental work, the second issue is related to the CFD simulation and the integration of the experimental data in the particle conversion model, the XDEM tool. The objective is to continue the development of the coupled CFD simulations with the XDEM model that were initialized during this work and obtain more details about the bed conversion on the grate and improve the gas-phase combustion inside the furnace.

BIBLIOGRAPHY

[1] European Commission, A Roadmap for Moving to a Competitive Low Carbon Economy in 2050, Brussels, 2011.

[2] U. Nations, Paris Agreement, (2015) 27. https://unfccc.int/sites/default/files/english_paris_agreement.pdf.

[3] European Comission, Stepping up Europe's 2030 climate ambition Investing in a climate-neutral future for the benefit of our people, Brussels, 2020.

[4] Bioenergy Europe, Bioenergy Landscape Statistical Report 2020, Brussels, 2020.

[5] Eurostat, Renewable energy statistics, (2022). https://ec.europa.eu/eurostat/statistics-explained/index.php?title=Renewable_energy_statistics (accessed February 7, 2022).

[6] R. Saidur, E.A. Abdelaziz, A. Demirbas, M.S. Hossain, S. Mekhilef, A review on biomass as a fuel for boilers, Renew. Sustain. Energy Rev. 15 (2011) 2262–2289. doi:10.1016/J.RSER.2011.02.015.

[7] M. Norton, A. Baldi, V. Buda, B. Carli, P. Cudlin, M.B. Jones, A. Korhola, R. Michalski, F. Novo, J. Oszlányi, F.D. Santos, B. Schink, J. Shepherd, L. Vet, L. Walloe, A. Wijkman, Serious mismatches continue between science and policy in forest bioenergy, GCB Bioenergy. 11 (2019) 1256–1263. doi:10.1111/gcbb.12643.

[8] F. Bilgili, E. Koçak, Ü. Bulut, S. Kuşkaya, Can biomass energy be an efficient policy tool for sustainable development?, Renew. Sustain. Energy Rev. 71 (2017) 830–845. doi:10.1016/j.rser.2016.12.109.

[9] A. Cowie, A. Cowie, M. Junginger, F. Ximenes, Response to Chatham House report "Woody Biomass for Power and Heat: Impacts on the Global Climate," (2017) 14.

[10] L. Gustavsson, S. Haus, C.A. Ortiz, R. Sathre, N. Le Truong, Climate effects of bioenergy from forest residues in comparison to fossil energy, Appl. Energy. 138 (2015) 36–50. doi:10.1016/j.apenergy.2014.10.013.

[11] A. Evans, V. Strezov, T.J. Evans, Sustainability considerations for electricity generation from biomass, Renew. Sustain. Energy Rev. 14 (2010) 1419–1427.

doi:10.1016/J.RSER.2010.01.010.

[12] M.A. Brown, A. Favero, V.M. Thomas, A. Banboukian, The economic and environmental performance of biomass as an “intermediate” resource for power production, Util. Policy. 58 (2019) 52–62. doi:10.1016/j.jup.2019.04.002.

[13] P. Carneiro, P. Ferreira, The economic, environmental and strategic value of biomass, Renew. Energy. 44 (2012) 17–22. doi:10.1016/J.RENENE.2011.12.020.

[14] G. Mao, N. Huang, L. Chen, H. Wang, Research on biomass energy and environment from the past to the future: A bibliometric analysis, Sci. Total Environ. 635 (2018) 1081–1090. doi:10.1016/j.scitotenv.2018.04.173.

[15] M. Banja, R. Sikkema, M. Jégard, V. Motola, J.-F. Dallemand, Biomass for energy in the EU – The support framework, Energy Policy. 131 (2019) 215–228. doi:10.1016/j.enpol.2019.04.038.

[16] IEA, Net Zero by 2050 - A Roadmap for the Global Energy Sector, 2021. https://iea.blob.core.windows.net/assets/deebef5d-0c34-4539-9d0c-10b13d840027/NetZeroby2050-ARoadmapfortheGlobalEnergySector_CORR.pdf.

[17] Deloitte, Towards an Integrated Energy System: Assessing Bioenergy’s Socio-Economic and Environmental Impact, 2022. https://bioenergyeurope.org/article/347-towards-an-integrated-energy-system-assessing-bioenergy-s-socio-economic-and-environmental-impact.html.

[18] D. da República, Decree-Law no. 64/2017, Diário da República n.º 113/2017, Série I de 2017-06-12, 2017.

[19] DGEG, Balanço Energético Nacional - 2020, 2020. https://www.dgeg.gov.pt/media/hmqkkm2m/dgeg-ben-2020.pdf.

[20] DGEG, Estatísticas rápidas - nº 206 - janeiro de 2022, 2022. https://www.dgeg.gov.pt/media/akjbntvo/dgeg-arr-2022-01_v2.pdf.

[21] ICNF, 6º Inventário Florestal Nacional - Áreas dos usos e das espécies florestais de Portugal Continental, 2015.

[22] H. Viana, W.B. Cohen, D. Lopes, J. Aranha, Assessment of forest biomass for use as energy. GIS-based analysis of geographical availability and locations of wood-fired power plants in Portugal, Appl. Energy. 87 (2010) 2551–2560. doi:10.1016/J.APENERGY.2010.02.007.

[23] Eurostat, Energy Statistics - Database Eurostat, (2021).

http://ec.europa.eu/eurostat/data/databse (accessed February 17, 2021).

[24] J. He, R. Zhu, B. Lin, Prospects, obstacles and solutions of biomass power industry in China, J. Clean. Prod. 237 (2019) 117783. doi:10.1016/J.JCLEPRO.2019.117783.

[25] IRENA, Renewable Energy Statistics 2021, 2022. https://www.irena.org/-/media/Files/IRENA/Agency/Publication/2021/Aug/IRENA_Renewable_Energy_Statistics_2021.pdf.

[26] Climate strategies & targets - European Commission, 2017. (n.d.). European Commission (accessed January 8, 2020).

[27] L. Gil, J. Bernardo, An approach to energy and climate issues aiming at carbon neutrality, Renew. Energy Focus. 33 (2020) 37–42. doi:10.1016/j.ref.2020.03.003.

[28] Portugal, Portuguese Government - Climate and Energy National Plan 2021 - 2030 (PNEC 2030), 2019.

[29] Portugal, Roadmap for Carbon Neutrality 2050 (RNC 2050), 2019.

[30] DGEG, Direcção Geral de Energia e Geologia. Renováveis - estatíticas rápidas nº 181, 2020.

[31] T. Nussbaumer, Combustion and Co-combustion of Biomass: Fundamentals, Technologies, and Primary Measures for Emission Reduction, Energy & Fuels. 17 (2003) 1510–1521. doi:10.1021/ef030031q.

[32] C. Yin, L.A. Rosendahl, Søren K., Grate-firing of biomass for heat and power production, Prog. Energy Combust. Sci. 34 (2008) 725–754. doi:10.1016/J.PECS.2008.05.002.

[33] European Commission, Directive 2009/28/EC, (2009) 47. https://eur-lex.europa.eu/legal-content/PT/TXT/PDF/?uri=CELEX:32009L0028&from=SK.

[34] K.M. Bryden, K.W. Ragland, Numerical Modeling of a Deep, Fixed Bed Combustor, Energy & Fuels. 10 (1996) 269–275. doi:10.1021/ef950193p.

[35] A. Demirbas, Potential applications of renewable energy sources, biomass combustion problems in boiler power systems and combustion related environmental issues, Prog. Energy Combust. Sci. 31 (2005) 171–192. doi:10.1016/j.pecs.2005.02.002.

[36] A.A. Bhuiyan, A.S. Blicblau, A.K.M.S. Islam, J. Naser, A review on thermo-chemical characteristics of coal/biomass co-firing in industrial furnace, J. Energy Inst. 91 (2018) 1–18. doi:10.1016/j.joei.2016.10.006.

[37] S. V. Vassilev, D. Baxter, L.K. Andersen, C.G. Vassileva, An overview of the chemical composition of biomass, Fuel. 89 (2010) 913–933. doi:10.1016/j.fuel.2009.10.022.

[38] P. McKendry, Energy production from biomass (part 2): conversion technologies, Bioresour. Technol. 83 (2002) 47–54. doi:10.1016/S0960-8524(01)00119-5.

[39] A. Demirbas, Combustion characteristics of different biomass fuels, Prog. Energy Combust. Sci. 30 (2004) 219–230. doi:10.1016/J.PECS.2003.10.004.

[40] G.V. Kuznetsov, S.S. Kropotova, A.G. Islamova, D.S. Romanov, Influence of forest fuel structure on thermophysical characteristics, Powder Technol. 366 (2020) 832–839. doi:10.1016/j.powtec.2020.03.031.

[41] I. Obernberger, F. Biedermann, T. Brunner, Biomass Energy Heat Provision in Modern Large-Scale Systems, in: Energy from Org. Mater., Springer New York, New York, NY, 2019: pp. 587–628. doi:10.1007/978-1-4939-7813-7_316.

[42] S. V. Vassilev, C.G. Vassileva, V.S. Vassilev, Advantages and disadvantages of composition and properties of biomass in comparison with coal: An overview, Fuel. 158 (2015) 330–350. doi:10.1016/J.FUEL.2015.05.050.

[43] B.. Jenkins, L.. Baxter, T.. Miles, T.. Miles, Combustion properties of biomass, Fuel Process. Technol. 54 (1998) 17–46. doi:10.1016/S0378-3820(97)00059-3.

[44] Z. Ilham, Biomass classification and characterization for conversion to biofuels, in: Value-Chain of Biofuels, Elsevier, 2022: pp. 69–87. doi:10.1016/B978-0-12-824388-6.00014-2.

[45] A. Demirbas, Biorefineries: Current activities and future developments, Energy Convers. Manag. 50 (2009) 2782–2801. doi:10.1016/j.enconman.2009.06.035.

[46] R. Mehrabian, A. Shiehnejadhesar, R. Scharler, I. Obernberger, Multi-physics modelling of packed bed biomass combustion, Fuel. 122 (2014) 164–178. doi:10.1016/j.fuel.2014.01.027.

[47] R. Mehrabian, S. Zahirovic, R. Scharler, I. Obernberger, S. Kleditzsch, S. Wirtz, V. Scherer, H. Lu, L.L. Baxter, A CFD model for thermal conversion of thermally thick biomass particles, Fuel Process. Technol. 95 (2012) 96–108. doi:10.1016/j.fuproc.2011.11.021.

[48] M. Hupa, O. Karlström, E. Vainio, Biomass combustion technology development – It is all about chemical details, Proc. Combust. Inst. 36 (2017) 113–134. doi:10.1016/J.PROCI.2016.06.152.

[49] H. Haykiri-Acma, S. Yaman, Effect of co-combustion on the burnout of lignite/biomass blends: A

Turkish case study, Waste Manag. 28 (2008) 2077–2084. doi:10.1016/j.wasman.2007.08.028.

[50] TNO, Database for the physico-chemical composition of biomass, (2022). https://phyllis.nl/ (accessed February 8, 2022).

[51] A. Williams, J.M. Jones, L. Ma, M. Pourkashanian, Pollutants from the combustion of solid biomass fuels, Prog. Energy Combust. Sci. 38 (2012) 113–137. doi:10.1016/J.PECS.2011.10.001.

[52] R. Saidur, E.A. Abdelaziz, A. Demirbas, M.S. Hossain, S. Mekhilef, A review on biomass as a fuel for boilers, Renew. Sustain. Energy Rev. 15 (2011) 2262–2289. doi:10.1016/j.rser.2011.02.015.

[53] I. Haberle, Ø. Skreiberg, J. Łazar, N.E.L. Haugen, Numerical models for thermochemical degradation of thermally thick woody biomass, and their application in domestic wood heating appliances and grate furnaces, Prog. Energy Combust. Sci. 63 (2017) 204–252. doi:10.1016/J.PECS.2017.07.004.

[54] M. Guerrero, M.P. Ruiz, M.U. Alzueta, R. Bilbao, A. Millera, Pyrolysis of eucalyptus at different heating rates: studies of char characterization and oxidative reactivity, J. Anal. Appl. Pyrolysis. 74 (2005) 307–314. doi:10.1016/j.jaap.2004.12.008.

[55] M.A. Gómez, J. Porteiro, D. Patiño, J.L. Míguez, Fast-solving thermally thick model of biomass particles embedded in a CFD code for the simulation of fixed-bed burners, Energy Convers. Manag. 105 (2015) 30–44. doi:10.1016/j.enconman.2015.07.059.

[56] H. Ström, H. Thunman, CFD simulations of biofuel bed conversion: A submodel for the drying and devolatilization of thermally thick wood particles, Combust. Flame. 160 (2013) 417–431. doi:10.1016/j.combustflame.2012.10.005.

[57] Y.A. Cengel, Heat transfer : a practical approach, Boston, USA, 1998.

[58] F. Incropera, D. DeWitt, Fundamentals of Heat and Mass Transfer, 3rd ed., New York : John Wiley, 1990.

[59] R. Mehrabian, R. Scharler, I. Obernberger, Effects of pyrolysis conditions on the heating rate in biomass particles and applicability of TGA kinetic parameters in particle thermal conversion modelling, Fuel. 93 (2012) 567–575. doi:10.1016/j.fuel.2011.09.054.

[60] Y. Yang, C. Ryu, A. Khor, N. Yates, V. Sharifi, J. Swithenbank, Effect of fuel properties on biomass

combustion. Part II. Modelling approach—identification of the controlling factors, Fuel. 84 (2005) 2116–2130. doi:10.1016/j.fuel.2005.04.023.

[61] K.M. Bryden, K.W. Ragland, C.J. Rutland, Modeling thermally thick pyrolysis of wood, Biomass and Bioenergy. 22 (2002) 41–53. doi:10.1016/S0961-9534(01)00060-5.

[62] R. Johansson, H. Thunman, B. Leckner, Influence of intraparticle gradients in modeling of fixed bed combustion, Combust. Flame. 149 (2007) 49–62. doi:10.1016/j.combustflame.2006.12.009.

[63] C. Yin, S. Li, Advancing grate-firing for greater environmental impacts and efficiency for decentralized biomass/wastes combustion, Energy Procedia. 120 (2017) 373–379. doi:10.1016/j.egypro.2017.07.220.

[64] U. Kleinhans, C. Wieland, F.J. Frandsen, H. Spliethoff, Ash formation and deposition in coal and biomass fired combustion systems: Progress and challenges in the field of ash particle sticking and rebound behavior, Prog. Energy Combust. Sci. 68 (2018) 65–168. doi:10.1016/J.PECS.2018.02.001.

[65] INEGI, Database of electric power plants based on renewable energy sources, (2017). http://e2p.inegi.up.pt/#Tec2 (accessed January 8, 2020).

[66] CINERGIA, Energy Sources - Renewable, (2019). https://www.cinergia.pt/pt/energia-pais/fontes-energia/ (accessed January 8, 2020).

[67] T.P. da Costa, P. Quinteiro, L.A. da C. Tarelho, L. Arroja, A.C. Dias, Environmental impacts of forest biomass-to-energy conversion technologies: Grate furnace vs. fluidised bed furnace, J. Clean. Prod. 171 (2018) 153–162. doi:10.1016/J.JCLEPRO.2017.09.287.

[68] I. Obernberger, F. Biedermann, T. Brunner, Biomass Energy Heat Provision in Modern Large-Scale Systems, in: Encycl. Sustain. Sci. Technol., Springer New York, New York, NY, 2017: pp. 1–43. doi:10.1007/978-1-4939-2493-6_316-3.

[69] B. Peters, Thermal Conversion of Solid Fuels, WIT Press, 2003.

[70] B. Peters, A. Džiugys, Comparison of the Heat-up of a Moving Bed on Forward and Backward Acting Grates, Numer. Heat Transf. Part A Appl. 62 (2012) 547–564. doi:10.1080/10407782.2012.703076.

[71] B. Peters, H. Raupenstrauch, Modeling Moving and Fixed Bed Combustion, Handb. Combust. 4

(2010). doi:10.1002/9783527628148.hoc061.

[72] S. Hermansson, H. Thunman, CFD modelling of bed shrinkage and channelling in fixed-bed combustion, Combust. Flame. 158 (2011) 988–999. doi:10.1016/j.combustflame.2011.01.022.

[73] B. Peters, Classification of combustion regimes in a packed bed of particles based on the relevant time and length scales, Combust. Flame. 116 (1999) 297–301. doi:10.1016/S0010-2180(98)00048-0.

[74] J. Blondeau, T. Museur, O. Demaude, P. Allard, F. Turoni, J. Mertens, Cost-effective flexibilisation of an 80 MW retrofitted biomass power plants: Improved combustion control dynamics using virtual air flow sensors, Case Stud. Therm. Eng. 21 (2020) 100680. doi:10.1016/j.csite.2020.100680.

[75] T. Nussbaumer, Combustion and Co-combustion of Biomass: Fundamentals, Technologies, and Primary Measures for Emission Reduction, Energy and Fuels. 17 (2003) 1510–1521. doi:10.1021/ef030031q.

[76] C. Yin, L.A. Rosendahl, S.K. Kær, Grate-firing of biomass for heat and power production, Prog. Energy Combust. Sci. 34 (2008) 725–754. doi:10.1016/j.pecs.2008.05.002.

[77] L. Rosendahl, Biomass combustion science, technology and engineering, Woodhead P, 2013.

[78] B.& Wilcox, Steam: its generation and use, 40th ed., Barberton, 1992.

[79] Y.B. Yang, C. Ryu, J. Goodfellow, V.N. Sharifi, J. Swithenbank, Modelling Waste Combustion in Grate Furnaces, Process Saf. Environ. Prot. 82 (2004) 208–222. doi:10.1205/095758204323065975.

[80] C. Yin, S. Li, Advancing grate-firing for greater environmental impacts and efficiency for decentralized biomass/wastes combustion, Energy Procedia. 120 (2017) 373–379. doi:10.1016/j.egypro.2017.07.220.

[81] A. Jančauskas, K. Buinevičius, Combination of Primary Measures on Flue Gas Emissions in Grate-Firing Biofuel Boiler, Energies. 14 (2021) 793. doi:10.3390/en14040793.

[82] E. Houshfar, T. Løvås, Ø. Skreiberg, Experimental Investigation on NOx Reduction by Primary Measures in Biomass Combustion: Straw, Peat, Sewage Sludge, Forest Residues and Wood Pellets, Energies. 5 (2012) 270–290. doi:10.3390/en5020270.

[83] E. Houshfar, R.A. Khalil, T. Løvås, Ø. Skreiberg, Enhanced NOx reduction by combined staged air and flue gas recirculation in biomass grate combustion, Energy and Fuels. 26 (2012) 9. doi:10.1021/ef300199g.

[84] J. Liu, X. Luo, S. Yao, Q. Li, W. Wang, Influence of flue gas recirculation on the performance of incinerator-waste heat boiler and NOx emission in a 500 t/d waste-to-energy plant, Waste Manag. 105 (2020) 450–456. doi:10.1016/j.wasman.2020.02.040.

[85] R. Pérez-Orozco, D. Patiño, J. Porteiro, A. Larrañaga, Flue Gas Recirculation during Biomass Combustion: Implications on PM Release, Energy & Fuels. 34 (2020) 11112–11122. doi:10.1021/acs.energyfuels.0c02086.

[86] H. Lamberg, O. Sippula, J. Tissari, J. Jokiniemi, Effects of Air Staging and Load on Fine-Particle and Gaseous Emissions from a Small-Scale Pellet Boiler, Energy & Fuels. 25 (2011) 4952–4960. doi:10.1021/ef2010578.

[87] H. Wiinika, R. Gebart, The influence of air distribution rate on particle emissions of fixed bed combustion of biomass, Combust. Sci. Technol. 177 (2005) 1747–1766. doi:10.1080/00102200590959468.

[88] B. Staiger, S. Unterberger, R. Berger, K.R.G. Hein, Development of an air staging technology to reduce NOx emissions in grate fired boilers, Energy. 30 (2005) 1429–1438. doi:10.1016/J.ENERGY.2004.02.013.

[89] M. Markovic, E.A. Bramer, G. Brem, Experimental investigation of wood combustion in a fixed bed with hot air, Waste Manag. 34 (2014) 49–62. doi:10.1016/J.WASMAN.2013.09.021.

[90] K.L. Jorgensen, R. Wessel, J. Strempek, Numerical Simulation of Combustion Air Systems for Large Industrial Boilers, in: ASME 2002 Int. Mech. Eng. Congr. Expo., New Orleans, Louisiana, USA, 2002: p. 8.

[91] H. Widell, Industrial-scale biomass combustion plants: engineering issues and operation, in: Biomass Combust. Sci. Technol. Eng., Elsevier, 2013: pp. 225–277. doi:10.1533/9780857097439.3.225.

[92] R. Saidur, J.U. Ahamed, H.H. Masjuki, Energy, exergy and economic analysis of industrial boilers, Energy Policy. 38 (2010) 2188–2197. doi:10.1016/J.ENPOL.2009.11.087.

[93] M.C. Barma, R. Saidur, S.M.A. Rahman, A. Allouhi, B.A. Akash, S.M. Sait, A review on boilers

energy use, energy savings, and emissions reductions, Renew. Sustain. Energy Rev. 79 (2017) 970–983. doi:10.1016/J.RSER.2017.05.187.

[94] M. Yan, X. Tian, Antoni, C. Yu, Z. Zhou, D. Hantoko, E. Kanchanatip, M.S. Khan, Influence of multi-temperature primary air on the characteristics of MSW combustion in a moving grate incinerator, J. Environ. Chem. Eng. 9 (2021) 106690. doi:10.1016/j.jece.2021.106690.

[95] L.B.. van Kessel, A.R.. Arendsen, P.D.. de Boer-Meulman, G. Brem, The effect of air preheating on the combustion of solid fuels on a grate, Fuel. 83 (2004) 1123–1131. doi:10.1016/j.fuel.2003.11.008.

[96] R.P. Van Der Lans, L.T. Pedersen, A. Jensen, P. Glarborg, K. Dam-Johansen, Modelling and experiments of straw combustion in a grate furnace, Biomass and Bioenergy. 19 (2000) 199–208. doi:10.1016/S0961-9534(00)00033-7.

[97] M. Hupa, O. Karlström, E. Vainio, Biomass combustion technology development – It is all about chemical details, Proc. Combust. Inst. 36 (2017) 113–134. doi:10.1016/J.PROCI.2016.06.152.

[98] B. Brandelet, C. Pascual, M. Debal, Y. Rogaume, A cleaner biomass energy production by optimization of the operational range of a fabric filter, J. Clean. Prod. 253 (2020) 119906. doi:10.1016/j.jclepro.2019.119906.

[99] F. Frandsen, J. Hansen, P.A. Jensen, K. Dam-Johansen, M. Montgomery, L.D. Fenger, J.N. Jensen, A. Karlsson, N. Henriksen, J.P. Jensen, Deposit Formation And Corrosion In The Air Pre-Heater Of A Straw-Fired Combined Heat And Power Production Boiler, IFRF Combust. J. (2002) 23.

[100] Y. Zhang, X. Du, M. Yue, M. Yan, Y. Shi, Heat transfer and ash deposition performance of heat exchange surface in waste incineration flue gas, Int. J. Heat Mass Transf. 155 (2020) 119691. doi:10.1016/j.ijheatmasstransfer.2020.119691.

[101] X. Meng, W. Zhou, E. Rokni, G. Chen, R. Sun, Y.A. Levendis, Release of Alkalis and Chlorine from Combustion of Waste Pinewood in a Fixed Bed, Energy & Fuels. 33 (2019) 1256–1266. doi:10.1021/acs.energyfuels.8b03970.

[102] G. Caposciutti, M. Antonelli, Experimental investigation on air displacement and air excess effect on CO, CO2 and NOx emissions of a small size fixed bed biomass boiler, Renew. Energy. 116 (2018) 795–804. doi:10.1016/J.RENENE.2017.10.001.

[103] H. Khodaei, F. Guzzomi, D. Patiño, B. Rashidian, G.H. Yeoh, Air staging strategies in biomass combustion-gaseous and particulate emission reduction potentials, Fuel Process. Technol. 157 (2017) 29–41. doi:10.1016/j.fuproc.2016.11.007.

[104] H. Khodaei, F. Guzzomi, G.H. Yeoh, A. Regueiro, D. Patiño, An experimental study into the effect of air staging distribution and position on emissions in a laboratory scale biomass combustor, Energy. 118 (2017) 1243–1255. doi:10.1016/j.energy.2016.11.008.

[105] E. Houshfar, Ø. Skreiberg, D. Todorović, A. Skreiberg, T. Løvås, A. Jovović, L. Sørum, NO x emission reduction by staged combustion in grate combustion of biomass fuels and fuel mixtures, Fuel. 98 (2012) 29–40. doi:10.1016/j.fuel.2012.03.044.

[106] E. Houshfar, Ø. Skreiberg, T. Løvås, D. Todorović, L. Sørum, Effect of excess air ratio and temperature on NOx emission from grate combustion of biomass in the staged air combustion scenario, Energy and Fuels. 25 (2011) 4643–4654. doi:10.1021/ef200714d.

[107] W. Zhao, Z. Li, G. Zhao, F. Zhang, Q. Zhu, Effect of air preheating and fuel moisture on combustion characteristics of corn straw in a fixed bed, Energy Convers. Manag. 49 (2008) 3560–3565. doi:10.1016/J.ENCONMAN.2008.07.006.

[108] J.R. Strempek, K.L. Jorgensen, Use of Numerical Modeling to Compare Overfire Air Systems on Stoker-Fired Furnaces, (2008) 9. doi:10.1115/IMECE2008-68348.

[109] Y.. Yang, V.. Sharifi, J. Swithenbank, Effect of air flow rate and fuel moisture on the burning behaviours of biomass and simulated municipal solid wastes in packed beds, Fuel. 83 (2004) 1553–1562. doi:10.1016/J.FUEL.2004.01.016.

[110] H. Thunman, Ignition and propagation of a reaction front in cross-current bed combustion of wet biofuels, Fuel. 80 (2001) 473–481. doi:10.1016/S0016-2361(00)00127-7.

[111] J.J. Saastammoinen, M. Horttanainen, P. Sarkomaa, Ignition Wave Propagation and Release of Volatiles in Beds of Wood Particles, Combust. Sci. Technol. 165 (2001) 41–60. doi:10.1080/00102200108935825.

[112] J.J. Saastamoinen, R. Taipale, M. Horttanainen, P. Sarkomaa, Propagation of the ignition front in beds of wood particles, Combust. Flame. 123 (2000) 214–226. doi:10.1016/S0010-2180(00)00144-9.

[113] W. Wei, F. Sun, Y. Shi, L. Ma, Theoretical prediction of acid dew point and safe operating

temperature of heat exchangers for coal-fired power plants, Appl. Therm. Eng. 123 (2017) 782–790. doi:10.1016/J.APPLTHERMALENG.2017.05.051.

[114] H. Chen, P. Pan, J. Jiao, Y. Wang, Q. Zhao, Low-temperature ash deposition and dewpoint corrosion of a coal-fired travelling grate boiler, Appl. Therm. Eng. 117 (2017) 752–761. doi:10.1016/J.APPLTHERMALENG.2017.02.052.

[115] B. Xiang, M. Zhang, H. Yang, J. Lu, Prediction of Acid Dew Point in Flue Gas of Boilers Burning Fossil Fuels, Energy & Fuels. 30 (2016) 3365–3373. doi:10.1021/acs.energyfuels.6b00491.

[116] B. Xiang, B. Tang, Y. Wu, H. Yang, M. Zhang, J. Lu, Predicting acid dew point with a semi-empirical model, Appl. Therm. Eng. 106 (2016) 992–1001. doi:10.1016/J.APPLTHERMALENG.2016.06.040.

[117] E. Vainio, H. Kinnunen, T. Laurén, A. Brink, P. Yrjas, N. DeMartini, M. Hupa, Low-temperature corrosion in co-combustion of biomass and solid recovered fuels, Fuel. 184 (2016) 957–965. doi:10.1016/J.FUEL.2016.03.096.

[118] Y. Wang, H. Ma, Z. Liang, H. Chen, Q. Zhao, X. Jin, Experimental study on dew point corrosion characteristics of the heating surface in a 65 t/h biomass-fired circulating fluidized bed boiler, Appl. Therm. Eng. 96 (2016) 76–82. doi:10.1016/J.APPLTHERMALENG.2015.10.151.

[119] S. Retschitzegger, T. Brunner, I. Obernberger, Low-Temperature Corrosion in Biomass Boilers Fired with Chemically Untreated Wood Chips and Bark, Energy & Fuels. 29 (2015) 3913–3921. doi:10.1021/acs.energyfuels.5b00365.

[120] M.J. Richardson, Thermal Analysis, in: Compr. Polym. Sci. Suppl., Elsevier, 1989: pp. 867–901. doi:10.1016/B978-0-08-096701-1.00036-7.

[121] S. Vyazovkin, K. Chrissafis, M.L. Di Lorenzo, N. Koga, M. Pijolat, B. Roduit, N. Sbirrazzuoli, J.J. Suñol, ICTAC Kinetics Committee recommendations for collecting experimental thermal analysis data for kinetic computations, Thermochim. Acta. 590 (2014) 1–23. doi:10.1016/j.tca.2014.05.036.

[122] J.E. White, W.J. Catallo, B.L. Legendre, Biomass pyrolysis kinetics: A comparative critical review with relevant agricultural residue case studies, J. Anal. Appl. Pyrolysis. 91 (2011) 1–33. doi:10.1016/J.JAAP.2011.01.004.

[123] A. Fernandez, J. Soria, R. Rodriguez, J. Baeyens, G. Mazza, Macro-TGA steam-assisted gasification

of lignocellulosic wastes, J. Environ. Manage. 233 (2019) 626–635. doi:10.1016/j.jenvman.2018.12.087.

[124] A. Williams, J.M. Jones, L. Ma, M. Pourkashanian, Pollutants from the combustion of solid biomass fuels, Prog. Energy Combust. Sci. 38 (2012) 113–137. doi:10.1016/j.pecs.2011.10.001.

[125] J. Silva, J. Teixeira, S. Teixeira, S. Preziati, J. Cassiano, CFD Modeling of Combustion in Biomass Furnace, in: Energy Procedia, Elsevier B.V., 2017: pp. 665–672. doi:10.1016/j.egypro.2017.07.179.

[126] J. Silva, L. Fraga, M.E. Ferreira, S. Chapela, J. Porteiro, S.F.C.F. Teixeira, J. Teixeira, Combustion Modelling of a 20 kW Pellet Boiler, in: Vol. 6B Energy, ASME, 2018: p. V06BT08A036. doi:10.1115/IMECE2018-88063.

[127] E. Biagini, L. Guerrini, C. Nicolella, Development of a variable activation energy model for biomass devolatilization, Energy and Fuels. 23 (2009) 3300–3306. doi:10.1021/ef9001499.

[128] L. Fraga, J. Silva, D.F. Soares, M. Ferreira, S.F. Teixeira, J.C. Teixeira, Study of Devolatilization Rates of Pine Wood and Mass Loss of Wood Pellets, in: ASME 2017 Int. Mech. Eng. Congr. Expo. Vol. 6 Energy, ASME, Tampa, Florida, USA, n.d.: p. 9. doi:10.1115/IMECE2017-71939.

[129] M.V. Gil, D. Casal, C. Pevida, J.J. Pis, F. Rubiera, Thermal behaviour and kinetics of coal/biomass blends during co-combustion, Bioresour. Technol. 101 (2010) 5601–5608. doi:10.1016/J.BIORTECH.2010.02.008.

[130] N.S. Yuzbasi, N. Selçuk, Air and oxy-fuel combustion characteristics of biomass/lignite blends in TGA-FTIR, Fuel Process. Technol. 92 (2011) 1101–1108. doi:10.1016/j.fuproc.2011.01.005.

[131] L.G. Fraga, J. Silva, J.C.F. Teixeira, M.E.C. Ferreira, D.F. Soares, S.F. Teixeira, The effect of the heating and air flow rate on the mass loss of pine wood particles, in: ECOS 2018 - Proc. 31st Int. Conf. Effic. Cost, Optim. Simul. Environ. Impact Energy Syst., Universidade do Minho. Departamento de Engenharia Mecânica, Guimarães, Portugal, 2018.

[132] C. Di Blasi, C. Branca, A. Santoro, E. Gonzalez Hernandez, Pyrolytic behavior and products of some wood varieties, Combust. Flame. 124 (2001) 165–177. doi:10.1016/S0010-2180(00)00191-7.

[133] D. Magalhães, F. Kazanç, J. Riaza, S. Erensoy, Ö. Kabaklı, H. Chalmers, Combustion of Turkish

lignites and olive residue: Experiments and kinetic modelling, Fuel. 203 (2017) 868–876. doi:10.1016/j.fuel.2017.05.050.

[134] Y. Su, Y. Luo, W. Wu, Y. Zhang, S. Zhao, Characteristics of pine wood oxidative pyrolysis: Degradation behavior, carbon oxide production and heat properties, J. Anal. Appl. Pyrolysis. 98 (2012) 137–143. doi:10.1016/J.JAAP.2012.07.005.

[135] M.A. Saeed, G.E. Andrews, H.N. Phylaktou, B.M. Gibbs, Global kinetics of the rate of volatile release from biomasses in comparison to coal, Fuel. 181 (2016) 347–357. doi:10.1016/J.FUEL.2016.04.123.

[136] R.K. Mishra, K. Mohanty, Pyrolysis kinetics and thermal behavior of waste sawdust biomass using thermogravimetric analysis, Bioresour. Technol. 251 (2018) 63–74. doi:10.1016/j.biortech.2017.12.029.

[137] A. Skreiberg, Ø. Skreiberg, J. Sandquist, L. Sørum, TGA and macro-TGA characterisation of biomass fuels and fuel mixtures, Fuel. 90 (2011) 2182–2197. doi:10.1016/j.fuel.2011.02.012.

[138] A. Magdziarz, M. Wilk, Thermogravimetric study of biomass, sewage sludge and coal combustion, Energy Convers. Manag. 75 (2013) 425–430. doi:10.1016/j.enconman.2013.06.016.

[139] P. Grammelis, P. Basinas, A. Malliopoulou, G. Sakellaropoulos, Pyrolysis kinetics and combustion characteristics of waste recovered fuels, Fuel. 88 (2009) 195–205. doi:10.1016/j.fuel.2008.02.002.

[140] S. Biswas, N. Choudhury, P. Sarkar, A. Mukherjee, S.G. Sahu, P. Boral, A. Choudhury, Studies on the combustion behaviour of blends of Indian coals by TGA and Drop Tube Furnace, Fuel Process. Technol. 87 (2006) 191–199. doi:10.1016/j.fuproc.2005.05.002.

[141] S. Vyazovkin, C.A. Wight, Isothermal and non-isothermal kinetics of thermally stimulated reactions of solids, Int. Rev. Phys. Chem. 17 (1998) 407–433. doi:10.1080/014423598230108.

[142] A. Garcia-Maraver, J.A. Perez-Jimenez, F. Serrano-Bernardo, M. Zamorano, Determination and comparison of combustion kinetics parameters of agricultural biomass from olive trees, Renew. Energy. 83 (2015) 897–904. doi:10.1016/j.renene.2015.05.049.

[143] S. Vyazovkin, A.K. Burnham, J.M. Criado, L.A. Pérez-Maqueda, C. Popescu, N. Sbirrazzuoli, ICTAC Kinetics Committee recommendations for performing kinetic computations on thermal analysis data, Thermochim. Acta. 520 (2011) 1–19. doi:10.1016/J.TCA.2011.03.034.

[144] A. Anca-Couce, C. Tsekos, S. Retschitzegger, F. Zimbardi, A. Funke, S. Banks, T. Kraia, P. Marques, R. Scharler, W. de Jong, N. Kienzl, Biomass pyrolysis TGA assessment with an international round robin, Fuel. 276 (2020) 118002. doi:10.1016/j.fuel.2020.118002.

[145] P.T. Williams, S. Besler, The influence of temperature and heating rate on the slow pyrolysis of biomass, Renew. Energy. 7 (1996) 233–250. doi:10.1016/0960-1481(96)00006-7.

[146] D. Vamvuka, S. Sfakiotakis, Combustion behaviour of biomass fuels and their blends with lignite, Thermochim. Acta. 526 (2011) 192–199. doi:10.1016/j.tca.2011.09.021.

[147] T. Mani, P. Murugan, J. Abedi, N. Mahinpey, Pyrolysis of wheat straw in a thermogravimetric analyzer: Effect of particle size and heating rate on devolatilization and estimation of global kinetics, Chem. Eng. Res. Des. 88 (2010) 952–958. doi:10.1016/J.CHERD.2010.02.008.

[148] A. Boriouchkine, V. Sharifi, J. Swithenbank, S.L. Jämsä-Jounela, A study on the dynamic combustion behavior of a biomass fuel bed, Fuel. 135 (2014) 468–481. doi:10.1016/j.fuel.2014.07.015.

[149] S.Y. Yorulmaz, A.T. Atimtay, Investigation of combustion kinetics of treated and untreated waste wood samples with thermogravimetric analysis, Fuel Process. Technol. 90 (2009) 939–946. doi:10.1016/j.fuproc.2009.02.010.

[150] D.K. Shen, S. Gu, K.H. Luo, A.V. Bridgwater, M.X. Fang, Kinetic study on thermal decomposition of woods in oxidative environment, Fuel. 88 (2009) 1024–1030. doi:10.1016/J.FUEL.2008.10.034.

[151] S.-S. Kim, J. Kim, Y.-H. Park, Y.-K. Park, Pyrolysis kinetics and decomposition characteristics of pine trees, Bioresour. Technol. 101 (2010) 9797–9802. doi:10.1016/J.BIORTECH.2010.07.094.

[152] D.K. Seo, S.S. Park, J. Hwang, T.U. Yu, Study of the pyrolysis of biomass using thermo-gravimetric analysis (TGA) and concentration measurements of the evolved species, J. Anal. Appl. Pyrolysis. 89 (2010) 66–73. doi:10.1016/j.jaap.2010.05.008.

[153] K. Slopiecka, P. Bartocci, F. Fantozzi, Thermogravimetric analysis and kinetic study of poplar wood pyrolysis, Appl. Energy. 97 (2012) 491–497. doi:10.1016/J.APENERGY.2011.12.056.

[154] D. Chen, Y. Zheng, X. Zhu, In-depth investigation on the pyrolysis kinetics of raw biomass. Part I: Kinetic analysis for the drying and devolatilization stages, Bioresour. Technol. 131 (2013) 40–46.

doi:10.1016/J.BIORTECH.2012.12.136.

[155] G. Mishra, J. Kumar, T. Bhaskar, Kinetic studies on the pyrolysis of pinewood, Bioresour. Technol. 182 (2015) 282–288. doi:10.1016/J.BIORTECH.2015.01.087.

[156] X. Wang, M. Hu, W. Hu, Z. Chen, S. Liu, Z. Hu, B. Xiao, Thermogravimetric kinetic study of agricultural residue biomass pyrolysis based on combined kinetics, Bioresour. Technol. 219 (2016) 510–520. doi:10.1016/J.BIORTECH.2016.07.136.

[157] D.K. Shen, S. Gu, B. Jin, M.X. Fang, Thermal degradation mechanisms of wood under inert and oxidative environments using DAEM methods, Bioresour. Technol. 102 (2011) 2047–2052. doi:10.1016/J.BIORTECH.2010.09.081.

[158] A. Anca-Couce, N. Zobel, A. Berger, F. Behrendt, Smouldering of pine wood: Kinetics and reaction heats, Combust. Flame. 159 (2012) 1708–1719. doi:10.1016/J.COMBUSTFLAME.2011.11.015.

[159] M.V. Kok, E. Özgür, Thermal analysis and kinetics of biomass samples, Fuel Process. Technol. 106 (2013) 739–743. doi:10.1016/j.fuproc.2012.10.010.

[160] A. Álvarez, C. Pizarro, R. García, J.L. Bueno, A.G. Lavín, Determination of kinetic parameters for biomass combustion, Bioresour. Technol. 216 (2016) 36–43. doi:10.1016/J.BIORTECH.2016.05.039.

[161] M.X. Fang, D.K. Shen, Y.X. Li, C.J. Yu, Z.Y. Luo, K.F. Cen, Kinetic study on pyrolysis and combustion of wood under different oxygen concentrations by using TG-FTIR analysis, J. Anal. Appl. Pyrolysis. 77 (2006) 22–27. doi:10.1016/J.JAAP.2005.12.010.

[162] M.G. Grønli, G. Várhegyi, C. Di Blasi, Thermogravimetric Analysis and Devolatilization Kinetics of Wood, Ind. Eng. Chem. Res. 41 (2002) 4201–4208. doi:10.1021/ie0201157.

[163] A. Saddawi, J.M. Jones, A. Williams, M.A. Wójtowicz, Kinetics of the Thermal Decomposition of Biomass, Energy & Fuels. 24 (2010) 1274–1282. doi:10.1021/ef900933k.

[164] L.I. Darvell, J.M. Jones, B. Gudka, X.C. Baxter, A. Saddawi, A. Williams, A. Malmgren, Combustion properties of some power station biomass fuels, Fuel. 89 (2010) 2881–2890. doi:10.1016/J.FUEL.2010.03.003.

[165] D.K. Seo, S.S. Park, J. Hwang, T.-U. Yu, Study of the pyrolysis of biomass using thermo-gravimetric analysis (TGA) and concentration measurements of the evolved species, J. Anal. Appl. Pyrolysis.

89 (2010) 66–73. doi:10.1016/J.JAAP.2010.05.008.

[166] P. Parthasarathy, K.S. Narayanan, L. Arockiam, Study on kinetic parameters of different biomass samples using thermo-gravimetric analysis, Biomass and Bioenergy. 58 (2013) 58–66. doi:10.1016/J.BIOMBIOE.2013.08.004.

[167] J.F. Saldarriaga, R. Aguado, A. Pablos, M. Amutio, M. Olazar, J. Bilbao, Fast characterization of biomass fuels by thermogravimetric analysis (TGA), Fuel. 140 (2015) 744–751. doi:10.1016/j.fuel.2014.10.024.

[168] R. Wadhwani, D. Sutherland, K.A.M. Moinuddin, P. Joseph, Kinetics of pyrolysis of litter materials from pine and eucalyptus forests, J. Therm. Anal. Calorim. 130 (2017) 2035–2046. doi:10.1007/s10973-017-6512-0.

[169] R. Xiao, W. Yang, X. Cong, K. Dong, J. Xu, D. Wang, X. Yang, Thermogravimetric analysis and reaction kinetics of lignocellulosic biomass pyrolysis, Energy. 201 (2020) 117537. doi:10.1016/j.energy.2020.117537.

[170] J.J. Alvarado Flores, J.G. Rutiaga Quiñones, M.L. Ávalos Rodríguez, J.V. Alcaraz Vera, J. Espino Valencia, S.J. Guevara Martínez, F. Márquez Montesino, A. Alfaro Rosas, Thermal Degradation Kinetics and FT-IR Analysis on the Pyrolysis of Pinus pseudostrobus, Pinus leiophylla and Pinus montezumae as Forest Waste in Western Mexico, Energies. 13 (2020) 969. doi:10.3390/en13040969.

[171] C. Di Blasi, Modeling chemical and physical processes of wood and biomass pyrolysis, Prog. Energy Combust. Sci. 34 (2008) 47–90. doi:10.1016/J.PECS.2006.12.001.

[172] R. Bilbao, J.F. Mastral, M.E. Aldea, J. Ceamanos, Kinetic study for the thermal decomposition of cellulose and pine sawdust in an air atmosphere, J. Anal. Appl. Pyrolysis. 39 (1997) 53–64. doi:10.1016/S0165-2370(96)00957-6.

[173] A. Garcia-Maraver, J.A. Perez-Jimenez, F. Serrano-Bernardo, M. Zamorano, Determination and comparison of combustion kinetics parameters of agricultural biomass from olive trees, Renew. Energy. 83 (2015) 897–904. doi:10.1016/J.RENENE.2015.05.049.

[174] X. Ren, J. Chen, G. Li, Y. Wang, X. Lang, S. Fan, Thermal oxidative degradation kinetics of agricultural residues using distributed activation energy model and global kinetic model, Bioresour. Technol. 261 (2018) 403–411. doi:10.1016/J.BIORTECH.2018.04.047.

[175] A. Dhahak, R. Bounaceur, C. Le Dreff-Lorimier, G. Schmidt, G. Trouve, F. Battin-Leclerc, Development of a detailed kinetic model for the combustion of biomass, Fuel. 242 (2019) 756–774. doi:10.1016/J.FUEL.2019.01.093.

[176] L.G. Fraga, J. Silva, S. Teixeira, D. Soares, M. Ferreira, J. Teixeira, Influence of Operating Conditions on the Thermal Behavior and Kinetics of Pine Wood Particles using Thermogravimetric Analysis, Energies. 13 (2020) 2756. doi:10.3390/en13112756.

[177] S. Munir, S.S. Daood, W. Nimmo, A.M. Cunliffe, B.M. Gibbs, Thermal analysis and devolatilization kinetics of cotton stalk, sugar cane bagasse and shea meal under nitrogen and air atmospheres, Bioresour. Technol. 100 (2009) 1413–1418. doi:10.1016/J.BIORTECH.2008.07.065.

[178] N.S. Yuzbasi, N. Selçuk, Air and oxy-fuel combustion characteristics of biomass/lignite blends in TGA-FTIR, Fuel Process. Technol. 92 (2011) 1101–1108. doi:10.1016/J.FUPROC.2011.01.005.

[179] F. Sher, S.Z. Iqbal, H. Liu, M. Imran, C.E. Snape, Thermal and kinetic analysis of diverse biomass fuels under different reaction environment: A way forward to renewable energy sources, Energy Convers. Manag. 203 (2020) 112266. doi:10.1016/j.enconman.2019.112266.

[180] A. Chouchene, M. Jeguirim, B. Khiari, F. Zagrouba, G. Trouvé, Thermal degradation of olive solid waste: Influence of particle size and oxygen concentration, Resour. Conserv. Recycl. 54 (2010) 271–277. doi:10.1016/j.resconrec.2009.04.010.

[181] M. Amutio, G. Lopez, R. Aguado, M. Artetxe, J. Bilbao, M. Olazar, Kinetic study of lignocellulosic biomass oxidative pyrolysis, Fuel. 95 (2012) 305–311. doi:10.1016/J.FUEL.2011.10.008.

[182] A.I. Moreno, R. Font, J.A. Conesa, Combustion of furniture wood waste and solid wood: Kinetic study and evolution of pollutants, Fuel. 192 (2017) 169–177. doi:10.1016/J.FUEL.2016.12.022.

[183] A. Álvarez, C. Pizarro, R. García, J.L. Bueno, A.G. Lavín, Determination of kinetic parameters for biomass combustion, Bioresour. Technol. 216 (2016) 36–43. doi:10.1016/j.biortech.2016.05.039.

[184] D. Yu, M. Chen, Y. Wei, S. Niu, F. Xue, An assessment on co-combustion characteristics of Chinese lignite and eucalyptus bark with TG–MS technique, Powder Technol. 294 (2016) 463–471. doi:10.1016/J.POWTEC.2016.03.016.

[185] A. Soria-Verdugo, E. Goos, N. García-Hernando, Effect of the number of TGA curves employed on the biomass pyrolysis kinetics results obtained using the Distributed Activation Energy Model, Fuel

Process. Technol. 134 (2015) 360–371. doi:10.1016/J.FUPROC.2015.02.018.

[186] Z. Chen, Q. Zhu, X. Wang, B. Xiao, S. Liu, Pyrolysis behaviors and kinetic studies on Eucalyptus residues using thermogravimetric analysis, Energy Convers. Manag. 105 (2015) 251–259. doi:10.1016/J.ENCONMAN.2015.07.077.

[187] A. Soria-Verdugo, L.M. Garcia-Gutierrez, L. Blanco-Cano, N. Garcia-Hernando, U. Ruiz-Rivas, Evaluating the accuracy of the Distributed Activation Energy Model for biomass devolatilization curves obtained at high heating rates, Energy Convers. Manag. 86 (2014) 1045–1049. doi:10.1016/J.ENCONMAN.2014.06.074.

[188] E. Granada, P. Eguía, J.A. Comesaña, D. Patiño, J. Porteiro, J.L. Miguez, Devolatilization behaviour and pyrolysis kinetic modelling of Spanish biomass fuels, J. Therm. Anal. Calorim. 113 (2013) 569–578. doi:10.1007/s10973-012-2747-y.

[189] P. Ghodke, R.N. Mandapati, Investigation of particle level kinetic modeling for babul wood pyrolysis, Fuel. 236 (2019) 1008–1017. doi:10.1016/J.FUEL.2018.09.084.

[190] H. Siddiqi, M. Bal, U. Kumari, B.C. Meikap, In-depth physiochemical characterization and detailed thermo-kinetic study of biomass wastes to analyze its energy potential, Renew. Energy. (2019). doi:10.1016/J.RENENE.2019.10.162.

[191] J. Chen, Y. Wang, X. Lang, X. Ren, S. Fan, Evaluation of agricultural residues pyrolysis under non-isothermal conditions: Thermal behaviors, kinetics, and thermodynamics, Bioresour. Technol. 241 (2017) 340–348. doi:10.1016/J.BIORTECH.2017.05.036.

[192] F.S. Akinrinola, L.I. Darvell, J.M. Jones, A. Williams, J.A. Fuwape, Characterization of Selected Nigerian Biomass for Combustion and Pyrolysis Applications, Energy & Fuels. 28 (2014) 3821–3832. doi:10.1021/ef500278e.

[193] M.V. Kok, E. Özgür, Thermal analysis and kinetics of biomass samples, Fuel Process. Technol. 106 (2013) 739–743. doi:10.1016/j.fuproc.2012.10.010.

[194] M. Amutio, G. Lopez, J. Alvarez, R. Moreira, G. Duarte, J. Nunes, M. Olazar, J. Bilbao, Pyrolysis kinetics of forestry residues from the Portuguese Central Inland Region, Chem. Eng. Res. Des. 91 (2013) 2682–2690. doi:10.1016/J.CHERD.2013.05.031.

[195] E. Biagini, A. Fantei, L. Tognotti, Effect of the heating rate on the devolatilization of biomass residues, Thermochim. Acta. 472 (2008) 55–63. doi:10.1016/J.TCA.2008.03.015.

[196] A.A.D. Maia, L.C. de Morais, Kinetic parameters of red pepper waste as biomass to solid biofuel, Bioresour. Technol. 204 (2016) 157–163. doi:10.1016/J.BIORTECH.2015.12.055.

[197] N. Aghamohammadi, N.M. Nik Sulaiman, M.K. Aroua, Combustion characteristics of biomass in SouthEast Asia, Biomass and Bioenergy. 35 (2011) 3884–3890. doi:10.1016/J.BIOMBIOE.2011.06.022.

[198] M.E. Sanchez, M. Otero, X. Gómez, A. Morán, Thermogravimetric kinetic analysis of the combustion of biowastes, Renew. Energy. 34 (2009) 1622–1627. doi:10.1016/J.RENENE.2008.11.011.

[199] S.Y. Yorulmaz, A.T. Atimtay, Investigation of combustion kinetics of treated and untreated waste wood samples with thermogravimetric analysis, Fuel Process. Technol. 90 (2009) 939–946. doi:10.1016/J.FUPROC.2009.02.010.

[200] X. Xu, R. Pan, R. Chen, Combustion Characteristics, Kinetics, and Thermodynamics of Pine Wood Through Thermogravimetric Analysis, Appl. Biochem. Biotechnol. 193 (2021) 1427–1446. doi:10.1007/s12010-020-03480-x.

[201] R. Chen, Q. Li, X. Xu, D. Zhang, R. Hao, Combustion characteristics, kinetics and thermodynamics of Pinus Sylvestris pine needle via non-isothermal thermogravimetry coupled with model-free and model-fitting methods, Case Stud. Therm. Eng. 22 (2020) 100756. doi:10.1016/j.csite.2020.100756.

[202] D. Cancellieri, V. Leroy-Cancellieri, X. Silvani, F. Morandini, New experimental diagnostics in combustion of forest fuels: microscale appreciation for a macroscale approach, Nat. Hazards Earth Syst. Sci. 18 (2018) 1957–1968. doi:10.5194/nhess-18-1957-2018.

[203] X. Fang, L. Jia, L. Yin, A weighted average global process model based on two–stage kinetic scheme for biomass combustion, Biomass and Bioenergy. 48 (2013) 43–50. doi:10.1016/J.BIOMBIOE.2012.11.011.

[204] X. Xu, R. Pan, R. Chen, Combustion Characteristics, Kinetics, and Thermodynamics of Pine Wood Through Thermogravimetric Analysis, Appl. Biochem. Biotechnol. 193 (2021) 1427–1446. doi:10.1007/s12010-020-03480-x.

[205] S. Fu, H. Chen, J. Yang, Z. Yang, Kinetics of thermal pyrolysis of Eucalyptus bark by using thermogravimetric-Fourier transform infrared spectrometry technique, J. Therm. Anal. Calorim. (2019). doi:10.1007/s10973-019-08763-y.

[206] L.Y. Vega, L. López, C.F. Valdés, F. Chejne, Assessment of energy potential of wood industry wastes through thermochemical conversions, Waste Manag. 87 (2019) 108–118. doi:10.1016/J.WASMAN.2019.01.048.

[207] Z. Cai, X. Ma, S. Fang, Z. Yu, Y. Lin, Thermogravimetric analysis of the co-combustion of eucalyptus residues and paper mill sludge, Appl. Therm. Eng. 106 (2016) 938–943. doi:10.1016/J.APPLTHERMALENG.2016.06.088.

[208] M. Lapuerta, J.J. Hernández, J. Rodríguez, Comparison between the kinetics of devolatilisation of forestry and agricultural wastes from the middle-south regions of Spain, Biomass and Bioenergy. 31 (2007) 13–19. doi:10.1016/J.BIOMBIOE.2006.05.003.

[209] M. Lapuerta, J.J. Hernández, J. Rodríguez, Kinetics of devolatilisation of forestry wastes from thermogravimetric analysis, Biomass and Bioenergy. 27 (2004) 385–391. doi:10.1016/j.biombioe.2003.11.010.

[210] M.G. Grønli, G. Várhegyi, C. Di Blasi, Thermogravimetric Analysis and Devolatilization Kinetics of Wood, Ind. Eng. Chem. Res. 41 (2002) 4201–4208. doi:10.1021/ie0201157.

[211] C. Di Blasi, Modeling and simulation of combustion processes of charring and non-charring solid fuels, Prog. Energy Combust. Sci. 19 (1993) 71–104. doi:10.1016/0360-1285(93)90022-7.

[212] T. Gu, C. Yin, W. Ma, G. Chen, Municipal solid waste incineration in a packed bed: A comprehensive modeling study with experimental validation, Appl. Energy. 247 (2019) 127–139. doi:10.1016/j.apenergy.2019.04.014.

[213] F. Shafizadeh, P.P.S. Chin, Thermal Deterioration of Wood, in: 1977: pp. 57–81. doi:10.1021/bk-1977-0043.ch005.

[214] A. Dernbecher, A. Dieguez-Alonso, A. Ortwein, F. Tabet, Review on modelling approaches based on computational fluid dynamics for biomass combustion systems, Biomass Convers. Biorefinery. 9 (2019) 129–182. doi:10.1007/s13399-019-00370-z.

[215] E. Ranzi, A. Cuoci, T. Faravelli, A. Frassoldati, G. Migliavacca, S. Pierucci, S. Sommariva, Chemical Kinetics of Biomass Pyrolysis, Energy & Fuels. 22 (2008) 4292–4300. doi:10.1021/ef800551t.

[216] A.G.W. Bradbury, Y. Sakai, F. Shafizadeh, A kinetic model for pyrolysis of cellulose, J. Appl. Polym. Sci. 23 (1979) 3271–3280. doi:10.1002/app.1979.070231112.

[217] S. Hameed, A. Sharma, V. Pareek, H. Wu, Y. Yu, A review on biomass pyrolysis models: Kinetic,

network and mechanistic models, Biomass and Bioenergy. 123 (2019) 104–122. doi:10.1016/J.BIOMBIOE.2019.02.008.

[218] C. Branca, A. Albano, C. Di Blasi, Critical evaluation of global mechanisms of wood devolatilization, Thermochim. Acta. 429 (2005) 133–141. doi:10.1016/J.TCA.2005.02.030.

[219] G. Várhegyi, Aims and methods in non-isothermal reaction kinetics, J. Anal. Appl. Pyrolysis. 79 (2007) 278–288. doi:10.1016/J.JAAP.2007.01.007.

[220] D.M. Grant, R.J. Pugmire, T.H. Fletcher, A.R. Kerstein, Chemical model of coal devolatilization using percolation lattice statistics, Energy & Fuels. 3 (1989) 175–186. doi:10.1021/ef00014a011.

[221] S. Niksa, Rapid coal devolatilization as an equilibrium flash distillation, AIChE J. 34 (1988) 790–802. doi:10.1002/aic.690340509.

[222] P.R. Solomon, D.G. Hamblen, R.M. Carangelo, M.A. Serio, G. V. Deshpande, General model of coal devolatilization, Energy & Fuels. 2 (1988) 405–422. doi:10.1021/ef00010a006.

[223] H. Kobayashi, J.B. Howard, A.F. Sarofim, Coal devolatilization at high temperatures, Symp. Combust. 16 (1977) 411–425. doi:10.1016/S0082-0784(77)80341-X.

[224] S. Niksa, Predicting the rapid devolatilization of diverse forms of biomass with bio-flashchain, Proc. Combust. Inst. 28 (2000) 2727–2733. doi:10.1016/S0082-0784(00)80693-1.

[225] M.A. Serio, A comprehensive model of biomass pyrolysis, 1997.

[226] C. Sheng, J.L.T. Azevedo, Modeling biomass devolatilization using the chemical percolation devolatilization model for the main components, Proc. Combust. Inst. 29 (2002) 407–414. doi:10.1016/S1540-7489(02)80054-2.

[227] M.-K. Bahng, C. Mukarakate, D.J. Robichaud, M.R. Nimlos, Current technologies for analysis of biomass thermochemical processing: A review, Anal. Chim. Acta. 651 (2009) 117–138. doi:10.1016/j.aca.2009.08.016.

[228] H.L. Friedman, Kinetics of thermal degradation of char-forming plastics from thermogravimetry. Application to a phenolic plastic, J. Polym. Sci. Part C Polym. Symp. 6 (1964) 183–195. doi:10.1002/polc.5070060121.

[229] T. Ozawa, A New Method of Analyzing Thermogravimetric Data, Bull. Chem. Soc. Jpn. 38 (1965) 1881–1886. doi:10.1246/bcsj.38.1881.

[230] J.H. Flynn, L.A. Wall, General treatment of the thermogravimetry of polymers, J. Res. Natl. Bur. Stand. Sect. A Phys. Chem. 70A (1966) 487. doi:10.6028/jres.070A.043.

[231] H. Kissinger, Variation of peak temperature with heating rate in differential thermal analysis, J. Res. Natl. Bur. Stand. (1934). 57 (1956) 217–221.

[232] H.E. Kissinger, Reaction Kinetics in Differential Thermal Analysis, Anal. Chem. 29 (1957) 1702–1706. doi:10.1021/ac60131a045.

[233] T. Akahira, T. Sunose, Method of determining activation deterioration constant of electrical insulating materials, Res Rep. Chiba Inst. Technol. (Sci. Technol.). 16 (1971) 22–31.

[234] M.. Starink, The determination of activation energy from linear heating rate experiments: a comparison of the accuracy of isoconversion methods, Thermochim. Acta. 404 (2003) 163–176. doi:10.1016/S0040-6031(03)00144-8.

[235] S. Vyazovkin, D. Dollimore, Linear and Nonlinear Procedures in Isoconversional Computations of the Activation Energy of Nonisothermal Reactions in Solids, J. Chem. Inf. Comput. Sci. 36 (1996) 42–45. doi:10.1021/ci950062m.

[236] S. Vyazovkin, Modification of the integral isoconversional method to account for variation in the activation energy, J. Comput. Chem. 22 (2001) 178–183. doi:10.1002/1096-987X(20010130)22:23.0.CO;2-#.

[237] A.W. Coats, J.P. Redfern, Kinetic Parameters from Thermogravimetric Data, Nature. 201 (1964) 68–69. doi:10.1038/201068a0.

[238] E.S. Freeman, B. Carroll, The Application of Thermoanalytical Techniques to Reaction Kinetics: The Thermogravimetric Evaluation of the Kinetics of the Decomposition of Calcium Oxalate Monohydrate, J. Phys. Chem. 62 (1958) 394–397. doi:10.1021/j150562a003.

[239] M.S. Duvvuri, S.P. Muhlenkamp, K.Z.W.J. Iqbal, Pyrolysis of natural fuels, J Fire Flammabl. (1975) 468–477.

[240] S. Vyazovkin, N. Sbirrazzuoli, Isoconversional Kinetic Analysis of Thermally Stimulated Processes in Polymers, Macromol. Rapid Commun. 27 (2006) 1515–1532. doi:10.1002/marc.200600404.

[241] V. Dhyani, T. Bhaskar, Kinetic Analysis of Biomass Pyrolysis, in: Waste Biorefinery, Elsevier, 2018: pp. 39–83. doi:10.1016/B978-0-444-63992-9.00002-1.

[242] J. Cai, D. Xu, Z. Dong, X. Yu, Y. Yang, S.W. Banks, A. V. Bridgwater, Processing thermogravimetric analysis data for isoconversional kinetic analysis of lignocellulosic biomass pyrolysis: Case study of corn stalk, Renew. Sustain. Energy Rev. 82 (2018) 2705–2715. doi:10.1016/J.RSER.2017.09.113.

[243] A. Khawam, D.R. Flanagan, Basics and Applications of Solid-State Kinetics: A Pharmaceutical Perspective, J. Pharm. Sci. 95 (2006) 472–498. doi:10.1002/jps.20559.

[244] L.G. Fraga, J. Silva, S. Teixeira, D. Soares, M. Ferreira, J. Teixeira, Thermal Conversion of Pine Wood and Kinetic Analysis under Oxidative and Non-Oxidative Environments at Low Heating Rate, Proceedings. 58 (2020) 23. doi:10.3390/WEF-06921.

[245] M.J. Starink, A new method for the derivation of activation energies from experiments performed at constant heating rate, Thermochim. Acta. 288 (1996) 97–104. doi:10.1016/S0040-6031(96)03053-5.

[246] H. Thunman, F. Niklasson, F. Johnsson, B. Leckner, Composition of volatile gases and thermochemical properties of wood for modeling of fixed or fluidized beds, Energy and Fuels. 15 (2001) 1488–1497. doi:10.1021/ef010097q.

[247] D. Neves, H. Thunman, A. Matos, L. Tarelho, A. Gómez-Barea, Characterization and prediction of biomass pyrolysis products, Prog. Energy Combust. Sci. 37 (2011) 611–630. doi:10.1016/j.pecs.2011.01.001.

[248] M. Hosseini Rahdar, F. Nasiri, B. Lee, A Review of Numerical Modeling and Experimental Analysis of Combustion in Moving Grate Biomass Combustors, Energy & Fuels. 33 (2019) 9367–9402. doi:10.1021/acs.energyfuels.9b02073.

[249] J. Silva, J. Teixeira, S. Teixeira, S. Preziati, J. Cassiano, CFD Modeling of Combustion in Biomass Furnace, in: Energy Procedia, 2017. doi:10.1016/j.egypro.2017.07.179.

[250] J. Silva, J. Teixeira, S. Teixeira, S. Chapela, J. Porteiro, Application of a biomass combustion model to an industrial boiler, in: ECOS 2018 - Proc. 31st Int. Conf. Effic. Cost, Optim. Simul. Environ. Impact Energy Syst., 2018. http://www.scopus.com/inward/record.url?eid=2-s2.0-85064182527&partnerID=MN8TOARS.

[251] J. Silva, J. Teixeira, S. Teixeira, S. Preziati, Analysis and Modeling of Combustion in Biomass Furnace, in: XXI Natl. Congr. Mech. Eng. Elche, Spain, 2016: p. 7.

[252] Y. Bin Yang, C. Ryu, A. Khor, V.N. Sharifi, J. Swithenbank, Fuel size effect on pinewood combustion in a packed bed, Fuel. 84 (2005) 2026–2038. doi:10.1016/j.fuel.2005.04.022.

[253] C. Ryu, Y. Bin Yang, A. Khor, N.E. Yates, V.N. Sharifi, J. Swithenbank, Effect of fuel properties on biomass combustion: Part I. Experiments - Fuel type, equivalence ratio and particle size, Fuel. 85 (2006) 1039–1046. doi:10.1016/j.fuel.2005.09.019.

[254] A.H. Mahmoudi, M. Markovic, B. Peters, G. Brem, An experimental and numerical study of wood combustion in a fixed bed using Euler-Lagrange approach (XDEM), Fuel. 150 (2015) 573–582. doi:10.1016/j.fuel.2015.02.008.

[255] J.C. Wurzenberger, S. Wallner, H. Raupenstrauch, J.G. Khinast, Thermal conversion of biomass: Comprehensive reactor and particle modeling, AIChE J. 48 (2002) 2398–2411. doi:10.1002/aic.690481029.

[256] A. Erić, S. Nemoda, M. Komatina, D. Dakić, B. Repić, Experimental investigation on the kinetics of biomass combustion in vertical tube reactor, J. Energy Inst. 92 (2019) 1077–1090. doi:10.1016/j.joei.2018.06.009.

[257] H.C. Ong, W.-H. Chen, Y. Singh, Y.Y. Gan, C.-Y. Chen, P.L. Show, A state-of-the-art review on thermochemical conversion of biomass for biofuel production: A TG-FTIR approach, Energy Convers. Manag. 209 (2020) 112634. doi:10.1016/j.enconman.2020.112634.

[258] C. Li, Z. Long, X. Jiang, P. Wu, X. Hou, Atomic spectrometric detectors for gas chromatography, TrAC Trends Anal. Chem. 77 (2016) 139–155. doi:10.1016/j.trac.2015.11.012.

[259] B.P. Regmi, M. Agah, Micro Gas Chromatography: An Overview of Critical Components and Their Integration, Anal. Chem. 90 (2018) 13133–13150. doi:10.1021/acs.analchem.8b01461.

[260] S. Wang, G. Dai, H. Yang, Z. Luo, Lignocellulosic biomass pyrolysis mechanism: A state-of-the-art review, Prog. Energy Combust. Sci. 62 (2017) 33–86. doi:10.1016/j.pecs.2017.05.004.

[261] M. Zaharescu, O.C. Mocioiu, Infrared Spectroscopy, in: Chem. Solut. Depos. Funct. Oxide Thin Film., Springer Vienna, Vienna, 2013: pp. 213–230. doi:10.1007/978-3-211-99311-8_9.

[262] Y.F. Huang, W.H. Kuan, P.T. Chiueh, S.L. Lo, Pyrolysis of biomass by thermal analysis–mass spectrometry (TA–MS), Bioresour. Technol. 102 (2011) 3527–3534. doi:10.1016/j.biortech.2010.11.049.

[263] M. Radojević, B. Janković, D. Stojiljković, V. Jovanović, I. Čeković, N. Manić, Improved TGA-MS

measurements for evolved gas analysis (EGA) during pyrolysis process of various biomass feedstocks. Syngas energy balance determination, Thermochim. Acta. 699 (2021) 178912. doi:10.1016/j.tca.2021.178912.

[264] M. Becidan, Ø. Skreiberg, J.E. Hustad, Products distribution and gas release in pyrolysis of thermally thick biomass residues samples, J. Anal. Appl. Pyrolysis. 78 (2007) 207–213. doi:10.1016/j.jaap.2006.07.002.

[265] T. Brunner, F. Biedermann, W. Kanzian, N. Evic, I. Obernberger, Advanced Biomass Fuel Characterization Based on Tests with a Specially Designed Lab-Scale Reactor, Energy & Fuels. 27 (2013) 5691–5698. doi:10.1021/ef400559j.

[266] G. Gauthier, T. Melkior, M. Grateau, S. Thiery, S. Salvador, Pyrolysis of centimetre-scale wood particles: New experimental developments and results, J. Anal. Appl. Pyrolysis. 104 (2013) 521–530. doi:10.1016/j.jaap.2013.05.017.

[267] A. Weissinger, In situ FT-IR spectroscopic investigations of species from biomass fuels in a laboratory-scale combustor: the release of nitrogenous species, Combust. Flame. 137 (2004) 403–417. doi:10.1016/j.combustflame.2004.02.010.

[268] H. Bennadji, K. Smith, S. Shabangu, E.M. Fisher, Low-Temperature Pyrolysis of Woody Biomass in the Thermally Thick Regime, Energy & Fuels. 27 (2013) 1453–1459. doi:10.1021/ef400079a.

[269] M. Nikku, A. Deb, E. Sermyagina, L. Puro, Reactivity characterization of municipal solid waste and biomass, Fuel. 254 (2019) 115690. doi:10.1016/j.fuel.2019.115690.

[270] Q. Hu, X. He, Z. Yao, Y. Dai, C.-H. Wang, Gaseous production kinetics and solid structure analysis during isothermal conversion of biomass pellet under different atmospheres, J. Energy Inst. 98 (2021) 53–62. doi:10.1016/j.joei.2021.06.009.

[271] B. Baumgarten, J. Reinhardt, C. Lepski, B. Risio, H. Thorwarth, Kinetics of Wood Devolatilization during Start-up, Energy & Fuels. 33 (2019) 11285–11291. doi:10.1021/acs.energyfuels.9b03030.

[272] L.N. Samuelsson, K. Umeki, M.U. Babler, Mass loss rates for wood chips at isothermal pyrolysis conditions: A comparison with low heating rate powder data, Fuel Process. Technol. 158 (2017) 26–34. doi:10.1016/j.fuproc.2016.12.003.

[273] N. Orang, H. Tran, Effect of feedstock moisture content on biomass boiler operation, TAPPI J. 14

(2015) 629–637. doi:10.32964/TJ14.10.629.

[274] M. Becidan, Ø. Skreiberg, J.E. Hustad, Experimental study on pyrolysis of thermally thick biomass residues samples: Intra-sample temperature distribution and effect of sample weight ("scaling effect"), Fuel. 86 (2007) 2754–2760. doi:10.1016/j.fuel.2007.03.007.

[275] C. Bruch, Modelling wood combustion under fixed bed conditions, Fuel. 82 (2003) 729–738. doi:10.1016/S0016-2361(02)00296-X.

[276] H.K. Versteeg, W. Malalasekera, An introduction to computational fluid dynamics: the finite volume method, Harlow, 1995.

[277] J. Chaney, H. Liu, J. Li, An overview of CFD modelling of small-scale fixed-bed biomass pellet boilers with preliminary results from a simplified approach, Energy Convers. Manag. 63 (2012) 149–156. doi:10.1016/j.enconman.2012.01.036.

[278] H. Khodaei, Y.M. Al-Abdeli, F. Guzzomi, G.H. Yeoh, An overview of processes and considerations in the modelling of fixed-bed biomass combustion, Energy. 88 (2015) 946–972. doi:10.1016/j.energy.2015.05.099.

[279] F.U. Rückert, D. Lehser-Pfeffermann, D. Theis, J.P. Kim, A. Schargen, I. Zorbach, J. Sohnemann, A new Simulation Model for Grate Firing Systems in OpenFOAM, Energy. 216 (2021) 119226. doi:10.1016/j.energy.2020.119226.

[280] W.P.Jones, R.P.Lindstedt, Global reaction schemes for hydrocarbon combustion, Combust. Flame. 73 (1988) 233–249.

[281] M. Yan, Antoni, J. Wang, D. Hantoko, E. Kanchanatip, Numerical investigation of MSW combustion influenced by air preheating in a full-scale moving grate incinerator, Fuel. 285 (2021) 119193. doi:10.1016/j.fuel.2020.119193.

[282] S.M. Mousavi, H. Fatehi, X.-S. Bai, Numerical study of the combustion and application of SNCR for NO reduction in a lab-scale biomass boiler, Fuel. 293 (2021) 120154. doi:10.1016/j.fuel.2021.120154.

[283] E. Ranzi, P.E.A. Debiagi, A. Frassoldati, Mathematical Modeling of Fast Biomass Pyrolysis and Bio-Oil Formation. Note I: Kinetic Mechanism of Biomass Pyrolysis, ACS Sustain. Chem. Eng. 5 (2017) 2867–2881. doi:10.1021/acssuschemeng.6b03096.

[284] Z. Xia, J. Long, S. Yan, L. Bai, H. Du, C. Chen, Two-fluid simulation of moving grate waste

incinerator: Comparison of 2D and 3D bed models, Energy. 216 (2021) 119257. doi:10.1016/j.energy.2020.119257.

[285] Z. Xia, P. Shan, C. Chen, H. Du, J. Huang, L. Bai, A two-fluid model simulation of an industrial moving grate waste incinerator, Waste Manag. 104 (2020) 183–191. doi:10.1016/j.wasman.2020.01.016.

[286] A. Zhou, H. Xu, X. Meng, W. Yang, R. Sun, Development of a numerical model for co-combustion of the blended solid waste fuel in the grate boiler, Chem. Eng. J. 405 (2021) 126604. doi:10.1016/j.cej.2020.126604.

[287] A. Zhou, H. Xu, M. Xu, W. Yu, Z. Li, W. Yang, Numerical investigation of biomass co-combustion with methane for NOx reduction, Energy. 194 (2020) 116868. doi:10.1016/j.energy.2019.116868.

[288] M.R. Karim, A.A. Bhuiyan, A.A.R. Sarhan, J. Naser, CFD simulation of biomass thermal conversion under air/oxy-fuel conditions in a reciprocating grate boiler, Renew. Energy. 146 (2020) 1416–1428. doi:10.1016/j.renene.2019.07.068.

[289] C. Netzer, T. Li, L. Seidel, F. Mauß, T. Løvås, Stochastic Reactor-Based Fuel Bed Model for Grate Furnaces, Energy & Fuels. 34 (2020) 16599–16612. doi:10.1021/acs.energyfuels.0c02868.

[290] T. Zadravec, C. Yin, F. Kokalj, N. Samec, B. Rajh, The impacts of different profiles of the grate inlet conditions on freeboard CFD in a waste wood-fired grate boiler, Appl. Energy. 268 (2020) 115055. doi:10.1016/j.apenergy.2020.115055.

[291] C.A. Bermúdez, J. Porteiro, L.G. Varela, S. Chapela, D. Patiño, Three-dimensional CFD simulation of a large-scale grate-fired biomass furnace, Fuel Process. Technol. 198 (2020) 106219. doi:10.1016/J.FUPROC.2019.106219.

[292] S. Chapela, J. Porteiro, M. Costa, Effect of the Turbulence–Chemistry Interaction in Packed-Bed Biomass Combustion, Energy & Fuels. 31 (2017) 9967–9982. doi:10.1021/acs.energyfuels.7b00516.

[293] M. Jiang, A.C.H. Lai, A.W.-K. Law, Solid Waste Incineration Modelling for Advanced Moving Grate Incinerators, Sustainability. 12 (2020) 8007. doi:10.3390/su12198007.

[294] S. Somwangthanaroj, S. Fukuda, CFD modeling of biomass grate combustion using a steady-state discrete particle model (DPM) approach, Renew. Energy. (2019).

doi:10.1016/J.RENENE.2019.10.042.

[295] A. Zhou, H. Xu, Y. Tu, F. Zhao, Z. Zheng, W. Yang, Numerical investigation of the effect of air supply and oxygen enrichment on the biomass combustion in the grate boiler, Appl. Therm. Eng. 156 (2019) 550–561. doi:10.1016/J.APPLTHERMALENG.2019.04.053.

[296] A. Zhou, Y. Tu, H. Xu, Y. Wenming, F. Zhao, S. Keng Boon, P. Subbaiah, Numerical investigation the effect of air supply on the biomass combustion in the grate boiler, Energy Procedia. 158 (2019) 272–277. doi:10.1016/J.EGYPRO.2019.01.088.

[297] A. Zhou, H. Xu, W. Yang, Y. Tu, M. Xu, W. Yu, S.K. Boon, P. Subbaiah, Numerical Study of Biomass Grate Boiler with Coupled Time-Dependent Fuel Bed Model and Computational Fluid Dynamics Based Freeboard Model, Energy & Fuels. 32 (2018) 9493–9505. doi:10.1021/acs.energyfuels.8b01823.

[298] C. Yin, L. Rosendahl, S. Kaer, H. Sorensen, Modeling and Experiments of Biomass Combustion in a Large-scale Grate Boiler, (n.d.).

[299] M. Syamlal, W. Rogers, T.J. O`Brien, MFIX documentation theory guide, Oak Ridge, TN, 1993. doi:10.2172/10145548.

[300] A. Rezeau, L.I. Díez, J. Royo, M. Díaz-Ramírez, Efficient diagnosis of grate-fired biomass boilers by a simplified CFD-based approach, Fuel Process. Technol. 171 (2018) 318–329. doi:10.1016/J.FUPROC.2017.11.024.

[301] Y. Tu, A. Zhou, M. Xu, W. Yang, K.B. Siah, P. Subbaiah, NOX reduction in a 40 t/h biomass fired grate boiler using internal flue gas recirculation technology, Appl. Energy. 220 (2018) 962–973. doi:10.1016/j.apenergy.2017.12.018.

[302] Y. Tu, A. Zhou, M. Xu, W. Yang, K.B. Siah, S. Prabakaran, Experimental and numerical study on the combustion of a 32 MW wood-chip grate boiler with internal flue gas recirculation technology, Energy Procedia. 143 (2017) 591–598. doi:10.1016/J.EGYPRO.2017.12.732.

[303] S. Patronelli, M. Antonelli, L. Tognotti, C. Galletti, Combustion of wood-chips in a small-scale fixed-bed boiler: Validation of the numerical model through in-flame measurements, Fuel. 221 (2018) 128–137. doi:10.1016/J.FUEL.2018.02.083.

[304] G. Caposciutti, F. Barontini, M. Antonelli, C. Galletti, L. Tognotti, U. Desideri, Biomass early stage combustion in a small size boiler: experimental and numerical analysis, Energy Procedia. 148

(2018) 1159–1166. doi:10.1016/j.egypro.2018.08.026.

[305] H. Mätzing, H.-J. Gehrmann, H. Seifert, D. Stapf, Modelling grate combustion of biomass and low rank fuels with CFD application, Waste Manag. 78 (2018) 686–697. doi:10.1016/J.WASMAN.2018.05.008.

[306] B. Rajh, C. Yin, N. Samec, M. Hriberšek, F. Kokalj, M. Zadravec, Advanced CFD modelling of air and recycled flue gas staging in a waste wood-fired grate boiler for higher combustion efficiency and greater environmental benefits, J. Environ. Manage. 218 (2018) 200–208. doi:10.1016/J.JENVMAN.2018.04.030.

[307] B. Rajh, C. Yin, N. Samec, M. Hriberšek, M. Zadravec, Advanced modelling and testing of a 13 MWth waste wood-fired grate boiler with recycled flue gas, Energy Convers. Manag. 125 (2016) 230–241. doi:10.1016/J.ENCONMAN.2016.02.036.

[308] M. Costa, N. Massarotti, V. Indrizzi, B. Rajh, C. Yin, N. Samec, Engineering bed models for solid fuel conversion process in grate-fired boilers, Energy. 77 (2014) 244–253. doi:10.1016/j.energy.2014.07.067.

[309] J. Ahn, J.H. Jang, Combustion characteristics of a 16 step grate-firing wood pellet boiler, Renew. Energy. 129 (2018) 678–685. doi:10.1016/J.RENENE.2017.06.015.

[310] J. Ahn, J.H. Jang, Combustion and heat transfer characteristics in a combustion chamber of a 13-step grate wood pellet firing boiler, J. Mech. Sci. Technol. 32 (2018) 1033–1040. doi:10.1007/s12206-018-0204-y.

[311] M.R. Karim, J. Naser, CFD modelling of combustion and associated emission of wet woody biomass in a 4 MW moving grate boiler, Fuel. 222 (2018) 656–674. doi:10.1016/J.FUEL.2018.02.195.

[312] M. Costa, C. Curcio, D. Piazzullo, V. Rocco, R. Tuccillo, RDF incineration modelling trough thermo-chemical conversion and gaseous combustion coupling, Energy. 161 (2018) 974–987. doi:10.1016/J.ENERGY.2018.07.142.

[313] M. Costa, N. Massarotti, A. Mauro, F. Arpino, V. Rocco, CFD modelling of a RDF incineration plant, Appl. Therm. Eng. 101 (2016) 710–719. doi:10.1016/J.APPLTHERMALENG.2016.01.073.

[314] M. Costa, V. Indrizzi, N. Massarotti, A. Mauro, Modeling and optimization of an incinerator plant for the reduction of the environmental impact, Int. J. Numer. Methods Heat Fluid Flow. 25 (2015)

1463–1487. doi:10.1108/HFF-10-2014-0300.

[315] M. Costa, M. Dell'Isola, N. Massarotti, Temperature and residence time of the combustion products in a waste-to-energy plant, Fuel. 102 (2012) 92–105. doi:10.1016/J.FUEL.2012.06.043.

[316] M. Costa, M. Dell'Isola, N. Massarotti, Numerical analysis of the thermo-fluid-dynamic field in the combustion chamber of an incinerator plant, Energy. 34 (2009) 2075–2086. doi:10.1016/J.ENERGY.2008.08.024.

[317] Y.B. Yang, Y.R. Goh, R. Zakaria, V. Nasserzadeh, J. Swithenbank, Mathematical modelling of MSW incineration on a travelling bed, Waste Manag. 22 (2002) 369–380. doi:10.1016/S0956-053X(02)00019-3.

[318] F. Wissing, S. Wirtz, V. Scherer, Simulating municipal solid waste incineration with a DEM/CFD method – Influences of waste properties, grate and furnace design, Fuel. 206 (2017) 638–656. doi:10.1016/J.FUEL.2017.06.037.

[319] E. Simsek, S. Wirtz, V. Scherer, H. Kruggel-Emden, R. Grochowski, P. Walzel, An Experimental and Numerical Study of Transversal Dispersion of Granular Material on a Vibrating Conveyor, Part. Sci. Technol. 26 (2008) 177–196. doi:10.1080/02726350801903772.

[320] H. Kruggel-Emden, E. Simsek, S. Wirtz, V. Scherer, A Comparative Numerical Study of Particle Mixing on Different Grate Designs Through the Discrete Element Method, J. Press. Vessel Technol. 129 (2007) 593–600. doi:10.1115/1.2767338.

[321] N.T.M. Duffy, J.A. Eaton, Investigation of 3D flow and heat transfer in solid-fuel grate combustion: Measures to reduce high-temperature degradation, Combust. Flame. 167 (2016) 422–443. doi:10.1016/J.COMBUSTFLAME.2015.12.032.

[322] N.T.M. Duffy, J.A. Eaton, Investigation of factors affecting channelling in fixed-bed solid fuel combustion using CFD, Combust. Flame. 160 (2013) 2204–2220. doi:10.1016/J.COMBUSTFLAME.2013.04.015.

[323] C.K. Westbrook, F.L. Dryer, Chemical kinetic modeling of hydrocarbon combustion, Prog. Energy Combust. Sci. 10 (1984) 1–57. doi:10.1016/0360-1285(84)90118-7.

[324] A.H. Mahmoudi, X. Besseron, F. Hoffmann, M. Markovic, B. Peters, Modeling of the biomass combustion on a forward acting grate using XDEM, Chem. Eng. Sci. 142 (2016) 32–41.

doi:10.1016/j.ces.2015.11.015.

[325] C. Galletti, V. Giomo, S. Giorgetti, P. Leoni, L. Tognotti, Biomass furnace for externally fired gas turbine: Development and validation of the numerical model, Appl. Therm. Eng. 96 (2016) 372–384. doi:10.1016/J.APPLTHERMALENG.2015.11.085.

[326] Q. Chen, X. Zhang, J. Zhou, V.N. Sharifi, J. Swithenbank, Effects of Flue Gas Recirculation on Emissions from a Small Scale Wood Chip Fired Boiler, Energy Procedia. 66 (2015) 65–68. doi:10.1016/J.EGYPRO.2015.02.034.

[327] S. Cordiner, A. Manni, V. Mulone, V. Rocco, A Detailed Study of a Multi-MW Biomass Combustor by Numerical Analysis: Evaluation of Fuel Characteristics Impact, Energy Procedia. 61 (2014) 751–755. doi:10.1016/J.EGYPRO.2014.11.958.

[328] A. Shiehnejadhesar, K. Schulze, R. Scharler, I. Obernberger, A new innovative CFD-based optimisation method for biomass combustion plants, Biomass and Bioenergy. 53 (2013) 48–53. doi:10.1016/j.biombioe.2013.02.005.

[329] D. Kurz, U. Schnell, G. Scheffknecht, Euler-Euler simulation of wood chip combustion on a grate - effect of fuel moisture content and full scale application, Prog. Comput. Fluid Dyn. An Int. J. 13 (2013) 322. doi:10.1504/PCFD.2013.055060.

[330] D. Kurz, U. Schnell, G. Scheffknecht, CFD simulation of wood chip combustion on a grate using an Euler–Euler approach, Combust. Theory Model. 16 (2012) 251–273. doi:10.1080/13647830.2011.610903.

[331] C. Yin, L. Rosendahl, S. Clausen, S.L. Hvid, Characterizing and modeling of an 88 MW grate-fired boiler burning wheat straw: Experience and lessons, Energy. 41 (2012) 473–482. doi:10.1016/J.ENERGY.2012.02.050.

[332] C. Jordan, M. Harasek, Improvement of a Combustion Unit Based on a Grate Furnace for Granular Dry Solid Biofuels Using CFD Methods, Heat Transf. Eng. 31 (2010) 774–781. doi:10.1080/01457630903501062.

[333] P. Saxena, F.A. Williams, Testing a small detailed chemical-kinetic mechanism for the combustion of hydrogen and carbon monoxide, Combust. Flame. 145 (2006) 316–323. doi:10.1016/J.COMBUSTFLAME.2005.10.004.

[334] X. Zhang, Q. Chen, R. Bradford, V. Sharifi, J. Swithenbank, Experimental investigation and

mathematical modelling of wood combustion in a moving grate boiler, Fuel Process. Technol. 91 (2010) 1491–1499. doi:10.1016/J.FUPROC.2010.05.026.

[335] Z. Yu, X. Ma, Y. Liao, Mathematical modeling of combustion in a grate-fired boiler burning straw and effect of operating conditions under air- and oxygen-enriched atmospheres, Renew. Energy. 35 (2010) 895–903. doi:10.1016/J.RENENE.2009.10.006.

[336] S.K. Kær, Numerical modelling of a straw-fired grate boiler, Fuel. 83 (2004) 1183–1190. doi:10.1016/J.FUEL.2003.12.003.

[337] P. Venturini, D. Borello, C. Iossa, D. Lentini, F. Rispoli, Modeling of multiphase combustion and deposit formation in a biomass-fed furnace, Energy. 35 (2010) 3008–3021. doi:10.1016/J.ENERGY.2010.03.038.

[338] D. Shin, S. Choi, The combustion of simulated waste particles in a fixed bed, Combust. Flame. 121 (2000) 167–180. doi:10.1016/S0010-2180(99)00124-8.

[339] E. Simsek, B. Brosch, S. Wirtz, V. Scherer, F. Krüll, Numerical simulation of grate firing systems using a coupled CFD/discrete element method (DEM), Powder Technol. 193 (2009) 266–273. doi:10.1016/J.POWTEC.2009.03.011.

[340] C. Yin, L. Rosendahl, S.K. Kær, S. Clausen, S.L. Hvid, T. Hille, Mathematical Modeling and Experimental Study of Biomass Combustion in a Thermal 108 MW Grate-Fired Boiler, Energy & Fuels. 22 (2008) 1380–1390. doi:10.1021/ef700689r.

[341] H. Zhou, A.D. Jensen, P. Glarborg, P.A. Jensen, A. Kavaliauskas, Numerical modeling of straw combustion in a fixed bed, Fuel. 84 (2005) 389–403. doi:10.1016/J.FUEL.2004.09.020.

[342] T. Klason, X.S. Bai, M. Bahador, T.K. Nilsson, B. Sundén, Investigation of radiative heat transfer in fixed bed biomass furnaces, Fuel. 87 (2008) 2141–2153. doi:10.1016/J.FUEL.2007.11.016.

[343] T. Klason, X.S. Bai, Combustion process in a biomass grate fired industry furnace: a CFD study, Prog. Comput. Fluid Dyn. An Int. J. 6 (2006) 278. doi:10.1504/PCFD.2006.010581.

[344] X.-S. Bai, L. Fuchs, Modelling of turbulent reacting flows past a bluff body: assessment of accuracy and efficiency, Comput. Fluids. 23 (1994) 507–521. doi:10.1016/0045-7930(94)90016-7.

[345] Y. Bin Yang, V.N. Sharifi, J. Swithenbank, Converting moving-grate incineration from combustion to gasification – Numerical simulation of the burning characteristics, Waste Manag. 27 (2007) 645–655. doi:10.1016/J.WASMAN.2006.03.014.

[346] Y. Bin Yang, R. Newman, V. Sharifi, J. Swithenbank, J. Ariss, Mathematical modelling of straw combustion in a 38 MWe power plant furnace and effect of operating conditions, Fuel. 86 (2007) 129–142. doi:10.1016/J.FUEL.2006.06.023.

[347] S.K. Kær, L.A. Rosendahl, L.L. Baxter, Towards a CFD-based mechanistic deposit formation model for straw-fired boilers, Fuel. 85 (2006) 833–848. doi:10.1016/J.FUEL.2005.08.016.

[348] S.K. Kær, Straw combustion on slow-moving grates—a comparison of model predictions with experimental data, Biomass and Bioenergy. 28 (2005) 307–320. doi:10.1016/J.BIOMBIOE.2004.08.017.

[349] K. Goerner, T. Klasen, Modelling, simulation and validation of the solid biomass combustion in different plants, Prog. Comput. Fluid Dyn. An Int. J. 6 (2006) 225. doi:10.1504/PCFD.2006.010031.

[350] C.D. Goddard, Y.B. Yang, J. Goodfellow, V.N. Sharifi, J. Swithenbank, J. Chartier, D. Mouquet, R. Kirkman, D. Barlow, S. Moseley, Optimisation study of a large waste-to-energy plant using computational modelling and experimental measurements, J. Energy Inst. 78 (2005) 106–116. doi:10.1179/014426005X50850.

[351] M. Huttunen, L. Kjäldman, J. Saastamoinen, Analysis of grate firing of wood with numerical flow simulation, IFRF Combust. J. (2004) 18.

[352] H.-H. Frey, B. Peters, H. Hunsinger, J. Vehlow, Characterization of municipal solid waste combustion in a grate furnace, Waste Manag. 23 (2003) 689–701. doi:10.1016/S0956-053X(02)00070-3.

[353] R. Scharler, T. Fleckl, I. Obernberge, Modification of a Magnussen Constant of the Eddy Dissipation Model for biomass grate furnaces by means of hot gas in-situ FT-IR absorption spectroscopy, Prog. Comput. Fluid Dyn. An Int. J. 3 (2003) 102. doi:10.1504/PCFD.2003.003776.

[354] R. Scharler, I. Obernberger, Numerical Modelling of Biomass Grate Furnaces, 5th Conf. Ind. Furn. Boil. (2000) 17.

[355] C. Ryu, D. Shin, S. Choi, Combined Simulation of Combustion and Gas Flow in a Grate-Type Incinerator, J. Air Waste Manage. Assoc. 52 (2002) 189–197. doi:10.1080/10473289.2002.10470769.

[356] N. Griselin, X.S. Bai, Particle Dynamics in a Biomass-Fired Furnace – Predictions of Solid

Residence Changes With Operation, IFRF Combust. J. (2000) 30.

[357] S. Kim, D. Shin, S. Choi, Comparative evaluation of municipal solid waste incinerator designs by flow simulation, Combust. Flame. 106 (1996) 241–251. doi:10.1016/0010-2180(95)00190-5.

[358] C. Yin, L.A. Rosendahl, S.K. Kær, S. Clausen, S.L. Hvid, T. Hille, Mathematical modeling and experimental study of biomass combustion in a thermal 108 MWth grate-fired boiler, Energy & Fuels. 22 (2008) 1380–1390.

[359] C. Yin, L. Rosendahl, S. Clausen, S.L. Hvid, Characterizing and modeling of an 88 MW grate-fired boiler burning wheat straw: Experience and lessons, Energy. 41 (2012) 473–482. doi:10.1016/j.energy.2012.02.050.

[360] C. Paper, F.A. Universit, M. Costa, I. National, A.M. Universit, T. Pegaso, Experimental and numerical analysis of a waste-to-energy plant operation, (2016).

[361] S.K. Kær, Numerical modelling of a straw-fired grate boiler, Fuel. 83 (2004) 1183–1190. doi:10.1016/j.fuel.2003.12.003.

[362] S.K. Kær, Straw combustion on slow-moving grates - A comparison of model predictions with experimental data, Biomass and Bioenergy. 28 (2005) 307–320. doi:10.1016/j.biombioe.2004.08.017.

[363] Z. Yu, X. Ma, Y. Liao, Mathematical modeling of combustion in a grate-fired boiler burning straw and effect of operating conditions under air- and oxygen-enriched atmospheres, Renew. Energy. 35 (2010) 895–903. doi:10.1016/j.renene.2009.10.006.

[364] X. Zhang, Q. Chen, R. Bradford, V. Sharifi, J. Swithenbank, Experimental investigation and mathematical modelling of wood combustion in a moving grate boiler, Fuel Process. Technol. 91 (2010) 1491–1499. doi:10.1016/j.fuproc.2010.05.026.

[365] M. Costa, M. Dell'Isola, N. Massarotti, Numerical analysis of the thermo-fluid-dynamic field in the combustion chamber of an incinerator plant, Energy. 34 (2009) 2075–2086. doi:10.1016/j.energy.2008.08.024.

[366] M. Costa, V. Indrizzi, N. Massarotti, A. Mauro, Modeling and optimization of an incinerator plant for the reduction of the environmental impact, Int. J. Numer. Methods Heat Fluid Flow. 25 (2015) 1463–1487. doi:10.1108/HFF-10-2014-0300.

[367] F. Wissing, S. Wirtz, V. Scherer, Simulating municipal solid waste incineration with a DEM/CFD

method – Influences of waste properties, grate and furnace design, Fuel. 206 (2017) 638–656. doi:10.1016/J.FUEL.2017.06.037.

[368] C. Jordan, M. Harasek, Improvement of a combustion unit based on a grate furnace for granular dry solid biofuels using CFD methods, Heat Transf. Eng. 31 (2010) 774–781. doi:10.1080/01457630903501062.

[369] N.T.M. Duffy, J.A. Eaton, Investigation of factors affecting channelling in fixed-bed solid fuel combustion using CFD, Combust. Flame. 160 (2013) 2204–2220. doi:10.1016/j.combustflame.2013.04.015.

[370] M.A. Gómez, J. Porteiro, D. Patiño, J.L. Míguez, Eulerian CFD modelling for biomass combustion. Transient simulation of an underfeed pellet boiler, Energy Convers. Manag. 101 (2015) 666–680. doi:10.1016/j.enconman.2015.06.003.

[371] B.E. Launder, D.B. Spalding, The numerical computation of turbulent flows, Comput. Methods Appl. Mech. Eng. 3 (1974) 269–289. doi:10.1016/0045-7825(74)90029-2.

[372] X. Lu, T. Wang, Investigation of radiation models in entrained-flow coal gasification simulation, Int. J. Heat Mass Transf. 67 (2013) 377–392. doi:10.1016/j.ijheatmasstransfer.2013.08.011.

[373] Y.B. Yang, H. Yamauchi, V. Nasserzadeh, J. Swithenbank, Effects of fuel devolatilisation on the combustion of wood chips and incineration of simulated municipal solid wastes in a packed bed, Fuel. 82 (2003) 2205–2221. doi:10.1016/S0016-2361(03)00145-5.

[374] B.F. Magnussen, B.H. Hjertager, On mathematical modeling of turbulent combustion with special emphasis on soot formation and combustion, Symp. Combust. 16 (1977) 719–729. doi:10.1016/S0082-0784(77)80366-4.

[375] B. Magnussen, On the structure of turbulence and a generalized eddy dissipation concept for chemical reaction in turbulent flow, in: 19th Aerosp. Sci. Meet., American Institute of Aeronautics and Astronautics, Reston, Virigina, 1981. doi:10.2514/6.1981-42.

[376] S. Chapela, J. Porteiro, M. Costa, Effect of the Turbulence–Chemistry Interaction in Packed-Bed Biomass Combustion, Energy & Fuels. 31 (2017) 9967–9982. doi:10.1021/acs.energyfuels.7b00516.

[377] A. Shiehnejadhesar, R. Mehrabian, R. Scharler, G.M. Goldin, I. Obernberger, Development of a gas phase combustion model suitable for low and high turbulence conditions, Fuel. 126 (2014)

177–187. doi:10.1016/j.fuel.2014.02.040.

[378] B. Rajh, C. Yin, N. Samec, M. Hriber??ek, M. Zadravec, Advanced modelling and testing of a 13 MWth waste wood-fired grate boiler with recycled flue gas, Energy Convers. Manag. 125 (2016) 230–241. doi:10.1016/j.enconman.2016.02.036.

[379] A. Shiehnejadhesar, R. Scharler, R. Mehrabian, I. Obernberger, Development and validation of CFD models for gas phase reactions in biomass grate furnaces considering gas streak formation above the packed bed, Fuel Process. Technol. 139 (2015) 142–158. doi:10.1016/j.fuproc.2015.07.029.

[380] D. Neves, H. Thunman, A. Matos, L. Tarelho, A. Gómez-Barea, Characterization and prediction of biomass pyrolysis products, Prog. Energy Combust. Sci. 37 (2011) 611–630. doi:10.1016/j.pecs.2011.01.001.

[381] K.W. Ragland, D.J. Aerts, A.J. Baker, Properties of wood for combustion analysis, Bioresour. Technol. 37 (1991) 161–168. doi:10.1016/0960-8524(91)90205-X.

[382] C. Di Blasi, C. Branca, A. Santoro, E. Gonzalez Hernandez, Pyrolytic behavior and products of some wood varieties, Combust. Flame. 124 (2001) 165–177. doi:10.1016/S0010-2180(00)00191-7.

[383] H. Khodaei, Y.M. Al-Abdeli, F. Guzzomi, G.H. Yeoh, An overview of processes and considerations in the modelling of fixed-bed biomass combustion, Energy. 88 (2015) 946–972. doi:10.1016/J.ENERGY.2015.05.099.

[384] EDP, Centrais Termoelétricas a Biomassa, (2015). http://www.a-nossa-energia.edp.pt/centros_produtores/fotos_videos.php?item_id=72&cp_type=te&section_type=fotos_videos (accessed May 14, 2015).

[385] I. Bonefacic, B. Frankovic, A. Kazagic, Cylindrical particle modelling in pulverized coal and biomass co-firing process, Appl. Therm. Eng. 78 (2015) 74–81. doi:https://doi.org/10.1016/j.applthermaleng.2014.12.047.

[386] P.E. Mason, L.I. Darvell, J.M. Jones, M. Pourkashanian, A. Williams, Single particle flame-combustion studies on solid biomass fuels, Fuel. 151 (2015) 21–30. doi:10.1016/j.fuel.2014.11.088.

[387] J. Riaza, J. Gibbins, H. Chalmers, Ignition and combustion of single particles of coal and biomass,

Fuel. 202 (2017) 650–655. doi:https://doi.org/10.1016/j.fuel.2017.04.011.

[388] H. Lu, E. Ip, J. Scott, P. Foster, M. Vickers, L.L. Baxter, Effects of particle shape and size on devolatilization of biomass particle, Fuel. 89 (2010) 1156–1168. doi:https://doi.org/10.1016/j.fuel.2008.10.023.

[389] G. Caposciutti, F. Barontini, C. Galletti, M. Antonelli, L. Tognotti, U. Desideri, Woodchip size effect on combustion temperatures and volatiles in a small-scale fixed bed biomass boiler, Renew. Energy. 151 (2020) 161–174. doi:10.1016/j.renene.2019.11.005.

[390] R. Brown, Thermochemical Processing of Biomass: Conversion into Fuels, Chemicals and Power, Second Edi, Wiley Series in Renewable Resources, 2019.

[391] S. Pang, A.S. Mujumdar, Drying of Woody Biomass for Bioenergy: Drying Technologies and Optimization for an Integrated Bioenergy Plant, Dry. Technol. 28 (2010) 690–701. doi:10.1080/07373931003799236.

[392] M. Hupa, O. Karlström, E. Vainio, Biomass combustion technology development – It is all about chemical details, Proc. Combust. Inst. 36 (2017) 113–134. doi:10.1016/J.PROCI.2016.06.152.

[393] P. Sommersacher, T. Brunner, I. Obernberger, Fuel Indexes: A Novel Method for the Evaluation of Relevant Combustion Properties of New Biomass Fuels, Energy & Fuels. 26 (2012) 380–390. doi:10.1021/ef201282y.

[394] R.T. Symonds, D.Y. Lu, V. Manovic, E.J. Anthony, Pilot-Scale Study of CO2 Capture by CaO-Based Sorbents in the Presence of Steam and SO2, Ind. Eng. Chem. Res. 51 (2012) 7177–7184. doi:10.1021/ie2030129.

[395] Y.B. Yang, J. Goodfellow, V. Nasserzadeh, J. Swithenbank, Study on the transient process of waste fuel incineration in a full-scale moving-bed furnace, Combust. Sci. Technol. 177 (2004) 127–150. doi:10.1080/00102200590883796.

[396] M. Markovic, E.A. Bramer, G. Brem, Experimental investigation of wood combustion in a fixed bed with hot air, Waste Manag. 34 (2014) 49–62. doi:10.1016/J.WASMAN.2013.09.021.

[397] H. Sabelstrom, Diffusion of solid fuel on a vibrating grate, Doctoral Thesis, Aalborg University, 2007.

[398] Y.H. Kiang, Predicting dew points of acid gases, Chem. Eng. 9 (1981) 127–128.

[399] F.H. Verhoff, J.T. Banchero, Predicting dew points of flue gases, Chem. Eng. Prog. 70 (1974) 71–

72.

[400] J.M. Blanco, F. Peña, Increase in the boiler's performance in terms of the acid dew point temperature: Environmental advantages of replacing fuels, Appl. Therm. Eng. 28 (2008) 777–784. doi:10.1016/J.APPLTHERMALENG.2007.06.024.

[401] F. Jappe Frandsen, Utilizing biomass and waste for power production—a decade of contributing to the understanding, interpretation and analysis of deposits and corrosion products, Fuel. 84 (2005) 1277–1294. doi:10.1016/J.FUEL.2004.08.026.

[402] R. Shah, Sekulic. Dursan, Fundamentals of Heat Exchanger Design, John Wiley & Sons, 2002.

[403] B. Kilkovsky, P. Stehlik, Z. Jegla, L.L. Tovazhnyansky, O. Arsenyeva, P.O. Kapustenko, Heat exchangers for energy recovery in waste and biomass to energy technologies – I. Energy recovery from flue gas, Appl. Therm. Eng. 64 (2014) 213–223. doi:10.1016/j.applthermaleng.2013.11.041.

[404] CentroPinus, A Fileira do Pinho em 2018 - Indicadores da Fileira do Pinho, 2019. https://gallery.mailchimp.com/617984157336295f77b5da6a8/files/2184e377-fc72-488b-8c4d-f826ac8c8431/Fileira_do_Pinho_2019.pdf.

[405] C. Alegria, N. Roque, T. Albuquerque, P. Fernandez, M.M. Ribeiro, Modelling Maritime Pine (Pinus pinaster Aiton) Spatial Distribution and Productivity in Portugal: Tools for Forest Management, Forests. 12 (2021) 368. doi:10.3390/f12030368.

[406] S. Ferreira, E. Monteiro, P. Brito, C. Vilarinho, Biomass resources in Portugal: Current status and prospects, Renew. Sustain. Energy Rev. 78 (2017) 1221–1235. doi:10.1016/J.RSER.2017.03.140.

[407] P.S. Duncker, S.M. Barreiro, G.M. Hengeveld, T. Lind, W.L. Mason, S. Ambrozy, H. Spiecker, Classification of Forest Management Approaches: A New Conceptual Framework and Its Applicability to European Forestry, Ecol. Soc. 17 (2012) art51. doi:10.5751/ES-05262-170451.

[408] I.M. Mirra, T.M. Oliveira, A.M.G. Barros, P.M. Fernandes, Fuel dynamics following fire hazard reduction treatments in blue gum (Eucalyptus globulus) plantations in Portugal, For. Ecol. Manage. 398 (2017) 185–195. doi:10.1016/j.foreco.2017.05.016.

[409] L.J.R. Nunes, L.M.E.F. Loureiro, L.C.R. Sá, H.F.C. Silva, Evaluation of the potential for energy recovery from olive oil industry waste: Thermochemical conversion technologies as fuel

improvement methods, Fuel. 279 (2020) 118536. doi:10.1016/j.fuel.2020.118536.

[410] S.E. Gustafsson, Transient plane source techniques for thermal conductivity and thermal diffusivity measurements of solid materials, Rev. Sci. Instrum. 62 (1991) 797–804. doi:10.1063/1.1142087.

[411] S.A. Al-Ajlan, Measurements of thermal properties of insulation materials by using transient plane source technique, Appl. Therm. Eng. 26 (2006) 2184–2191. doi:10.1016/j.applthermaleng.2006.04.006.

[412] Hot Disk, Hot Disk Thermal Constants Analyser - Instruction Manual, 2019.

[413] TA Instruments, SDT 2960 Simultaneous DSC-TGA Manual, 2000.

[414] A. Friedl, E. Padouvas, H. Rotter, K. Varmuza, Prediction of heating values of biomass fuel from elemental composition, Anal. Chim. Acta. 544 (2005) 191–198. doi:10.1016/j.aca.2005.01.041.

[415] M. Pronobis, Evaluation of the influence of biomass co-combustion on boiler furnace slagging by means of fusibility correlations, Biomass and Bioenergy. 28 (2005) 375–383. doi:10.1016/j.biombioe.2004.11.003.

[416] P. Teixeira, H. Lopes, I. Gulyurtlu, N. Lapa, P. Abelha, Evaluation of slagging and fouling tendency during biomass co-firing with coal in a fluidized bed, Biomass and Bioenergy. 39 (2012) 192–203. doi:10.1016/j.biombioe.2012.01.010.

[417] Q. Guo, Z. Cheng, G. Chen, B. Yan, L. Hou, F. Ronsse, Optimal strategy for clean and efficient biomass combustion based on ash deposition tendency and kinetic analysis, J. Clean. Prod. 271 (2020) 122529. doi:10.1016/j.jclepro.2020.122529.

[418] ANSYS, ANSYS FLUENT Theory Guide, (2013).

[419] B. Peters, M. Baniasadi, M. Baniasadi, X. Besseron, A.E. Donoso, M. Mohseni, G. Pozzetti, XDEM multi-physics and multi-scale simulation technology: Review of DEM–CFD coupling, methodology and engineering applications, Particuology. 44 (2019) 176–193. doi:10.1016/j.partic.2018.04.005.

[420] B. Peters, A. Džiugys, R. Navakas, Simulation of thermal conversion of solid fuel by the discrete particle method, Lith. J. Phys. 51 (2011) 91–105. doi:10.3952/lithjphys.51204.

[421] H.K. Versteeg, W. Malalasekera, An Introduction to Computational Fluid Dynamics - The Finite

Volume Method, Technical, Harlow, 1995.

[422] T.-H. Shih, W.W. Liou, A. Shabbir, Z. Yang, J. Zhu, A new k-ϵ eddy viscosity model for high reynolds number turbulent flows, Comput. Fluids. 24 (1995) 227–238. doi:10.1016/0045-7930(94)00032-T.

[423] K. Samiei, Assessment of implicit and explicit algorithms in numerical simulation of granular matter, University of Luxembourg, 2012.

[424] M. Michael, A Discrete Approach to Describe the Kinematics between Snow and a Tire Tread, University of Luxembourg, 2014.

[425] A.H. Mahmoudi, Prediction of heat-up, drying and gasification of fixed and moving beds by the Discrete Particle Method (DPM), University of Luxembourg, 2016.

[426] C. Di Blasi, Modeling chemical and physical processes of wood and biomass pyrolysis, Prog. Energy Combust. Sci. 34 (2008) 47–90. doi:10.1016/j.pecs.2006.12.001.

[427] R.B. Bird, W.E. Stewart, E.N. Lightfoot, Transport Phenomena, John Wiley & Sons, 780.

[428] N. Wakao, S. Kaguei, Heat And Mass Transfer In Packed Beds, Gordon and Breach, Science Publisher, Inc, 1982.

[429] N. Wakao, S. Kaguei, T. Funazkri, Effect of fluid dispersion coefficients on particle-to-fluid heat transfer coefficients in packed beds, Chem. Eng. Sci. 34 (1979) 325–336. doi:10.1016/0009-2509(79)85064-2.

[430] N. Wakao, T. Funazkri, Effect of fluid dispersion coefficients on particle-to-fluid mass transfer coefficients in packed beds, Chem. Eng. Sci. 33 (1978) 1375–1384. doi:10.1016/0009-2509(78)85120-3.

[431] K.-E. Saarela, L. Harju, J. Rajander, J.-O. Lill, S.-J. Heselius, A. Lindroos, K. Mattsson, Elemental analyses of pine bark and wood in an environmental study, Sci. Total Environ. 343 (2005) 231–241. doi:10.1016/j.scitotenv.2004.09.043.

[432] P. McKendry, Energy production from biomass (part 1): overview of biomass, Bioresour. Technol. 83 (2002) 37–46. doi:10.1016/S0960-8524(01)00118-3.

[433] K.L. Kenney, W.A. Smith, G.L. Gresham, T.L. Westover, Understanding biomass feedstock variability, Biofuels. 4 (2013) 111–127. doi:10.4155/bfs.12.83.

[434] L.J.R. Nunes, J.C.O. Matias, J.P.S. Catalão, Biomass combustion systems: A review on the

physical and chemical properties of the ashes, Renew. Sustain. Energy Rev. 53 (2016) 235–242. doi:10.1016/J.RSER.2015.08.053.

[435] P.E. Mason, L.I. Darvell, J.M. Jones, A. Williams, Comparative Study of the Thermal Conductivity of Solid Biomass Fuels, Energy & Fuels. 30 (2016) 2158–2163. doi:10.1021/acs.energyfuels.5b02261.

[436] B.M. Suleiman, J. Larfeldt, B. Leckner, M. Gustavsson, Thermal conductivity and diffusivity of wood, Wood Sci. Technol. 33 (1999) 465–473. doi:10.1007/s002260050130.

[437] W. Guo, C.J. Lim, X. Bi, S. Sokhansanj, S. Melin, Determination of effective thermal conductivity and specific heat capacity of wood pellets, Fuel. 103 (2013) 347–355. doi:10.1016/j.fuel.2012.08.037.

[438] J.M. Jones, A. .Saddawi, B. Dooley, E.J.S. Mitchella, J.Werner, D.J. Waldron, S. Weatherstone, A. Williams, Low temperature ignition of biomass, Fuel Process. Technol. 134 (2015) 372–377. doi:10.1016/j.fuproc.2015.02.019.

[439] S. V. Vassilev, C.G. Vassileva, Y.-C. Song, W.-Y. Li, J. Feng, Ash contents and ash-forming elements of biomass and their significance for solid biofuel combustion, Fuel. 208 (2017) 377–409. doi:10.1016/j.fuel.2017.07.036.

[440] H. Hartmann, T. Böhm, P.D. Jensenb, M. Temmerman, F. Rabierc, M. Golser, Methods for size classification of wood chips, Biomass and Bioenergy. 30 (2006) 944–953. doi:10.1016/j.biombioe.2006.06.010.

[441] D. Kuptz, K. Schreiber, F. Schulmeyer, S. Lesche, T. Zeng, F. Ahrens, V. Zelinski, C. Schön, A. Pollex, H. Borchert, V. Lenz, A. Loewen, M. Nelles, H. Hartmann, Evaluation of combined screening and drying steps for the improvement of the fuel quality of forest residue wood chips—results from six case studies, Biomass Convers. Biorefinery. 9 (2019) 83–98. doi:10.1007/s13399-019-00389-2.

[442] P. Shrivastava, P. Khongphakdi, A. Palamanit, A. Kumar, P. Tekasakul, Investigation of physicochemical properties of oil palm biomass for evaluating potential of biofuels production via pyrolysis processes, Biomass Convers. Biorefinery. 11 (2021) 1987–2001. doi:10.1007/s13399-019-00596-x.

[443] P. Jensen, H. Hartmann, T. Bohm, M. Temmerman, F. Rabier, M. Morsing, Moisture content determination in solid biofuels by dielectric and NIR reflection methods, Biomass and Bioenergy.

30 (2006) 935–943. doi:10.1016/j.biombioe.2006.06.005.

[444] L. Sanchez-Silva, D. López-González, J. Villaseñor, P. Sánchez, J.L. Valverde, Thermogravimetric–mass spectrometric analysis of lignocellulosic and marine biomass pyrolysis, Bioresour. Technol. 109 (2012) 163–172. doi:10.1016/J.BIORTECH.2012.01.001.

[445] J.A. Conesa, A. Marcilla, J.A. Caballero, R. Font, Comments on the validity and utility of the different methods for kinetic analysis of thermogravimetric data, J. Anal. Appl. Pyrolysis. 58–59 (2001) 617–633. doi:10.1016/S0165-2370(00)00130-3.

[446] R. Chen, Q. Li, X. Xu, D. Zhang, R. Hao, Combustion characteristics, kinetics and thermodynamics of Pinus Sylvestris pine needle via non-isothermal thermogravimetry coupled with model-free and model-fitting methods, Case Stud. Therm. Eng. 22 (2020) 100756. doi:10.1016/j.csite.2020.100756.

[447] J.L. Figueiredo, C. Valenzuela, A. Bernalte, J.M. Encinar, Pyrolysis of holm-oak wood: influence of temperature and particle size, Fuel. 68 (1989) 1012–1016. doi:10.1016/0016-2361(89)90067-7.

[448] B. Rajh, C. Yin, N. Samec, CFD modeling and experience of waste-to-energy plant burning waste wood, 14th Int. Waste Manag. Landfill Symp. (2013) 13. http://vbn.aau.dk/files/154851236/390.pdf.

[449] C. Choi, W.S. Choi, J.H. Choi, W.J. Kim, D. Shin, Reducing CO emissions through a secondary air nozzle retrofit based on the jet penetration factor and the momentum flux ratio of a commercial wood waste incinerator, Appl. Therm. Eng. 118 (2017) 101–112. doi:10.1016/j.applthermaleng.2017.02.068.

[450] H.R. Trechsel, M.T. Bomberg, C. Carll, A.C. Wiedenhoeft, Moisture-Related Properties of Wood and the Effects of Moisture on Wood and Wood Products, in: Moisture Control Build. Key Factor Mold Prev. Ed., ASTM International, 100 Barr Harbor Drive, PO Box C700, West Conshohocken, PA 19428-2959, n.d.: pp. 54-54–26. doi:10.1520/MNL11544M.

LIST OF PUBLICATIONS

Papers in Scientific Journals

1) **João Silva,** Senhorinha Teixeira, Élson Grilo, Bernhard Peters, and José Teixeira, *"Analysis and monitoring of the combustion performance in a biomass power plant"*, Cleaner Engineering and Technology, 5, 100334, 2021, doi.org/10.1016/j.clet.2021.100334.

2) **João Silva,** Ana Ferreira, Senhorinha Teixeira, Eduardo Ferreira, Luis Martins and José Teixeira, *"Sawdust Drying Process in a Large-Scale Pellets Facility: An Energy and Exergy Analysis"*, Cleaner Environmental Systems, 2, 100037, 2021, doi.org/10.1016/j.cesys.2021.100037.

3) Ana Ferreira, **João Silva,** Senhorinha Teixeira, José Carlos Teixeira and Silvia Nebra, *"Assessment of the Stirling engine performance comparing two renewable energy sources: Solar energy and biomass"* Renewable Energy, 154, 581–597, 2020, doi: 10.1016/j.renene.2020.03.020.

4) Lelis Fraga, **João Silva,** Senhorinha Teixeira, Manuel Ferreira and José Teixeira, *"Influence of Operating Conditions on the Thermal Behavior and Kinetics of Pine Wood Particles using Thermogravimetric Analysis".* Energies, 13, 2756, 2020, doi.org/10.3390/en13112756.

5) **João Silva,** Lelis Fraga, Senhorinha Teixeira, Manuel Ferreira and José Teixeira, *"Thermal conversion of pine wood and kinetic analysis under oxidative and non-oxidative environments at low heating rate"*, Proceedings, 58(1):23, 2020, doi.org/10.3390/WEF-06921.

Proceedings in Scientific Conferences

1) Ana Cristina Ferreira, **João Silva**, Senhorinha Teixeira, and José Teixeira, *"A brief review on decarbonization and energy transition of Portuguese industry: renewable energies incorporation and efficiency measures"*, 35th ECOS (accepted).

2) **João Silva,** Senhorinha Teixeira, and José Teixeira, "*Experimental and Numerical Study of Biomass Combustion in a Small-scale Reactor",* CPOTE 2022 (accepted).

3) **João Silva,** Senhorinha Teixeira, and José Teixeira, *"An Experimental Setup to Study the Fundamental Phenomena associated with Biomass Combustion",* ASME 2022 (accepted).

4) Carlos Castro, José Carlos Teixeira, Cândida Vilarinho, **João Silva,** Margarida Gonçalves, André Ribeiro and Nuno Pacheco, *"The influence of fuel mix on the devolatilization of RDF based coal"*, ICoWEFS 2022 (accepted).

5) **João Silva,** Ana Cristina Ferreira, Senhorinha Teixeira and José Carlos Teixeira *"Decentralized Forest Biomass Residues Thermal Power Plant Potential: An Economic and Environmental Perspective,"* Proceedings of the 34th International Conference On Efficiency, Cost, Optimization,

Simulation And Environmental Impact Of Energy Systems (ECOS), 2021, 28 June – 2 July 2021, Online.

6) **João Silva,** Ana Cristina Ferreira, Senhorinha Teixeira and José Carlos Teixeira *"Potential of Forest Biomass Residues: Thermal and Economic Perspectives,"* Proceedings of the Circular and Bioeconomics – CIBEK 2021, April 1, 2021, Belgrade, Serbia.

7) **João Silva**, Lelis Fraga, Senhorinha Teixeira, and José Teixeira, *"Numerical tools developed to predict the combustion behavior inside a 20 kW Pellet Boiler",* Proceedings of the LAMBDA Big Data Analytics Summer School, Doctoral Workshop, 17 September 2021, Online.

8) **João Silva,** Senhorinha Teixeira, Bernhard Peters and José Teixeira, *"Survey of Existing Literature Data on the Biomass Combustion Behavior in Industrial Grate-fired Boilers",* Proceedings of the ASME 2021 International Mechanical Engineering Congress and Exposition. Volume 8A: Energy. Virtual, Online. November 1–5, 2021. V08AT08A008. ASME, doi:10.1115/IMECE2021-73567.

9) **João Silva,** Vitor Guedes, Senhorinha Teixeira, Pedro Lobarinhas, José Teixeira and Nelson Rodrigues, *"Numerical Simulation of the Flow inside a Horizontal Closed Refrigerated Display Cabinet",* Proceedings of the ASME 2021 International Mechanical Engineering Congress and Exposition. Volume 10: Fluids Engineering. Virtual, Online. November 1–5, 2021. V010T10A055. ASME. doi:10.1115/IMECE2021-73589.

10) **João Silva,** Lelis Fraga, Senhorinha Teixeira, Manuel Ferreira and José Teixeira, *"Thermal conversion of pine wood and kinetic analysis under oxidative and non-oxidative environments at low heating rate"*, The First World Energies Forum—Current and future Energy Issues, 14–16 September 2020, Online.

11) Ana Cristina Ferreira, **João Silva,** Senhorinha Teixeira, José Carlos Teixeira and Silvia Nebra, "*Analysis of the different renewable energy sources in the performance of a Stirling engine"*, Proceedings of the 32nd International Conference On Efficiency, Cost, Optimization, Simulation And Environmental Impact Of Energy Systems (ECOS), 23-28 June 2019 in Wroclaw, Poland.

12) **João Silva,** Lelis Fraga, Sergio Chapela, Jacobo Porteiro, Manuel Ferreira, Senhorinha Teixeira, José Teixeira, *"CFD Modeling of a 20 kW Pellet Boiler"*, Proceedings of the ASME 2018 International Mechanical Engineering Congress and Exposition. Volume 6B: Energy. Pittsburgh, Pennsylvania, USA. November 9–15, 2018. V06BT08A036. ASME. doi:10.1115/IMECE2018-88063.

13) **João Silva,** Sergio Chapela, Jacobo Porteiro, Senhorinha Teixeira and José Teixeira, *"Application of a Biomass Combustion Model in an Industrial Boiler"*, Proceedings of the 31st International Conference on Efficiency, Cost, Optimization, Simulation and Environmental Impact of Energy Systems (ECOS), 15–21 June 2018 in Guimarães, Portugal.

14) Lelis Fraga, **João Silva,** José Teixeira, Manuel Ferreira, Delfim Soares and Senhorinha Teixeira, *"The effect of the heating and air flow rate on the mass loss of pine wood particles"*, Proceedings of the 31st International Conference on Efficiency, Cost, Optimization, Simulation and Environmental Impact of Energy Systems (ECOS), 15–21 June 2018 in Guimarães, Portugal.

Abstracts in Scientific Conferences

1) Bernhard Peters, **João Silva,** Senhorinha Teixeira, and José Teixeira, *"Meeting the Challenge to Resolve Biomass Combustion in Industrial Furnaces",* 17th OpenFOAM Workshop, 11-14 July 2022, Cambridge, United Kingdom.

2) **João Silva,** Senhorinha Teixeira, José Carlos Teixeira, Bernhard Peters *"Kinetics Study of the Main Forest Residues Used in a Portuguese Power Plant"*, 17th International Congress on Thermal Analysis and Calorimetry, 29 Aug. – 3 Sept. 2021, Online.

3) **João Silva,** Senhorinha Teixeira, José Carlos Teixeira, Bernhard Peters *"Characterization of the Forest Residues Combustion by Thermogravimetric Analysis",* 17th International Congress on Thermal Analysis and Calorimetry, 29 Aug. – 3 Sept. 2021, Online.

4) **João Silva,** João Marques, Rita Amaral, Senhorinha Teixeira, José Teixeira, Susete Marques, Mariana Dias, Isabel Martins, Catarina Santos, Ana Xambre, Helena Alvelos, André Mendes, and Filipe Alvelos *"Integração dos Modelos de Rothermel e do Tempo Mínimo de Transmissão para Modelação da Propagação do Fogo"*, XXI APDIO Congress, IO2021 – 7 and 8 November 2021 in Figueira da Foz, Portugal.

5) **João Silva,** Senhorinha Teixeira, Eduardo Ferreira, Luis B. Martins and José Teixeira, *"Energy and Exergy Analyses of a Sawdust Rotary Dryer Integrated with Biomass Furnace"*, 14th International Conference on Energy for a Clean Environment, 8-12 September 2019 in Funchal, Madeira, Portugal.

6) **João Silva,** Élson Grilo, Carlos Ferreira, Senhorinha Teixeira and José Carlos Teixeira, *"The Influence of the Primary Air on the Combustion Performance in an Industrial Biomass Boiler",* 27th European Biomass Conference & Exhibition (EUBCE), 27-30 May 2019 in Lisbon, Portugal.

ANNEXES

Annex A – Biomass Power Plants in Portugal

Table 41: Dedicated Biomass Power Plants in Portugal. Source: Adapted from: [65,66].

Power Plant	Date	Location	Electric Power (MW)
Altri – Termoelétrica Centroliva	1998	Vila Velha de Rodão	5
Altri – Termoelétrica de Mortágua	1999	Mortágua	9
Altri – Termoelétrica de Rodão	2007	Vila Velha de Rodão	12.5
Termoelétrica Terras de Sta. Maria	2008	Oliveira de Azeméis	10
The Navigator Company – Termoelétrica de Cacia	2009	Aveiro	12.5
Altri – Termoelétrica da Figueira da Foz	2009	Figueira da Foz	26
The Navigator Company – Termoelétrica de Setúbal	2009	Setúbal	12.5
Altri – Termoelétrica de Constância	2009	Constância	12.5
Termoelétrica de Belmonte	2010	Belmonte	2
Termoelétrica de PALSER	2010	Sertã	3
Central de Biomassa de Famalicão I	2017	Famalicão	10
Termoflorestal	2017	Batalha	5
Central de Biomassa de Famalicão II	2018	Famalicão	10
Central de Biomassa do Fundão	2019	Fundão	15
Central de Biomassa de Viseu	2019	Viseu	15
Central de Biomassa do Juncal	2019	Juncal	5
Central de Biomassa da Chamusca	2019	Chamusca	3
Central de Biomassa de Mangualde	2020	Mangualde	10
Altri – Celbi 2*	2020	Figueira da Foz	30
		Total:	**208**

*construction in progress

Table 42: Cogeneration Biomass Power Plants in Portugal. Source: Adapted from: [65,66]**.**

Power Plant	Date	Location	Electric Power (MW)
Altri – Cogeração Celbi	1987	Figueira da Foz	70.96
Altri – Cogeração Celtejo	1992	Vila Velha de Ródão	30
Cogeração SIAF	1996	Mangualde	3.8
Altri – Cogeração Caima	2001	Constância	12.8
Cogeração EUROPA&C Energia Viana, S.A	2002	Viana do Castelo	26
Cogeração Amorim	2004	Santa Maria da Feira	1
The Navigator Company – Cogeração da Figueira da Foz	2004	Figueira da Foz	95
The Navigator Company –Cogeração Setúbal	2004	Setúbal	53.9
The Navigator Company – Cogeração Cacia	2005	Aveiro	35.2
Costa Ibérica	2011	Viseu	0.3
		Total:	**328.96**

Annex B – Moisture Control Procedure Validation

Since the moisture content of the samples can vary in a wide range, a procedure to ensure a constant and equal moisture content in the different samples was used. The development of this procedure is important to avoid the influence of the moisture content in the thermal properties, differences in the thermal conversion behavior, and to allow an effective comparison between the different biomass species. The procedure used in this work is based on the equilibrium moisture content concept between the environment and the solid particles. It is known that moisture content in solid biomass particles is time-dependent as presents a dependency on ambient conditions (temperature, pressure, and relative humidity). This is because biomass is hygroscopic and at a certain temperature and relative humidity, biomass will equilibrate to specific moisture content and will maintain until a new modification of the environmental conditions. Hence, the creation of controlled environmental conditions in a closed volume where the samples are stored is essential and makes possible a constant moisture content in the biomass samples.

Therefore, this principle only requires the achievement of known environmental conditions, which can be obtained economically through the utilization of a salt solution. The salt solutions provide a known target relative humidity, and since the temperature in the laboratory does not present a significant variation, the moisture content of the biomass samples can be previously known. The maximum possible moisture content in biomass using this procedure is around 20% and for this is necessary an atmosphere with a relative humidity of 97 to 99%. This is only possible with a salt solution of potassium sulfate. More details about the equilibrium moisture content for a given temperature and humidity can be found in Trechsel et al. [450].

Considering the previous information, the principle was verified using two samples, with around 10 to 14% of moisture, in a desiccator with a potassium sulfate solution in the lower part. The relative humidity inside the desiccator was continuously monitored using a humidity sensor, SHT31 Smart Gadget with an accuracy of ± 2%, allowing to monitor its value over time. During the experiment, the samples were removed from the desiccator in order to verify if their weight had changed. Figure 98 presents the variation of the mass of the samples along the time, and it is possible to observe that the moisture of the samples was increased along the time and two weeks are necessary to achieve and ensure a 20% of moisture content in the samples.

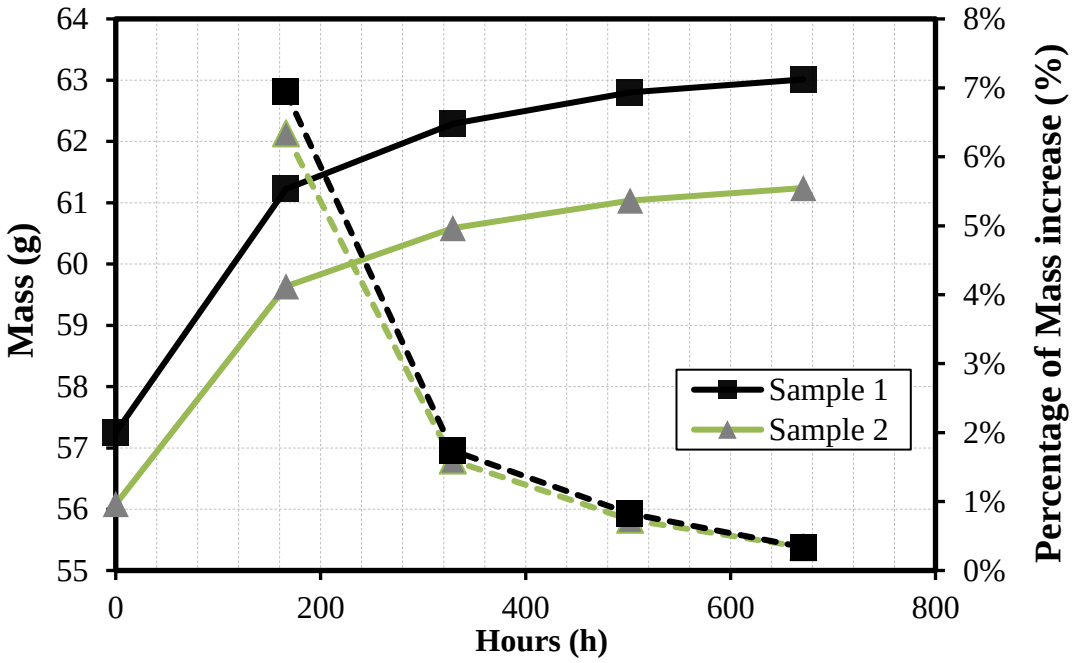

Figure 98: Variation of the mass of the samples along the time.

Although the experiment was successful, due to the long period the particles were subjected to a very humid atmosphere, as can be seen in Figure 99, the formation of mold on the surface of the particles was observed. Thus, the particles should not be exposed to a very humid environment for more than three weeks.

a) b)

Figure 99: Appearance of the particles at: a) beginning and b) end of the experiment.

Annex C – TGA Experiments

Auxiliary Experiments

Blank Experiments

In a TG experiment the temperature increase at which the air is subjected cause a variation in its density. This effect cannot be neglected since the air density variation leads to an effect denominated buoyancy effect and which is important to consider since the experiment involves a reduced amount of mass. This effect depends on different factors such as the flow rate and the heating rate. Therefore, it is important to account for this effect in order to report the effective mass of the sample during the experiment. Hence, blank experiments are necessary to subsequently correct the result from the TGA. Taking into account the heating rates selected to develop the TGA, a simple run for each heating rate was performed with the crucible empty. Figure 100 presents the weight variation considering the initial weight report in the TG equipment. As can be seen in this figure, the buoyancy effect is more remarkable, reaching the decimal point of the initial weight of the sample. For the lower heating rate, 5 °C/min, the buoyancy effect is not visible and an increase of the weight along the heating program was verified. This phenomenon happens due to the configuration of the TG equipment, and the movement of the fluid flow overlaps the buoyancy effect since the temperature increase occurs slowly.

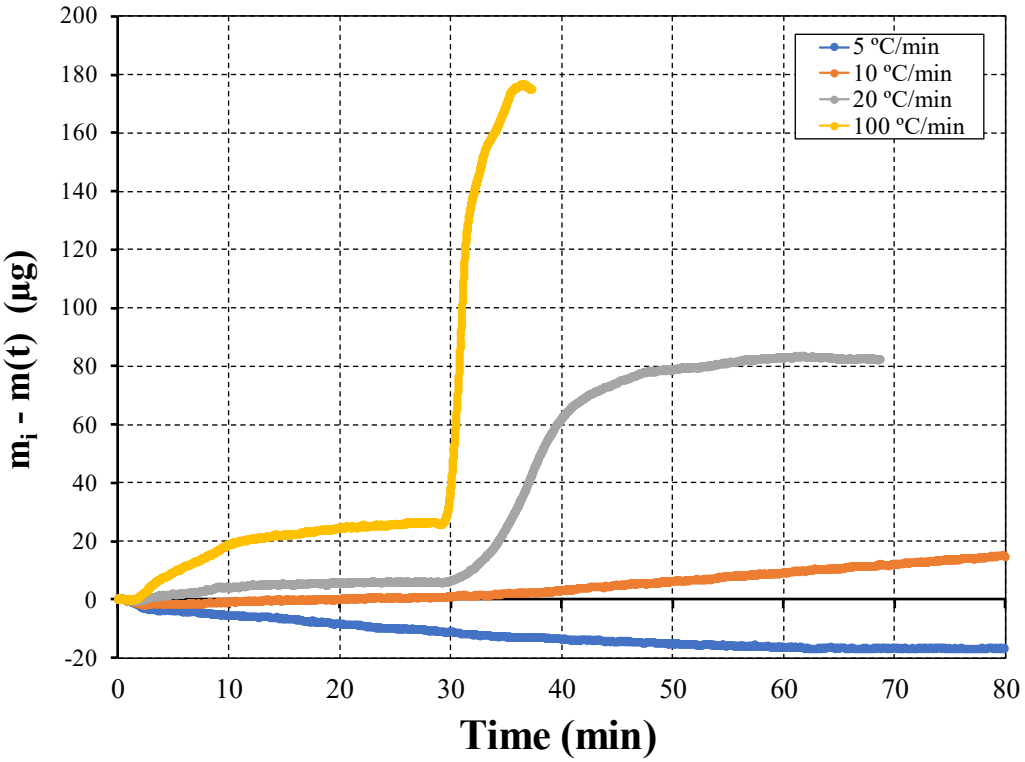

Figure 100: Blank experiments with different heating rates.

The variations presented in Figure 100 were defined as background weight signals and were subtracted in every experiment, and the real mass was computed.

Influence of the Initial Conditions

In order to better understand the influence of the different variables involved in the TG experiments, a parametric analysis was initially developed. Hence, preliminary experiments to observe mainly the influence of the atmosphere, the air flow rate, and the particle size were developed [176,244]. This study is particularly important to define earlier the key variables and avoid diffusion limitations and keep kinetic controlled conditions during the TG experiments.

The first issue analyzed was the atmosphere, this should be oxidant in order to guarantee a chemical-kinetic reaction control similar to the conditions in industrial equipment. With this condition, the complexity of the thermal conversion of biomass is addressed since the appearance of gas-phase reaction between the volatiles and the air supplied is promoted as well as the char combustion is enhanced [244]. Consequently, experiments with oxidative atmosphere provided the following parameters higher than inert experiments: i) maximum mass loss rate 15% higher; ii) average char combustion rate 5 times higher; iii) heat released reaches 3.44 times higher. Therefore, this modification from inert to oxidant atmosphere will result in a variation of the kinetic analysis. Furthermore, the oxidizing flow rate is important to be sufficient to avoid secondary reactions near the biomass sample. In the preliminary experiments developed with different air flow rates, as represented in Figure 101, similar results were obtained although with 100 mL/min more heat was released and detected in the Differential Scanning Calorimetry.

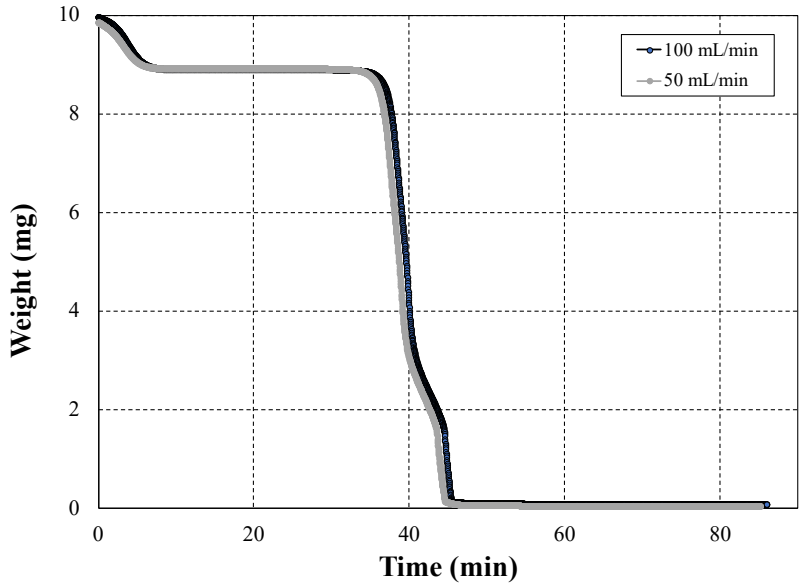

Figure 101: Influence of the air flow rate in experiments with the same conditions.

Lower and higher values of the air flow rate were considered inappropriate due to the incapacity to avoid secondary reactions or to be excessive and modify the thermal conversion [176]. Thus, 100 mL/min was defined as the air flow rate necessary to carry out the experiments.

The second issue addressed was the particle size and initial mass of the sample. It is known that larger particles and initial mass are related to heat and mass transfer effects, since spatial temperature gradients are caused, and the diffusion of the air is increased leading to a diffusion regime. Considering the knowledge acquired from the previous experiments [176], it was defined that to avoid heat transfer and mass transfer limitations, the particle size should be smaller than 1 mm and the initial mass should be around 10 mg.

Additionally, the heating program with in-situ drying was defined as a crucial step to minimize the influence of the heterogeneity of the samples. Hence, if the samples present different moisture contents, the thermal behavior will not be affected. The final temperature was adjusted in order to be enough to obtain a complete decomposition. Initial 700 °C was defined however, some constituents of the solid biomass present a conversion at higher temperatures. In this way, the final temperature was defined as 900 °C.

Raw Data Assessment

Table 43: Characteristic parameters considered for thermal analysis evaluation and comparison.

Fuel	β (°C/min)	Temperatures					Mass Loss				Time			Indexes			
		T_{ig}	T_b	T_1	T_2	T_{max}	DTG_{mean}	DTG_{max}	R_1	R_2	m_b	t_{ig}	t_b	I	V	B	C
ET	5	241.78	423.96	309.02	416.42	416.42	21.20	0.58	59.41	33.64	0.155	55.28	90.01	4.26E-03	2.64E-06	1.70	4.97E-07
	10	239.78	436.98	318.90	423.89	423.89	23.01	1.17	61.80	32.25	0.145	41.44	60.03	9.25E-03	2.87E-06	1.88	1.07E-06
	20	238.42	448.47	328.18	423.93	328.18	24.93	2.14	56.98	30.92	0.184	35.75	45.59	1.53E-02	3.33E-06	2.19	2.09E-06
	100	237.36	561.91	350.87	451.07	350.87	122.71	9.98	62.45	27.48	0.481	29.95	32.93	1.24E-01	1.47E-05	3.24	3.87E-05
EB	5	239.47	476.82	313.68	435.70	313.68	2.90	0.57	48.66	41.82	0.448	54.68	102.18	5.19E-04	3.16E-07	1.95	5.99E-08
	10	220.59	503.16	321.57	446.47	446.47	5.64	1.10	42.97	45.59	0.453	40.65	68.84	2.02E-03	6.36E-07	2.26	2.53E-07
	20	207.92	530.03	336.67	451.63	451.63	14.57	2.15	42.48	45.30	0.391	33.71	49.72	8.69E-03	1.81E-06	2.80	1.37E-06
	100	152.94	638.04	342.43	457.31	342.43	63.39	9.94	51.04	38.28	0.296	29.11	33.57	6.49E-02	1.05E-05	4.22	4.22E-05
EBA	5	240.55	432.91	315.18	428.77	315.18	6.21	0.57	51.62	39.23	0.490	55.06	93.41	1.21E-03	7.21E-07	1.69	1.41E-07
	10	234.19	429.65	326.22	419.17	419.17	36.34	1.12	55.07	34.86	0.318	40.90	59.40	1.50E-02	5.12E-06	2.10	1.72E-06
	20	233.37	428.77	335.65	408.17	408.17	35.47	2.05	51.71	31.66	0.536	35.54	44.62	2.24E-02	6.25E-06	2.69	3.11E-06
	100	148.60	547.86	356.69	726.63	356.69	89.77	9.52	53.41	32.40	0.914	27.95	31.54	1.02E-01	4.58E-06	1.08	7.06E-05
PT	5	251.92	445.11	316.35	436.46	316.35	7.14	0.55	51.85	36.78	0.007	57.25	95.76	1.30E-03	7.46E-07	1.61	1.39E-07
	10	247.39	450.12	328.17	440.06	440.06	24.05	1.09	54.60	33.21	0.102	43.28	62.54	8.89E-03	2.65E-06	1.81	9.52E-07
	20	242.06	484.53	339.58	444.82	339.58	27.88	2.19	57.14	32.38	0.175	35.15	47.19	1.68E-02	3.22E-06	2.30	2.16E-06
	100	240.67	579.16	374.80	505.04	374.80	111.47	9.98	61.99	27.83	0.192	29.62	32.74	1.15E-01	9.49E-06	2.60	3.32E-05
PB	5	232.17	443.93	298.05	433.13	298.05	3.46	0.54	47.61	38.96	0.24	54.09	96.29	6.64E-04	3.70E-07	1.57	7.60E-08
	10	206.23	461.45	307.79	423.42	423.42	22.61	1.08	47.94	38.07	0.36	37.99	63.45	9.38E-03	3.08E-06	2.21	1.06E-06
	20	199.27	494.73	315.32	430.09	430.09	23.03	2.11	48.77	37.45	0.27	32.70	47.49	1.48E-02	3.19E-06	2.57	1.69E-06
	100	170.05	589.39	323.58	411.21	323.58	111.16	10.31	54.54	38.18	0.31	28.72	32.57	1.19E-01	2.31E-05	4.79	1.75E-05
AT	5	238.62	421.24	308.75	404.83	308.75	5.08	0.57	54.83	36.22	0.56	54.46	90.78	1.03E-03	7.18E-07	1.90	1.20E-07
	10	225.80	424.92	316.04	411.38	411.38	20.68	1.13	54.07	36.95	0.25	40.46	59.00	8.66E-03	3.04E-06	2.09	1.08E-06
	20	217.41	417.51	312.98	389.47	312.98	58.08	2.11	51.09	36.14	0.15	34.93	44.18	3.76E-02	1.12E-05	2.62	6.22E-06
	100	196.59	539.53	321.96	457.54	321.96	146.91	10.50	58.49	36.33	0.10	29.23	32.35	1.55E-01	1.71E-05	2.53	7.40E-05
AB	5	236.71	471.81	304.35	417.05	304.35	2.71	0.57	54.50	37.74	0.48	54.73	101.62	4.87E-04	3.34E-07	2.09	5.89E-08
	10	210.91	505.79	317.73	511.51	317.73	5.27	1.15	57.11	35.51	0.30	37.58	66.84	2.10E-03	4.06E-07	1.52	2.69E-07
	20	200.77	527.77	321.61	510.10	321.61	10.67	2.27	57.17	35.34	0.32	33.18	49.21	6.53E-03	8.77E-07	1.73	1.14E-06
	100	165.86	680.97	332.70	504.08	332.70	57.00	10.03	56.09	34.19	0.37	28.63	33.38	5.96E-02	6.03E-06	3.01	3.05E-05
OB	5	240.99	437.76	313.61	429.19	313.61	6.67	0.57	58.18	32.75	0.02	55.33	94.43	1.28E-03	7.63E-07	1.70	1.49E-07
	10	229.04	445.48	327.79	438.42	438.42	24.56	1.15	60.08	32.11	0.11	40.25	61.21	9.97E-03	2.96E-06	1.96	1.20E-06
	20	224.65	451.47	336.07	428.49	428.49	30.05	2.24	60.34	31.13	0.18	34.45	44.99	1.94E-02	4.31E-06	2.45	2.96E-06
	100	218.13	558.84	354.60	433.67	354.60	122.13	10.50	67.48	27.25	0.19	28.70	31.78	1.34E-01	2.00E-05	4.31	4.82E-05

Annex D – Debugging the Small-scale Reactor Experimental System

Temperature Calibration

Before the experimental campaign using the small-scale reactor, it was required to calibrate the equipment in terms of the temperature set point. This preliminary experiment was essential to obtain the relationship between the reactor display temperature and the real temperature inside the furnace. In this way, with this information, it was possible to define the correct temperature in the controller.

The procedure was performed using three thermocouples (precalibrated) introduced in different positions inside the reactor. Figure 102 presents the experimental apparatus used during this debugging test. As shown in Figure 103, to obtain the desired setpoint temperatures to develop the experiments (400, 500, 600, 700, and 800 °C) a higher temperature needs to be defined in the temperature controller. During the normal operation of the small-scale reactor, the thermocouple that is connected to the controller is placed in the middle of the reactor wall but, during this test, the thermocouple used was the one placed in the middle of the reactor. This was carried out to obtain more easily the deviation between both temperatures since the temperature mentioned for each experiment is based on the temperature where the basket with the biomass samples will be placed.

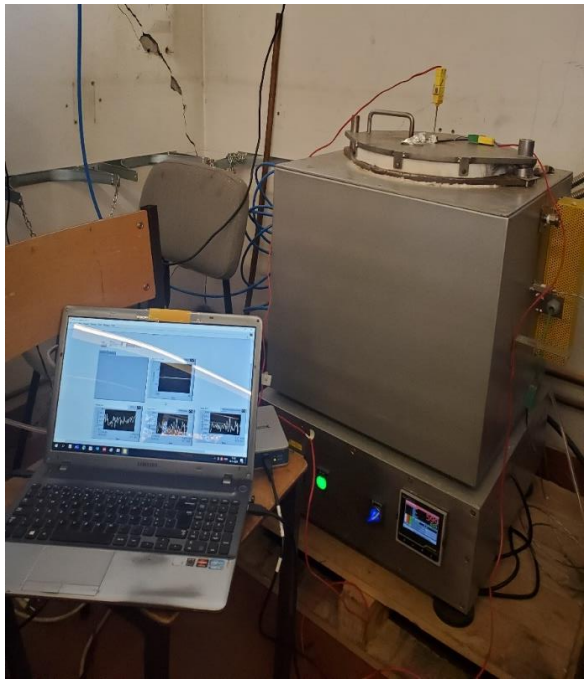

Figure 102: Experimental apparatus used for temperature calibrations.

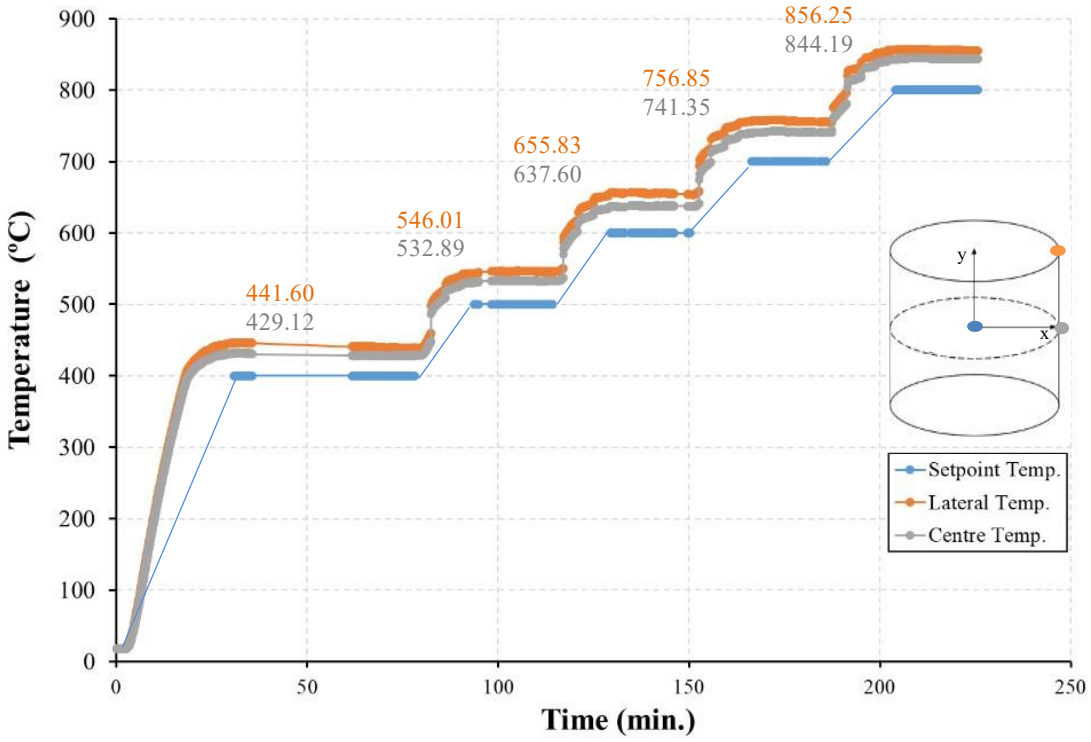

Figure 103: Temperature variation inside the reactor at different positions.

Thus, the deviation between the desired and the display temperature is between 30 to 40 °C. Hence, for each desired isothermal experiment the deviation between the temperatures was known and the new value to be defined for each corresponding experiment was defined.

Weighing Variation

The sensitivity of the scale to the temperature change and the flow induced on the basket were initially evaluated. Although the temperature affects the result of the scale, to avoid this issue, the experiment only starts after the interior of the reactor is at the desired temperature and, before the introduction of the sample in the basket, in the LabVIEW, a signal is sent to the scale to null the scale. In this way, the effects from the expansion of metal wire, or related to the buoyancy promoted by the reduction of the gas density will not be taken into account using this procedure. Regarding the influence of the flow in the wight measurements, after some modifications in the lid and in the connection of the wire that connects the basket to the scale, preliminary experiments with the basket empty and different air flow rates (including the maximum possible in the experimental apparatus – 70 L/min) were carried out. The results are presented in Figure 104 and, as it is possible to observe, the variation of the scale measurement is minimal when compared to the initial mass used in the experiments (20 g).

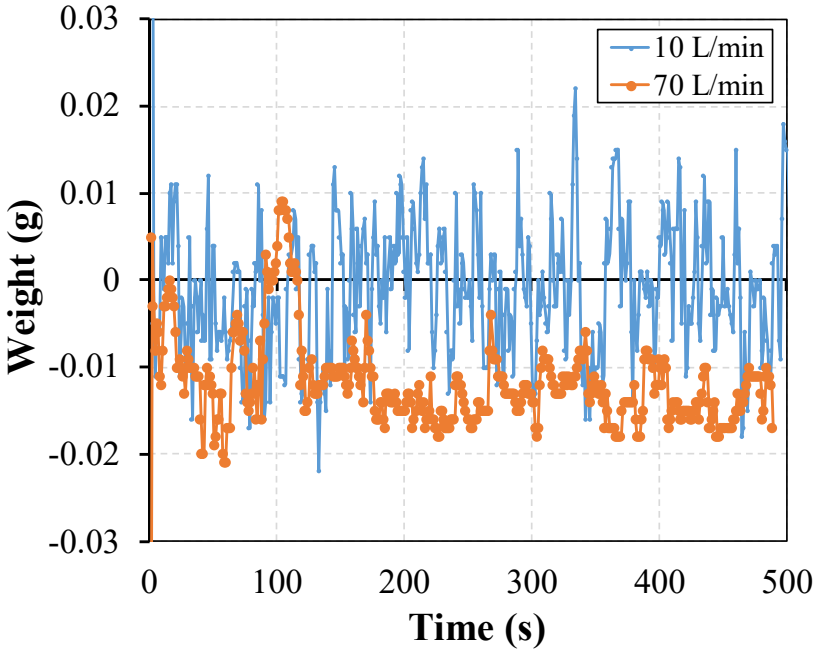

Figure 104: Weight variation along with a blank experiment.

Analysis of the Operating Conditions

After the calibration process of the small-scale reactor and understand the influence of the operating conditions on the weight measurements, combustion experiments were developed to observe the influence of the air flow rate and the particle size on the combustion behavior, and also the influence of the air flow rate in the gas collection. Figure 105 presents the influence of the air flow rate on the combustion behavior of eucalyptus samples.

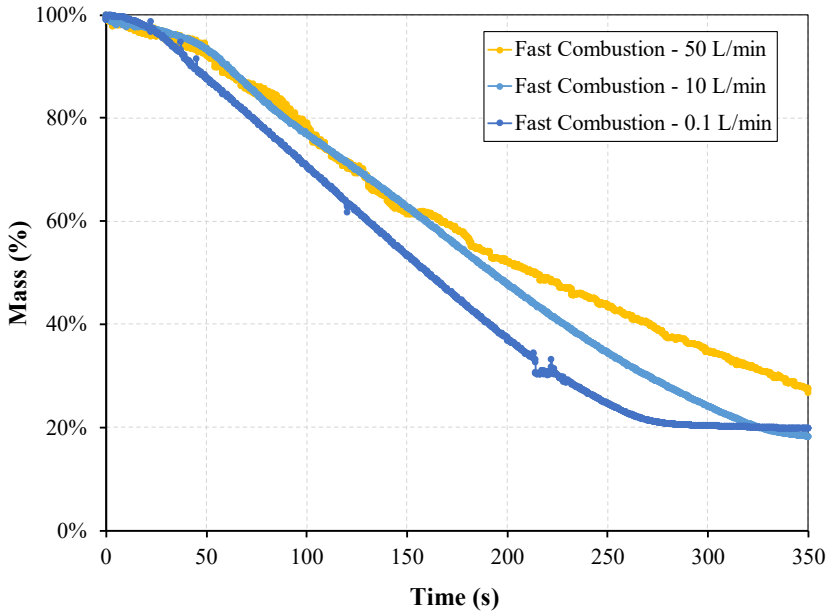

Figure 105: Influence of the air flow rate during experiments with the same operating conditions.

The air flow rate, as expected, presents a determinant profile in the combustion behavior of the solid biomass particles. Although there are significant differences, the critical aspect of these experiments was to understand the limit value to collect a gas sample and determine the volatiles composition. After some modifications to the experimental procedure to collect the gas sample, the best configuration to capture a sample during the first stages of the thermal conversion, was to introduce a probe in the middle of the lid, close to the wire that connects the scale to the basket, and using the lower air flow rate as possible, 0.1 L/min.

Regarding the influence of the particle size of the samples, two samples of eucalyptus particles were prepared. One sample was composed of a random set of particles collected after the milling process while the other one was composed of sieved particles with a size between 16 and 50 mm. As observed in Figure 106 at 400 °C, the difference between the mass loss profile of both samples is insignificant. Furthermore, more experiments were carried out with similar samples and with different reactor temperatures, and only a small difference was detected at the beginning of the thermal conversion process. The differences were not higher than 0.1% of the weight of the sample. Therefore, these results suggest that mass loss is not dependent on the size of the particle.

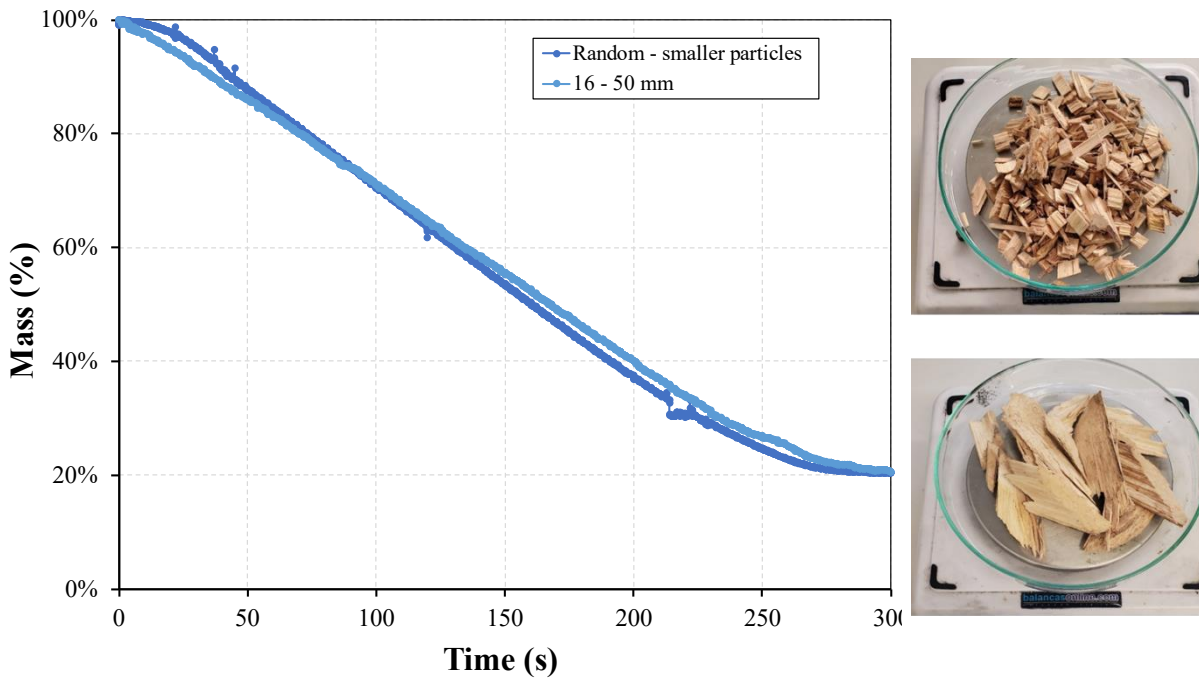

Figure 106: Comparison of the mass loss behavior for experiments using particles with different sizes.

To verify this result, samples with different dimensions were carefully prepared to understand which dimension is controlling the combustion of a set of woodchips. Figure 107 presents the particles produced at the laboratory with a length of 30 or 60 mm and a thickness of 10 or 20 mm. A set of combustion experiments was carried out with these particles and as represented in Figure 108, the thickness of the particles is the geometrical dimension that limits the combustion behavior for larger particles. Therefore, as woodchips are thin particles and, although there are particles of different lengths, the combustion profile is always similar. These experiments were useful to understand this phenomenon and justify the particles used in this work.

Figure 107: Particles produced to analyze the influence of different dimensions on the mass loss behavior.

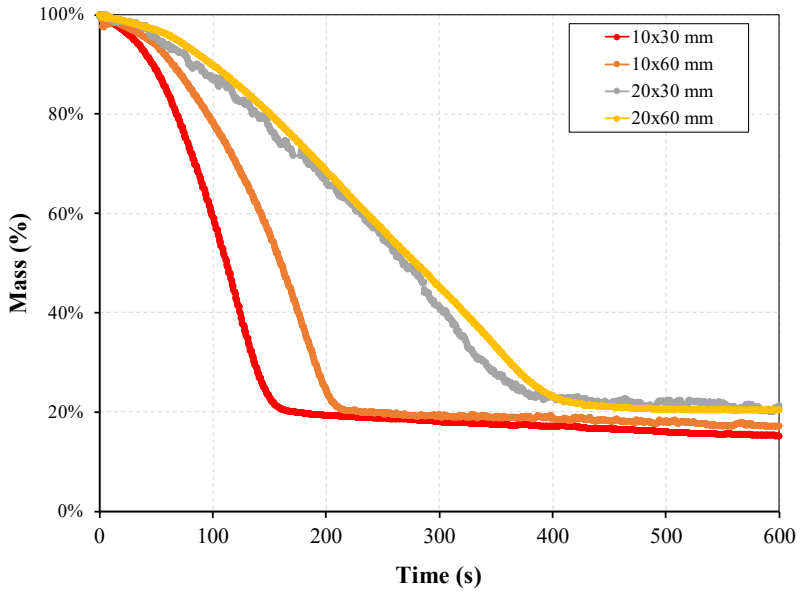

Figure 108: Comparison of the mass loss behavior for particles with different lengths and thicknesses.

Annex E – Technical Drawing of the Grate-fired Boiler

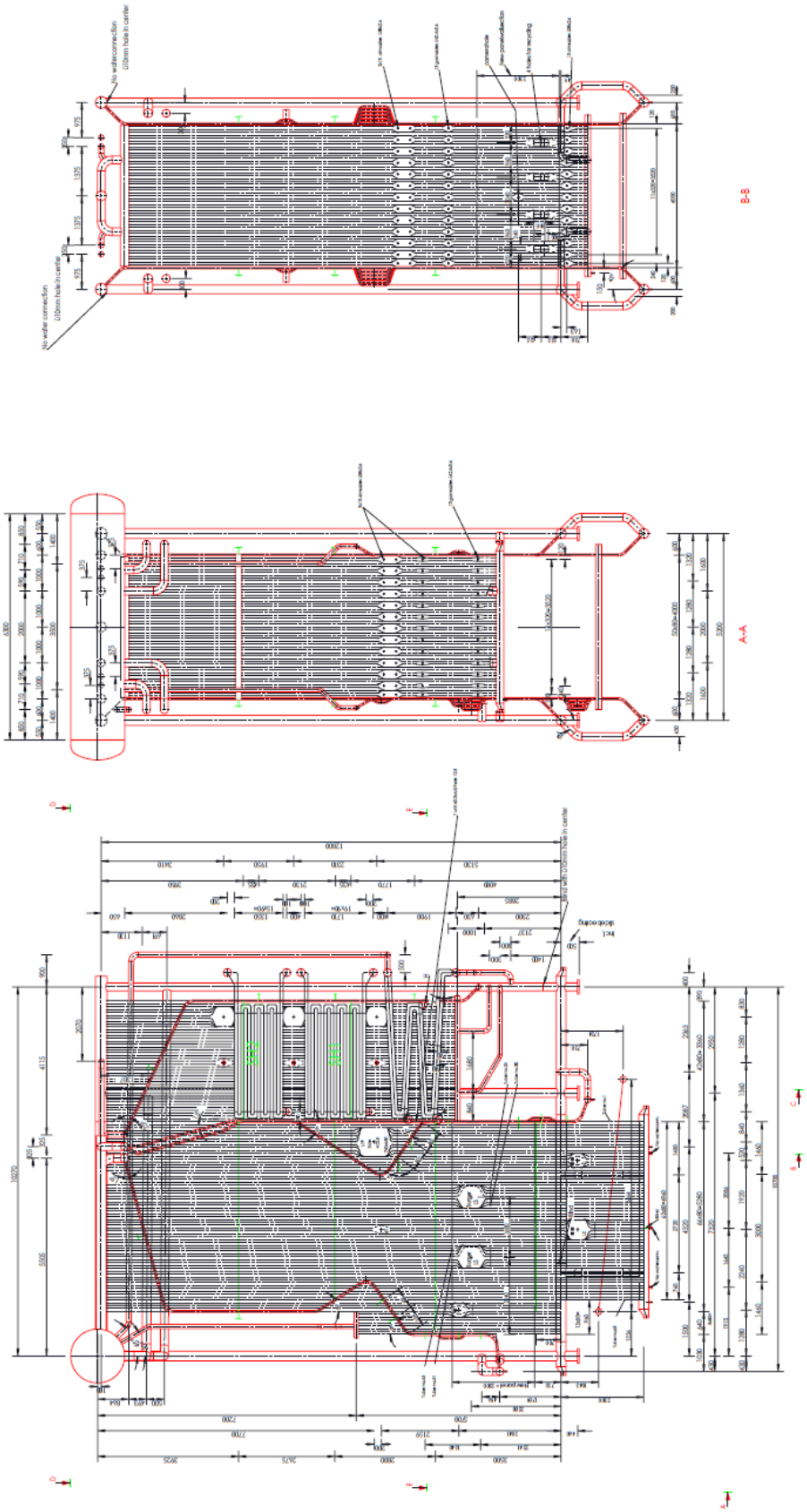

Figure 109: Technical drawing of the grate-fired boiler from the Mortágua Power Plant.